

ADVANCED HYBRID PARTICULATE COLLECTOR

Final Topical Report for Phase III

Reporting Period September 30, 1999, to September 29, 2001

Prepared for:

AAD Document Control
U.S. Department of Energy
National Energy Technology Laboratory
PO Box 10940, MS 921-107
Pittsburgh, PA 15236-0940

DOE Cooperative Agreement No. DE-FC26-99FT40719
Contracting Officer's Representative: William Aljoe

Prepared by:

Ye Zhuang
Stanley J. Miller
Michelle R. Olderbak

Energy & Environmental Research Center
University of North Dakota
PO Box 9018
Grand Forks, ND 58202-9018

Rich Gebert

W.L. Gore & Associates, Inc.
101 Lewisville Road
Elkton, MD 21922-1100

DISCLAIMER

This report was prepared as an account of work sponsored by the United States Government. Neither the United States, any agency thereof, nor any of their employees, makes any warranty, express or implied, or assumes any legal liabilities or responsibility for the accuracy, completeness, or usefulness of any information, apparatus, product, or process disclosed, or represents that its use would not infringe privately owned rights. Reference herein to any specific commercial product, process, or service, by trade name, trade mark, manufacturer, or otherwise, does not necessarily constitute or imply its endorsement, recommendation, or favoring by the United States or any agency thereof. The views and opinions of authors expressed herein do not necessarily state or reflect those of the United States Government or any agency thereof.

This report is available to the public from the National Technical Information Service, U.S. Department of Commerce, 5285 Port Royal Road, Springfield, VA 22161; phone orders accepted at (703) 487-4650.

ACKNOWLEDGMENT

This report was prepared with the support of the U.S. Department of Energy (DOE) National Energy Technology Laboratory Contract No. DE-FC26-99FT40719. However, any opinions, findings, conclusions, or recommendations expressed herein are those of the authors(s) and do not necessarily reflect the views of DOE.

EERC DISCLAIMER

LEGAL NOTICE This research report was prepared by the Energy & Environmental Research Center (EERC), an agency of the University of North Dakota, as an account of work sponsored by National Energy Technology Laboratory. Because of the research nature of the work performed, neither the EERC nor any of its employees makes any warranty, express or implied, or assumes any legal liability or responsibility for the accuracy, completeness, or usefulness of any information, apparatus, product, or process disclosed, or represents that its use would not infringe privately owned rights. Reference herein to any specific commercial product, process, or service by trade name, trademark, manufacturer, or otherwise does not necessarily constitute or imply its endorsement or recommendation by the EERC.

ADVANCED HYBRID PARTICULATE COLLECTOR

ABSTRACT

A new concept in particulate control, called an advanced hybrid particulate collector (AHPC), is being developed under funding from the U.S. Department of Energy. The AHPC combines the best features of electrostatic precipitators (ESPs) and baghouses in an entirely novel manner. The AHPC concept combines fabric filtration and electrostatic precipitation in the same housing, providing major synergism between the two methods, both in the particulate collection step and in transfer of dust to the hopper. The AHPC provides ultrahigh collection efficiency, overcoming the problem of excessive fine-particle emissions with conventional ESPs, and solves the problem of reentrainment and re-collection of dust in conventional baghouses.

Phase I of the development effort consisted of design, construction, and testing of a 5.7-m³/min (200-acfm) working AHPC model. Results from both 8-hr parametric tests and 100-hr proof-of-concept tests with two different coals demonstrated excellent operability and greater than 99.99% fine-particle collection efficiency.

Since all of the developmental goals of Phase I were met, the approach was scaled up in Phase II to a size of 255 m³/min (9000 acfm) (equivalent in size to 2.5 MW) and was installed on a slipstream at the Big Stone Power Plant. For Phase II, the AHPC at Big Stone Power Plant was operated continuously from late July 1999 until mid-December 1999. The Phase II results were highly successful in that ultrahigh particle collection efficiency was achieved, pressure drop was well controlled, and system operability was excellent.

For Phase III, the AHPC was modified into a more compact configuration, and components were installed that were closer to what would be used in a full-scale commercial design. The modified AHPC was operated from April to July 2000. While operational results were acceptable during this time, inspection of bags in the summer of 2000 revealed some membrane damage to the fabric that appeared to be caused by electrical effects. Subsequently, extensive theoretical, bench-scale, and pilot-scale investigations were completed to find an approach to prevent bag damage without compromising AHPC performance. Results showed that the best bag protection and AHPC performance were achieved by using a perforated plate installed between the discharge electrodes and bags. This perforated-plate design was then installed in the 2.5-MW AHPC at Big Stone Power Plant in Big Stone City, South Dakota, and the AHPC was operated from March to June 2001. Results showed that the perforated-plate design solved the bag damage problem and offered even better AHPC performance than the previous design. All of the AHPC performance goals were met, including ultrahigh collection efficiency, high air-to-cloth ratio, reasonable pressure drop, and long bag-cleaning interval.

TABLE OF CONTENTS

ABSTRACT	i
LIST OF FIGURES	vi
LIST OF TABLES	xv
UNITS AND ACRONYMS USED	xvi
EXECUTIVE SUMMARY	xviii
1.0 INTRODUCTION	1-1
1.1 Background	1-1
1.2 Phase I Summary	1-2
1.3 Phase II Summary	1-4
1.4 Phase III Objectives	1-8
2.0 THEORY AND CONCEPT	2-1
2.1 Fine-Particle Collection Efficiency	2-1
2.2 GORE-TEX® Membrane Filtration Media	2-2
2.2.1 GORE-TEX® Membrane–GORE-TEX® Felt Filter Bags	2-4
2.2.2 GORE-NO-STAT® Filter Bags (GORE-TEX® Membrane/GORE-TEX® Antistatic Felt, 20 oz/yd ²)	2-5
2.2.3 GORE-NO-STAT® Filter Bag (GORE-TEX® Antistatic Membrane/ GORE-TEX® Antistatic Felt)	2-5
2.3 Flow Theory and Performance Evaluation Criteria	2-6
2.4 AHPC Concept Description	2-9
3.0 RESULTS AND DISCUSSIONS	3-1
3.1 Scope of the Phase III Work	3-1
3.2 AHPC Upgrade and Field Study at Big Stone Power Plant (September 1999 – June 2000)	3-3
3.2.1 System Modification at the AHPC Big Stone Unit at the Start of Phase III	3-3
3.2.1.1 Data Acquisition and Control	3-3
3.2.1.1.1 Hardware: National Instrument “Field Point” Module	3-3
3.2.1.1.2 Software: Server–Client Program Developed by National Instrument “Lookout”	3-4
3.2.1.2 AHPC Modification at the Big Stone Unit	3-10
3.2.1.2.1 Single-Side Transition Inlet	3-10
3.2.1.2.2 Discharge Electrodes and Plates	3-11

Continued . . .

TABLE OF CONTENTS (cont.)

3.2.1.2.3	Plate Spacing	3-13
3.2.1.2.4	Bag Spacing, Tube Sheet, and Pulse Tube Changes	3-13
3.2.2	Results for Test Period 1 (April 18, 2000 – May 17, 2000)	3-15
3.2.2.1	Plant Conditions and AHPC Operating Parameters	3-15
3.2.2.2	Results Discussion	3-17
3.2.2.3	A/C Ratio Experiments	3-21
3.2.2.4	Pulse Trigger Pressure Experiments	3-25
3.2.3	Results for Test Period 2 (May 31, 2000 – July 21, 2000)	3-28
3.2.3.1	Plant Conditions and AHPC Operating Parameters	3-28
3.2.3.2	Testing Results Discussion	3-28
3.2.3.3	Additional A/C Ratio and Pulse Trigger Pressure Experiments	3-34
3.2.4	Bag Analysis	3-41
3.2.4.1	Visual Analysis	3-42
3.2.4.2	Media Analysis	3-45
3.2.4.3	Dimensional Analysis	3-46
3.2.4.4	Air Permeability Analysis	3-46
3.2.4.5	Mechanical Strength Analysis	3-48
3.2.4.6	Summary of Bag Evaluation	3-48
3.2.5	Fly Ash Resistivity Analysis	3-48
3.2.6	Summary for April–July 2000 Testing	3-50
3.3	AHPC Pilot- and Bench-Scale Studies at the EERC (August – December 2000)	3-51
3.3.1	Pilot-Scale Cold-Flow Tests at the EERC	3-51
3.3.1.1	Effect of Electrodes on V–I Characteristics and Current to Bags	3-54
3.3.1.2	EERC Electrode Tests	3-59
3.3.1.2.1	Spacing Ratio Experiments	3-61
3.3.1.2.2	Plate-Spacing Experiments	3-62
3.3.1.2.3	2-Wire Grid Experiments	3-62
3.3.1.3	ELEX Electrode Tests	3-63
3.3.1.3.1	Spacing Ratio Experiments	3-64
3.3.1.3.2	Bag-Type Experiments	3-65
3.3.1.3.3	Grounded-Grid Experiments	3-66
3.3.1.4	ENELCO Electrode Tests	3-67
3.3.1.4.1	Spacing Ratio Experiments	3-67
3.3.1.4.2	Bag-Type Experiments	3-68
3.3.1.5	Summary of Pilot-Scale Cold-Flow Tests at the EERC	3-70
3.3.2	Pilot-Scale Coal Combustion Hot-Flow Tests at the EERC	3-72
3.3.2.1	PTC-CR-621 Series Tests	3-72
3.3.2.1.1	PTC-CR-621-1	3-73
3.3.2.1.2	PTC-CR-621-2	3-73
3.3.2.1.3	PTC-CR-621-3	3-76

Continued . . .

TABLE OF CONTENTS (cont.)

3.3.2.1.4	PTC-CR-621-4	3-80
3.3.2.1.5	PTC-CR-621-5	3-82
3.3.2.2	PTC-CR-622 and PTC-CR-623 Series Tests	3-85
3.3.2.2.1	Test Configuration Description	3-85
3.3.2.2.2	Results for PTC-CR-622 Test	3-88
3.3.2.2.3	Results for Test PTC-CR-623	3-94
3.3.2.2.4	Evaluation of ESP Performance in the AHPC Unit under the Perforated-Plate Configuration	3-104
3.3.2.2.5	Summary of Perforated-Plate Testing	3-105
3.3.3	Bench-Scale Experiments and Theoretical Calculation for AHPC Perforated-Plate Configuration	3-106
3.3.3.1	Effect of Perforated-Plate Hole Size on Bag Current	3-106
3.3.3.2	Electrical Field Distribution in the Perforated-Plate Configuration	3-111
3.4	AHPC Field Study at Big Stone Power Plant (January – July 2001)	3-115
3.4.1	Modifications of the Perforated-Plate AHPC at Big Stone Power Plant	3-115
3.4.2	Overview for March 15, 2001 – June 28, 2001	3-122
3.4.3	Results for Test Period 1 (March 15 – May 8, 2001)	3-124
3.4.3.1	Plant Conditions – Fuel, Load, and Temperature	3-124
3.4.3.2	Electrical Conditions	3-126
3.4.3.3	Perforated-Plate AHPC Performance	3-128
3.4.3.4	Pulse Trigger Pressure Experiments	3-135
3.4.3.5	A/C Ratio Experiments	3-137
3.4.3.6	Secondary Current Experiments	3-139
3.4.3.7	Pulse-Cleaning Experiments	3-140
3.4.4	Results for Test Period 2 (May 16 – June 15, 2001)	3-146
3.4.4.1	Plant Conditions – Fuel, Load, and Temperature	3-146
3.4.4.2	Electrical Conditions	3-147
3.4.4.3	Perforated-Plate AHPC Performance	3-148
3.4.4.4	Fixed Bag-Cleaning Interval Experiments	3-150
3.4.4.5	Pulse Sequence Experiments with Cross-Row Pulsing	3-151
3.4.5	Results for Test Period 3 (June 17–28, 2001)	3-155
3.4.5.1	Electrical Conditions	3-155
3.4.5.2	Pulse Sequence Experiments	3-156
3.4.5.3	Humidification Experiments	3-158
3.4.6	AHPC Filter Bag Analysis	3-162
3.4.6.1	Filter Bag Drag Analysis	3-163
3.4.6.2	Filter Bag Field Analysis	3-165
3.4.6.3	Visual Observation	3-167
3.4.6.4	Filter Bag Microscope Analysis	3-167

Continued . . .

TABLE OF CONTENTS (cont.)

3.4.6.5	Air Permeability Analysis	3-169
3.4.6.6	Dimensional and Mechanical Strength Analysis	3-170
3.4.7	Coal and Fly Ash Resistivity Analyses	3-171
3.4.8	Particulate Emissions of the Perforated-Plate AHPC System	3-172
4.0	CONCLUSIONS AND DISCUSSIONS	4-1
5.0	REFERENCES	5-1

LIST OF FIGURES

2.2-1	Comparison of GORE-TEX [®] membrane to conventional copolyimide fiber (P-84)	2-3
2.4-1	Top view of the 9000-acfm (255-m ³ /min) AHPC installed at the Big Stone Power Plant at the start of Phase III	2-11
3.2-1	Overall process layout screen	3-6
3.2-2	SIR II control screen for changing the operation of the ESP power supply	3-6
3.2-3	SIR II readings screen	3-7
3.2-4	SIR II alarms screen	3-7
3.2-5	Screen used for controlling the backpulse and rapper-cleaning sequences	3-8
3.2-6	Ash removal control screen	3-8
3.2-7	Screen for following the differential pressure across the bags in the AHPC	3-9
3.2-8	Cleaning cycle statistics screen	3-9
3.2-9	AHPC unit installed at Big Stone with new inlet ducting and side transition inlet configuration	3-12
3.2-10	Inlet transition baffle distributor plates at the entrance to the AHPC	3-12
3.2-11	Top view of the modified AHPC at the start of Phase III	3-14
3.2-12	Gross load for Big Stone for the period April 18 – May 17, 2000	3-17
3.2-13	Bag-cleaning interval for April 21 – May 15, 2000, while the AHPC is operated in the multibank pulsing mode	3-19
3.2-14	Bag-cleaning interval for April 21–27, 2000, while the AHPC is operated in the multibank pulsing mode	3-19
3.2-15	Residual drag for April 21 – May 15, 2000, during periods of operation in the multibank pulsing mode	3-20
3.2-16	K ₂ C _i values for April 21 – May 15, 2000, during periods of operation in the multibank pulsing mode	3-20

Continued . . .

LIST OF FIGURES (cont.)

3.2-17 A/C ratio for the test period to determine the effect of A/C ratio on bag-cleaning interval 3-22

3.2-18 Tube sheet pressure drop for the test period to determine the effect of A/C ratio on bag-cleaning interval 3-23

3.2-19 Drag values for the test period to determine the effect of A/C ratio on bag-cleaning interval 3-23

3.2-20 Bag-cleaning intervals during the times when the A/C ratio was changed 3-24

3.2-21 Effect of pulse-cleaning set point on bag-cleaning interval at constant A/C ratio . . 3-26

3.2-22 Pressure drop for May 15, 2000 3-26

3.2-23 A/C ratio for May 15, 2000 3-27

3.2-24 Bag-cleaning interval for May 15, 2000 3-27

3.2-25 Big Stone Power Plant gross load and ESP inlet temperature for May 24 – July 21, 2000 3-29

3.2-26 Varying bag-cleaning interval with time of day 3-29

3.2-27 Bag-cleaning interval for June 16–24, 2000 3-30

3.2-28 K_2C_i for June 16–24, 2000 3-31

3.2-29 Residual drag for the period from June 16–24, 2000 3-31

3.2-30 Daily average pressure drop for June 28 – July 5, 2000 3-33

3.2-31 Residual drag for June 28 – July 5, 2000 3-33

3.2-32 Bag-cleaning interval for June 28 – July 5, 2000 3-35

3.2-33 K_2C_i for June 28 – July 5, 2000 3-35

3.2-34 Pressure drop for July 7, 2000 3-37

3.2-35 Bag-cleaning interval for July 7, 2000 3-37

Continued . . .

LIST OF FIGURES (cont.)

3.2-36 K_2C_i for July 7, 2000 3-38

3.2-37 K_2C_i versus difference in pressure drop before and after bag cleaning
for July 7, 2000 3-38

3.2-38 A/C ratio for July 9, 2000 3-39

3.2-39 Pressure drop for July 9, 2000 3-40

3.2-40 Bag-cleaning interval for July 9, 2000 3-40

3.2-41 K_2C_i versus bag-cleaning interval for July 9, 2000 3-41

3.2-42 R2B2 after brushing 3-43

3.2-43 Fly ash resistivity of AHPC hopper ash samples for Cordero Rojo complex and
Black Thunder coals 3-50

3.3-1 Percent bag current of measurement total current for EERC and ELEX electrodes . 3-55

3.3-2 Percent bag current of measurement total current for ENELCO electrodes 3-55

3.3-3 Effect of electrode on V-I characteristics 3-58

3.3-4 Effect of electrode on V-I characteristics 3-58

3.3-5 Effect of electrode on current to bags 3-60

3.3-6 Effect of electrode on current to bags 3-60

3.3-7 Effect of spacing ratio on bag current 3-61

3.3-8 Effect of plate spacing on bag current 3-62

3.3-9 Effect of grid on bag current 3-63

3.3-10 Effect of ratio on current to the bags 3-64

3.3-11 Effect of bag type on current to the bags 3-65

3.3-12 Effect of bag type on current to the bags 3-66

Continued . . .

LIST OF FIGURES (cont.)

3.3-13 Effect of grounded grid on current to the bags 3-67

3.3-14 Effect of ratio on current to the bags 3-68

3.3-15 Effect of ratio on current to the bags 3-69

3.3-16 Effect of bag type on current to the bags 3-69

3.3-17 Effect of bag type on current to the bags in the presence of a grounded grid 3-70

3.3-18 Current and voltage for PTC-CR-621-1 3-74

3.3-19 Bag-cleaning interval for PTC-CR-621-1 3-74

3.3-20 K_2C_i for PTC-CR-621-1 3-75

3.3-21 Residual drag for PTC-CR-621-1 3-75

3.3-22 Bag-cleaning interval for PTC-CR-621-2 3-76

3.3-23 K_2C_i for PTC-CR-621-2 3-77

3.3-24 Residual drag for PTC-CR-621-2 3-77

3.3-25 Bag-cleaning interval for PTC-CR-621-3 3-78

3.3-26 K_2C_i for PTC-CR-621-3 3-79

3.3-27 Residual drag for PTC-CR-621-3 3-79

3.3-28 Bag-cleaning interval for PTC-CR-621-4 3-80

3.3-29 K_2C_i for PTC-CR-621-4 3-81

3.3-30 Residual drag for PTC-CR-621-4 3-81

3.3-31 Bag-cleaning interval for PTC-CR-621-5 3-83

3.3-32 Residual drag for PTC-CR-621-5 3-83

3.3-33 K_2C_i for PTC-CR-621-5 3-84

Continued . . .

LIST OF FIGURES (cont.)

3.3-34 AHPC pilot-scale configuration at the EERC 3-86

3.3-35 Photo showing the 1.5-in. (38-mm) holes uniformly distributed over the perforated plate in a staggered pattern 3-89

3.3-36 Bag-cleaning interval for PTC-CR-622-1 3-89

3.3-37 Residual drag for PTC-CR-622-1 3-90

3.3-38 K_2C_i for PTC-CR-622-1 3-91

3.3-39 Fly ash-deposited pattern on the perforated plates at the pilot-scale AHPC 3-91

3.3-40 Bag-cleaning intervals for PTC-CR-622-2 and PTC-CR-622-3 3-93

3.3-41 K_2C_i for PTC-CR-622-2 and PTC-CR-622-3 3-93

3.3-42 Residual drag for PTC-CR-622-2 and PTC-CR-622-3 3-94

3.3-43 A nonuniform hole distribution on perforated plates 3-96

3.3-44 Pressure drop for PTC-CR-623-1 3-96

3.3-45 Pressure drop for PTC-CR-623-3 3-97

3.3-46 Bag-cleaning interval for PTC-CR-623-1 3-97

3.3-47 Bag-cleaning interval for PTC-CR-623-3 3-98

3.3-48 Residual drag for PTC-CR-623-1 3-98

3.3-49 Residual drag for PTC-CR-623-3 3-99

3.3-50 K_2C_i for PTC-CR-623-1 3-99

3.3-51 K_2C_i for PTC-CR-623-3 3-100

3.3-52 Effect of corona current on respirable mass in AHPC 3-105

3.3-53 Schematic of the bench-scale AHPC 3-106

Continued . . .

LIST OF FIGURES (cont.)

3.3-54 Current to the bags as a function of spacing between the electrode and the bag . . 3-108

3.3-55 Current to the bags as a function of spacing between the electrode and the bag . . 3-108

3.3-56 Current to the bag in the presence of different perforated plates 3-110

3.3-57 Current to the bag in the presence of different perforated plates 3-110

3.3-58 Current to the bag in the presence of different perforated plates 3-111

3.3-59 Electrical potential distributed in the pilot unit AHPC with the 1.0-in.
(25-mm)-hole-size perforated plates 3-113

3.3-60 Electrical potential distributed in the pilot unit AHPC with the 2.0-in.
(51-mm)-hole-size perforated plates 3-113

3.3-61 Electrical potential distributed in the pilot unit AHPC with the 2.5-in.
(64-mm)-hole-size perforated plates 3-114

3.3-62 Electric potential distribution in the AHPC pilot unit without the perforated plates 3-114

3.4-1 Top view of the 9000-acfm (255-m³/min) AHPC, as modified at
the start of Phase III 3-116

3.4-2 Top view of the perforated-plate configuration for the 9000-acfm
(255-m³/min) AHPC 3-116

3.4-3 Photo of the back side of the perforated plate showing the
uniform hole distribution pattern 3-117

3.4-4 Installing the perforated plates in the 9000-acfm (255-m³/min) AHPC at the
Big Stone Power Plant, March 2001 3-119

3.4-5 Perforated plates as installed in the 9000-acfm (255-m³/min) AHPC before
the tube sheet is replaced. Bags fit inside each pair of perforated plates 3-119

3.4-6 Photo showing the bidirectional discharging electrodes 3-120

3.4-7 AHPC pulse system (top view) 3-120

Continued . . .

LIST OF FIGURES (cont.)

3.4-8	Photo showing the newly installed cross-row pulse system with Goyen pulse valves	3-121
3.4-9	Daily average A/C ratio	3-123
3.4-10	Daily average pressure drop	3-124
3.4-11	Daily average bag-cleaning interval	3-125
3.4-12	Daily average K_2C_i	3-125
3.4-13	Daily average residual drag	3-126
3.4-14	Big Stone Power Plant gross load and ESP inlet temperature (test period March 15 – May 8, 2001)	3-127
3.4-15	Number of sparks per day (Test Period 1)	3-127
3.4-16	AHPC bag-cleaning interval (March 27–28, 2001)	3-129
3.4-17	AHPC residual drag (March 27–28, 2001)	3-129
3.4-18	AHPC K_2C_i (March 27–28, 2001)	3-130
3.4-19	AHPC bag-cleaning interval (April 5–23, 2001)	3-130
3.4-20	AHPC K_2C_i (April 5–23, 2001)	3-131
3.4-21	AHPC residual drag (April 5–23, 2001)	3-131
3.4-22	AHPC bag-cleaning interval (April 25 – May 8, 2001)	3-132
3.4-23	AHPC residual drag (April 25 – May 8, 2001)	3-132
3.4-24	AHPC K_2C_i (April 25 – May 8, 2001)	3-133
3.4-25	Trigger pressure effect on AHPC K_2C_i (April 23–27, 2001)	3-135
3.4-26	Trigger pressure effect on AHPC residual drag (April 23–27, 2001)	3-136
3.4-27	Trigger pressure effect on AHPC bag-cleaning interval (April 23–27, 2001)	3-136

Continued . . .

LIST OF FIGURES (cont.)

3.4-28	A/C ratio effect on AHPC K_2C_i (April 11–19, 2001)	3-137
3.4-29	A/C ratio effect on AHPC residual drag (April 11–19, 2001)	3-138
3.4-30	A/C ratio effect on AHPC bag-cleaning interval (April 11–19, 2001)	3-138
3.4-31	Current effect on AHPC K_2C_i (May 3–4, 2001)	3-140
3.4-32	Current effect on AHPC residual drag (May 3–4, 2001)	3-141
3.4-33	Current effect on AHPC bag-cleaning interval (May 3–4, 2001)	3-141
3.4-34	Pulse pressure effect on AHPC residual drag (March 21–25, 2001)	3-142
3.4-35	Pulse pressure effect on AHPC residual drag (April 19–21, 2001)	3-143
3.4-36	Pulse pressure effect on AHPC bag-cleaning interval (March 21–25, 2001)	3-144
3.4-37	Pulse pressure effect on AHPC bag-cleaning interval (April 19–21, 2001)	3-144
3.4-38	Photo showing the nonuniform ash pattern on the perforated plates caused by the electrical field in the AHPC vessel	3-145
3.4-39	Photo showing a very clean perforated plate with only a thin uniform ash deposit after a power-off rap	3-145
3.4-40	Photo showing the extremely clean bag surface after brush-off	3-146
3.4-41	Big Stone Power Plant gross load and ESP inlet temperature (Test Period May 16 – June 15, 2001)	3-147
3.4-42	Number of sparks per day (May 16 – June 16, 2001)	3-148
3.4-43	A/C ratio effect on AHPC bag-cleaning interval (May 17–18, 2001)	3-149
3.4-44	A/C ratio effect on AHPC K_2C_i (May 17–18, 2001)	3-149
3.4-45	A/C ratio effect on AHPC residual drag (May 17–18, 2001)	3-150
3.4-46	AHPC residual drag performance at 10- and 30-min bag-cleaning intervals (May 18–21, 2001)	3-151

Continued . . .

LIST OF FIGURES (cont.)

3.4-47 AHPC K_2C_i performance at 10- and 30-min bag-cleaning intervals (May 18–21, 2001) 3-152

3.4-48 Pulse sequence effect on AHPC bag-cleaning interval (June 7–13, 2001) 3-153

3.4-49 Pulse sequence effect on AHPC residual drag (June 7–13, 2001) 3-153

3.4-50 Pulse sequence effect on AHPC K_2C_i (June 7–13, 2001) 3-154

3.4-51 Number of sparks per day (June 18–28, 2001) 3-155

3.4-52 Pulse sequence effect on AHPC bag-cleaning interval (June 17–20, 2001) 3-156

3.4-53 Pulse sequence effect on AHPC residual drag (June 17–20, 2001) 3-157

3.4-54 Pulse sequence effect on AHPC K_2C_i (June 17–20, 2001) 3-157

3.4-55 Humidification effect on AHPC bag-cleaning interval (June 25–26, 2001) 3-158

3.4-56 Humidification effect on AHPC residual drag (June 25–26, 2001) 3-159

3.4-57 Humidification effect on K_2C_i (June 25–26, 2001) 3-159

3.4-58 Humidification effect on K_2C_i (June 27, 2001) 3-162

3.4-59 Average filter drag per row 3-165

3.4-60 Location of removed bags for analysis 3-166

3.4-61 Photo showing the top cuff, R3B4, and top of the bag 3-166

3.4-62 R3B5 membrane surface at 10–50× magnification 3-168

3.4-63 Fly ash resistivity at Big Stone Power Plant 3-173

3.4-64 Respirable mass concentration at the outlet of the AHPC unit at the Big Stone Power Plant 3-175

LIST OF TABLES

3.2-1	AHPC Settings and Results While Operating in the Multibank Pulsing Mode	3-18
3.2-2	AHPC Settings on July 7, 2000	3-36
3.2-3	Filter Media Permeability as Measured in Lab	3-47
3.2-4	Coal Usage Schedule and Analysis Results	3-49
3.3-1	Electrode Type and Discharge Points	3-52
3.3-2	Cold-Flow Electrode Tests	3-56
3.3-3	AHPC Configurations Tested in PTC-CR-621 Series	3-72
3.3-4	Experimental Parameters for the AHPC Pilot Test	3-88
3.3-5	Residual Dust Cake Weights	3-101
3.3-6	Calculated Results of K_2 "	3-103
3.3-7	Calculated Results of K_2	3-103
3.3-8	Parameters Evaluated in the Bench-Scale Experiments	3-107
3.4-1	AHPC Settings and Results at Different A/C Ratios	3-139
3.4-2	AHPC Settings at Different Pulse-Cleaning Pressures	3-142
3.4-3	AHPC Settings and Results at Different Pulse Sequence Modes	3-154
3.4-4	AHPC Settings and Results with and Without Humidification	3-160
3.4-5	Filter Drag Test Dates and AHPC Operating Parameters	3-164
3.4-6	Filter Media Permeability as Measured in Lab	3-170
3.4-7	Coal Usage Schedule and Analysis Results	3-172
3.4-8	AHPC Dust-Loading Measurements	3-173

UNITS AND ACRONYMS USED

AB	Allen-Bradley
acfm	actual cubic feet per minute
AHPC	advanced hybrid particulate collector
APS	aerodynamic particle sizer
A/C	air-to-cloth (ratio)
C	Celsius
CBCM	conductive bag, conductive membrane
CBNM	conductive bag, nonconductive membrane
cfm	cubic feet per minute
cm	centimeter
cm ³	cubic centimeter
DC	direct current
DOE	U.S. Department of Energy
dP	differential pressure
EERC	Energy & Environmental Research Center
EFE	electric field effect
EPA	U.S. Environmental Protection Agency
ePTFE	expanded polytetrafluoroethylene
ESD	electrostatic discharge
ESP	electrostatic precipitator
ETB	electrode-to-bag
ETP	electrode-to-plate
F	Fahrenheit
FFs	fabric filters
ft	foot
ft ²	square foot
g	gram
gr	grain
HAP	hazardous air pollutant
hr	hour
HV	high voltage
ID	induced draft, inside diameter
in.	inch
I/O	input/output
kPa	kilopascal
kV	kilovolt
m	meter
m ²	square meter
m ³	cubic meter
mA	milliampere
mg	milligram
µg	microgram
min	minute

NBCM	nonconductive bag, conductive membrane
NBNM	nonconductive bag, nonconductive membrane
pc	pulverized coal
PID	proportional integral derivative
PJFF	pulse-jet fabric filter
PLC	programmable logic controller
PM	particulate matter
ppm	parts per million
psig	pounds per square inch gage
PRB	Powder River Basin
PRDA	Program Research and Development Announcement
PTB	plate-to-bag
PTP	plate-to-plate
RTU	remote terminal unit
s	second
SCA	specific collection area
SCADA	Supervisory Control and Data Acquisition
scf	standard cubic feet
SIR	switched integrated rectifier
TCP/IP	transport control protocol/Internet protocol
tr	transformer rectifier
UND	University of North Dakota
W.C.	water column

ADVANCED HYBRID PARTICULATE COLLECTOR

PHASE III DRAFT FINAL REPORT

EXECUTIVE SUMMARY

A new concept in particulate control, called an advanced hybrid particulate collector (AHPC), is being developed at the Energy & Environmental Research Center (EERC) with U.S. Department of Energy (DOE) funding. In addition to DOE and the EERC, the project team includes W.L. Gore & Associates, Inc.; Allied Environmental Technologies, Inc.; and Otter Tail Power Company, which operates the Big Stone Power Plant. The Big Stone Power Plant is co-owned by Montana–Dakota Utilities, NorthWestern Public Service, and Otter Tail Power Company. The AHPC combines the best features of electrostatic precipitators (ESPs) and baghouses in a unique approach to develop a compact but highly efficient system. Filtration and electrostatics are employed in the same housing, providing major synergism between the two collection methods, both in the particulate collection step and in the transfer of dust to the hopper. The AHPC provides ultrahigh collection efficiency, overcoming the problem of excessive fine-particle emissions with conventional ESPs, and solves the problem of reentrainment and re-collection of dust in conventional baghouses.

The objective is to develop a highly reliable AHPC that can provide >99.99% particulate collection efficiency for particle sizes from 0.01 to 50 μm , is applicable for use with all U.S. coals, and is less costly than existing technologies.

Phase I of the development effort consisted of design, construction, and testing of a 200-acfm (5.7 m^3/min) working AHPC model. Results from both 8- and 100-hr tests showed that the concept worked well, achieving greater than 99.99% collection efficiency for fine particles at high filtration velocities.

Since all the developmental goals of Phase I were met, the approach was scaled up in Phase II to a size of 9000 acfm (255 m^3/min) and was installed on a slipstream at the Big Stone Power Plant.

For Phase II, the AHPC at the Big Stone Power Plant was operated continuously from late July 1999 until mid-December 1999, except for a 3-week down period in September corresponding to an annual plant outage. The Phase II results were highly successful in that ultrahigh particle collection efficiency was achieved, pressure drop was well controlled, and system operability was excellent.

The developmental objective for the more recent testing in Phase III was to obtain the necessary engineering data to facilitate scaleup of the AHPC to the full-scale demonstration size for near-term commercialization of this technology. As part of the initial Phase III work, the AHPC field unit was operated from April to July 2000. The results showed that the AHPC exceeded the performance goals of a 10-min bag-cleaning interval at an air-to-cloth (A/C) ratio of 12 ft/min (3.7 m/min) and 8-in. W.C. (2.0 kPa) pressure drop.

During the summer of 2000, some membrane damage appearing to be electrical in nature was observed on the bags. Extensive studies were carried out to determine the reason for the observed bag damage and to find possible solutions without compromising AHPC performance. The best solution to prevent the bag damage was found to be perforated plates installed between the electrodes and the bags to block the electric field from the bag surface and intercept current to the bags. The perforated plate not only solved the bag damage problem, but also appeared to offer many other advantages such as operation at higher A/C ratios, lower pressure drop, and an even more compact geometric arrangement.

Based on experimental data from additional pilot studies with the 200-acfm (5.7-m³/min) AHPC, design modifications were made and implemented on the 9000-acfm (255-m³/min) AHPC field unit at the Big Stone Power Plant. The modified Big Stone AHPC was started in March 2001 and operated through June 2001, completing the Phase III experimental work.

Conclusions from the Phase III project are as follows:

- At the start of Phase III, the 9000-acfm (255-m³/min) AHPC was modified, including a side transition inlet, different discharge electrodes and plates, closer bag and plate spacing, and addition of preionization zone. The AHPC field unit was then successfully operated for a period of about 3 months from April to July 2000. The modified AHPC with a significantly closer bag row spacing and bag-to-electrode spacing functioned very well according to theoretical expectations and within the previously established goals of a 10-min bag-cleaning interval at an A/C ratio of 12 ft/min (3.7 m/min) and 8.0 in. W.C. (2.0 kPa) pressure drop. Acceptable performance was achieved in spite of dealing with a fine-particle size, high-resistivity ash.
- The AHPC performance in summer 2000 demonstrated the bag-cleaning interval was quite sensitive to the A/C ratio and could be significantly increased by a small reduction in A/C ratio under a constant pulse-trigger pressure. Alternatively, the average pressure drop across the system could be significantly reduced by a small reduction in A/C ratio at a constant bag-cleaning interval. These results suggest there is a trade-off between pressure drop and A/C ratio.
- The use of high-resistivity fly ash (higher than 4×10^{11} ohm-cm) limits AHPC performance by affecting ESP operation.
- The filter bags were analyzed after more than 3 months' operation at the Big Stone unit in summer 2000. The results showed the filter bags retained permeability and strength. However, some damage was observed on the membrane, which appeared to be caused by electrical effects such as back corona, rather than from abrasion, temperature, or chemical attack.
- Bench- and pilot-scale tests were conducted to evaluate the effects of electrode type, bag type, spacing ratio, plate-to-plate spacing, and grounded grids on the current to the bags. It was found that the ELEX electrode induced the highest bag current and was less

directional than either the EERC electrode or ENELCO-type electrodes. The bag current can be significantly reduced by increasing spacing ratio, meaning that the greater the distance from the electrode to the filter bags, the lower the current to the filter bags. The GORE-NO STAT[®] filter bag (GORE-TEX[®] antistatic membrane/GORE-TEX[®] felt) induced less current than the GORE-NO STAT[®] filter bags (GORE-TEX[®] membrane/GORE-TEX[®] felt).

- Among the several configurations tested in the pilot AHPC unit at the EERC, perforated plates installed between the discharge electrodes and the filter bags provided excellent protection of the filter bags from electrical damages and also improved AHPC performance in terms of longer bag-cleaning intervals and lower K_2C_i and residual drag.
- Perforated plates with two different hole sizes of 1.5 and 2.0 in. (38 and 51 mm) were evaluated in hot-combustion tests at the EERC, with the spacing between the perforated plate and the filter bags varied from 2.0 to 3.0 in. (51 and 76 mm). Very low bag current was maintained for all the different filter bags tested under the perforated-plate configurations. The 2.0-in. (51-mm)-diameter hole perforated plate demonstrated somewhat better AHPC performance than the 1.5-in. (38-mm) hole perforated plate in terms of longer bag-cleaning interval, lower K_2C_i , and lower residual drag. However, the 1.5-in. (38-mm) perforated plates may provide better bag protection.
- A perforated-plate configuration for the 9000-acfm (255-m³/min) AHPC at the Big Stone Power Plant was installed in January–March 2001, and 3 months of successful testing were conducted from March to June 2001 with the larger-scale AHPC.
- AHPC performance with the perforated-plate configuration was excellent for several different subbituminous fuels, with ash resistivity over 10¹² ohm-cm. This demonstrates flexibility and ruggedness under varying and challenging conditions. With high-resistivity dust, some reduction in performance is expected compared to operation with moderate-resistivity ash. However, by a small reduction in A/C ratio or increase in pressure drop, the AHPC can adequately handle dusts with very high ash resistivity.

Overall, AHPC performance with the perforated plates was better than with the previous design.

- The cross-row pulsing configuration appeared to be as effective as the more conventional in-row pulsing approach. This means that additional flexibility is available to facilitate design of both new and retrofit applications for the AHPC. Adequate pulse cleaning was achieved for several different pulse sequences with the cross-row pulsing. Pulse order sequence appeared to be of minor significance.
- Pulse-cleaning pressure appears to be critical to adequately control residual drag. Significantly lower residual drag was achieved by increasing the pulse pressure from 50 to 65 psi (345 to 448 kPa). Stable, longer-term operation has been demonstrated with a pulse pressure of 75 psi (517 kPa).
- Particulate collection efficiency was again demonstrated to be well above the performance goal of 99.99%, and outlet emissions were measured to be cleaner than the surrounding ambient air.
- Short-term tests with humidification showed that the AHPC performance significantly improved when it was not limited by high ash resistivity. Operation at an A/C ratio of 13.9 ft/min (4.2 m/min) was achieved with humidification, demonstrating the potential of the AHPC to operate at much higher A/C ratios when conditions are more ideal.
- After 2300 hr of operation, the filter bags still maintained excellent permeability, retained their dimensional stability, and showed no decrease in mechanical strength. No sign of membrane damage, either from electrical effects or other factors such as abrasion, temperature, and chemical attack, was found under microscope analysis, proving excellent bag protection with the perforated-plate design.

ADVANCED HYBRID PARTICULATE COLLECTOR

PHASE III DRAFT FINAL REPORT

1.0 INTRODUCTION

1.1 Background

The University of North Dakota (UND) Energy & Environmental Research Center (EERC) responded to the U.S. Department of Energy (DOE) Program Research and Development Announcement (PRDA) No. DE-RA22-94PC92291, Advanced Environmental Control Technologies for Coal-Based Power Systems Phases I and II, under Topic 7: Advanced Concepts for Control of Fine Particles and Vapor-Phase Toxic Emissions. The EERC proposal was subsequently selected for DOE funding, and the EERC was awarded Contract DE-AC22-95PC95258. Phase I work consisted of initial development of a new concept in fine-particle control called an advanced hybrid particulate collector (AHPC). The AHPC concept consists of a combination of fabric filtration and electrostatic precipitation in the same housing, providing major synergism between the two collection methods, both in the particulate collection step and in the transfer of dust to the hopper. The AHPC provides ultrahigh collection efficiency, overcoming the problem of excessive fine-particle emission with conventional electrostatic precipitators (ESPs), and it solves the problem of reentrainment and re-collection of dust in conventional baghouses. Following highly successful results from the Phase I work, the EERC submitted a Phase II downselection proposal to DOE to continue development of the AHPC. The Phase II contract was awarded in March 1998 and included additional 200-acfm ($5.7\text{-m}^3/\text{min}$) testing, similar to the tests completed in Phase I, as well as the design, construction, and testing of a 9000-acfm ($255\text{-m}^3/\text{min}$) (2.5-MW equivalent) version of the AHPC. The 2.5-MW AHPC was installed on a slipstream of the Big Stone Power Plant and was operated continuously from late July 1999 until mid-December 1999. The project team included the EERC as the main contractor; Allied Environmental Technologies Company (ALENTEC) as a subcontractor; W.L. Gore & Associates, Inc. (Gore), as a technical and financial partner; and Otter Tail Power Company, which operates the Big Stone Power Plant. The Big Stone Power Plant is co-owned by Montana–Dakota Utilities, NorthWestern Public Service, and Otter Tail Power Company. The

results from Phase I and II were presented in the final report to DOE as well as a number of scientific conferences (1–8).

This Phase III project was awarded under DOE Program Solicitation DE-PA26-99FT40251 and specifically addresses Technical Topical Area 3 – Primary PM Emissions Control. Phase III is a logical continuation of the development toward full-scale commercialization of the AHPC. The Phase III project covered a period of 2 years from October 1999 through September 2001. This report is the final project report for Phase III.

1.2 Phase I Summary

The Phase I objective was to develop a highly reliable AHPC that can provide >99.99% particulate collection efficiency for all particle sizes from 0.01 to 50 μm , be applicable for use with all U.S. coals, and be less costly than existing technologies.

Phase I of the development effort included design and construction of a 200-acfm ($5.7\text{-m}^3/\text{min}$) working AHPC model. The first experimental tests were cold-flow tests with air for the purpose of adjusting the bag-cleaning parameters to achieve the best interaction between the ESP and filtration zones. Reentrained dust (fly ash) was injected into the carrier air upstream of the AHPC, operating at an air-to-cloth (A/C) ratio of 12 ft/min (3.7 m/min). After successful completions of the cold-flow tests, 8-hr verification tests where the AHPC was required to collect fly ash from real flue gas produced from coal combustion were completed. These tests were followed by 100-hr tests with subbituminous and bituminous coals to evaluate the longer-term operability of the AHPC over multiple cleaning cycles. Initial tests were conducted with the ESP power on and bags removed to approximate the amount of dust precollected. Without the bags, the particulate emissions ranged between 0.28 to 0.37 g/m^3 , corresponding to a collection of about 95%. This result was encouraging because 90%–95% efficiency for the ESP was the basis for the concept. Data collected with an aerodynamic particle sizer (APS) indicated 83% collection efficiency of respirable mass compared to 95% total mass. This result was also encouraging because it showed that the ESP also removed a substantial portion of the fine-particle mass. Precollection of smaller as well as larger particles was desirable because if only

the smaller particles reached the filter, the pressure drop may have been difficult to control.

The objectives of the 8-hr tests on coal were to:

- Evaluate AHPC performance under real flue gas conditions firing Absaloka subbituminous and Blacksville bituminous coals.
- Evaluate on-line versus off-line cleaning.
- Test A/C ratio at 12 and 16 ft/min (3.7 m/min and 4.9 m/min).

The 8-hr tests provided the following results:

- The AHPC achieved particulate collection efficiencies of 99.99% for particle sizes from 0.01 to 50 μm .
- Excellent AHPC performance was achieved for both the subbituminous and bituminous coals, with reasonable bag-cleaning intervals.
- No significant difference in time intervals between bag-cleaning cycles with on-line and off-line cleaning was observed.

The objectives of the 100-hr tests on coal were to:

- Determine operability of the AHPC for an extended period at steady-state conditions.
- Determine baseline information of the fate of seven trace metals using the AHPC system.
- Evaluate the effect of carbon injection on mercury emissions and system operability.

The 100-hr tests provided the following results:

- Particulate collection efficiencies greater than 99.99% for all particle sizes from 0.01 to

50 μm were achieved.

- Pressure drop was well controlled and steady. Injection of carbon did not adversely affect pressure drop. Time intervals between bag-cleaning cycles ranged from 25 to 35 min at the end of the 100-hr tests.
- Emissions of seven trace elements—arsenic, cadmium, chromium, lead, mercury, nickel, and selenium—were measured. Only two elements, mercury and selenium, were detected in measurable quantities in vapor form at the outlet.
- With sorbent injection, total mercury removal efficiency ranged between 50% and 75%.
- No increased particulate emissions were noted during mercury sorbent injection.

1.3 Phase II Summary

The overall Phase II project objective was the same as for Phase I: to develop a highly reliable AHPC that can provide >99.99% particulate collection efficiency for all particle sizes from 0.01 to 50 μm , is applicable for use with all U.S. coals, and is less costly than existing technologies. The developmental objective for Phase II was to take the concept from Maturity Level II, which was achieved in Phase I, through Maturity Level III, engineering development scale.

Since all of the developmental goals of Phase I were met, the approach was scaled up in Phase II to a size of 9000 acfm (255 m^3/min) (equivalent in size to 2.5 MW) and was installed on a slipstream at the Big Stone Power Plant in Big Stone City, South Dakota. For Phase II, the AHPC at the Big Stone Power Plant was operated continuously from late July 1999 until mid-December 1999. The Phase II results were highly successful in that ultrahigh particle collection efficiency was achieved, pressure drop was well controlled, and system operability was excellent.

Additional 200-acfm (5.7- m^3/min) tests were completed to help design the scaled-up unit with the appropriate geometric configuration and to determine if the AHPC could be designed in a more compact configuration than was tested in Phase I without compromising performance.

Bag-to-plate spacing was reduced to 10 in. and 8 in. (254 mm and 203 mm) for comparison with the 14-in. (356-mm) spacing tested in Phase I. A bottom inlet configuration was also tested using 10-in. (254-mm) bag-to-plate spacing.

Results showed that the AHPC can function well with much closer bag-to-plate spacings than were tested in Phase I. This is a highly encouraging result because it indicates that the AHPC can be configured in a very compact geometric arrangement, leading to lower cost of construction. The side inlet configuration with a 10-in. (254-mm) bag-to-plate spacing appeared to provide somewhat better performance than an 8-in. (203-mm) bag-to-plate spacing, but the AHPC functioned well with both configurations. The AHPC also functioned well with a bottom inlet. This indicates that exact baffling for the inlet flow is not critical and that the AHPC would function well with a very simple inlet configuration.

The goal for the scaleup tests was to evaluate the AHPC under the most realistic conditions achievable, including the use of full-scale components where possible. The 9000-acfm (255-m³/min) size represented a large, pilot-scale (2.5-MW electrical equivalent) unit that appeared to provide the best combination of being large enough to allow meaningful tests with full-scale components, but yet small enough to be transportable and cost-effective. Since a side inlet and 10-in. (254-mm) bag-to-plate spacing provided the best performance in the 200-acfm (5.7-m³/min) tests, that configuration was used as the basis for the design of the 9000-acfm (255-m³/min) AHPC.

The AHPC vessel and main components were fabricated and assembled in the EERC high-bay facility for system component shakedown prior to shipping the unit to the Big Stone Power Plant.

Following installation and shakedown of the field AHPC at Big Stone, the unit was operated continuously from late July through mid-December 1999, except for 3 weeks in September which included the annual Big Stone Power Plant maintenance outage. The primary purpose of these Phase II field tests was to provide long-term operating data rather than to test a large number of variables. An important objective was to demonstrate that longer-term bag life

could be achieved when operating at an A/C ratio of 12 ft/min (3.7 m/min), using commercially available bags provided by Gore. A second important objective was to demonstrate ultrahigh particulate collection over an extended time period. The only major test parameter change was operation at higher A/C ratios in the range from 14–16 ft/min (4.3–4.9 m/min) for the last month of testing. Particulate monitoring was completed during the first and last months of operation.

A summary of the Phase II conclusions is as follows:

- The AHPC demonstrated ultrahigh particulate collection efficiency for submicron particles, respirable mass particulate matter, and total particulate mass. Collection efficiency was proven to exceed 99.99% by one to two orders of magnitude over the entire range of particles from 0.01 to 50 μm . The flue gas exiting the AHPC was as clean as pristine ambient air, with a $\text{PM}_{2.5}$ level of 5 $\mu\text{g}/\text{m}^3$. This level of control would not only meet current and possible near-term stricter standards, but would also appear to meet any standard well into the foreseeable future.
- The 2.5-MW field demonstration AHPC functioned exceptionally well within theoretical expectations over the 4.5-month test period. All particulate emission tests and visual inspections of the clean air plenum indicate that ultrahigh collection efficiency was maintained throughout the tests. The electric field captured the majority of the dust during normal filtration, and observation of the bag pulsing showed that the dust coming off the bags was propelled back into the ESP zone and trapped according to theoretical expectations.
- A high level of ruggedness of the AHPC concept was demonstrated. In spite of numerous unplanned shutdowns and start-ups with dew point excursions (caused by short plant shutdowns) and several times where water leakage around an insulator caused high-voltage power shutdown, the AHPC recovered very well each time. There were no mechanical failures such as electrode breakage or misalignment, rapper failures, pulsing system failures, or mechanical bag failures. Ruggedness was achieved even though this was the first attempt at building an AHPC larger than laboratory scale.

- Pressure drop at < 8 in. W.C. (2 kPa) at a bag-cleaning interval of at least 10 min at an A/C ratio of 12 ft/min (3.7 m/min) was clearly demonstrated. The best AHPC performance was seen during Test Period 1 when the ash resistivity was somewhat lower. For an extended time, the average pressure drop was controlled at 7.5 in. W.C. (1.89 kPa) with a typical bag-cleaning interval of 20 to 30 min and an average A/C ratio of 12 ft/min (3.7 m/min). Test Period 2 results suggest that some loss in AHPC performance is expected when the ash resistivity approaches 10^{12} ohm-cm. However, the results show that acceptable bag-cleaning intervals can be maintained with a small increase in pressure drop. In either case, the AHPC demonstrated the ability to function very well with high-resistivity ash.
- Results show that operation at higher A/C ratios than 12 ft/min (3.7 m/min) with very-high-resistivity ash will be difficult. Operation at 16 ft/min (4.9 m/min) was demonstrated, but these results indicate that design modifications of the AHPC may be necessary to operate at higher A/C ratios and deal with high ash resistivity at the same time.
- Bag life of at least 3.5 months was demonstrated. While much longer-term bag life will need to be proven, these results are highly encouraging because they show that in the first AHPC demonstration attempt with full-scale bags, no serious problems occurred. In spite of hundreds of thousands of sparks over the test period, there was never an indication of any sparking to the bags. This means that the directional discharge electrodes with the appropriate spacing performed flawlessly according to theoretical and design expectations.
- Better AHPC performance was observed at lower operating temperatures, likely as a result of lower ash resistivity. This result is encouraging first because it shows that the AHPC can perform reasonably well at the higher-resistivity conditions and second because it provides a design basis for the AHPC. For high-resistivity ash, a more conservative approach might be required, while for lower-resistivity ash, there is confidence that the AHPC will perform very well at high A/C ratios.

- The dependence of AHPC performance on a specific inlet baffling configuration appears to be minimal. The best performance was observed for the baffling configuration with the most significant flow maldistribution. Again, this is encouraging because it indicates that an exact inlet design is not critical for adequate performance.
- Preliminary economic analysis of the AHPC compared with conventional ESPs and baghouses indicates that the AHPC is economically competitive with either of these technologies for meeting current standards. For meeting a possible stricter fine-particle standard or 99.99% control of total particulate matter, the AHPC is the economic choice over either ESPs or baghouses by a wide margin.

1.4 Phase III Objectives

The objective of the Phase III project is to develop a highly reliable AHPC that can provide >99.99% particulate collection efficiency for all particle sizes from 0.01 to 50 μm , is applicable for use with all U.S. coals, and is less costly than existing technologies. This goal has remained unchanged since the concept was originally proposed in 1994. The approach objective with the AHPC is to utilize filtration and electrostatic mechanisms in a unique manner that is superior to conventional fabric filters (FFs) and ESPs. The developmental objective for Phase III was to obtain the necessary engineering data to facilitate scaleup of the AHPC to the full-scale demonstration size for near-term commercialization of this technology.

2.0 THEORY AND CONCEPT

2.1 Fine-Particle Collection Efficiency

The goal in developing a new approach for particulate control is to achieve as high a level of control as is practically possible, while at the same time providing high reliability, smaller size, and economic benefits. For dusts that are primarily larger than 20 μm , inertial separation methods, such as cyclones, are reasonably effective and are much more economical than conventional ESPs or baghouses. However, fine particles smaller than 2.5 μm pass through cyclones with little or no collection. If emission of even a small amount of fine dust is unacceptable, then cyclones are not a viable control method, and only ESPs and baghouses are capable of achieving any reasonable level of control. Fabric filters collect fine particles much better than ESPs because FFs do not have the same theoretical (and actual) minimum collection efficiency for particles in the range from 0.1 to 0.3 μm . For these particles, the collection efficiency of a cyclone is close to zero, the efficiency of a modern ESP could approach about 99%, and the efficiency of a well-designed fabric filter would be about 99.9%. Higher levels of control might be possible with an ESP, but only by a significant increase in the size or specific collection area (SCA). Since the goal for the AHPC is to be much smaller and more economical than conventional approaches, achieving better fine-particle collection with electrostatic collection alone does not appear to be viable. That means that the advanced concept must employ filtration or some combination of electrostatics and filtration to achieve an ultrahigh fine-particle collection efficiency.

Fabric filters cannot routinely achieve 99.9% fine-particle collection efficiency for all coals within economic constraints, and studies have shown that collection efficiency is likely to deteriorate significantly when the face velocity is increased (9, 10). An approach to make FFs more economical is to employ smaller baghouses that operate at much higher A/C ratios. The challenge is to increase the A/C ratio for economic benefits and to achieve ultrahigh collection efficiency at the same time. To achieve high collection efficiency, the pores in the filter media must be effectively bridged (assuming they are larger than the average particle size). With conventional fabrics at low A/C ratios, the residual dust cake serves as part of the collection

medium, but at high A/C ratios, only a very light residual dust cake is acceptable, so the cake cannot be relied on to help achieve high collection efficiency. The solution is to employ a sophisticated fabric that can ensure ultrahigh collection efficiency and endure frequent high-energy cleaning. In addition, the fabric should be reliable under the most severe chemical environment likely to be encountered (such as high SO₃). A fabric that meets these requirements is GORE-TEX[®] membrane on GORE-TEX[®] felt, which can achieve very high collection efficiencies at high A/C ratios. Although GORE-TEX[®] membrane filter medium is more expensive than conventional fabrics, the much smaller surface area required for the AHPC will make the use of the GORE-TEX[®] membrane filter medium economical.

2.2 GORE-TEX[®] Membrane Filtration Media

Gore manufactures uniquely constructed filter bags for FF collectors used in many industrial applications, including metal, coal-fired boiler, incineration, chemical, and mineral-based applications. GORE-TEX[®] membrane filter bags consist of a microporous expanded polytetrafluoroethylene (ePTFE) membrane laminated to a felted or fabric backing material. The substrate is chosen based on the temperature and chemical composition of the gas stream entering the fabric filter. The ePTFE membrane is inert to most chemicals and can withstand continuous operating temperatures of 500EF (260EC).

Presently, two filtration technologies are used in fabric filtration: membrane surface filtration and depth filtration. Depth filtration depends upon a two-stage dust cake development. The primary dust cake is located within the weave of the filter media and is the first to develop. The secondary dust cake builds upon the primary dust cake. Primary dust cake maintenance is extremely important because the primary dust cake is responsible for particulate matter (PM) capture, that is, maintaining low PM emissions. However, the secondary dust cake is responsible for increased static pressure loss and must be removed by the action of the cleaning cycle. Excessive cleaning disturbs the primary dust cake and can lead to excessive PM emissions.

The GORE-TEX[®] membrane utilizes surface filtration to collect the PM which impinges upon it. Consequently, even fine, nonagglomerative PM does not penetrate or pass through the filter media. Significant improvements in filtration efficiency, especially for submicron PM, are realized. Figure 2.2-1 is a scanning electron microphotograph comparing the GORE-TEX[®] membrane to conventional copolyimide (P-84[®]) felt filter media. The views of each material are at a magnification of 200×. Corresponding incremental micron-sized particles are included for reference. This comparison reveals why this membrane is capable of capturing even submicron-sized PM, whereas conventional filter media require the establishment of a primary dust cake to achieve acceptable filtration performance. Thus ePTFE membrane laminate construction allows the filter bags to operate on the principle of surface filtration; that is, PM is collected on the surface of the GORE-TEX[®] membrane and not within the interstices of the felted or woven fabric. This allows the filter bag to operate at lower pressure differentials and higher fabric filter A/C ratios.

For over 20 years, GORE-TEX[®] membrane filter media have been utilized within FFs to capture all fine PM and submicron PM produced. Many of these applications needed ePTFE membrane filter media to ensure that PM and other hazardous air pollutant (HAP) emissions would be below those levels required by state or federal regulatory authorities.

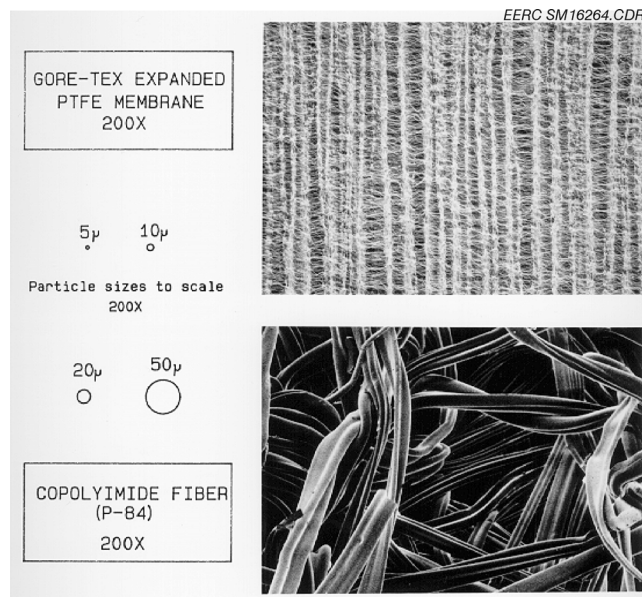


Figure 2.2-1. Comparison of GORE-TEX[®] membrane to conventional copolyimide fiber (P-84).

Currently, there are more than 40 incineration facilities that utilize GORE-TEX[®] membrane filter bags in their FFs. Included in these are municipal solid waste incinerators, hazardous waste combustors, medical waste incinerators, contaminated soil thermal desorption units, and tire-to-energy facilities. Additionally, GORE-TEX[®] membrane filter bags are used in more than 30 industrial boilers as the final control mechanism in their primary boiler FFs. These boiler applications include circulating fluid-bed combustors, stoker-fired facilities, and pulverized-coal units. They burn a wide range of fuels varying between coal types (subbituminous and bituminous), waste coal types (anthracite culm and bituminous gob), agricultural mass waste, petroleum coke, hog fuel, and miscellaneous oil mixtures. Bag life has also been shown to be excellent, typically at least 3–5 years. In one application, bag life is currently over 8 years and continuing. Possible GORE-TEX[®] fabrics that might be used with the AHPC are described in the following sections.

2.2.1 GORE-TEX[®] Membrane–GORE-TEX[®] Felt Filter Bags

The GORE-TEX[®] membrane–GORE-TEX[®] felt filter media combine an ePTFE felt with an ePTFE membrane. The felt is chemically inert and can withstand continuous operating temperatures as high as 500EF (260EC). The GORE-TEX[®] membrane has high particle capture efficiency and excellent surface filtration. Filter bag applications include waste incinerators, titanium dioxide chlorinators, oxidizing agent recovery, carbon black drying, and pharmaceuticals production.

The components of the GORE-TEX[®] felt include the fiber, scrim, and sewing thread. The ePTFE fibers have excellent chemical resistance to mineral and organic acids, alkalies, oxidizing agents, and organic solvents. The high tenacity and low shrinkage characteristics of the ePTFE fibers allow the filter bags to retain optimum levels of durability and dust removal after extended operation in aggressive pulse-jet FFs (PJFFs). The enhanced cleaning produces lower operating pressure drop across the FF and higher airflow per filter bag.

The GORE-TEX[®] membrane collects dust particles on the surface of the media. The high particle capture efficiency of the membrane eliminates the need for a dust cake to form on the

felt surface to achieve a high efficiency. When cleaned by compressed air, the collected dust cake is removed. This allows the filter bag to operate at lower pressure differentials and higher A/C ratios.

2.2.2 GORE-NO-STAT[®] Filter Bags (GORE-TEX[®] Membrane/GORE-TEX[®] Antistatic Felt, 20 oz/yd²)

The GORE-NO-STAT[®] filter bag is an ePTFE felt containing antistatic-carbon-filled ePTFE fibers and an ePTFE membrane. The antistatic fibers in the felt allow electrical charge to be transferred through the media to the cage. The charge can then be carried to a suitable grounded conductor, thereby dissipating the charge. The conductive fiber continuously drains charges from the filter media and prevents static buildup on the filter bags.

Electrostatic charges can build up on dust particles as they move through an air stream because of the triboelectric effects of the dust particles interacting with ions in the air and other dust particles. As the dust particles are collected and built up on the surface of a filter bag, the electrical charges can accumulate. A filter media with a high electrical resistance can isolate the charge between the dust and the metal wire of the filter cage. If a static discharge occurs, an electric arc or spark can travel through the media. This can damage the filter media and/or produce conditions for dust explosions internal to the air pollution device. The antistatic felt is used to control electrostatic charge on the filter bags. GORE-NO STAT[®] fiber bags retain the chemical resistance and operating temperature performance levels of the GORE-TEX[®] membrane/GORE-TEX[®] felt filter media.

2.2.3 GORE-NO-STAT[®] Filter Bag (GORE-TEX[®] Antistatic Membrane/GORE-TEX[®] Antistatic Felt)

The filter bags selected for the most recent AHPC testing were GORE-NO STAT[®] filter bags (GORE-TEX[®] antistatic membrane/GORE-TEX[®] antistatic felt). The filter media is similar to the GORE-NO STAT[®] material described above, but it contains an antistatic membrane as well as an antistatic felt backing material. This material provides the best electrical charge

dissipation of the bags tested to date. The enhanced antistatic characteristics of this GORE-NO-STAT[®] filter bag, along with the enhanced durability and chemical resistance of the ePTFE felt and dust removal ability of the ePTFE membrane, make this media optimally designed for operation within an AHPC system.

2.3 Flow Theory and Performance Evaluation Criteria

For viscous flow, pressure drop across a fabric filter is dependent on three components:

$$dP = K_f V + K_2 W_R V + K_2 C_i V^2 t / 7000 \quad [\text{Eq. 2.3-1}]$$

where:

- dP = differential pressure across baghouse tube sheet (in. W.C.) (kPa)
- K_f = fabric resistance coefficient (in. W.C.-min/ft) (kPa-min/m)
- V = face velocity or A/C ratio (ft/min) (m/min)
- K₂ = specific dust cake resistance coefficient (in. W.C.-ft-min/lb) (kPa-m-min/kg)
- W_R = residual dust cake weight (lb/ft²) (kg/m²)
- C_i = inlet dust loading (grains/acf) (g/m³)
- t = filtration time between bag cleaning (min)

The first term in Eq. 2.3-1 accounts for the pressure drop across the fabric. For conventional fabrics, the pore size is quite large, and the corresponding fabric permeability is high, so the pressure drop across the fabric alone is negligible. To achieve better collection efficiency, the pore size can be significantly reduced, without making fabric resistance a significant contributor to pressure drop. The GORE-TEX[®] fabric allows for this optimization by providing a microfine pore structure while maintaining sufficient fabric permeability to permit operation at high A/C ratios. A measure of the new fabric permeability is the Frazier number, which is the volume of gas that will pass through a ft² of fabric sample at a pressure drop of 0.5 in. W.C. (0.12 kPa). The Frazier number of the bags for the Phase III tests is in the range from 4 to 8 ft/min (1.22 to 2.44 m/min). Through the filter, viscous (laminar) flow conditions exist so the pressure drop varies directly with flow velocity. Assuming a new fabric Frazier number of 6 ft/min

(1.8 m/min), the pressure drop across the fabric alone would be 1.0 in. W.C. (0.25 kPa) at an A/C ratio (filtration velocity) of 12 ft/min (3.7 m/min).

The second term in Eq. 2.3-1 accounts for the pressure drop contribution from the permanent residual dust cake that exists on the surface of the fabric. For operation at high A/C ratios, the bag cleaning must be sufficient to maintain a very light residual dust cake and ensure that the pressure drop contribution from this term is reasonable. The contribution to pressure drop from this term is one of the most important indicators of longer-term bag cleanability.

The third term in Eq. 1 accounts for the pressure drop contribution from the dust accumulated on the bags since the last bag cleaning. K_2 is determined primarily by the fly ash particle-size distribution and the porosity of the dust cake. Typical K_2 values for a full dust loading of pulverized coal (pc)-fired fly ash range from about 4 to 20 in. W.C.-ft-min/lb (0.5 to 2.5 kPa-m-min/kg), but may, in extreme cases, cover a wider range. Within this term, the bag-cleaning interval, t , is the key performance indicator. The goal is to operate with as long of a bag-cleaning interval as possible, since more frequent bag pulsing can lead to premature bag failure and require more energy consumption from compressed air usage. For Phase III, the stated goal was to operate with a pulse interval of at least 10 min while operating at an A/C ratio of 12 ft/min (3.7 m/min).

Total tube sheet pressure drop is another key indicator of overall performance of the AHPC. Here, the stated Phase III goal was to operate with a tube sheet pressure drop of 8 in. W.C. (2.0 kPa) at an A/C ratio of 12 ft/min (3.7 m/min). Note that the average pressure drop is not the same as the pulse-cleaning trigger point. For many of the previous and current tests, the pulse trigger point was set at 8 in. W.C. (2.0 kPa), but the average pressure drop was significantly lower.

To help analyze filter performance, the terms in Eq. 2.3-1 can be normalized to the more general case by dividing by velocity. The dP/V term is commonly referred to as drag or total tube sheet drag, D_T .

$$\frac{dP}{V} = D_T = K_f + K_2 W_R + \frac{K_2 C_i V t}{7000} \quad [Eq. 2.3-2]$$

The new fabric drag and the residual dust cake drag are typically combined into a single term called residual drag, D_R .

$$D_T = D_R + \frac{K_2 C_i V t}{7000} \quad [Eq. 2.3-3]$$

The residual drag term then is the key indicator of how well the bags are cleaning over a range of A/C ratios, but may still be somewhat dependent on A/C ratio. For example, it may be more difficult to overcome a dP of 10 in. W.C. (2.5 kPa) to clean the bags than to clean at a dP of 5 in. W.C. (1.3 kPa). For most baghouses, the residual drag typically climbs somewhat over time and must be monitored carefully to evaluate the longer-term performance.

Between bag cleanings, from the second term in Eq. 2.3-3, the drag increases linearly with K_2 (dust cake resistance coefficient), C_i (inlet dust concentration), V (filtration velocity), and t (filtration time). For conventional baghouses, the C_i term is easily determined from an inlet dust loading measurement, and approximate K_2 values can be determined from the literature or by direct measurement. However, for the AHPC, the concentration of the dust that reaches the bags is generally not known and would be very difficult to measure experimentally. From the Phase I laboratory tests, results indicated approximately 90% of the dust was precollected and did not reach the fabric. However, this amount is likely to fluctuate significantly with changes to the electrical field and with the dust resistivity. Since C_i is not known, for evaluation of AHPC performance, the K_2 and C_i can be considered together.

$$K_2 C_i = \frac{(D_T + D_R) 7000}{V t} \quad [Eq. 2.3-4]$$

Evaluation of K_2C_i can help in assessing how well the ESP portion of the AHPC is functioning, especially by comparing with the K_2C_i during short test periods in which the ESP power was shut off.

Eq. 2.3-4 can be solved for the bag-cleaning interval, t , as shown in Eq. 2.3-5. It is clear that the bag-cleaning interval is inversely proportional to the face velocity, V , and the K_2C_i term and directly proportional to the change in drag before and after cleaning (delta drag). The delta drag term is dependent on the cleaning set point or maximum pressure drop as well as the residual drag. The face velocity, delta drag, and K_2C_i terms are relatively independent of each other and should all be considered when evaluating the bag-cleaning interval. However, as mentioned above, the drag may be somewhat dependent on velocity if the dust does not clean off the bags as well at high velocity as at low velocity. Similarly, the K_2C_i is somewhat dependent on velocity for a constant plate collection area. At the greater flow rates, the SCA of the precipitator is reduced, which will result in a greater dust concentration, C_i , reaching the bags.

$$t = \frac{(D_T + D_R) 7000}{VK_2C_i} \quad [Eq. 2.3-5]$$

2.4 AHPC Concept Description

While very large ESPs are required to achieve >99% collection of the fine particles, a small ESP can remove 90% to 95% of the dust. Including rapping puffs, 90% to 95% collection efficiency can be achieved with full-scale precipitators with an SCA of less than 20 m² of collection area/m³/s (100 ft² of collection area/1000 acfm) (11). In the AHPC concept, the goal is to employ only enough ESP plate area to remove approximately 90% of the dust. Similarly, the cloth area should be held to a minimum to keep the cost reasonable. If the fabric is operated at an A/C ratio of 12 ft/min (3.7 m/min) and the SCA of the ESP is 83 ft²/1000 acfm (17 m²/m³/s), the filtration collection area will be the same as the plate collection area. An SCA of 83 ft²/1000 acfm (17 m²/m³/s) should be sufficient to easily remove at least 90% of the dust (note that an alternative definition of SCA is simply the inverse of A/C ratio multiplied by 1000). A

baghouse operating at an A/C ratio of 2 ft/min (0.6 m/min) has the same collection area as an ESP with an SCA of 500 ft²/1000 acfm (100 m²/m³/s). Both of these are typical of the size of collectors employed for new power plants. Therefore, an AHPC operating at an A/C ratio of 12 ft/min (3.7 m/min) and an SCA of 83 ft²/1000 acfm (17 m²/m³/s) would offer an 83% reduction in fabric area over a conventional baghouse operating at 2 ft/min (0.6 m/min) and an 83% reduction in plate area over a conventional ESP with an SCA of 500 ft²/1000 acfm (100 m²/m³/s). The combined collection area in the AHPC would be 67% lower than either the conventional baghouse or the ESP.

The geometric configuration of the AHPC concept can be understood by comparing the configuration with a conventional pulse-jet baghouse. In a typical pulse-jet baghouse, the individual bags or filtration tubes are 4–6 in. (102–152 mm) in diameter and 8–26 ft (2.4–8.0 m) long and mounted in and suspended from a tube sheet. The dust is collected on the outside of the bags while the flue gas passes through the fabric to the inside, then exits through the top of the bags into the clean air plenum and subsequently out the stack. Cages are installed inside the bags to prevent them from collapsing during normal filtration. Air nozzles are installed above each bag to clean the bags with a quick burst of high-pressure air directed inside the bags. The burst of air, or cleaning pulse, causes a rapid expansion of the bag and momentarily reverses the direction of gas through the bag, which both help to clean the dust off the bags. Typically, pulse-jet bags are oriented in a rectangular array spaced only a few inches apart. The bags are usually pulse-cleaned one row at a time in sequence, with approximately 15 bags per row. Because of the narrow bag spacing and forward filtration through the two adjacent rows, much of the dust that is removed from one row of bags is simply re-collected on the adjacent bags. Only very large agglomerates of dust reach the hopper after pulsing. The phenomenon of redispersion and re-collection of dust after bag cleaning is one of the major obstacles to operation of baghouses at higher filtration velocity (also called A/C ratio).

In the AHPC concept, rows of pulse-cleaned bags are centered between ESP collection plates, and high-voltage corona discharge electrodes are installed on both sides of the bags (see Figure 2.4-1, which is a top view of the 9000-acfm AHPC installed at the Big Stone Power Plant at the start of Phase III). The spacing from the discharge electrodes to the plates is less than

the spacing from the discharge electrodes to the bags, which forces any sparking to the plates rather than to the bags. Conventional discharge electrodes may be employed, but the preferred configuration is to use directional corona electrodes that force the corona to the plate side rather than to the bag side. An optional variation of the configuration to help protect the bags is a row of grounded wires or grid between the high-voltage electrode and the bags; however, this extra row of grounded wires is not necessary, except under severe sparking conditions or back corona conditions.

Operation of the AHPC can be considered a two-step process. In Step 1, the particles are collected on either the grounded plates or the filtration surface, and in Step 2, the dust is transferred to the hopper. In Step 1, dirty gas flow enters the AHPC vessel and is directed into the ESP zone by appropriate baffling. The particles in the ESP zone immediately become charged and migrate toward the grounded plate at a velocity (electrical migration velocity) dependent

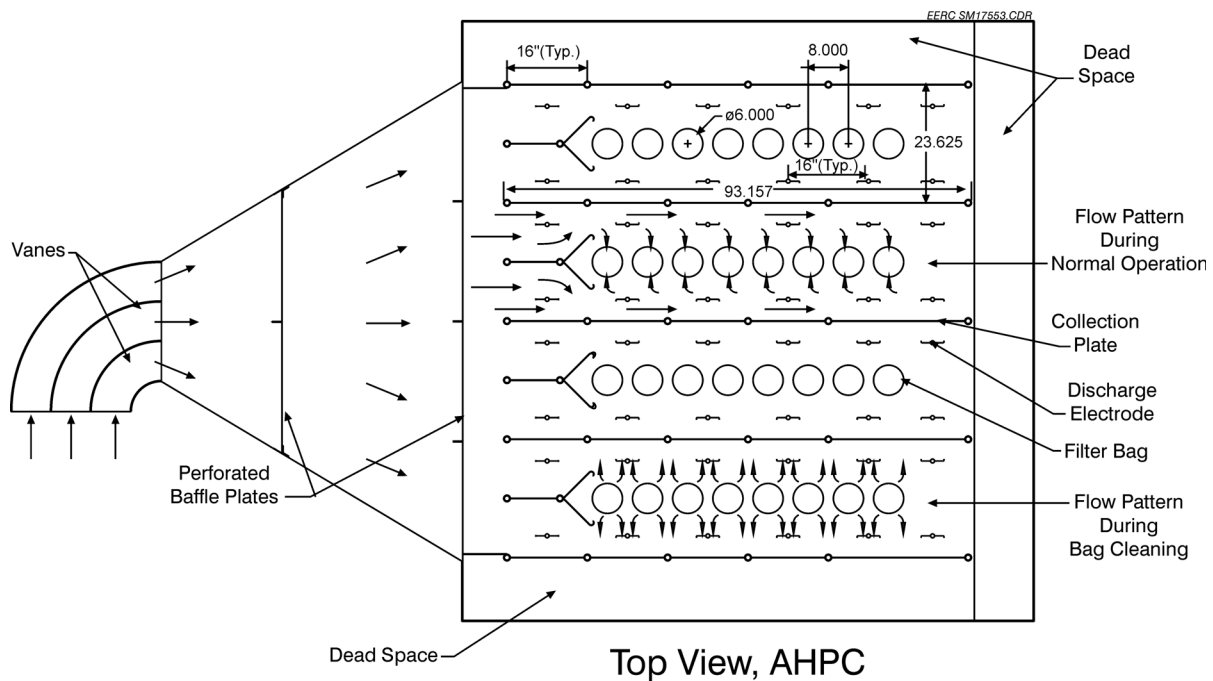


Figure 2.4-1. Top view of the 9000-acfm (255-m³/min) AHPC installed at the Big Stone Power Plant at the start of Phase III.

upon the particle charge and electric field strength. For 10- μm particles, the actual migration velocity is approximately 2 ft/s (0.61 m/s) or 10 times the filtration velocity of 12 ft/min (3.7 m/min) or 0.2 ft/s (0.061 m/s). This rapid movement of dust toward the grounded plate pulls some of the gas flow with it and, along with electric wind effects from the movement of charged gas molecules toward the plate, produces a “suction action” of the gas flow toward the plate. The gas cannot accumulate at the plate, so there is a resulting recirculation pattern produced by the combination of the forward entrance velocity parallel to the plate and the migration velocity perpendicular to the plate. Since all of the gas flow must eventually pass through the bags, a portion of the recirculation flow is drawn toward the bags. The particles that reach the filtration surface will likely retain some charge. Charged particles are more readily collected because there is an additional coulombic force to drive the particles to a grounded or neutral surface. In addition, a dust cake formed from charged particles will be more porous, which produces a lower pressure drop. Ultrahigh fine-particle collection is achieved by removing over 90% of the dust before it reaches the fabric, precharging the particles, and using a GORE-TEX[®] membrane fabric to collect the particles that reach the filtration surface.

In Step 2, the dust that accumulates on the grounded plates and filtration surfaces must be periodically removed and transferred from the bags and plates to the hopper. When the bags are cleaned, a few larger agglomerates may fall directly to the hopper; however, much of the dust is reentrained into particles too small to fall directly to the hopper. In conventional baghouses, these particles would immediately be re-collected on the bags. In the AHPC, the unique method of bag cleaning prevents the re-collection of dust on the filter surface. The bags are pulsed with sufficient energy and volume to propel the reentrained dust past the high-voltage wires and back into the ESP zone, where they immediately become charged and are trapped on the plates. Since this reentrained cloud is composed of agglomerated particles larger than originally collected on the bags, they are trapped in the ESP zone much more easily than the original fine particles. The alternative rows of bags, wires, and plates act as an “electronic trap” to prevent the reentrained dust from being re-collected on the same bags, and the plates prevent the dust from being re-collected on adjacent rows of bags. This effect greatly reduces the accumulation of a residual dust cake and makes control of pressure drop at high A/C ratios much easier. Since most of the dust collects on the grounded plates, these plates are rapped periodically, and the dust is released

from the plates in large agglomerates that easily reach the hopper. Any fine dust that penetrates the ESP zone is collected at an ultrahigh efficiency by the bags. This completely eliminates any spike in emissions due to a rapping puff and makes redundant downstream fields completely unnecessary, compared to conventional ESPs that require multiple fields to minimize rapping reentrainment. In the AHPC, there is major synergism between the ESP and filtration modes, each improving the operation of the other. The filter collects the excess ESP emissions during normal operation and during rapping, and the ESP collects the reentrained dust from the bags upon cleaning, which greatly enhances the ability to control pressure drop and operate at high A/C ratios. The AHPC is also superior to ESPs because the AHPC completely eliminates the problem of sneackage in conventional ESPs; in the AHPC, all of the flow must pass through the bags.

3.0 RESULTS AND DISCUSSIONS

3.1 Scope of the Phase III Work

Following Phase II, modifications were made on the field AHPC unit during September 1999–March 2000 to improve overall AHPC performance. The primary modifications included:

- A new data acquisition and control system.
- Installation of a side inlet transition section.
- Design, construction, and installation of different discharge electrodes and collecting plates.
- A more compact plate- and bag-spacing arrangement.
- A modified pulsing system.

The field unit was then operated from April 18, 2000, to July 21, 2000, to obtain long-term operating data that could be used to scale up the AHPC for application to a full-scale boiler. The operating parameters such as A/C ratio (6–12 ft/min [1.8–3.7 m/min]), pulse trigger pressure (6–8.5 in. W.C. [1.5–2.1 kPa]), pulse-cleaning pressure (67–80 psi [462–552 kPa]), pulse duration time (200–800 ms), and corona current (30–80 mA) were varied to investigate their effect on AHPC performance.

After bag damage was observed during the summer of 2000, systematic bench- and pilot-scale tests were completed at the EERC to investigate the reason for the bag damage and find a practical method to solve the problem. Cold-flow tests were conducted at the EERC for six different types of filter bags combined with various electrodes and geometry alignment. Subsequently, several conditions from the cold-flow tests were selected and further evaluated for their effect on bag protection and AHPC performance in hot-flow coal combustion tests. The current to bag, bag-cleaning ability, and ESP performance were evaluated under the modified AHPC configuration. The filter bags after the hot-flow tests were examined for possible electric damage. Among all the proposed configurations, perforated plates installed between the filter bags and the discharge electrodes appeared to be the best solution to prevent bag damage.

Moreover, the experimental data obtained from the EERC pilot scale tests demonstrated the perforated-plate configuration also significantly improved overall AHPC performance. Theoretical study and bench-scale experiments also were completed to understand the interactions between the electric field and the filter bags in the presence of the perforated plate and to determine the optimized perforated-plate configuration (hole size and percent open area).

Based on results from the theoretical, bench-, and pilot-scale studies, a perforated-plate configuration was designed (1.5-in. [38-mm]-hole diameter with 45% open area, 3.0 in. [76 mm] spacing between bags and the perforated plate) and installed on the 9000-acfm (255 m³/min) slipstream field unit at the Big Stone Power Plant. The modified Big Stone AHPC was successfully started in March 2001 and operated for a testing period of 3.5 months through June 2001. Operating variables such as A/C ratio, ESP current, and pulse-cleaning pressure were tested. A cross-row pulsing system was also installed and tested in the AHPC system to compare its effectiveness on bag-cleaning ability with that of the conventional in-row pulsing system. In order to reduce high fly ash resistivity, a limiting factor for the present AHPC operation, a humidification system was installed and briefly tested to examine AHPC performance under more ideal ash resistivity conditions.

In addition to the Phase III results presented in the following section of this report, interim results were also presented at several scientific conferences (12–14).

3.2 AHPC Upgrade and Field Study at Big Stone Power Plant (September 1999 – June 2000)

3.2.1 System Modification at the AHPC Big Stone Unit at the Start of Phase III

Improvements to the field AHPC unit were made to support the Phase III tests. These improvements included a new data acquisition and control system, installation of additional heaters, a modified ash collection and discharge system, and changes to the roof to facilitate access and prevent water leaking. Based on the request of commercialization partners, a single side transition inlet, different discharge electrodes, and different collecting plates were designed and installed at the AHPC Big Stone unit.

3.2.1.1 Data Acquisition and Control

The laboratory-grade Fluke data logger system, used in the Phase II study, was limited to about 20 points and had no control capabilities. Because of the limited data collection capability of the data acquisition system and no automated controls, it always required personnel to remain on-site to make manual adjustments of the AHPC unit and to record data. The data acquisition equipment was significantly upgraded in the Phase III study to incorporate automated control to provide more data collection flexibility on the AHPC demonstration unit at Big Stone Power Plant. The new acquisition system not only provided for much better monitoring of the AHPC operation but also provided much better control of the entire process either on-site or from a remote location.

3.2.1.1.1 Hardware: National Instrument “Field Point” Module

For Phase II AHPC operation, a preprogrammed Allen-Bradley (AB) programmable logic controller (PLC) simultaneously controlled the pulse bag-cleaning cycle using measured differential pressure as a set point and the plate and electrode cleaning rappers based upon a time interval. The pulse-cleaning duration of the bags and rappers was determined by preset values

that were switch-selectable by the operator. In addition, the rapper-cleaning interval (cycle time) was selectable using preset switches.

The ABB switched integrated rectifier (SIR) II power supply used for energizing the ESP was controlled by a microprocessor integrated into the T/R (transformer/rectifier) set, which was then controlled via a local RTU (remote terminal unit) module or the Gateway communication module. The latter method allowed remote access to the power supply using the MODBUS serial communication protocol purchased with the ESP power supply. Using the Gateway module, all of the functions and data related to ESP operation could be retrieved or controlled digitally. Previously, only two analog data points, the ESP current and voltage, could be recorded by the data acquisition system. Any remaining data had to be recorded manually by an on-site operator.

For upgrading the data acquisition system, National Instrument's "FieldPoint" modular distributed I/O (input/output) system using an RS-485 serial communication network was selected. All analog input modules are 16-bit resolution, while the analog output modules use 12-bit resolution. Each module is "hot-swappable," allowing replacement, if necessary, without shutting down the system. The FieldPoint hardware is designed to be used for industrial applications and will withstand operating temperatures as low as -40EC.

The data acquisition hardware is designed for use with a personal computer operating under a Windows (95/98/NT) environment. A Gateway 400-MHz Celeron computer equipped with a modem for remote call-in access and a Windows 98 operating system was used on-site to run the program. A multiport RS-485/422 serial interface card from National Instruments communicated with the FieldPoint networking module.

3.2.1.1.2 Software: Server-Client Program Developed by National Instrument "Lookout"

In order to automatically control the AHPC system and interface all the hardware with an operator, an application program is required to record, communicate, log, and display the data collected by the field hardware. In addition, the program is able to supervise the operation of the

AHPC to 1) alarm that an event has occurred or 2) to correct the situation automatically, if possible, without operator input.

For this purpose, National Instruments “Lookout” was acquired for use as the Supervisory Control and Data Acquisition package (SCADA). One of the major advantages of this package is that the programming can be altered on the fly without shutting down the system or the process. The software also comes standard with all of the necessary software drivers to communicate with MODBUS, Allen-Bradley PLCs, and FieldPoint hardware. Lookout also allows remote access to the server (in this case, the remotely located computer monitoring the AHPC) using the Internet, a local area network, or a modem using TCP/IP (transport control protocol/Internet protocol) networking protocol.

Both the server and the client application were developed for the remote operation of the AHPC. The server is intimately connected to the hardware and “serves” up the data to be used by the client application. The client application is transportable and can be loaded on any computer with a modem to gain access to the server. The client is capable of changing the operation of the AHPC by relaying commands through the server. The server and client interfaces appear identical to the user, but different connections and programming are required. Communications were successfully established to all hardware devices. In addition, remote access was established using both ethernet and modem networking capabilities. The client software was developed in parallel with the server software and presently is capable of changing the remote hardware (based on simulated bench tests) used to control the AHPC.

The interface, designed using the Lookout software program, consists of a series of windows for viewing and controlling AHPC operation. Eight screens were developed as a minimum requirement for controlling operation of the AHPC. Figures 3.2-1–3.2-8 show examples of these screens. Figure 3.2-1 is an overall process layout and acts as a menu to reach other screens and to display and acknowledge alarms. Figure 3.2-2 shows the SIR II control screen for changing the operation of the ESP power supply. From this screen, the SIR II

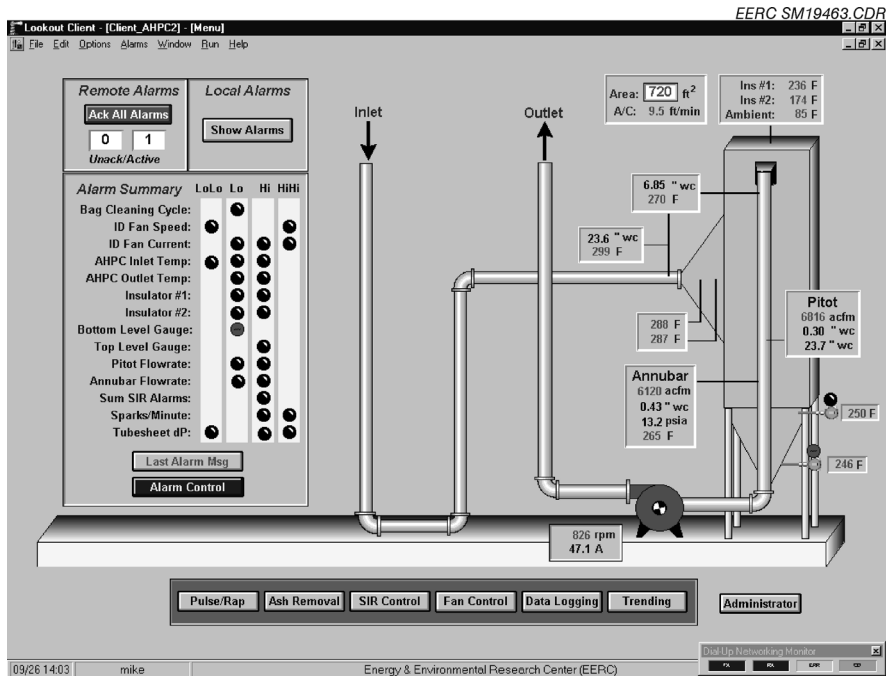


Figure 3.2-1. Overall process layout screen.

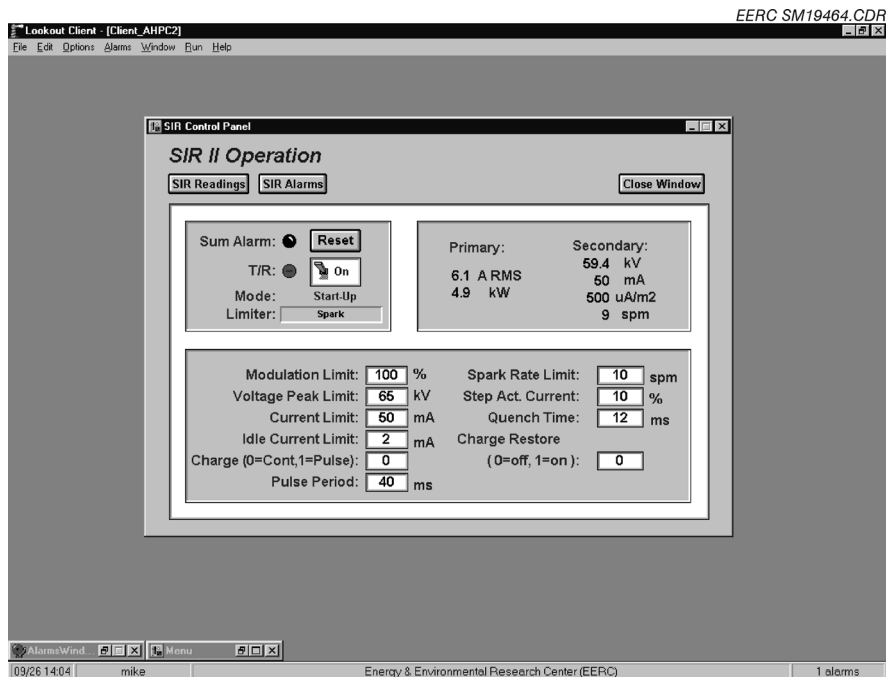


Figure 3.2-2. SIR II control screen for changing the operation of the ESP power supply.

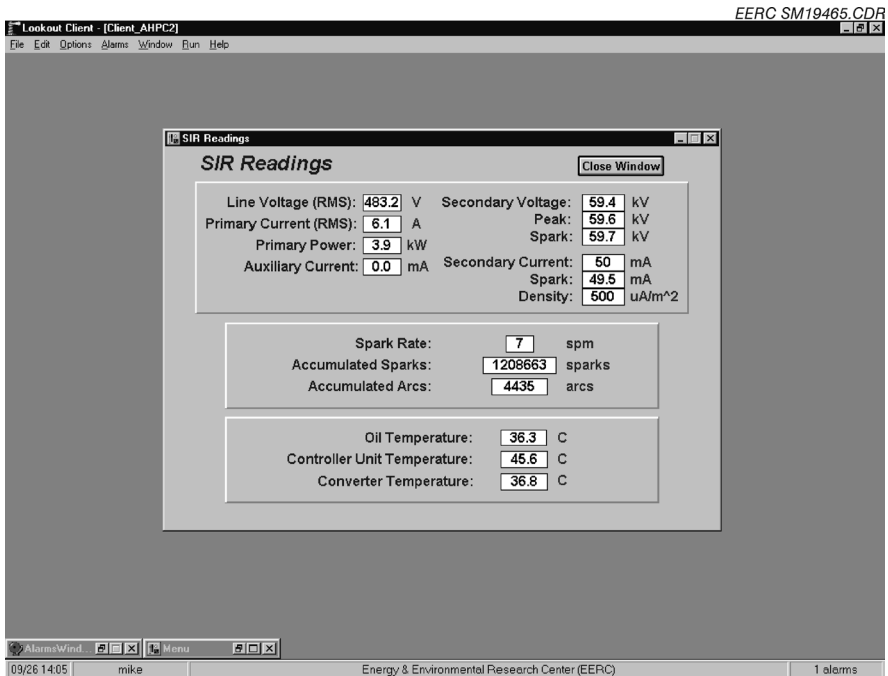


Figure 3.2-3. SIR II readings screen.

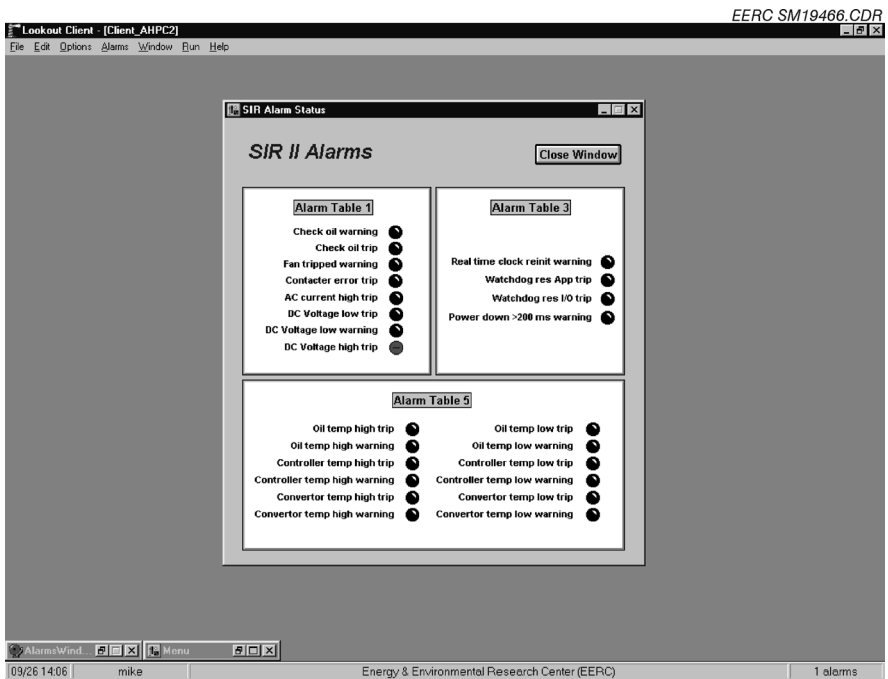


Figure 3.2-4. SIR II alarms screen.

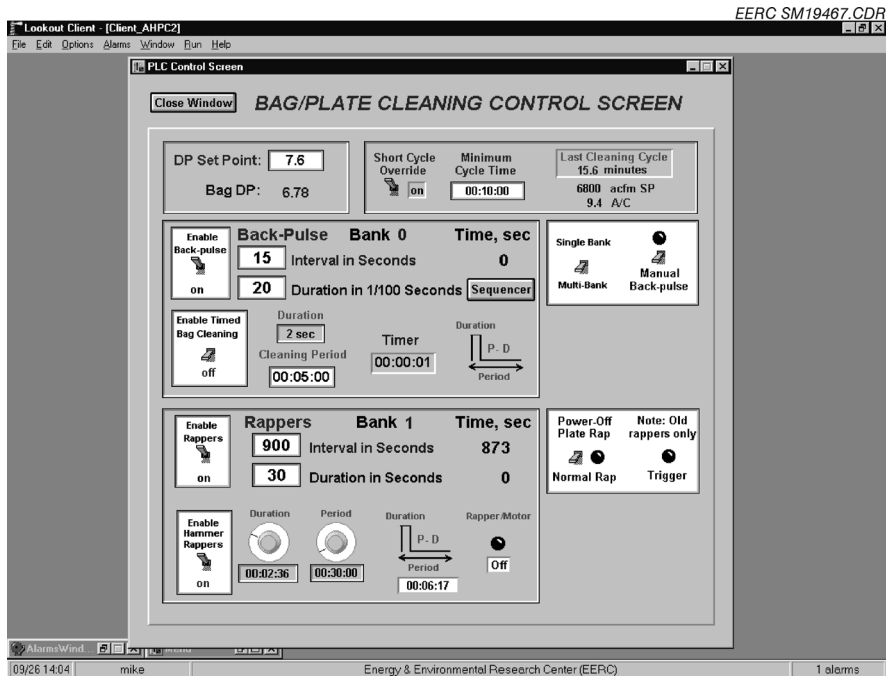


Figure 3.2-5. Screen used for controlling the backpulse and rapper-cleaning sequences.

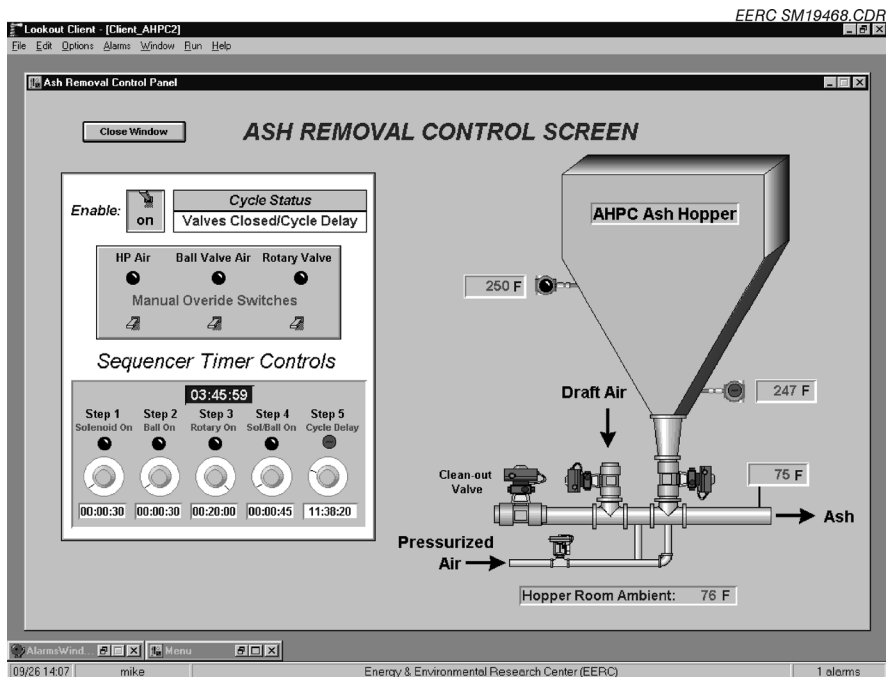


Figure 3.2-6. Ash removal control screen.

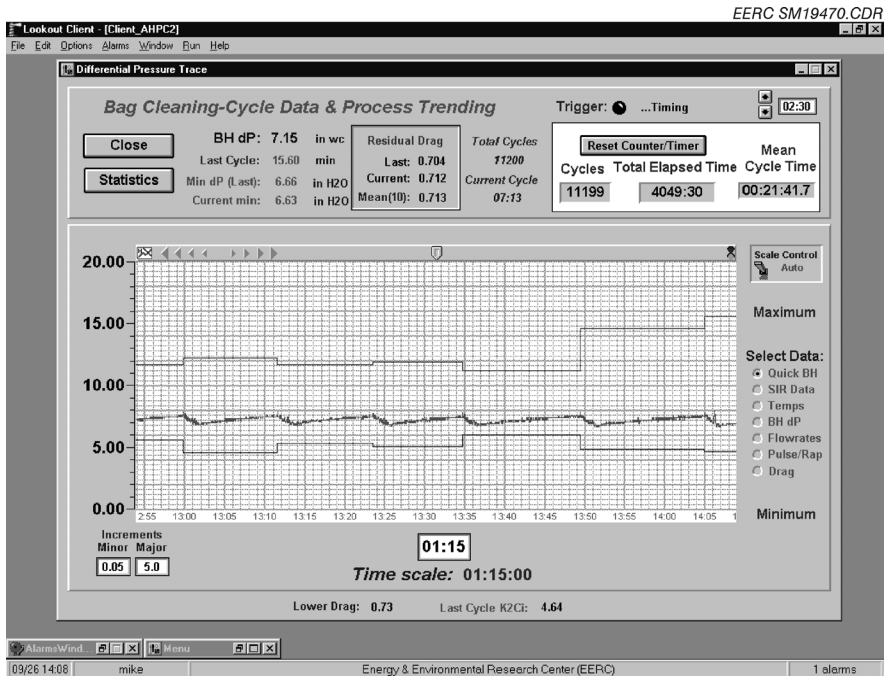


Figure 3.2-7. Screen for following the differential pressure across the bags in the AHPC.

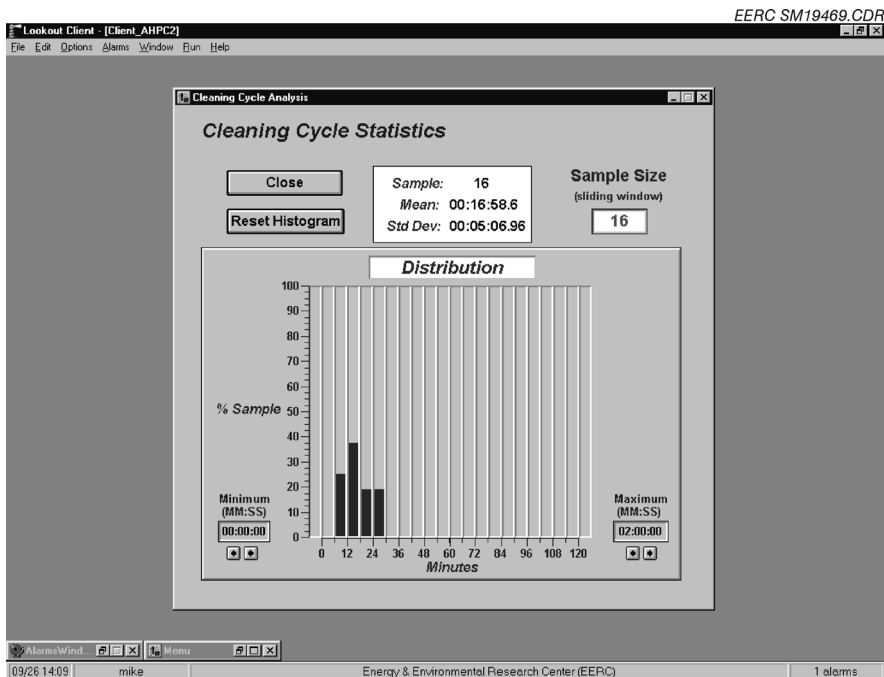


Figure 3.2-8. Cleaning cycle statistics screen.

readings screen, shown in Figure 3.2-3, can be reached, and the SIR II alarms screen, Figure 3.2-4, can be viewed. For controlling the backpulse and rapper-cleaning sequences, the screen shown in Figure 3.2-5 is used. From this screen, the PLC is programmable, allowing changes in cleaning interval and duration. Control of the ash collected in the hopper is reached through the ash removal screen seen in Figure 3.2-6. This screen allows the user to control the timing of the sequencer used for opening and closing valves. Probably the most “fluid” of the data screens are the ones used to view the performance of the process, by showing real-time tracking of a number of process variables. Figure 3.2-7, as an example, shows a screen for following the differential pressure across the bags in the AHPC. This screen provides a graphical presentation, as well as showing cleaning cycle information. From Figure 3.2-7, a statistics screen concerning cleaning cycle time and distribution can be accessed, as shown in Figure 3.2-8.

The data appearing on the data screens in Figures 3.2-1–3.2-8 are transient values seen by the hardware at that moment or stored in a memory buffer. These data are then written to disk files as a permanent record for reporting and analysis. Logging frequency, grouping, and file designation are also established for each potential data point.

Process control logic allows the computerized system to perform tasks as required without requiring operator attention. The ash removal system and the bag-cleaning cycle are examples of the automated process control. The A/C ratio is also automatically controlled by using a PID (proportional integral derivative) loop to vary the speed of the ID (induced-draft) fan, controlling the process flow rate.

3.2.1.2 AHPC Modification at the Big Stone Unit

3.2.1.2.1 Single-Side Transition Inlet

To facilitate transport and test flexibility, the 9000-acfm (255 m³/min) AHPC in Phase II was designed with an inlet that entered a manifold which then distributed the flow to opposite sides of the vessel. To reach the entrance slots for each row of bags required that the flow make

four 90 degree turns, which caused severe flow maldistribution among the different bag rows. Subsequently, additional baffling was installed to improve flow distribution from row to row. However, significant turbulence was imparted to the flow, showing that the flow was not uniform from top to bottom and did not uniformly move into each row of bags. According to the advice of the commercialization team, a gradual transition-type inlet similar to the inlet transition configuration used in commercial ESPs was installed in the Phase III study (see Figure 3.2-9). The inlet was installed on only one side of the vessel so that it no longer has the flexibility of two opposite-side inlets. This modification greatly improved the flow maldistribution problem. As shown in Figure 3.2-9, the inlet transition installation required cutting out almost one whole side of the vessel, installing the transition, and significant changing to the inlet piping. The inlet transition has turning vanes to help minimize turbulence through the 90 degree bend at the entrance to the transition and then two rows of baffle distributor plates (see Figure 3.2-10) within the transition to help equalize the flow at the entrance to the main AHPC collector.

3.2.1.2.2 Discharge Electrodes and Plates

The discharge electrodes used in Phase II were custom-built by a different commercial ESP vendor, and they functioned well for the tests. However, the commercialization team decided to install ELEX discharge electrodes for the Phase III study. The collecting plates used in the Phase II study were custom-designed and fabricated at the EERC. These plates had stiffeners with a sharp edge, resulting in significant back corona emitting from the stiffener edges observed during the Phase II field study. The new plates, more similar to the commercial design without sharp-edged stiffeners, were then constructed to minimize the back corona problem. The rapping cleaning of the plates was also marginal in Phase II, so improvements to the plate suspension to facilitate better rapping were implemented.



Figure 3.2-9. AHPC unit installed at Big Stone with new inlet ducting and side transition inlet configuration.

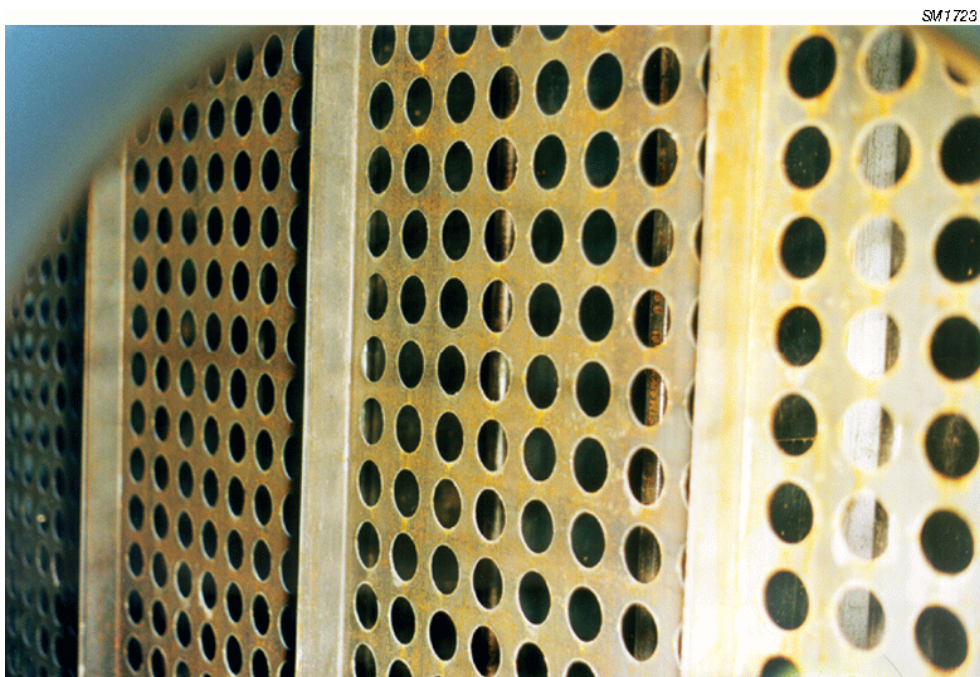


Figure 3.2-10. Inlet transition baffle distributor plates at the entrance to the AHPC.

3.2.1.2.3 Plate Spacing

The plate-to-plate spacing, which was 29 in. (736.6 mm) in the Phase II study, was reduced to 23.6 in. (600 mm) in the new plate configuration. This decision was based on the fact that no sparking to the bags was observed in Phase II, which implied that the spacing could be reduced without compromising AHPC performance. A more compact geometric arrangement is desirable because it makes for a smaller device, leading to cost savings. The 23.6-in. (600-mm) spacing has also been employed on commercial ESP units.

3.2.1.2.4 Bag Spacing, Tube Sheet, and Pulse Tube Changes

Using narrower plate spacing necessitated several other changes. Since the bags were centered between two adjacent plates, a change in plate spacing required a change in bag spacing. The change in bag spacing was accomplished by modifying the tube sheet to accommodate the narrower bag spacing, which also required that the pulse tube spacing be changed to the new bag-spacing dimensions. The top view of the modified AHPC is shown in Figure 3.2-11. Moving the plates closer together resulted in some extra space behind the two end collection plates (labeled as dead space in Figure 3.2-11), as well as space behind the old entrance baffle wall at the opposite side to the inlet transition. In order to make use of the extra space, on the inlet side, a short preionization zone was added between the exit of the second perforated baffle plate and the first bag in each row. The main collection plates were extended toward the entrance, a short y-shaped plate was added at the beginning of each row of bags, and a discharge electrode was placed in this section (see Figure 3.2-11).

As the fly ash particles pass through this section, they are electrically charged and some precipitate on the extended collection plates and the y-shaped plates before they reach the filter bags. Also, it is helpful to direct the flow primarily between the discharge electrodes and plates as the flow enters the filtration area.

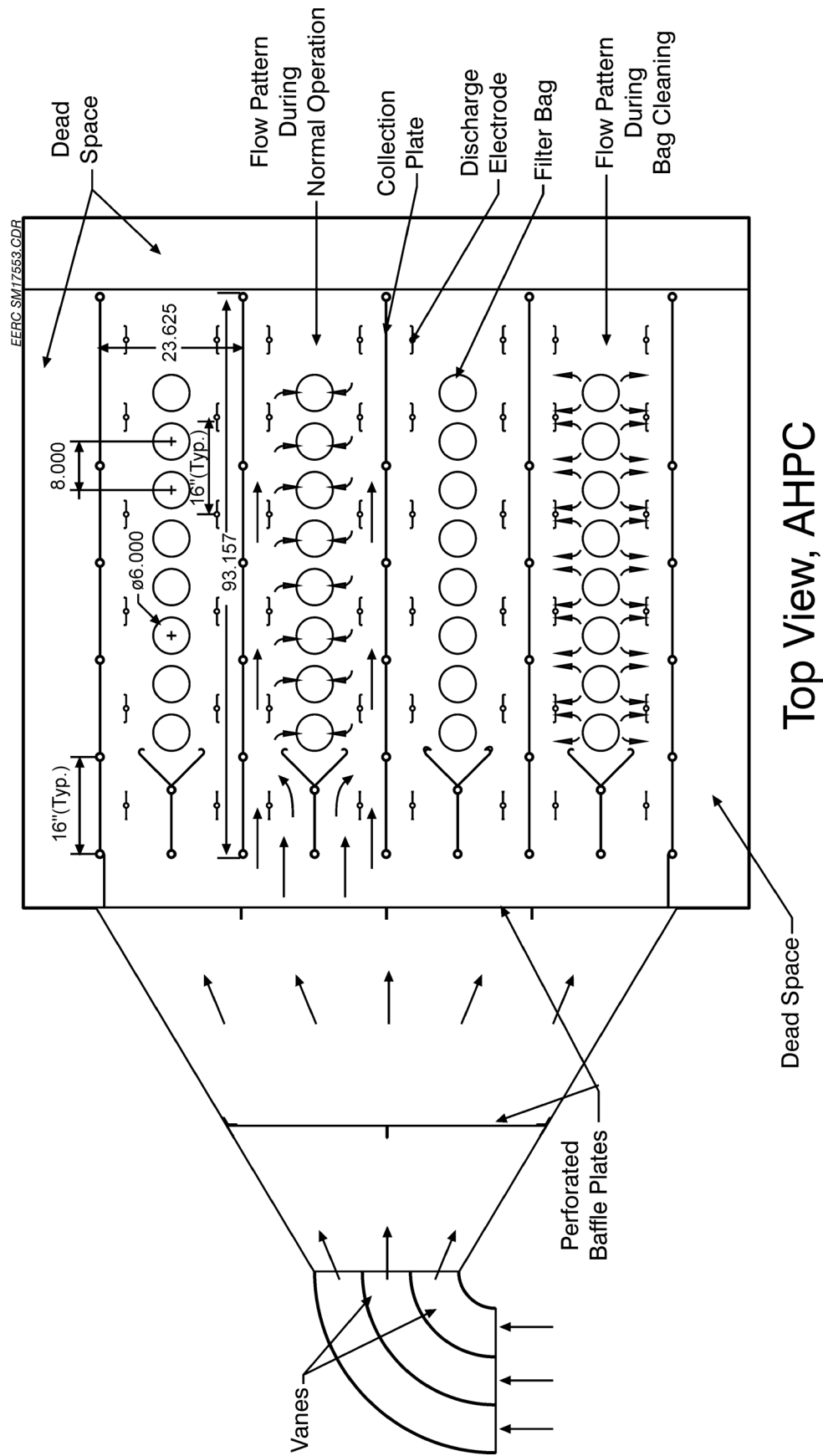


Figure 3.2-11. Top view of the modified AHPC at the start of Phase III.

3.2.2 Results for Test Period 1 (April 18, 2000 – May 17, 2000)

One additional modification to the AHPC configuration was the installation of an inlet air dilution port just downstream from the inlet shutoff damper. The port consists of a short section of 18-in. (0.46-m) diameter pipe mounted perpendicularly to the main 24-in. (0.61-m)-diameter inlet duct. The port was installed to allow cold-flow testing and is large enough so that the AHPC can be flow-tested under full flow conditions with the inlet damper completely shut. The port can also serve as a controlled air dilution source to allow testing at lower temperatures.

Prior to start-up of the AHPC with flue gas on April 18, 2000, cold-flow velocity measurements were made from inside the vessel with a handheld vane anemometer to determine the uniformity of flow at the exit of the second perforated plate baffle. Results showed that flow was reasonably uniform from top to bottom and side to side. However, somewhat higher velocities were noted in the Row 4 bag channel (top row in Figure 3.2-11); some vertical downflow was noted coming into the hopper at the inlet to the preionization zone; and some vertical upward flow was noted in the hopper near the back of the bag rows. After 1 month of operation, the AHPC was shut down to coincide with the annual plant outage and was restarted again on May 31, 2000. During this downtime, a portion of the baffle plate was blocked to correct the high-velocity area in the Row 4 bag channel, and a diverter plate was installed below the preionization zone to correct the downward flow to the hopper. Additional cold-flow measurements following these modifications showed that the flow was more uniform.

3.2.2.1 Plant Conditions and AHPC Operating Parameters

The AHPC was started at an A/C ratio of 12 ft/min (3.7 ft/min) with a pulse trigger pressure of 6.0 in. W.C. (1.5 kPa) and a low current of 30 mA on April 18, 2000, and was operated continuously until May 5, 2000, when the Big Stone Power Plant had an unplanned outage. The unit was started again on May 8, 2000, and operated continuously through May 17, 2000, when it was shut down for the planned annual Big Stone maintenance outage. The gross load of the Big Stone Power Plant during this testing period is plotted as a function of time and shown in Figure 3.2-12. The power plant operated at full load of 465 MW for most of the testing

period and dropped to around 340 MW occasionally at night. The flue gas temperature at the ESP inlet (also shown in Figure 3.2-12) was quite steady, ranging from 260E to 300EF (127E to 149EC) for most of the testing time except for the power plant outage.

As in previous start-ups, arcing occurred around the electrode insulators for the first hour, preventing the application of high voltage. However, after the insulators were heated to operating temperature, the arcing subsided, and full power could be applied to the AHPC.

The initial bag-cleaning interval was 35 min, but after 24 hr, it was as low as 5 min, so the pulse set point was increased to 7 in. W.C. (1.74 kPa) and the current increased to 50 mA. The pulse interval subsequently increased to 25 min overnight and then fluctuated between 10 and 20 min until midmorning on April 21, 2000, when it dropped below 10 min. At this point, the pulse set point was increased to 7.5 in. W.C. (1.8 kPa) where it remained for the entire month, except for times when it was deliberately lowered for testing at lower A/C ratios.

The pulse cleaning was switched several times between “single-bank” mode and “multibank” mode in this testing period. In the single-bank mode, only one row of bags is pulsed when the dP set point is reached, and the second row is pulsed the next time the set point is reached. In the multibank mode, all four rows of bags are pulsed in sequence within a short time, usually less than 1 min. The single-bank mode is more typical of full-scale operation and results in less fluctuation in the flow rate, but more information on how well the bags clean can be obtained in the multibank mode. For example, the residual drag and K_2C_i terms can be determined only in multibank mode. After several iterations in both modes, it was determined that the automatic PID control of the fan produced very rapid response so that the flow rate could be held constant in either mode.

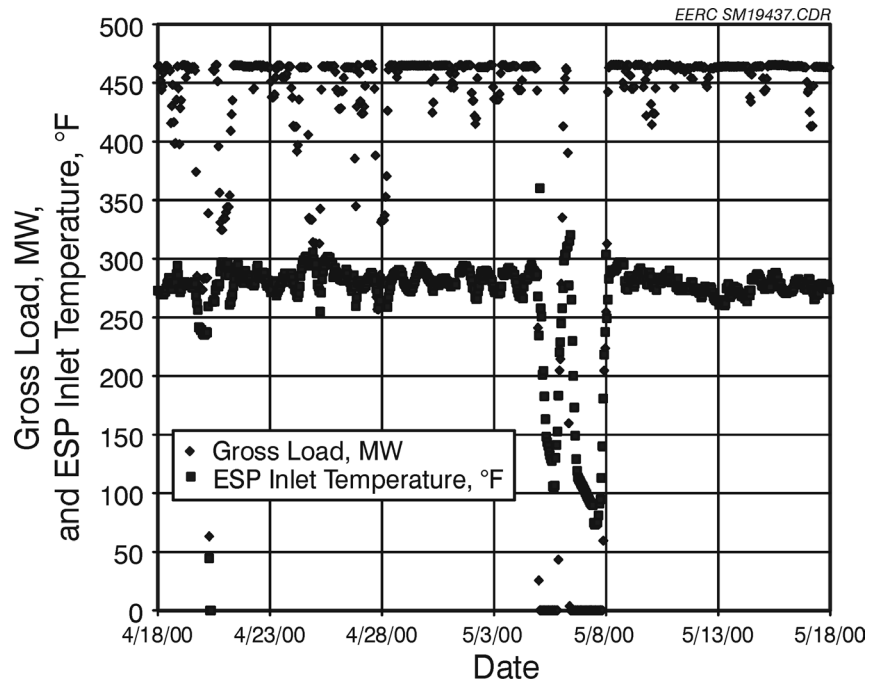


Figure 3.2-12. Gross load for Big Stone for the period April 18 – May 17, 2000.

3.2.2.2 Results Discussion

From April 21, 2000, 9:00 p.m. through April 27, 2000, 9:00 a.m., the AHPC was operated under steady-state conditions in the multibank pulsing mode. The pulse trigger pressure was set at 7.5 in. W.C. (1.9 kPa) with a current level of 50 mA. The pulse-cleaning pressure was 67 psi (462 kPa) with a pulse-duration time of 800 ms. In addition, shorter tests were conducted May 3–4, 2000, and May 15–16, 2000, in the multibank mode. Operating conditions for these tests are summarized in Table 3.2-1. The pulse cleaning was increased from 67 to 80 psi (462 to 552 kPa) for the May 3–4, 2000, test, and the current was increased from 50 to 66 mA for the third test.

The resultant bag-cleaning interval, residual drag, and K_2C_i for these test periods are shown in Figures 3.2-13–3.2-16, and average values are given in Table 3.2-1. Figure 3.2-13 shows the 3-hr average bag-cleaning intervals for all three test periods. It is seen that the bag-cleaning interval varied widely in the first test, ranging from 26 min to as low as 5 min, while the intervals

TABLE 3.2-1

AHPC Settings and Results While Operating in the Multibank Pulsing Mode			
Test Dates	4/21/00–4/27/00	5/3/00–5/4/00	5/15/00–5/16/00
Operational Setting			
Test Duration, hr	138	33	12
A/C Ratio, ft/min (m/min)	12 (3.7)	12 (3.7)	12 (3.7)
Cleaning Type	Multi	Multi	Multi
Pulse-Cleaning Pressure, psi (kPa)	67 (462)	80 (552)	80 (552)
Pulse Duration, ms	800	800	800
Pulse Trigger Pressure, in. H ₂ O (kPa)	7.5 (1.9)	7.5 (1.9)	7.5 (1.9)
Current Set Point, mA	50	50	66
Operational Results			
Average Tube Sheet dP, in. H ₂ O (kPa)	6.9 (1.7)	6.97 (1.7)	7.03 (1.8)
Average Residual Drag	0.50	0.53	0.53
Average Bag-Cleaning Interval, min	12.30	7.25	10.2
Average K ₂ C _i	6.44	7.54	5.69

did not change as much for the second and third test periods. The observed wide variation of the bag-cleaning interval during the tests is probably caused by the fluctuating flue gas temperature, which significantly affects ESP performance because of the dependence of fly ash resistivity on temperature. In order to examine the temperature effect in more detail, the bag-cleaning interval for Test 1 (April 21–27, 2000) is plotted as a function of operating time and shown in Figure 3.2-14. The bag-cleaning interval during April 24 and 25, 2000, reached its peak level when the flue gas temperature was at the lowest of 250E–260EF (121E–127EC) at 6 a.m., and then was reduced in the range from 5–10 min when the inlet temperature was at its highest of 290E–300EF (143E–149EC). On the other hand, because of a more constant flue gas temperature ranging from 270E–290EF (132E–143EC) in Tests 2 and 3, the bag-cleaning interval was maintained steady as shown in Figure 3.2-14. By increasing the current from 50 to 66 mA, the bag-cleaning interval did not increase significantly.

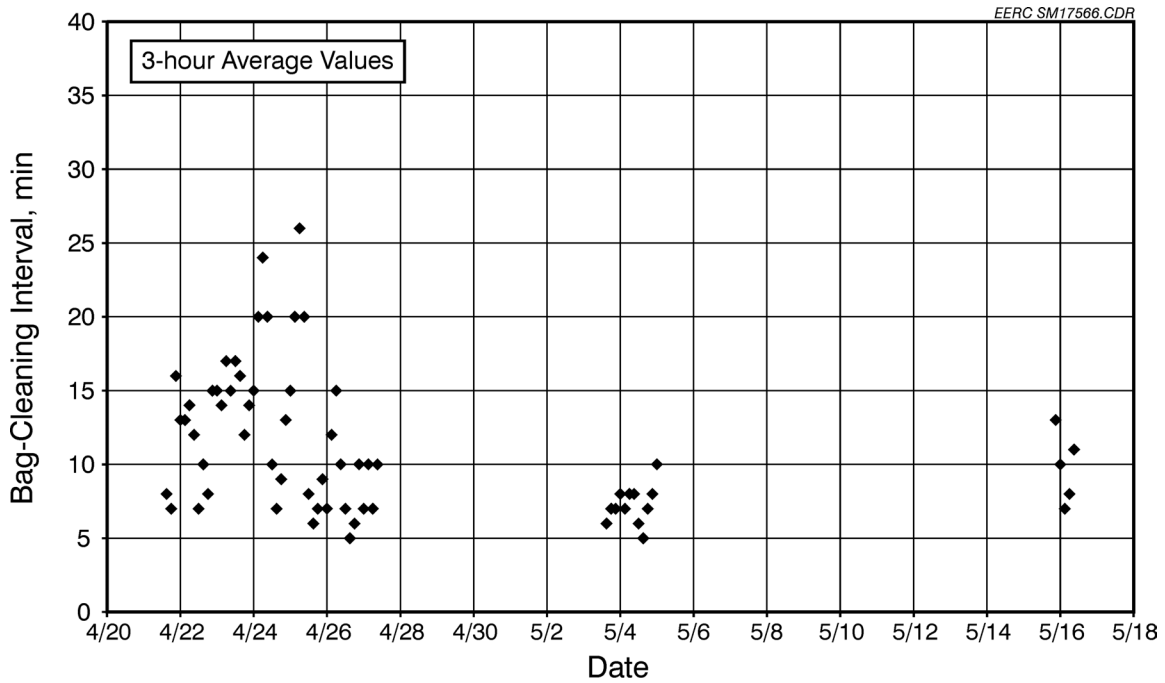


Figure 3.2-13. Bag-cleaning interval for April 21 – May 15, 2000, while the AHPC is operated in the multibank pulsing mode.

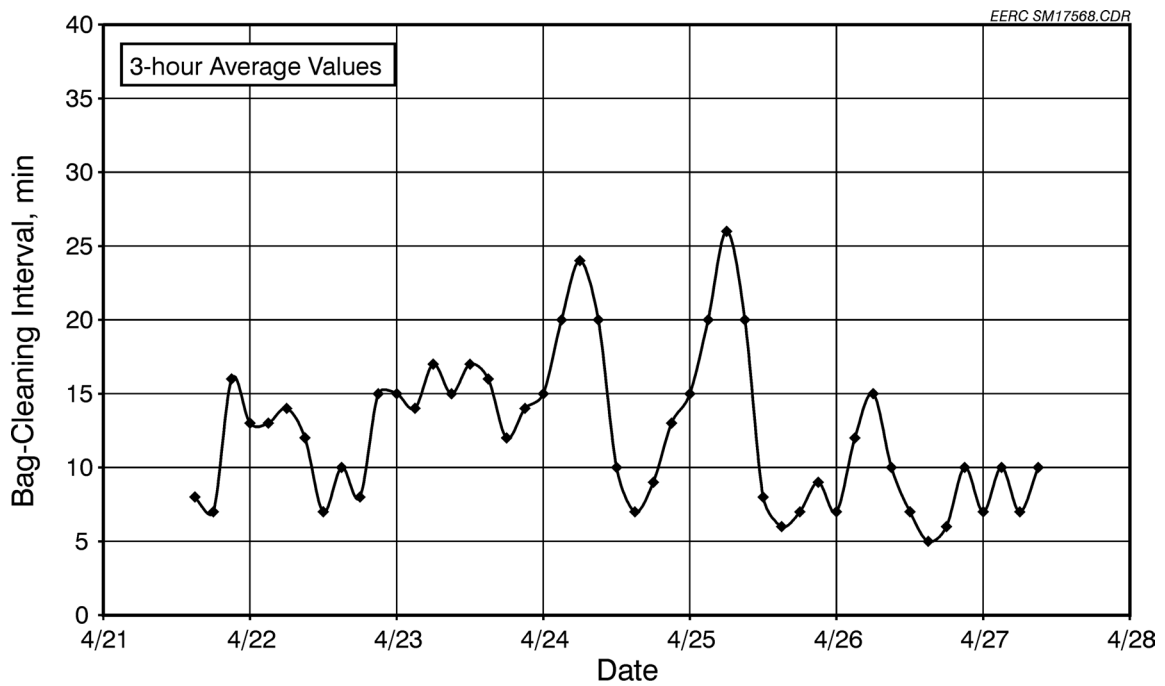


Figure 3.2-14. Bag-cleaning interval for April 21–27, 2000, while the AHPC is operated in the multibank pulsing mode.

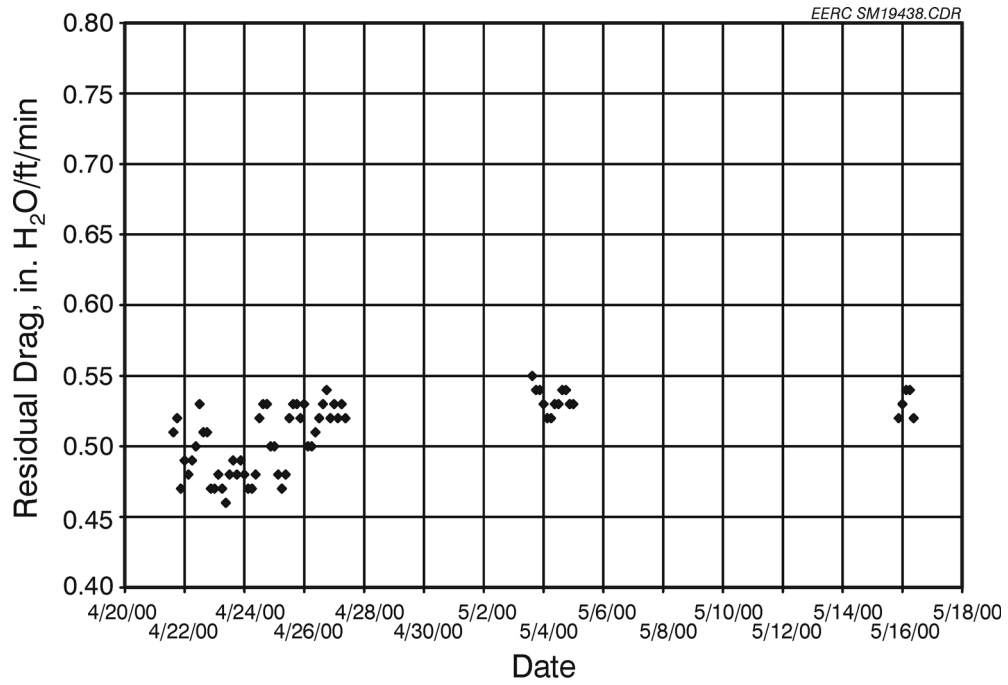


Figure 3.2-15. Residual drag for April 21 – May 15, 2000, during periods of operation in the multibank pulsing mode.

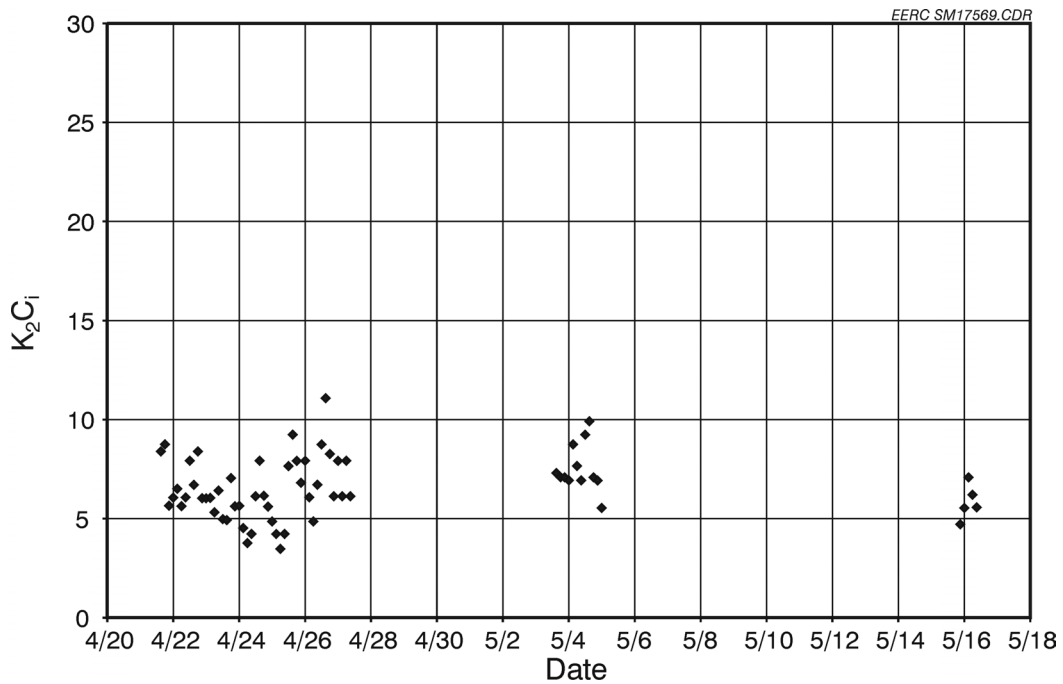


Figure 3.2-16. K_2C_i values for April 21 – May 15, 2000, during periods of operation in the multibank pulsing mode.

The residual drag (Figure 3.2-15) appears to be very constant ranging from 0.47 to 0.53 for the first test period and 0.51 to 0.54 in the second and third test periods. The residual drag typically goes down somewhat with an increase in bag-cleaning interval. This could be the result of better bag cleaning with better electrical conditions (i.e., more of the dust is trapped in the ESP zone after pulsing when the temperature and ash resistivity are lowest). Since the residual drag between the second and third test periods was constant, the AHPC appears to have reached a fairly steady state of operation.

The K_2C_1 data (Figure 3.2-16), an indicator of the ESP performance, are in a fairly narrow range from 4 to 10 for all the three periods. The lowest values (3 to 4) occurred when the flue gas temperature was at its lowest level, resulting in the longest bag-cleaning intervals, which, again, can be explained by better ESP performance occurring at these times. Average values (Table 3.2-1) for the three periods are very close, but the lowest is for the third test period. This may be the result of the higher current set point which should produce somewhat better ESP performance.

As described earlier, the goal for AHPC performance is to achieve at least a 10-min bag-cleaning interval at a pressure drop of 8 in. W.C. (2.0 kPa) and an A/C of 12 ft/min (3.7 m/min). From Table 3.2-1, it is seen that the average pressure drops across the system for each of the tests are only about 7 in. W.C. (1.7 kPa). The average bag-cleaning intervals are above 10 min for Test Periods 1 and 3 but only 7.25 min for Test Period 2. However, by increasing the average pressure drop to 8 in. W.C. (2.0 kPa), the bag-cleaning interval would be well over 10 min for all three tests. The AHPC during this first month of operation clearly exceeded the performance goal.

3.2.2.3 A/C Ratio Experiments

Several short-term tests from May 12 to 13 were conducted to evaluate the effect of A/C ratio on the AHPC performance with the pulse trigger pressure at 7.5 in. W.C. (1.87 kPa) and a current level of 66 mA. The A/C ratio (Figure 3.2-17), initially at 12 ft/min (3.7 m/min), was

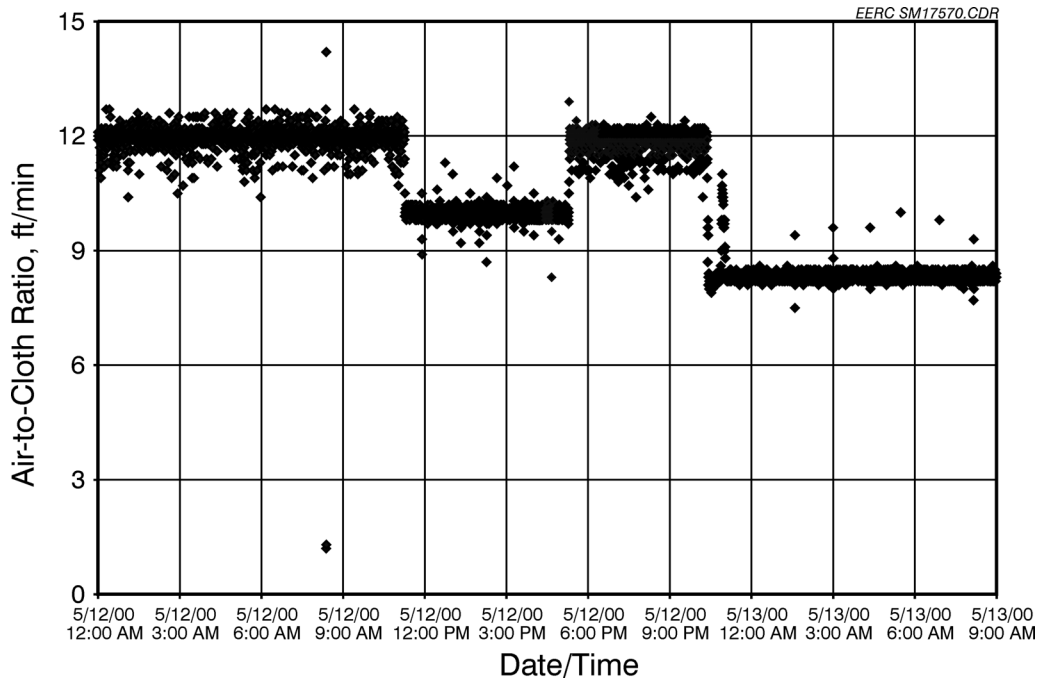


Figure 3.2-17. A/C ratio for the test period to determine the effect of A/C ratio on bag-cleaning interval.

reduced to 10 ft/min (3.1 m/min) for 6 hr and then back to 12 ft/min (3.7 m/min). Next, the A/C ratio was further decreased to 8.3 ft/min (2.5 m/min) until May 13, 2000 9:00 a.m. The AHPC system was operated in single-bank cleaning mode during this testing period, so no residual drag and K_2C_1 were obtained. The resultant bag-cleaning interval, pressure drop, and drag are shown in Figures 3.2-18–3.2-20. The pressure drop across the system is plotted as a function of operating time. The upper values of the pressure drop are determined by the pulse trigger set point and, as shown, remain constant at 7.5 in. W.C. (1.9 kPa). The observed scatter points above 7.5 in. W.C. (1.87 kPa) (Figure 3.2-18) are those cases when the data happened to log during the bag pulse where there was a momentary surge in dP above the 7.5 in. W.C. (1.9 kPa). The AHPC unit operated at a lower average pressure drop level when the A/C ratio was reduced to 8 ft/min (2.4 m/min) compared to the results at 12 ft/min (3.7 m/min). In order to evaluate filter performance, the pressure drop was divided by the filtration face velocity (A/C ratio), referred to as drag, and plotted in Figure 3.2-19. Since the pulse trigger pressure setting point was constant in the tests, the upper drag values (Figure 3.2-19) increase with a decrease in velocity as

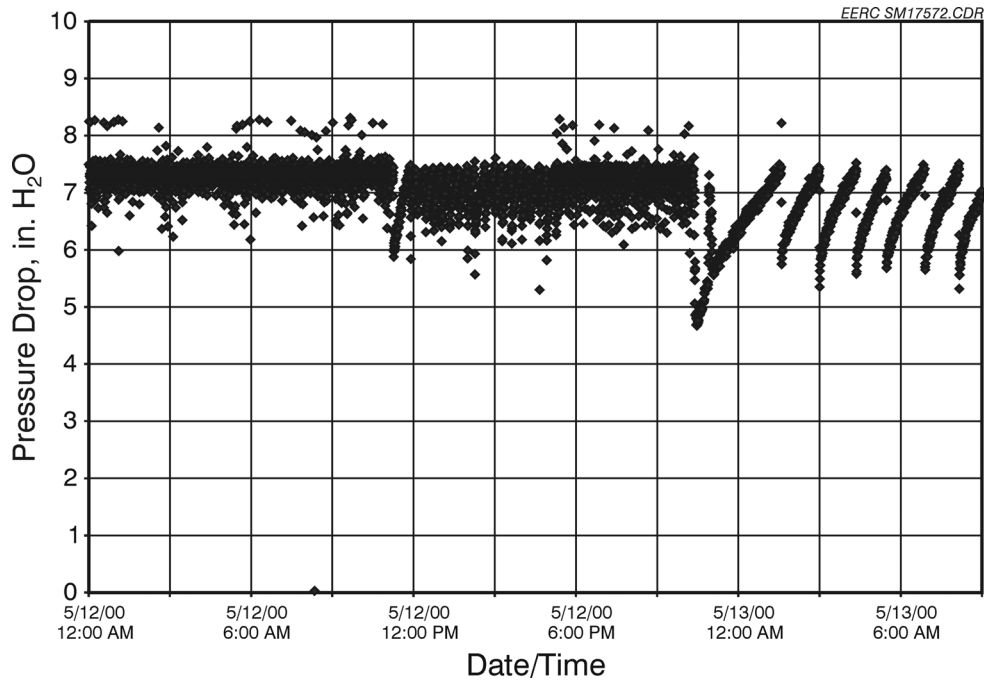


Figure 3.2-18. Tube sheet pressure drop for the test period to determine the effect of A/C ratio on bag-cleaning interval.

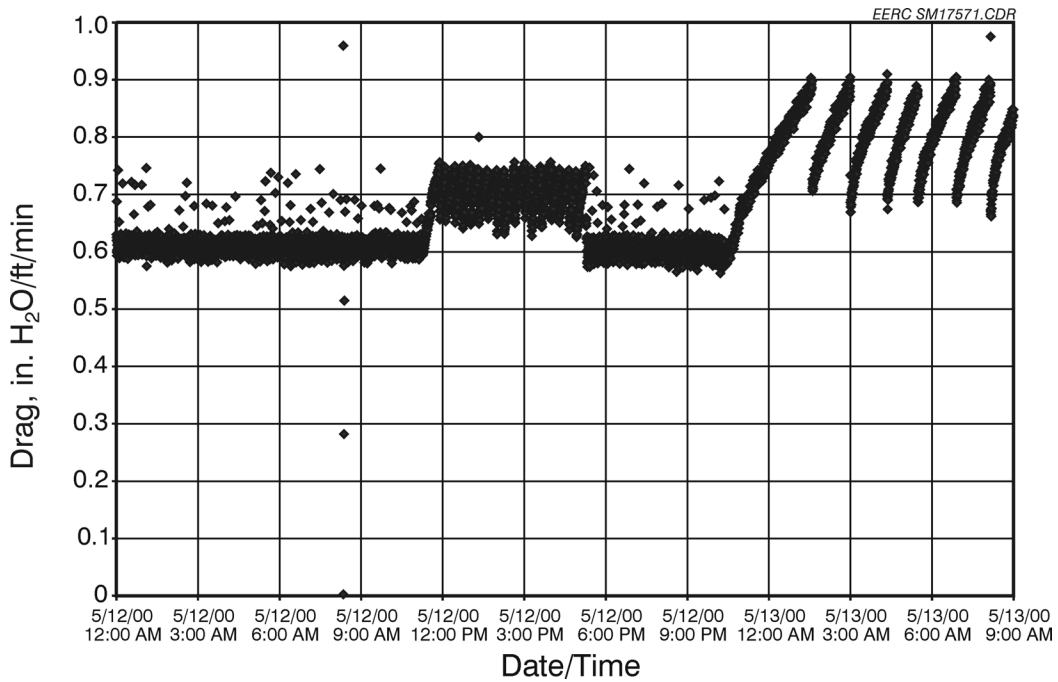


Figure 3.2-19. Drag values for the test period to determine the effect of A/C ratio on bag-cleaning interval.

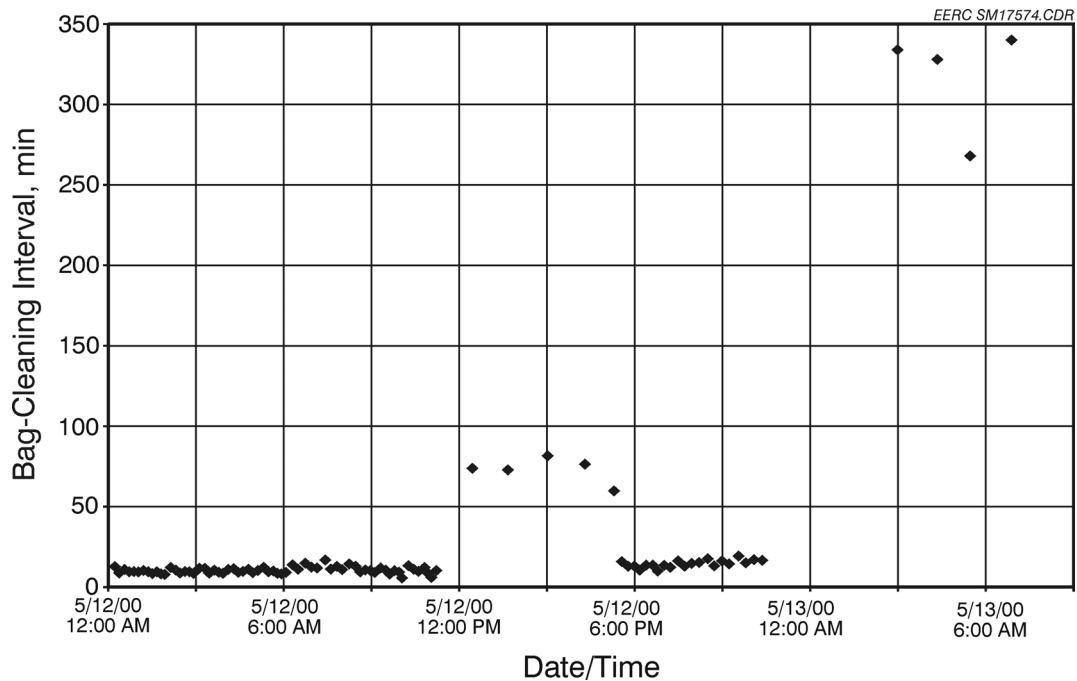


Figure 3.2-20. Bag-cleaning intervals during the times when the A/C ratio was changed.

expected. The after-pulse drag values shown in Figure 3.2-19 also increase with a decrease in velocity, but this is misleading because for each pulse only $\frac{1}{4}$ of the bags are pulsed. The true residual drag after pulsing all four rows of bags would be much lower than the values shown.

The effect of the reduced A/C ratio on bag cleaning (Figure 3.2-20) is significant, increasing from the range of 8–20 min at 12 ft/min (3.7 m/min) to 75 min at 10 ft/min (3.1 m/min) and 315 min at 8.3 ft/min (2.5 m/min). An explanation of the effect can be obtained from Eq. 2.3-1. Among the parameters determining the bag-cleaning interval, both dP and K_2C_i are in first-order correlation with bag-cleaning interval, while the A/C ratio has a reversed secondary-order correlation with bag-cleaning interval, which means even a slight change of A/C ratio might result in a dramatic variation of bag-cleaning interval. Since the single-bank mode was employed and both the residual drag and K_2C_i are unknown, we must approximate one of the values to calculate the other. For the 10-ft/min (3.1-m/min) test, if we assume a residual drag value of 0.4, the K_2C_i would be 3.2. This is in the range of the lower values observed at 12 ft/min (3.7 m/min) and appears to be reasonable. It is also likely to decrease somewhat with a

decrease in velocity. Assuming a residual drag of 0.3 at 8.3 ft/min (2.5 m/min), the calculated K_2C_i is 1.6. Again, this appears reasonable since the K_2C_i tends to be lowest at night when the test occurred and would also be lower because of the lower velocity.

3.2.2.4 Pulse Trigger Pressure Experiments

Pulse trigger pressure is another very important operating parameter for the AHPC performance. It not only determines the pressure drop across the system but also the bag-cleaning interval. Several additional short-term tests were completed at 10 ft/min (3.1 m/min) to investigate the pulse trigger pressure effect on the bag-cleaning interval. The AHPC was operated at a single-bank pulse mode with a 80 psi (552 kPa) pulse-cleaning pressure, a pulse duration time of 800 ms, and the current at 66 mA. The bag-cleaning interval results are plotted as a function of the pulse trigger pressure (Figure 3.2-21) and show a proportional correlation between the pulse trigger pressure and the bag-cleaning interval. The higher setting pulse trigger pressure results in an extended bag-cleaning interval.

Long bag-cleaning intervals are desirable because of the likely benefit to bag life, but in some cases, operation at a lower pressure drop may be more important. On May 15, 2000, short-term tests were conducted to examine the combined effects of A/C ratio and pulse trigger pressure on the resultant bag-cleaning interval. Figures 3.2-22 and 3.2-23 show the variations of pressure drop and the A/C ratio during the tests, and Figure 3.2-24 shows the resultant bag-cleaning interval. On May 15, from 12:00 a.m. to 8:30 a.m., the A/C ratio was 10 ft/min (3.1 m/min) with a pulse trigger pressure set at 6.8 in. W.C. (1.7 kPa). The corresponding bag-cleaning interval was in the range of 47–68 min. By increasing the A/C ratio to 12 ft/min (3.7 m/min) and pulse trigger pressure to 7.5 in. W.C. (1.9 kPa) (May 15, 2000, 8:30 a.m. – 1:30 p.m.), the bag-cleaning interval was significantly reduced to 10 min. The tests were repeated from May 15, 2000, 1:30 p.m. to May 16, 2000, 12:00 a.m. and demonstrated similar results as shown in Figure 3.2-24. The above experimental data suggest A/C ratio has a stronger effect on bag-cleaning interval than pulse trigger pressure. In order to obtain a bag-cleaning interval of

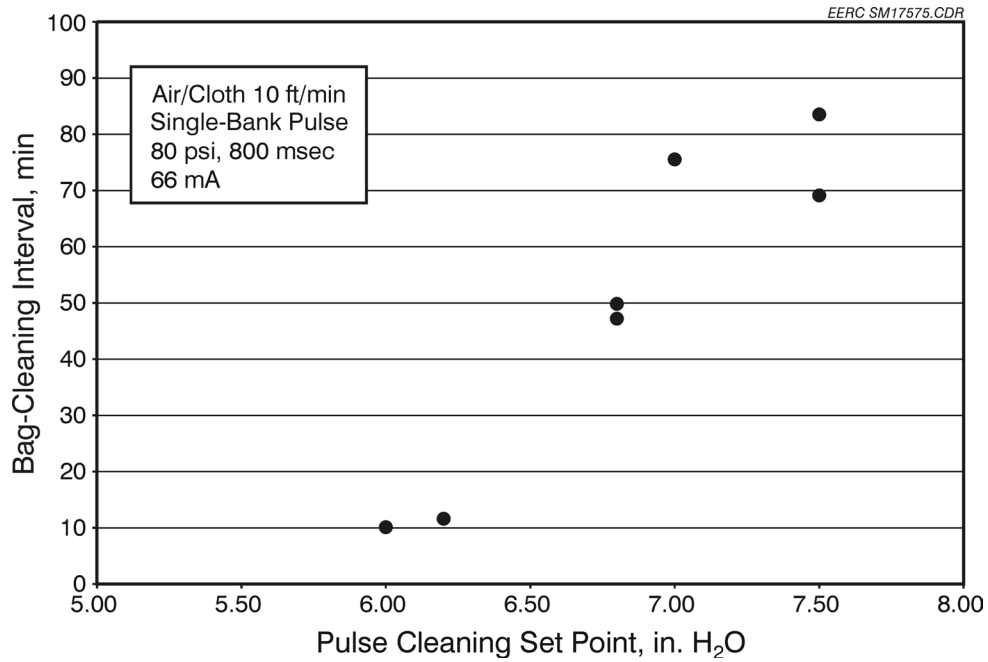


Figure 3.2-21. Effect of pulse-cleaning set point on bag-cleaning interval at constant A/C ratio.

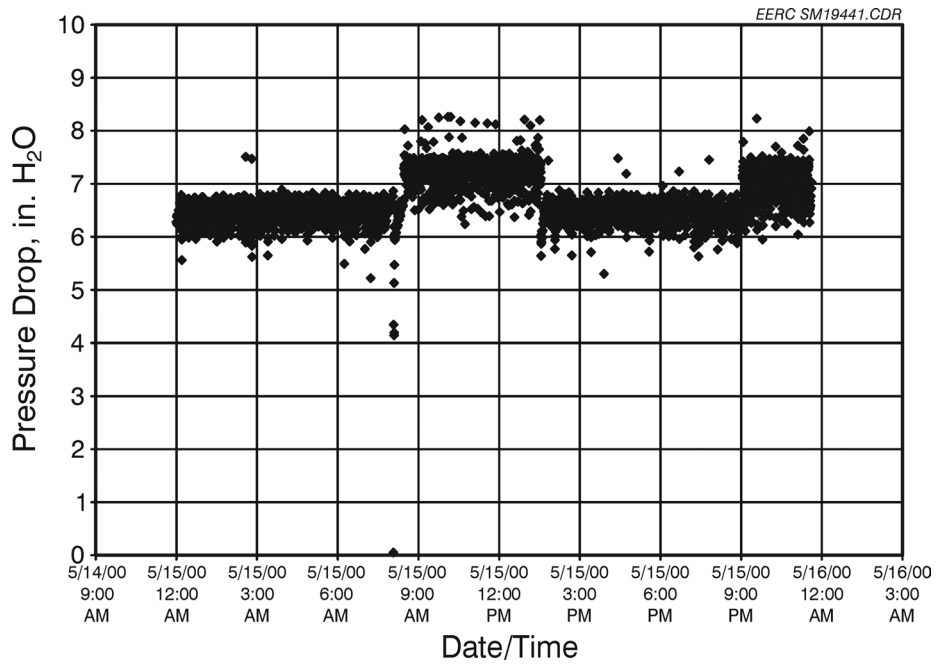


Figure 3.2-22. Pressure drop for May 15, 2000.

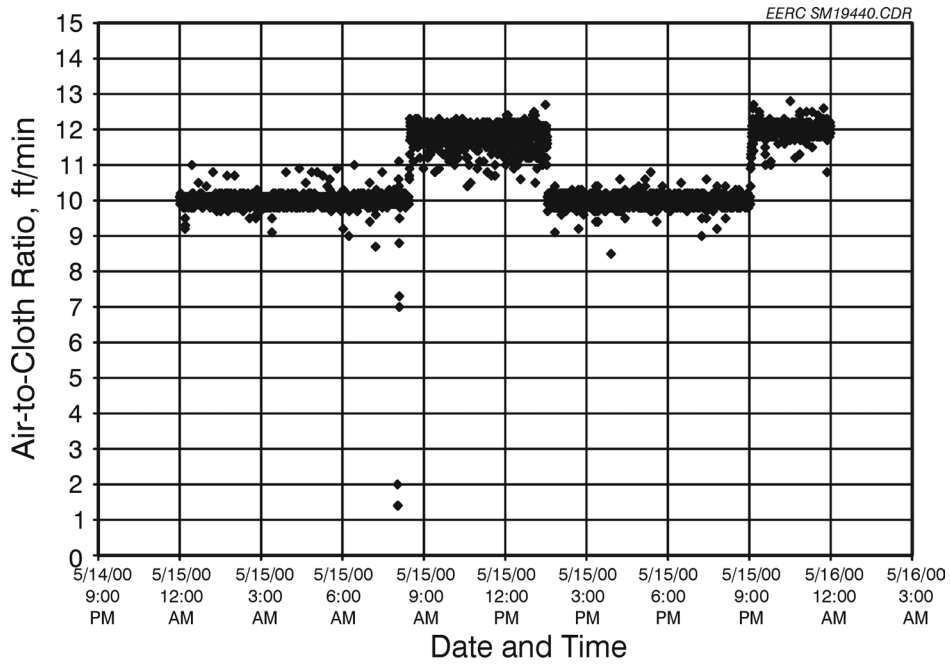


Figure 3.2-23. A/C ratio for May 15, 2000.

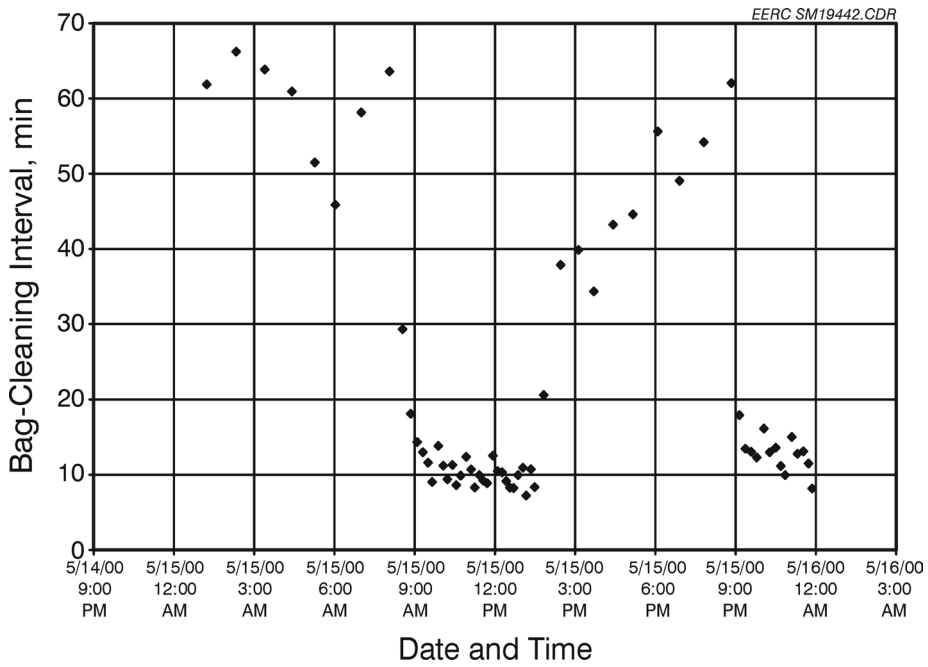


Figure 3.2-24. Bag-cleaning interval for May 15, 2000.

10 min, the AHPC can be operated either at 12 ft/min (3.7 m/min) with a pulse trigger pressure set point of 7.5 in W.C. (1.9 kPa) (shown in Figure 3.2-24) or at a reduced 10 ft/min (3.1 m/min) A/C ratio with a lower set point of 6.0 in. W.C. (1.5 kPa) (shown in Figure 3.2-21), suggesting that there is a trade-off between pressure drop and A/C ratio.

3.2.3 Results for Test Period 2 (May 31, 2000 – July 21, 2000)

3.2.3.1 Plant Conditions and AHPC Operating Parameters

Following the plant outage, the AHPC was started again May 31, 2000, with the same bags at an A/C ratio of 12 ft/min (3.7 m/min), a pulse trigger pressure set at 7.5 in. W.C. (1.9 kPa), and a current of 66 mA. In the 1½-month test, the power plant experienced several unplanned short outages which occurred on June 21, 2000, and July 17, 2000. Also, the power plant gross load fluctuated, having a full load of 460 MW during the day and dropping to 300–400 MW at night (shown in Figure 3.2-25). The flue gas temperature (also shown in Figure 3.2-25) varied in the range of 270E–325EF (132E–163EC). Another complicating factor was a switch of coal from the Cordero Rojo Complex burned in April and May to Black Thunder, which was burned in June. The Black Thunder ash appeared to be more sticky and, subsequently, more difficult to clean off the bags. In early July, the power plant switched coal again to another Powder River Basin (PRB) coal from the Belle Ayr Mine. These varying power plant operating conditions created a challenging environment for AHPC performance.

3.2.3.2 Testing Results Discussion

The bag-cleaning interval was maintained in the range from 70 to 80 min on May 31, 2000, but following a 30-min period when the high-voltage SIR power was shut off on June 1, the bag-cleaning interval dramatically reduced to 5–10 min. It was not clear whether the power-off period was the main contributor to this effect or whether a seasoning effect of the bags was occurring. Consequently, on June 3, 2000, the A/C ratio was reduced to 10 ft/min (3.1 m/min) and the pulse set point to 6.8 in. W.C. (1.7 kPa). AHPC operation was steady under these conditions for several days, with bag-cleaning interval changing with time of day as shown in Figure 3.2-26. The bag-cleaning interval was 15–30 min at night when the flue gas temperature was at its lowest level

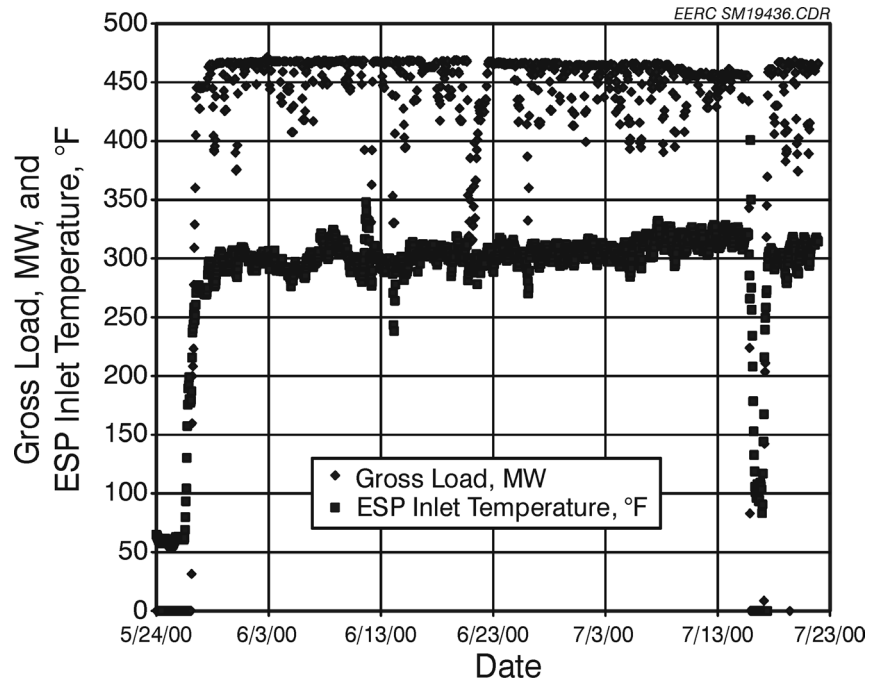


Figure 3.2-25. Big Stone Power Plant gross load and ESP inlet temperature for May 24 - July 21, 2000.

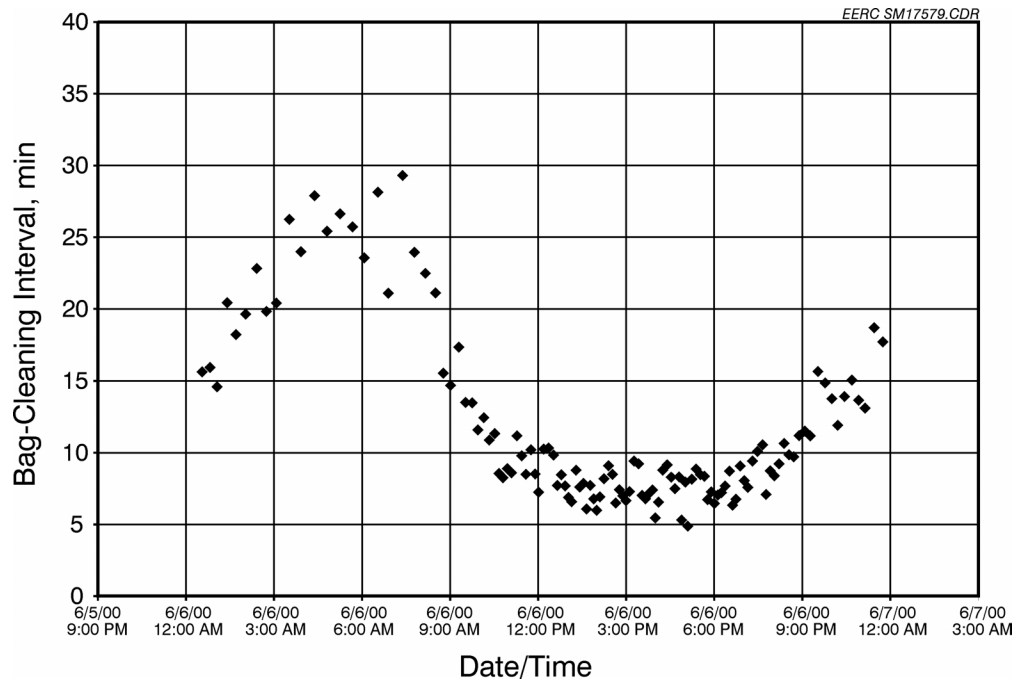


Figure 3.2-26. Varying bag-cleaning interval with time of day.

and decreased to 5–10 min during the day when the flue gas temperature reached its highest level.

From June 7, 2000, until June 9, 2000, the A/C was increased again to 12 ft/min (3.7 m/min) and the pulse set point to 8 in. W.C. (2.0 kPa). The bag-cleaning interval during this time was short, ranging from 45 sec to 2 min, so that the AHPC fell into a continuous pulse cleaning mode. Therefore, the A/C was reduced to 10 ft/min (3.1 kPa) again. The bag-cleaning interval as well as the pressure drop across the system, however, did not return to the previous levels before the continuous cleaning. This suggests that the continuous cleaning episode may have had a permanent negative effect on bag-cleaning ability. Since the AHPC was operated in the single-bank pulse mode during the above testing periods, the K_2C_i and residual drag are not available.

From June 16, 2000, through June 24, 2000, the AHPC operated in the multibank mode to obtain more information on the AHPC performance. The A/C ratio was 10 ft/min (3.1 m/min), and the pulse trigger pressure was 8 in. W.C. (2.0 kPa). The bag-cleaning interval, K_2C_i , and residual drag results are shown in Figures 3.2-27–3.2-29. The bag-cleaning interval

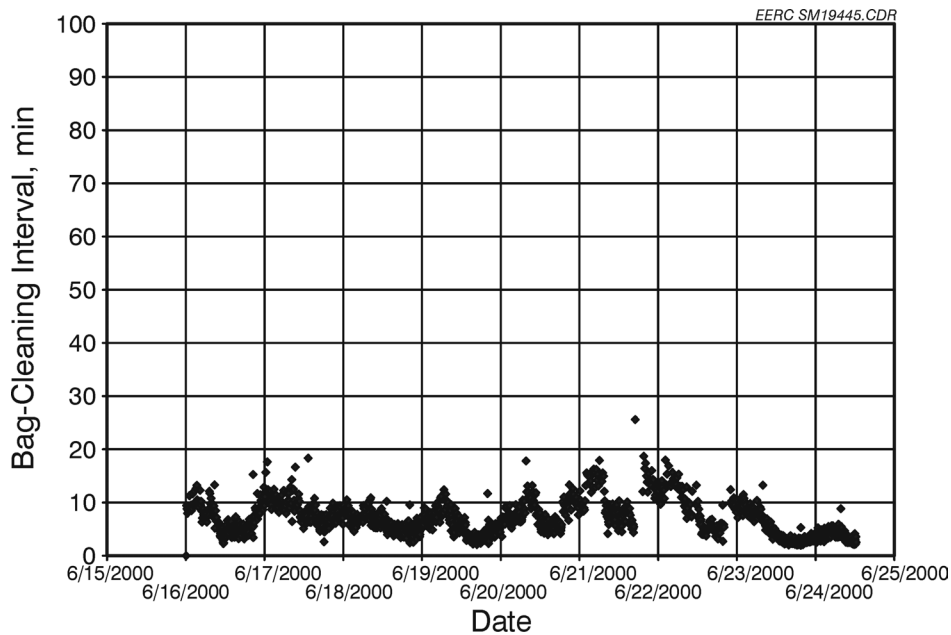


Figure 3.2-27. Bag-cleaning interval for June 16–24, 2000.

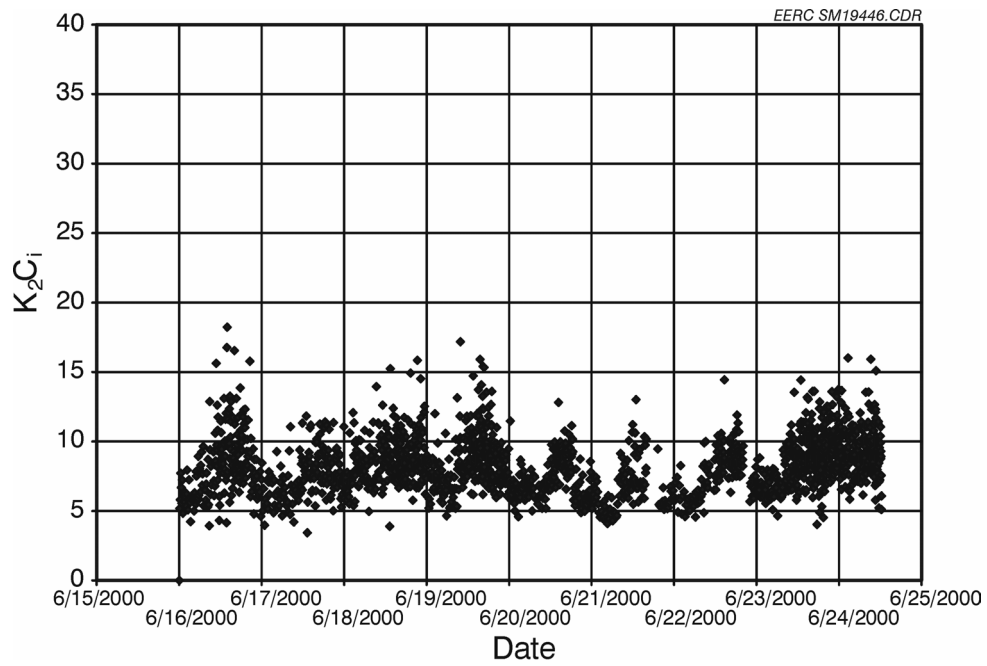


Figure 3.2-28. K_2C_i for June 16–24, 2000.

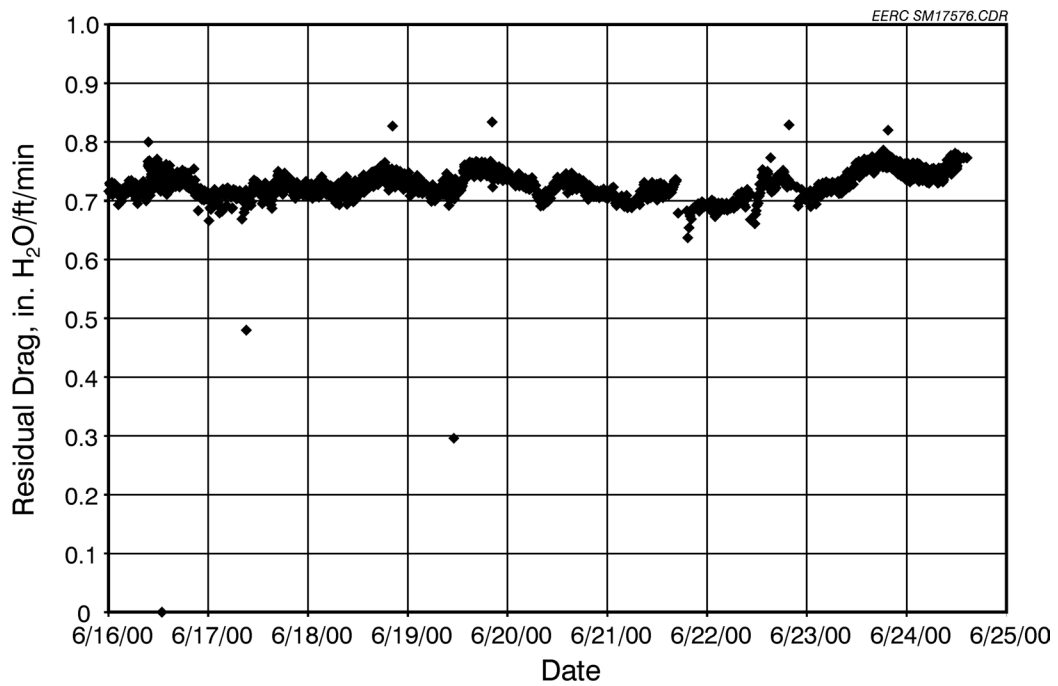


Figure 3.2-29. Residual drag for the period from June 16–24, 2000.

(Figure 3.2-27) during most of the testing period ranged from 2–15 min. The observed periodic variation of the bag-cleaning interval is due to the corresponding fluctuating flue gas temperature. The short bag-cleaning intervals are the results of deteriorated ESP performance and bag-cleaning ability, as indicated by the high K_2C_i (Figure 3.2-28) and residual drag (Figure 3.2-29). The K_2C_i varied from 5 to as high as over 25, indicating the ESP did not function efficiently to remove most of the fly ash, resulting in a high dust loading to the filter bags. When the bag-cleaning interval dropped below 7 min, the K_2C_i term increased substantially, suggesting that for acceptable AHPC performance, the bag-cleaning interval should not be allowed to go below a critical minimum. The residual drag for this period (Figure 3.2-29) was high, but stable, ranging from 0.68 to 0.78. The high residual drag implies that more fly ash was still sticking to the filter bags after pulse cleaning because of the more cohesive fly ash from Black Thunder coal compared to that from the Cordero Rojo Complex.

After several other unsuccessful short-term tests to see if the residual drag could be reduced with off-line rapping and off-line pulsing, the AHPC was shut down on June 27, 2000. Several bags were removed for inspection and replaced with new bags, and the rest of the bags were hand-cleaned with a soft brush. Most of the residual dust was easily removed by brushing except for small intermittent nodules which covered the entire bag surface. A possible cause of the nodules would be a condensation mist which may have occurred during the second start-up.

The AHPC was brought on-line again on June 28, 2000, at an A/C ratio of 10 ft/min (3.1 m/min) and a current of 55 mA. The pulse trigger pressure was set at 7.0 in. W.C. (1.7 kPa), and the AHPC operated in the multibank pulsing mode through July 5, 2000. The purpose of these tests was to further evaluate the trade-off between A/C ratio and pressure drop. The daily average pressure drop across the system and the corresponding residual drag from June 28, 2000, to July 5, 2000, are plotted in Figures 3.2-30 and 3.2-31. The average pressure drop started at 6.0 in. W.C. (1.5 kPa) on June 28, 2000, and by the next day climbed to 6.5 in. W.C. (1.6 kPa) where it remained steady through July 5, 2000. The residual drag demonstrated the same trend. Initially, it was at 0.3 in. W.C./ft/min (0.25 kPa/m/min), and after 2 days of operation, it reached

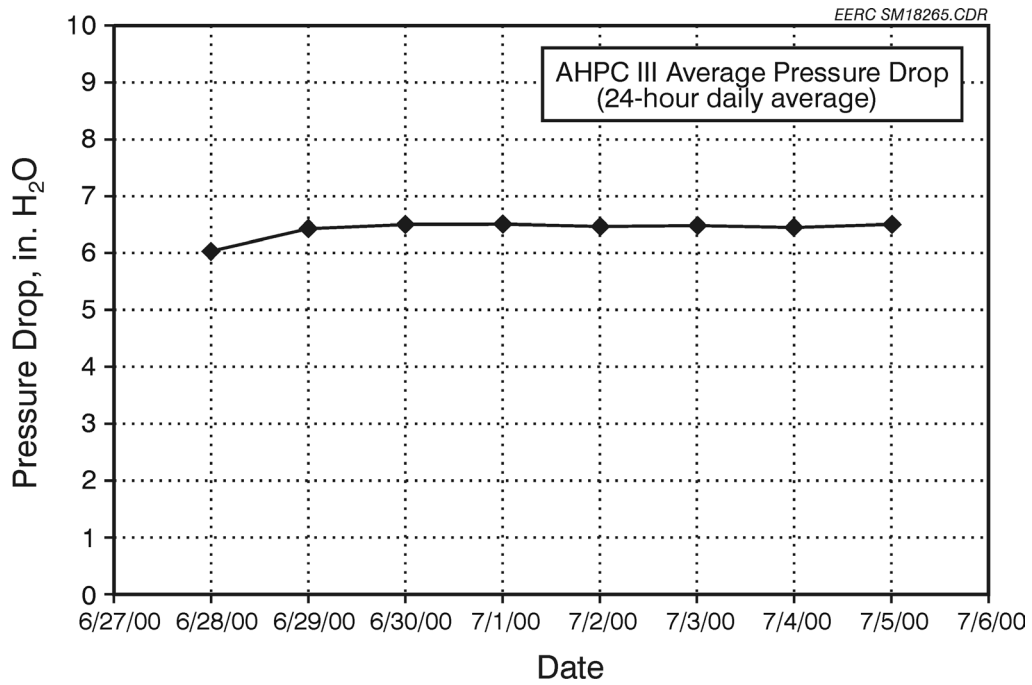


Figure 3.2-30. Daily average pressure drop for June 28 – July 5, 2000.

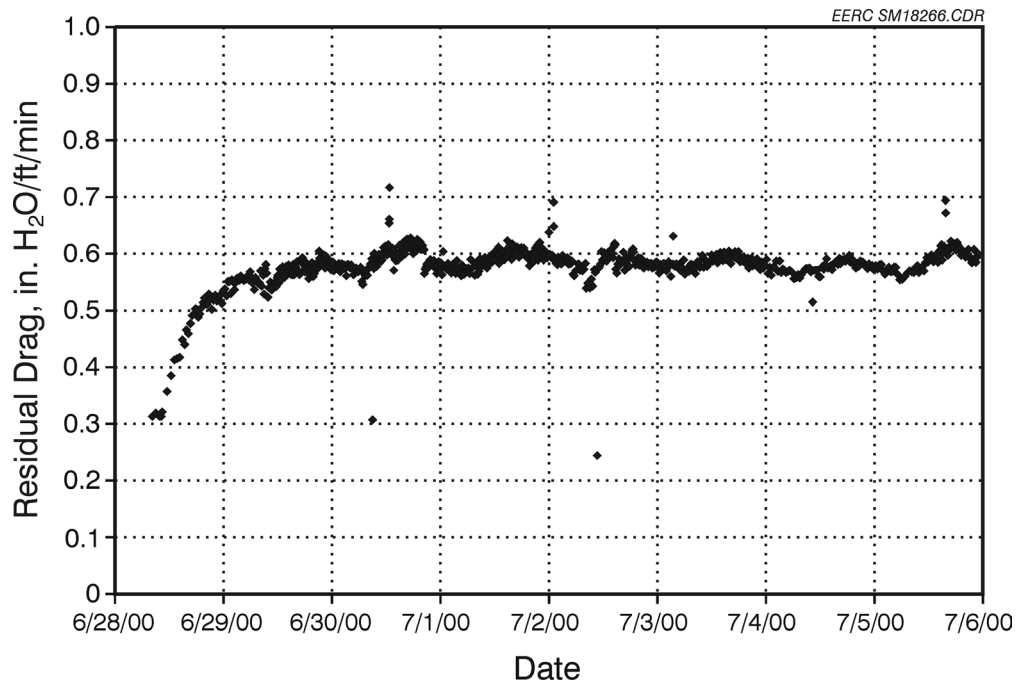


Figure 3.2-31. Residual drag for June 28 – July 5, 2000.

a steady condition ranging from 0.55 to 0.62 in W.C./ft/min (0.45–0.50 kPa/m/min). The observed residual drag was lower than that of the previous operation at 8.0 in. W.C. (2.0 kPa) pulse trigger pressure and 12 ft/min (3.7 m/min) A/C ratio, indicating an improvement in bag-cleaning ability under the reduced A/C ratio and pulse trigger pressure conditions. The bag-cleaning interval and the calculated K_2C_i are shown in Figures 3.2-32 and 3.2-33. The bag-cleaning interval, ranging from 5 to 36 min (Figure 3.2-32), is longer than 10 min for the majority of this testing period, which is reasonably acceptable for the AHPC performance. The average bag-cleaning interval during this test of 15.2 min was higher than the average 6.3 min observed in the previous tests (June 16–24, 2000), even though current was actually reduced from 66 mA to 55 mA. The periodic change of the bag-cleaning interval shown in Figure 3.2-32 was again caused by the fluctuating flue gas temperature during the day and night. The calculated K_2C_i (Figure 3.2-33) varied from 2.26 to 20 with an average of 6.87, lower than the 8.37 obtained in the previous test (June 16–24, 2000), proving better ESP performance.

The reasons for the improved AHPC performance, however, are complex. One of the possible reasons was the switch of coal, in early July, from Black Thunder to PRB coal from the Belle Ayr Mine, which produces ash easier to capture by the ESP. The exact trade-off between the pulse trigger pressure and the A/C ratio is also dependent on the coal. The results show it is possible to have lower average pressure drop and longer bag-cleaning intervals with a small decrease in A/C ratio for either coal type. Avoiding operation with continuous pulsing might have also been a factor.

3.2.3.3 Additional A/C Ratio and Pulse Trigger Pressure Experiments

Further short-term tests were carried out after July 6, 2000, to evaluate the combined effects of A/C and pulse trigger pressure drop on AHPC performance. The high voltage (HV) power was also shut down several times to investigate the relationship between bag-cleaning interval and K_2C_i .

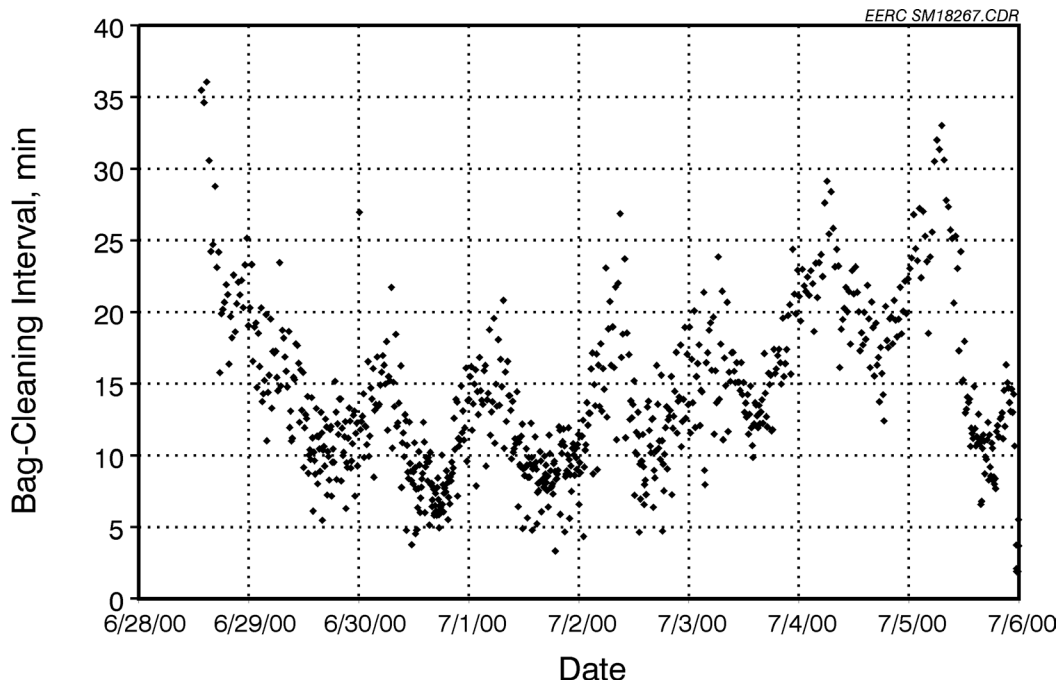


Figure 3.2-32. Bag-cleaning interval for June 28 – July 5, 2000.

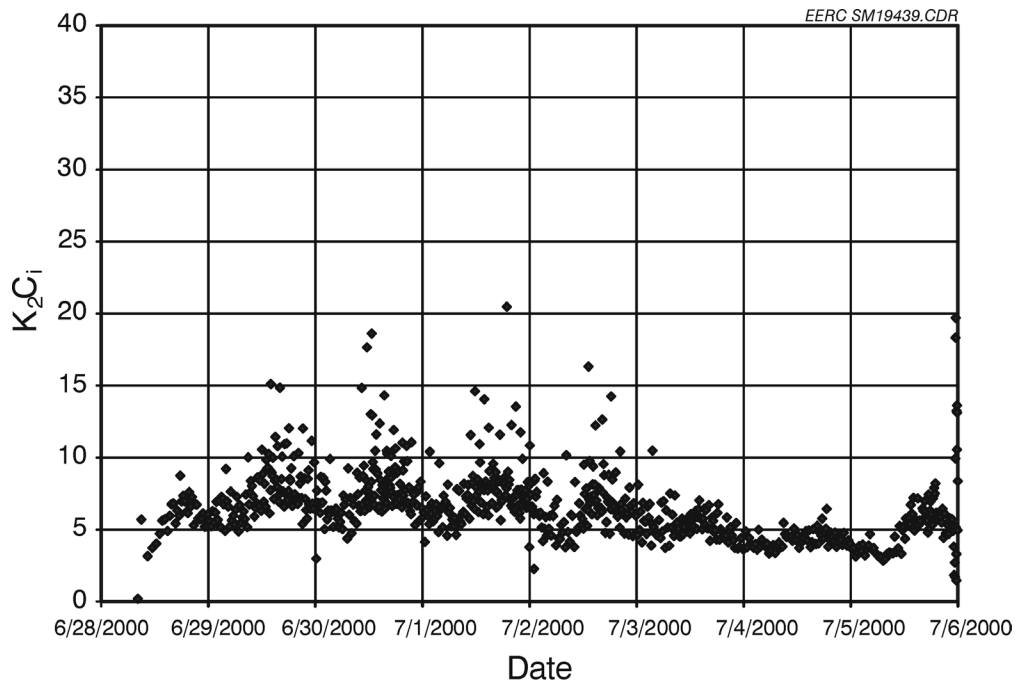


Figure 3.2-33. K_2C_i for June 28 – July 5, 2000.

During the test on July 7, 2000, the A/C ratio was maintained at 8 ft/min (2.44 m/min) until 9:00 p.m., when the A/C was set at 10 ft/min (3.1 m/min). The pulse trigger pressure was set to 5.5 in. W.C. (1.4 kPa) initially from 12:00 a.m. to 9:00 a.m. and then changed to 7.5 in. W.C. (1.9 kPa) for the rest of the test period. A summary of the testing matrix is given in Table 3.2-2.

TABLE 3.2-2

AHPC Settings on July 7, 2000			
Test Time	12:00 a.m. – 9:00 a.m.	9:00 a.m. – 9:00 p.m.	9:00 p.m. – 12:00 p.m.
Operational Setting			
A/C Ratio, ft/min (m/min)	8 (2.4)	8 (2.4)	10 (3.1)
Pulse Trigger Pressure, in. H ₂ O (kPa)	5.5 (1.4)	7.5 (1.9)	7.5 (1.9)
Current Set Point, mA	68	68	68

The pressure drop and bag-cleaning interval results are shown in Figures 3.2-34 and 3.2-35. The upper level of the pressure drop across the system (Figure 3.2-34) is determined by the pulse trigger pressure setting point, while the lower values represent the bag-cleaning ability. With the same A/C ratio of 8 ft/min (2.4 m/min), the bag-cleaning interval increased significantly from around 20 to 80–100 min when the pulse trigger pressure was elevated from 5.5 in. W.C. (1.4 kPa) to 7.5 in. W.C. (1.9 kPa). The observed short bag-cleaning interval of 5–7 min (9:00 a.m.–9:30 a.m.) was due to the shutdown of the SIR HV power supply at that time, demonstrating that ESP performance is very critical to AHPC operation. When the A/C ratio was increased to 10 ft/min (3.1 m/min) at 9:00 p.m., while the pulse trigger pressure was held constant, the bag-cleaning interval dropped to 11–13 min, indicating a strong influence of A/C ratio on AHPC performance. The calculated K_2C_i was plotted as a function of operating time in Figure 3.2-36. When the pulse trigger pressure was increased from 5.5 in. W.C. (1.4 kPa) to 7.5 in. W.C. (1.9 kPa) at a constant A/C ratio of 8 ft/min (2.4 m/min), the K_2C_i slightly decreased except for the test period when the HV power was shut off. To clarify the pulse trigger pressure effect on K_2C_i in more detail, the calculated K_2C_i is plotted as a function of pressure drop difference (before and after bag cleaning), as shown in Figure 3.2-37. The results demonstrated a weak dependence of K_2C_i on dP. When the SIR HV power supply was off, the AHPC was

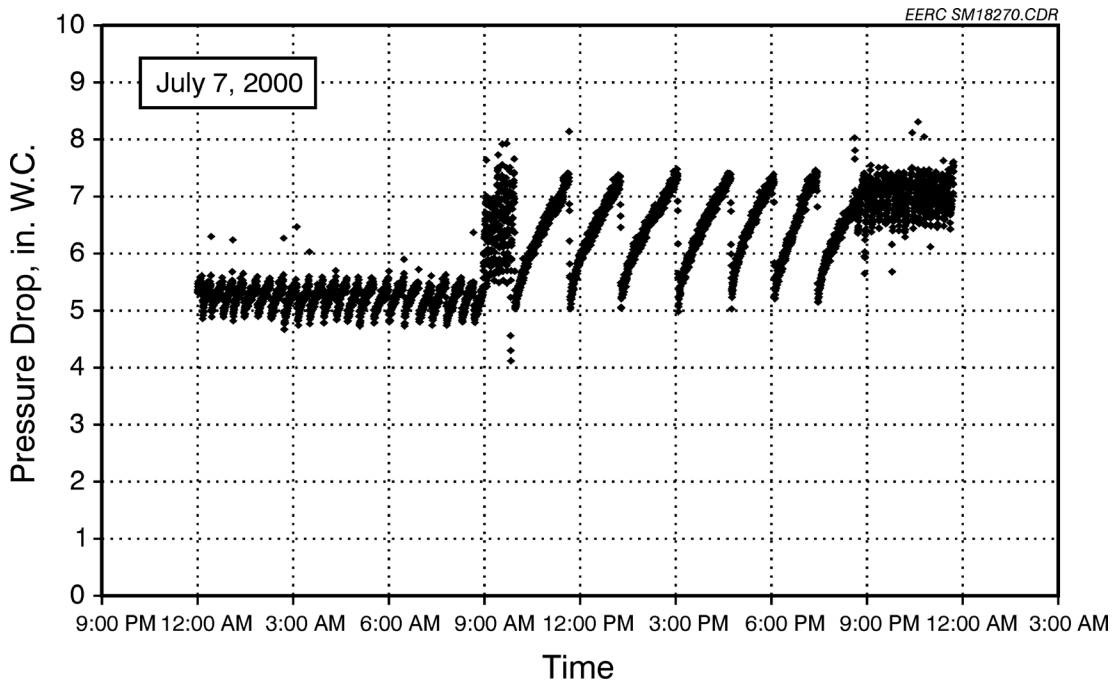


Figure 3.2-34. Pressure drop for July 7, 2000.

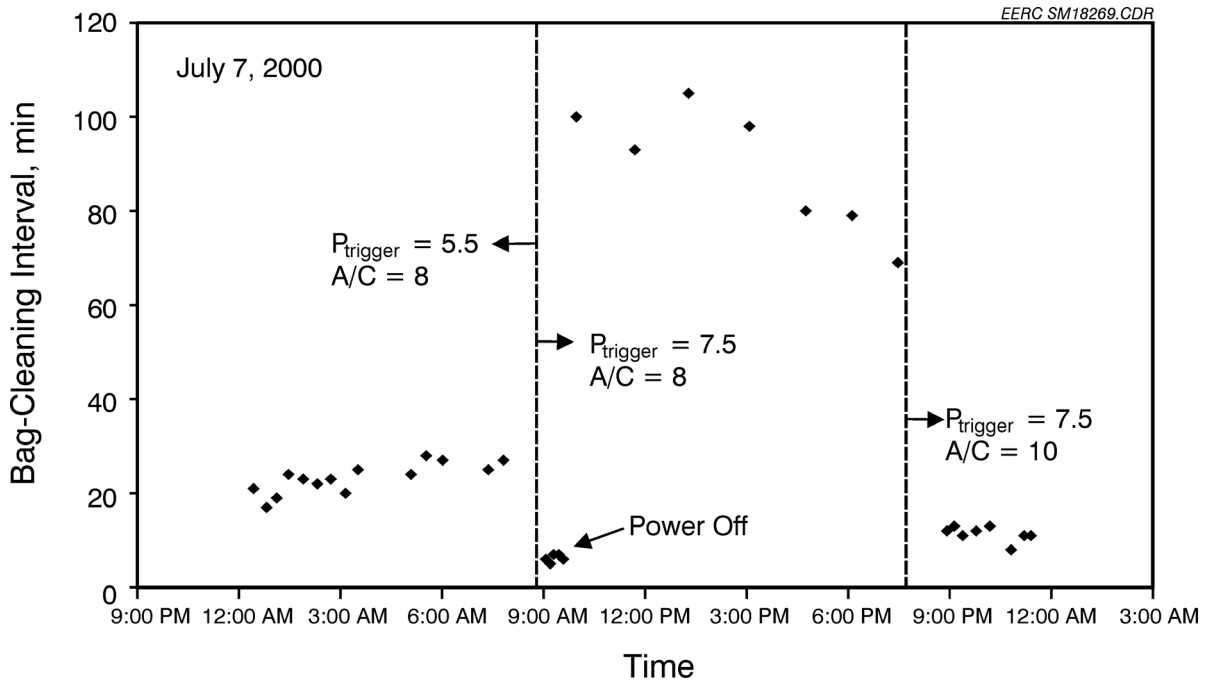


Figure 3.2-35. Bag-cleaning interval for July 7, 2000.

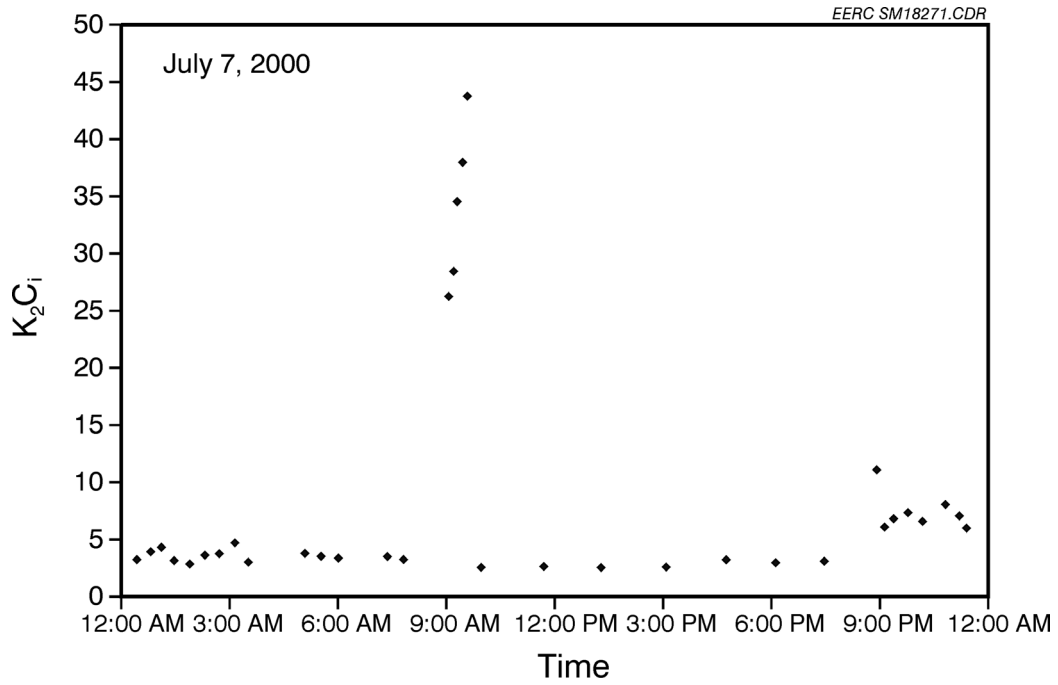


Figure 3.2-36. K_2C_i for July 7, 2000.

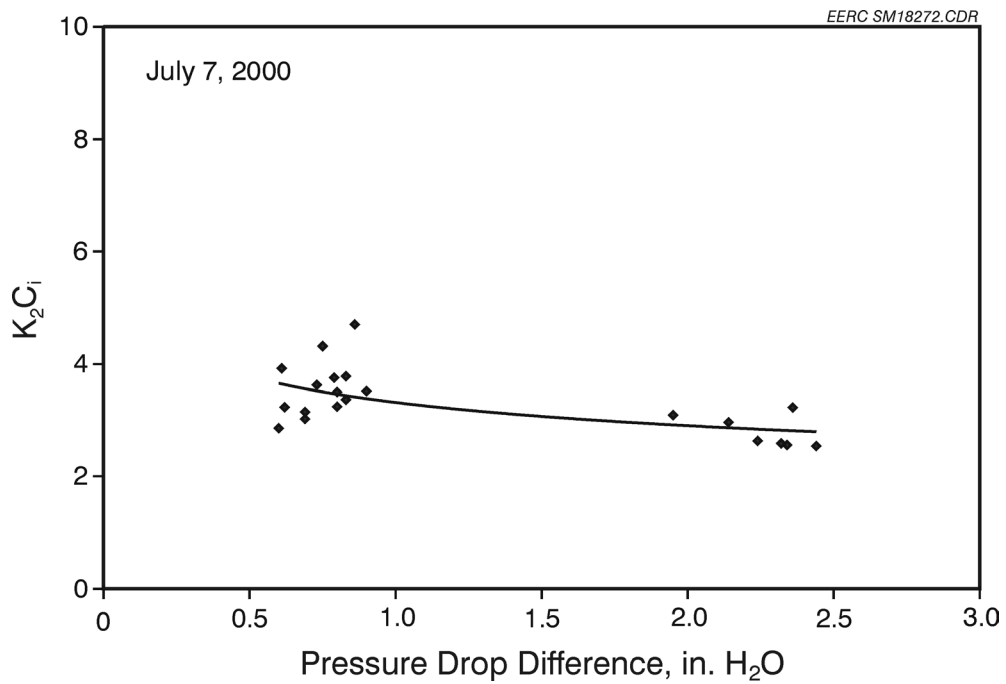


Figure 3.2-37. K_2C_i versus difference in pressure drop before and after bag cleaning for July 7, 2000.

operated in a conventional baghouse mode where all the fly ash was collected on the filter bags, resulting in a high K_2C_i of 45. By increasing the A/C ratio to 10 ft/min (3.1 m/min), K_2C_i was observed to increase in the range of 5–10, indicating the ESP performance deteriorated to some extent because of the reduced residence time of fly ash in the ESP zone.

On July 9, 2000, the A/C ratio (shown in Figure 3.2-38) was set at 6, 8, and 10 ft/min (2.1, 2.4, and 3.1 m/min), and the corresponding pulse trigger pressure was set at 7.5, 6.0, 7.5, and 6.5 in. W.C. (1.9, 1.5, 1.9, and 1.6 kPa) to examine their combined effect on bag-cleaning interval. The recorded pressure drop is plotted in Figure 3.2-39, showing a low A/C ratio causes a reduced pressure drop across the system. The bag-cleaning interval results are plotted in Figure 3.2-40. The bag-cleaning interval increased significantly from around 10 min at the A/C of 10 ft/min (3.1 m/min) and 7.5 in. W.C. (1.9 kPa) pulse trigger to 120 min at an A/C ratio of 6 ft/min (1.8 m/min) with a reduced pulse trigger pressure of 6 in. W.C. (1.5 kPa), demonstrating again the greater effect of A/C ratio on bag-cleaning interval than that of pulse trigger pressure. By increasing the A/C ratio to 8 ft/min (2.4 m/min) with an elevated pulse trigger pressure of

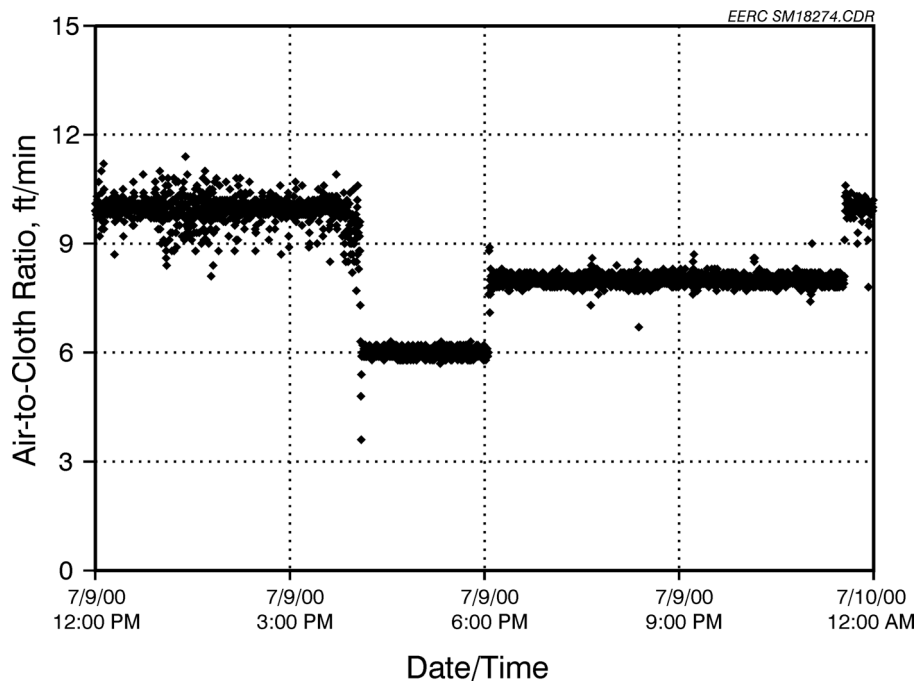


Figure 3.2-38. A/C ratio for July 9, 2000.

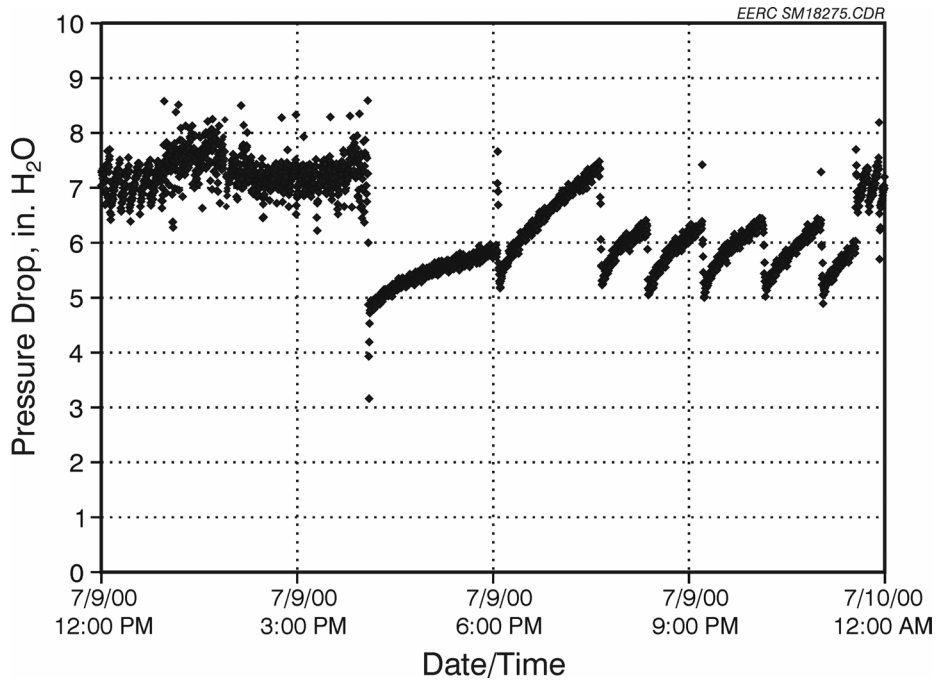


Figure 3.2-39. Pressure drop for July 9, 2000.

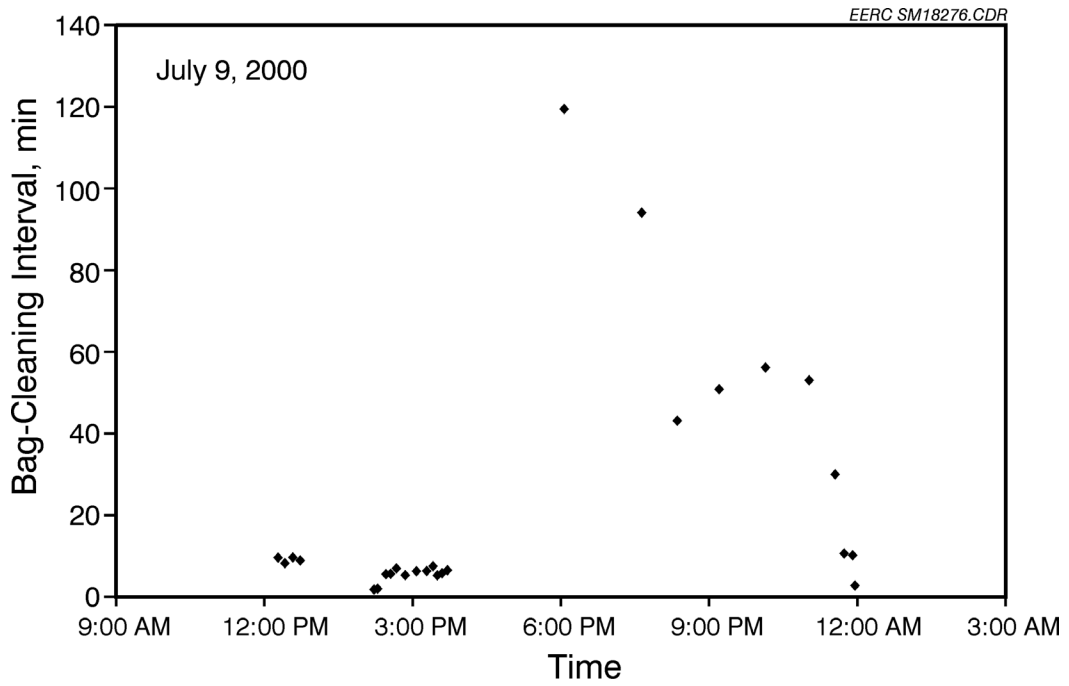


Figure 3.2-40. Bag-cleaning interval for July 9, 2000.

7.5 in W.C. (1.89 kPa), the interval was reduced to 100 min, and it was further decreased to 50–60 min when the pulse trigger was lowered to 6.5 in. W.C. (1.6 kPa) while the A/C ratio was held constant. The K_2C_i was calculated and plotted as a function of the bag-cleaning interval, as shown in Figure 3.2-41. The approximately inverse dependence of bag-cleaning interval on K_2C_i ($t \propto (K_2C_i)^{-0.55}$) is demonstrated.

3.2.4 Bag Analysis

GORE-NO STAT[®] filter bags were installed and precoated with the fly ash dust from the Big Stone Power Plant ESP prior to start-up of the AHPC Phase III testing on April 18, 2000. The filter bags contain an antistatic ePTFE fiber. The conductive felt fibers help to dissipate electrical charge buildup across the surface of the filter bags. A filter media that can dissipate electrical charge is desirable in the AHPC because of the presence of electrical charges on the dust or in the gas.

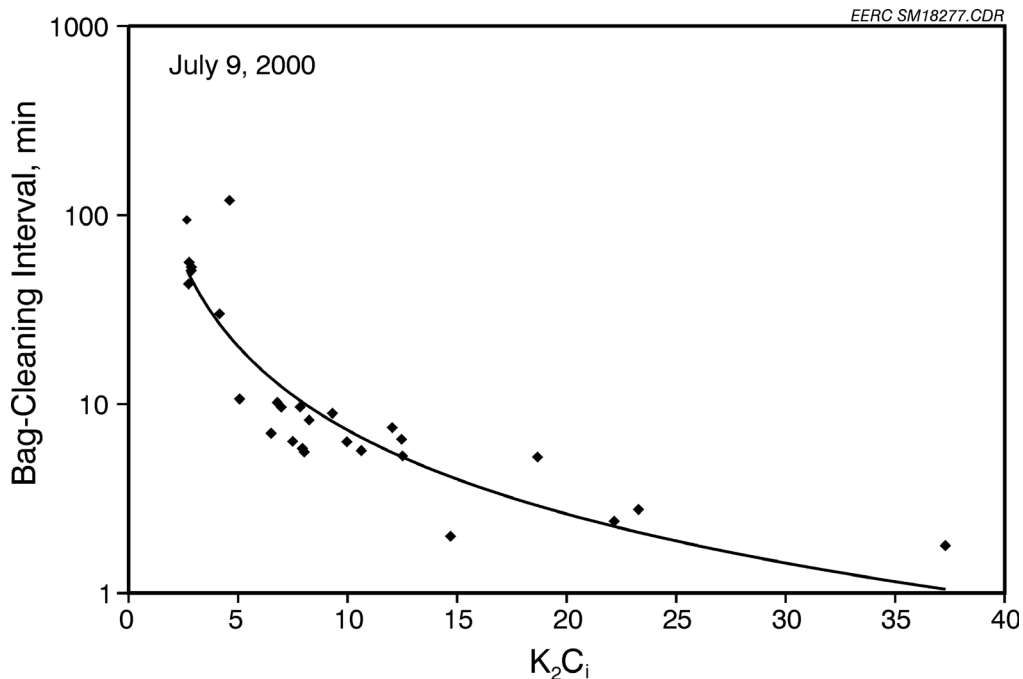


Figure 3.2-41. K_2C_i versus bag-cleaning interval for July 9, 2000.

The filter media is also required to withstand the high-temperature and corrosive conditions encountered in many coal-fired boiler fabric filter dust collectors. GORE-NO STAT[®] filter bag is chemically inert and can withstand continuous operating temperatures as high as 500EF (260EC). The ePTFE fibers have excellent chemical resistance to mineral and organic acids, alkalies, oxidizing agents, and organic solvents.

During the first 2 months, operating parameters were varied, and the power plant coal source changed a number of times. Several unscheduled maintenance outages and a planned annual outage subjected the AHPC to system upsets. The unscheduled Big Stone boiler shutdowns resulted in immediate loss of airflow and power to the AHPC, and the subsequent restarts may have exposed the bags to flue gas dew point excursions.

Seven filter bags were removed from the AHPC unit for inspection and analysis on June 27, 2000, after 1360 hr of operation. New filter bags replaced the ones removed in June. On July 21, 2000, additional filter bag inspection included one of the new bags that had been installed in June.

AHPC testing was stopped on May 5–8, 2000, for an unscheduled power plant outage, on May 17–30, 2000, for Big Stone's annual maintenance outage, and again on June 27, 2000, for filter bag inspection. The shutdown procedure followed for the maintenance outage and filter bag inspection included cleaning bags on-line and off-line to remove dust cake from the bag surface. Seven bags were returned to Gore for lab analysis from the following locations: Row 3/Bag 3 (R3B3), R3B6, R4B4, R4B7, R2B1, R2B2, and R1B5. For reference, the location of Row 1 is closest to the collector flue gas outlet pipe side, and Bag 1 is closest to the pulse system manifold and valve side.

3.2.4.1 Visual Analysis

All seven filter bags contained a thin layer of dust on the membrane surface, typical of most coal-fired boiler applications. The primary dust cake was easily brushed off and revealed a

membrane that looked white with 0.4- to 0.12-in. (10- to 3-mm)-diameter dust nodules interspersed on the membrane surface along the entire length and circumference of the filter bags. A larger concentration of nodules was found 7 to 10 in. (0.18 to 0.25 m) from the top and then from 24 in. (0.61 m) to the bottom of the filter bags. A photograph was taken of R2B2's surface after light brushing (see Figure 3.2-42) showing the nodules. Past experience has shown nodules are an indication that the filter bags were exposed to flue gas dew point excursions similar to what may have occurred during the unscheduled outage. Using fly ash from the new coal types as a precoat may have contributed to the formation of the nodules. The hygroscopic properties of fly ash vary with its properties and type. When exposed to moisture during flue gas temperature excursions, nodules can form on the filter bags. In the past, this problem was not seen on the previously used coal. After this filter bag evaluation, new procedures were implemented to correct the problem. The new procedure requires precoating the bags with crushed limestone prior to start-up. The limestone acts to absorb the moisture and, unlike some fly ash, does not form a cementitious nodule adhering to the surface of the bag. After the filter bag is cleaned, the limestone is removed, and the bag resumes normal operation at the now-appropriate temperature and operating conditions.



Figure 3.2-42. R2B2 after brushing.

The filter bags were examined for membrane damage from sparking, high flue gas velocity abrasion, chemical/temperature degradation, and possible pulse-jet overcleaning. There was no indication of membrane damage from abrasion, temperature, or chemical attack.

On most of the filter bags inspected, membrane damage was observed along two areas of the filter bag that began 24 to 27 in. (0.61 to 0.69 m) from the top of the bag and extended to the bottom of the bag. The majority of visual damage was located along the vertical cage wires that were adjacent to the position of the discharge electrodes. Typically, the damage occurred along four of the twelve cage wires, two groups of two on opposite sides of the filter bag that were closest to the discharge electrodes. The observations of small holes 0.02–0.08 in. (0.5–2 mm) in diameter and their location indicate the possibility of some type of electrically induced damage.

The bags in positions in the rear of the AHPC opposite the inlet had greater damage. The bags at the inlet had very little to no damage. The major operating difference between these two sections is the presence of extreme back corona from the collecting plates in the back of the AHPC because of heavy deposits of dust on the plates from ineffective cleaning or rapping of the plates.

The location of the damage close to the discharge electrodes indicates that back corona may have occurred between the discharge electrodes and filter bags. During testing, numerous visual observations through the site ports were made during both daytime and nighttime hours of the interior of the AHPC to evaluate discharge electrode corona intensity and collecting plate back corona intensity and location. Several engineers and operators observed electrode corona discharge toward the plate and back corona at several locations on the plate. No sparking to or back corona from the filter bags was observed. The conductive felt is designed to dissipate the charge buildup on the surface of the bags as well as keep the filter media conductive and reduce any voltage drop across it. Since the membrane damage occurred along the cage wires directly opposite the discharge electrodes and no sparking to the bags was observed, back corona is the suspected cause of the damage. However, the lack of visibility of back corona from the bags indicates the back corona may be very weak, yet possibly able to damage the bags.

On July 21, 2000, AHPC operation was idled to remove and inspect R4B7, which had been installed on June 26, 2000. The filter bag after 670 hr of operation had a thin layer of dust present that was easily brushed off. Similar observations were made on this bag as on the aforementioned bags. Membrane damage was observed in the middle and bottom of the bag along the vertical cage wires closest to the discharge electrodes. At the bottom, some membrane damage occurred between the cage wires. There was no membrane damage in the top 28 in. (0.71 m) of the filter bag. This is another important point. While the discharge electrode masts start at a point 10 in. (0.25 m) below the tube sheet, the directional corona discharge tabs of the electrodes start at a point 28 in. (0.71 m) below the tube sheet in the exact vertical location the bag damaged started. This suggests that the bag damage is related to the corona discharge location and possible electric field effects as the dust is charged and collected on the plate just opposite of the bags.

3.2.4.2 Media Analysis

Laboratory analysis of the chemical and elemental material properties of the damaged membrane areas was carried out on two of the filter bags along with a brand new one for comparison purposes. R3B6's membrane surface was analyzed at the top and along a vertical cage wire. The results indicate the remaining dust on the membrane surface is made up of inorganic sulfate, aluminum, calcium, magnesium, sodium, and silicon which would all be expected in fly ash. The R2B1 surface was also analyzed at the middle and on the cuff bottom where a small portion of the cuff was blackened. The media analysis reveals a breakdown in the chemical structure of the ePTFE membrane at the location where the damage is noted. This is usually due to high temperatures. Because the damage was localized on the media, the effects are not the result of flue gas temperature excursions. The media breakdown is likely the result of electrical spark or back corona-induced high-temperature effects. The small areas of damage localized near the cage wires did not result in evidence of increased emissions as indicated by the spotless condition of the clean air plenum when the bags were removed.

The changes in the design of the AHPC from Phase II to Phase III included new discharge electrodes, new plates, smaller spacing between the bags, and discharge electrodes. One or several of these may have contributed to the media damage.

3.2.4.3 Dimensional Analysis

The flat width of the bags was 9.02 to 9.21 in. (0.229 to 0.234 m) as measured in the lab after 8 weeks of operation. The bag width of new bags was measured as 9.02 in. (0.229 m). All the bags were cut and manufactured to the identical flat-width specifications. The bags maintained their dimensional stability during the 8 weeks of operation.

3.2.4.4 Air Permeability Analysis

The air permeability analysis of the AHPC filter bag media was performed in the lab using the Frazierometer. This device measures the amount of air that flows through a flat sample of media 3.5 in. (89 mm) in diameter and correlates it to a Frazier number. The Frazier number describes the volume of air (cfm) passing through 1 square foot of media at a differential pressure of 0.5 in. W.C. (0.125 kPa). A value of 1.0 Frazier, which equals 1 cfm/ft² at 0.5 in. W.C. (0.125 kPa). Canceling sq² units; Frazier number units are expressed as ft/min at 0.5 in. W.C. (0.125 kPa).

Samples of the AHPC filter bag media were cut from the top, middle, and bottom bag locations. The sample size was 5 in. (127 mm) in vertical bag length direction along the entire circumference of the bag. This enabled three measurements to be taken per bag location. The test produces a total of nine data points for each filter bag. A sample is tested for permeability in the condition it was received from the field application and labeled (as received). The nine readings are then averaged to create a bag permeability number.

Additional testing of the same samples is completed to determine the permeability condition of the membrane. A very soft brush is used to lightly remove the dust particles on the

surface of the membrane. Care is taken to prevent brushing the dust into the membrane or smearing the dust cake across the surface. The permeability of the samples is tested to make sure the test heads match up exactly with the test area previously measured. An average of the nine measurements is compared to the new permeability of the media for changes in condition and as an indicator for performance.

The data from the seven bags are displayed in Table 3.2-3. As a baseline, the new Frazier number of the media used in Phase III tests is within the range of 4.0 to 8.0 ft/min (1.2 to 2.4 m/min) at 0.5 in. W.C. (0.125 kPa). The as-received media appeared to retain much of the dust cake that was present during bag removal. The average as-received Frazier number was 2.42 after 8 weeks (1360 hr) of operation at a 12 ft/min (3.7 m/min) A/C ratio. After brushing, the average Frazier number was 6.57. The after-brushing Frazier number is within the range of the new media permeability. This indicates the membrane is capturing the particles on the surface of the media while retaining most of its original permeability.

The air permeability analysis of the AHPC Filter Bag R4B7 after 670 hr of operation was performed in the lab using the Frazierometer. The identical procedure for the time period of April to June was followed (see Table 3.2-3). The average as-received Frazier number for R4B7 was 2.22 and, after brushing, 5.44.

TABLE 3.2-3

Filter Media Permeability as Measured in Lab				
Time Period Bags in Operation (2000)	Hours of Operation	Bag Position	As-Received Average of Nine Data Points, ft/min at 0.5 in. H ₂ O	After-Brushing Average of Nine Data Points, ft/min at 0.5 in. H ₂ O
April 18 to June 26	1360	R3B3	2.48	5.82
April 18 to June 26	1360	R3B6	2.86	5.91
April 18 to June 26	1360	R4B4	1.77	4.37
April 18 to June 26	1360	R4B7	1.53	5.61
April 18 to June 26	1360	R2B1	2.33	4.78
April 18 to June 26	1360	R1B5	2.82	5.92
April 18 to June 26	1360	R2B2	3.17	7.00
		Average	2.42	6.57
June 26 to July 21	670	R4B7	2.22	5.44

3.2.4.5 Mechanical Strength Analysis

A Mullen Burst test was run on Filter Bag R4B7 after 670 hr of operation. The sample was removed from the center of the filter bag to determine if any weakening of the bag had occurred. The test gradually applies increasing pressure behind the filter bag sample until the test unit's rubber diaphragm penetrates the sample. The sample burst at 1000 psi (6895 kPa), indicating no chemical or thermal attack had occurred. The Mullen Burst strength for a new bag typically falls in the range of 500 to 1000 psi (3447 to 6895 kPa).

3.2.4.6 Summary of Bag Evaluation

- The filter bags retained permeability and recovered from system upsets, including switches to different coal sources.
- The bags retained their dimensional stability and mechanical strength.
- The damage to the membrane was due to electrical effects on the bags. The change in components and spacing may have contributed to these effects.

3.2.5 *Fly Ash Resistivity Analysis*

Three different coals were burned at the Big Stone Power Plant in summer 2000. The Big Stone Power Plant burned Cordero Rojo Complex during April and May and switched to Black Thunder in June and Belle Ayr in July. The coal usage schedule and coal analysis results for the three coals are listed in Table 3.2-4. The varying coal usage resulted in challenging operating conditions for the AHPC system, such as variation of fly ash resistivity and particle size. Among these parameters, sodium content in coal is critical to AHPC performance, since a higher sodium content in the coal correlates with lower fly ash resistivity.

TABLE 3.2-4

Coal Usage Schedule and Analysis Results			
	Cordero Rojo	Black Thunder	Belle Ayr
Time	April–May	June	July
Moisture, %, as received	29.4	28.2	29.5
Ash, %, as received	5.86	4.97	4.37
Btu/lb, %, as received	8423	8721	8621
Sulfur, %, as received	0.32	0.31	0.29
NaO, %, as received	1.22	1.39	1.42

The fly ash samples were collected during the tests and analyzed for electric resistivity under a controlled 11% moisture condition, a normal moisture content in the flue gas from Belle Ayr. The results are plotted as a function of testing temperature and shown in Figure 3.2-43. The fly ash resistivity ranged from 4 to 8×10^{11} ohm-cm over the operating temperature from 250EF to 300EF (121E to 149EC), the normal operating temperature for the AHPC. This resistivity range is high enough to cause back corona and limit ESP performance. The fly ash from Black Thunder coal has a relatively lower resistivity (but still high enough to limit ESP performance) than that from the Cordero Rojo Complex, which is in agreement with the sodium content in the raw coals. Also, considering the more cohesive characteristics of the fly ash from Black Thunder than the ash from either the Cordero Rojo Complex or Belle Ayr, the Black Thunder coal appears to be more difficult to deal with for AHPC operation. The high resistivity of the fly ash caused back corona observed through the sight ports on the plates near the back wall of the AHPC (opposite the inlet side) for all of the testing. However, back corona was not observed on the bags. For most of the tests, the sparking was minimal, typically less than one spark per minute. This implies that even better performance could be achieved by increasing the current limit and subsequent ESP power for lower-resistivity coals.

No outlet dust-loading measurements were conducted at this time, but based on the pristine clean air plenum when several bags were pulled for inspection at the end of June, the fine-

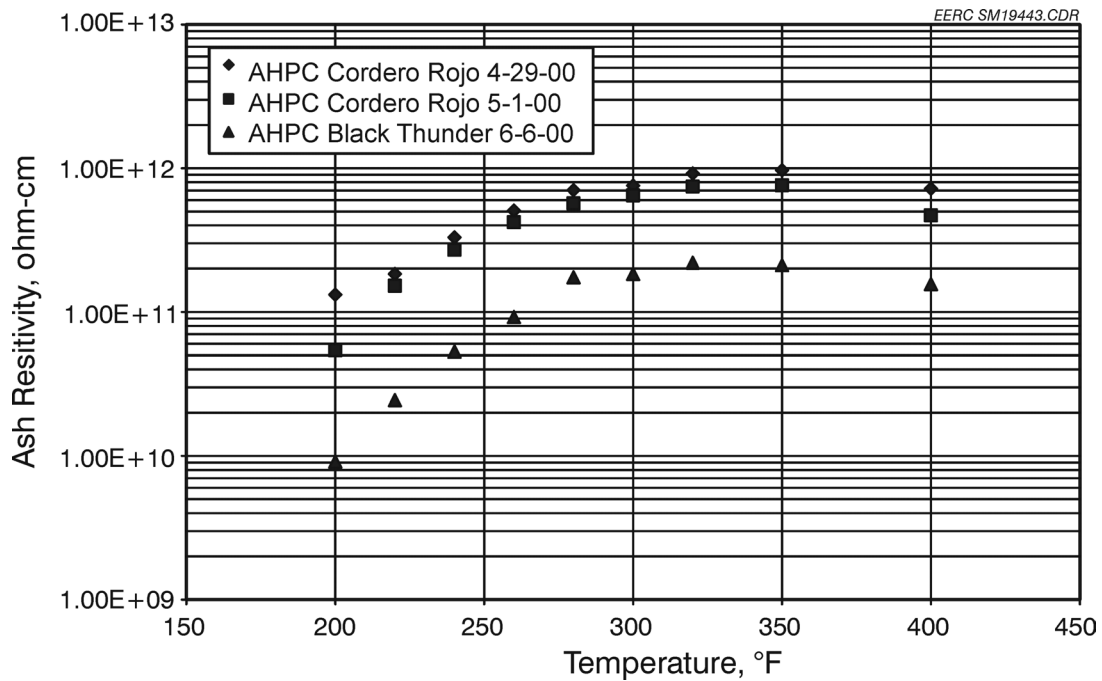


Figure 3.2-43. Fly ash resistivity of AHPC hopper ash samples for Cordero Rojo complex and Black Thunder coals.

particle collection efficiency was likely well above 99.99%, similar to actual measurements taken in 1999 from the Phase II testing and later measurements taken in Phase III.

3.2.6 Summary for April–July 2000 Testing

Except for part of the period in June, AHPC performance in summer 2000 was highly successful. The results show the AHPC unit functioned well according to theoretical expectations under significantly closer bag row spacing and bag-to-electrode spacing. Bag-cleaning interval, residual drag, and K_2C_i were all acceptable. However, further studies were needed to find a way to protect the filter bags without compromising overall AHPC performance.

3.3 AHPC Pilot- and Bench-Scale Studies at the EERC (August – December 2000)

3.3.1 Pilot-Scale Cold-Flow Tests at the EERC

The filter bag damage observed in the field tests summer 2000 was believed to be electrically induced. Consequently, pilot-scale experiments were carried out at the EERC to investigate the interactions between electrostatics and the filter bags under different operating conditions. The 200-acfm (5.7-m³/min) AHPC was first operated under cold-flow conditions without fly ash. The current to bags was measured for the six different types of filter bags combined with various electrodes and geometry alignment. The experimental parameters tested are summarized below:

Electrode type: EERC, ELEX, ENELCO 3-mast, ENELCO 2-mast, pipe

Bag type: GORE-TEX[®] felt filter bag/GORE-TEX[®] membrane (nonconductive bag, nonconductive membrane [NBNM])
GORE-TEX[®] felt filter bag/GORE-TEX[®] antistatic membrane (nonconductive bag, conductive membrane [NBCM])
GORE-NO STAT[®] filter bags (GORE-TEX[®] membrane/GORE-TEX[®] felt) (conductive bag, nonconductive membrane [CBNM])
GORE-NO STAT[®] filter bag (GORE-TEX[®] antistatic membrane/GORE-TEX[®] felt) (conductive bag, conductive membrane [CBCM])
SUPERFLEX[®] filter bags
RYTON[®] felt (no membrane)

Plate spacing: 600, 700, 800 mm

Spacing ratio: 1.00, 1.25, 1.65, 2.00

Grounded grid: 2-wire grid, 3-wire grid, diamond mesh

A total of five different electrodes were used in the cold-flow test to examine their effects on current to the bags. Detailed information about these electrodes is listed in Table 3.3-1.

TABLE 3.3-1

Electrode Type and Discharge Points				
Electrode Type	Spacing Between Electrode Masts, cm	Electrodes Used per Side	Discharge Points per Electrode	Total Discharge Points
EERC	10	7	34	476
ELEX	38	2	16	64
ENELCO 2-mast	19	2	22	88
ENELCO 3-mast	38	3	22	132
Pipe	19	3	0	0

Because of more discharge points on the electrodes (listed in Table 3.3-1), it is expected that the EERC electrodes would provide the highest corona current among the five electrodes under the same applied voltage.

The GORE bags were evaluated for their ability to dissipate electrical charge buildup on the filter surface. They were tested in the cold-flow tests to systematically investigate their responses under various operating conditions.

A number called the “spacing ratio” was created to compare the distances and position of the discharge electrode relative to the filter bag and collecting plate. The ratio is equal to the distance of the bag to the electrode divided by the distance of the electrode to the plate. By adjusting the electrode position between the filter bags and the collection plates, the current to bags was measured under different spacing ratios, ranging from 1.00 to 2.00, to examine the geometric alignment effect on bag current.

In order to suppress the back corona observed on the bag surface, metal-grounded grids were installed between the bags and electrodes to intercept the ion current flowing toward the filter bags and reduce the electric field around the bags. Three different types of grounded grids, called 2-wire, 3-wire, and diamond mesh, were initially tested. The 2-wire grid consisted of two

vertical wires, 0.12 in. (3 mm) in diameter, spaced 2.36 in. (60 mm) apart in front of each filter bag. The total number of wires per bag side was eight. These were placed 0.98 in. (25 mm) from the bag surface. The 3-wire was similar, except with three wires in front of each bag. The diamond mesh was a diamond pattern plate grid of expanded metal with a diamond hole size of 0.79 in × 1.18 in (20 mm × 30 mm). Each plate was positioned 1.18 in. (30 mm) from the bag's surface between the bags and the discharge electrodes.

The variables were the measurement of the electrical current flow through the bags, cages, and the collecting plates and the observations of back corona. The cages, bags, and collecting plates were isolated from grounded points, and each cage and plate had an independent ground wire.

A negative-polarity HV power supply, capable of producing 10 mA at up to 100 kV, was used to apply negative HV to the discharge electrodes. Typically, the 10-mA current limit was reached between 60 and 75 kV. The ground wires connected to each filter cage and collecting plate traveled through independent current meters to an earth ground. Six current readings were taken simultaneously: four from the bags and two from the collecting plates. The current meter always displayed a negative value and did not switch polarity when back corona was observed. All the measurements were totaled and compared to the current output by the HV power supply. Calculating the sum of the total bag current and the plate current as a percentage of the total current produced by the power supply yielded percentages of 92%–100% without a grounded grid, showing good current balances. Replicate tests were completed showing very accurate and repeatable results.

Observations of the corona discharge from the electrodes and the back corona from the filter bags were made through site ports of the AHPC pilot unit. All other entry points of light were eliminated so that total darkness was produced inside the AHPC chamber. After one's eyes adjusted to the darkness, observations of corona and back corona were noted.

3.3.1.1 Effect of Electrodes on V–I Characteristics and Current to Bags

Current to bags was measured at a fixed applied voltage of 55 kV for different electrodes such as EERC, ELEX, ENELCO-2-mast and ENELCO-3-mast with various plate-to-plate spacings and spacing ratios. The percentage of the bag current of the total corona current was calculated and plotted in Figures 3.3-1 and 3.3-2. The labels shown in the figures are test numbers (see Table 3.3-2). Figure 3.3-1 shows the percentage of bag current ranged from 0.2% to 16.9% (depending on the plate-to-plate spacing and spacing ratio) for the EERC electrode at the negative voltage of 55 kV. The percentage of bag current for ELEX electrode with negative voltage was as high as 43.8% at a plate-to-plate spacing of 23.6 in. (600 mm) with a spacing ratio of 1.25 and dramatically decreased to 0.1% by adjusting the spacing ratio to 2.0 and using a 2-wire grid. When applying a positive polarity power to the collection plates, both EERC and ELEX electrodes show a very low current level to the filter bags. The bag current percentages for ENELCO-2-mast and ENELCO-3-mast electrodes are shown in Figure 3.3-2 at 55 kV. Again, when negative voltage was applied on the electrodes, the percentage of bag current was varied from 18.9% to 0.2% for both the electrodes, depending on plate-to-plate spacing, spacing ratio, and the use of a grounded grid. The positive voltage on the collection plate also resulted in a low bag current percentage.

A series of experiments was then carried out to examine the correlations between applied voltage and corona current for the different type electrodes. Plate spacing was set to 23.6 in. (600 mm), and GORE-NO STAT[®] filter bags (GORE-TEX[®] membrane/GORE-TEX[®]felt) were used. A total of five electrode types were tested under the two different spacing ratios of 1.25 and 1.65. Total generated corona currents were plotted as a function of the applied voltage, shown in Figures 3.3-3 and 3.3-4. Under both the spacing ratios of 1.25 and 1.65, the EERC electrode produced the highest total corona current followed by ELEX, ENELCO-3-mast, and ENELCO-2-mast type electrodes at the same applied voltage. The corona current, for example, at the spacing ratio of 1.25 and the applied voltage of 60 kV was 9.77 mA for the EERC electrode and reduced to less than 8 mA for the other electrodes. The pipe electrodes produced a much lower corona current because of the absence of discharging points on the smooth pipe.

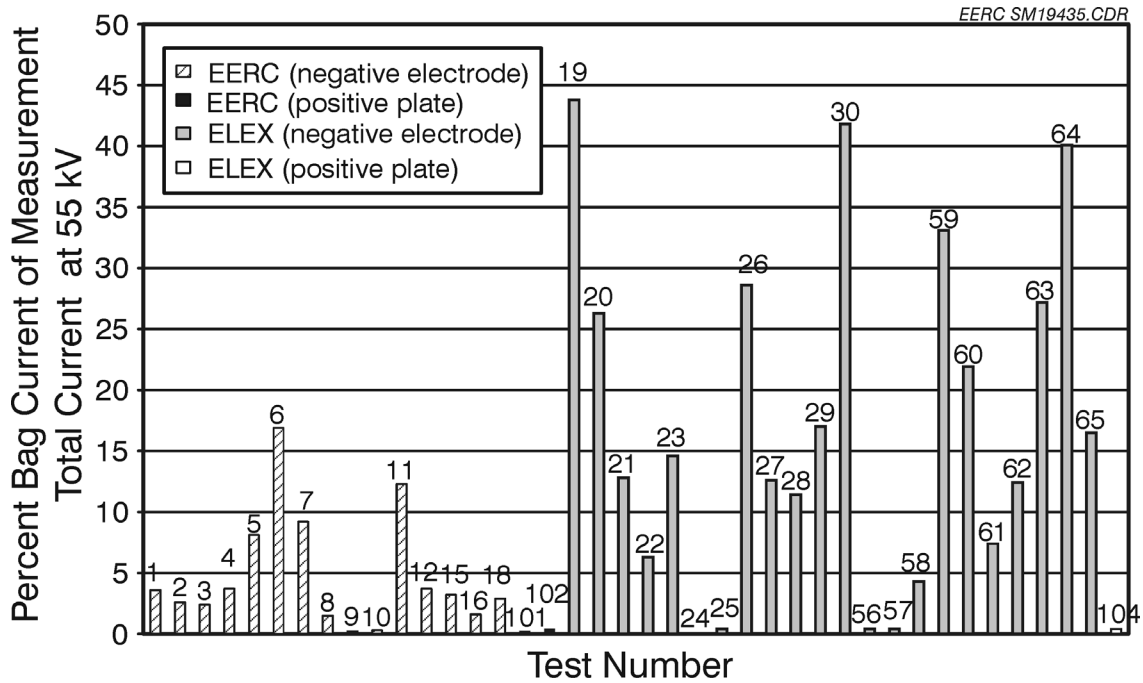


Figure 3.3-1. Percent bag current of measurement total current for EERC and ELEX electrodes.

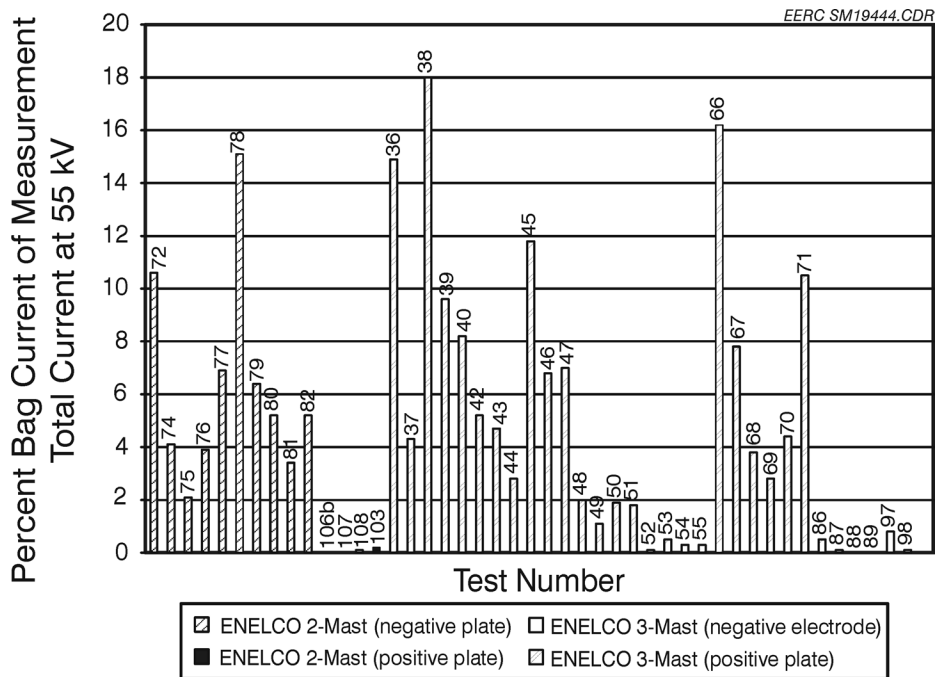


Figure 3.3-2. Percent bag current of measurement total current for ENELCO electrodes.

TABLE 3.3-2

Cold-Flow Electrode Tests

Test Number	Electrode	Grid	Total Bag Current at 55 kV, mA	Percent Bag Current of Measurement Total at 55 kV
1	EERC	None	0.1	3.6
2	EERC	None	0.07	2.6
3	EERC	None	0.07	2.4
4	EERC	None	0.11	3.7
5	EERC	None	0.17	8.1
6	EERC	None	0.3	16.9
7	EERC	2 wire	0.15	9.2
8	EERC	2 wire	0.04	1.5
9	EERC	2 wire	0.01	0.2
10	EERC	None	0.02	0.3
11	EERC	None	0.76	12.3
12	EERC	None	0.28	3.7
15	EERC	None	0.33	3.2
16	EERC	2 wire	0.17	1.6
18	EERC	2 wire	0.24	2.9
19	ELEX	None	2.52	43.8
20	ELEX	None	1.52	26.3
21	ELEX	2 wire	0.63	12.8
22	ELEX	2 wire	0.43	6.3
23	ELEX	None	1.09	14.6
24	ELEX	Diamond mesh	0.01	0.1
25	ELEX	Diamond mesh	0.01	0.4
26	ELEX	None	1.3	28.6
27	ELEX	None	0.93	12.6
28	ELEX	None	0.83	11.4
29	ELEX	None	1.33	17
30	ELEX	None	2.33	41.8
31	Pipe	None	0.15	22.8
32	Pipe	None	0.2	36.6
33	Pipe	None	0.09	32.8
34	Pipe	None	0.06	26.1
35	Pipe	Diamond mesh	0.0005	0.3
36	ENELCO 3-mast	None	0.84	14.9
37	ENELCO 3-mast	None	0.21	4.3
38	ENELCO 3-mast	None	1.06	18
39	ENELCO 3-mast	2 wire	0.52	9.6
40	ENELCO 3-mast	None	0.65	8.2
42	ENELCO 3-mast	None	0.21	5.2
43	ENELCO 3-mast	None	0.2	4.7
44	ENELCO 3-mast	None	0.15	2.8
45	ENELCO 3-mast	None	0.34	11.8
46	ENELCO 3-mast	None	0.18	6.8
47	ENELCO 3-mast	None	0.19	7
48	ENELCO 3-mast	None	0.11	2
49	ENELCO 3-mast	None	0.06	1.1
50	ENELCO 3-mast	3-5 wire	0.09	1.9
51	ENELCO 3-mast	3-5 wire	0.09	1.8

Cont. . . .

TABLE 3.3-2

Cold-Flow Electrode Tests (cont.)

Test Number	Electrode	Grid	Total Bag Current at 55 kV, mA	Percent Bag Current of Measurement Total at 55 kV
52	ENELCO 3-mast	3-5 wire	0.01	0.1
53	ENELCO 3-mast	3-5 wire	0.03	0.5
54	ENELCO 3-mast	3-5 wire	0.02	0.3
55	ENELCO 3-mast	3-5 wire	0.01	0.3
56	ELEX	3-5 wire	0.01	0.4
57	ELEX	3-5 wire	0.01	0.4
58	ELEX	3-5 wire	0.14	4.3
59	ELEX	None	1.11	33.1
60	ELEX	None	0.97	21.9
61	ELEX	None	0.5	7.4
62	ELEX	None	0.63	12.4
63	ELEX	None	1.69	27.2
64	ELEX	None	2.23	40.1
65	ELEX	None	1.23	16.5
66	ENELCO 3-mast	None	0.91	16.2
67	ENELCO 3-mast	None	0.58	7.8
68	ENELCO 3-mast	None	0.38	3.8
69	ENELCO 3-mast	None	0.27	2.8
70	ENELCO 3-mast	None	0.34	4.4
71	ENELCO 3-mast	None	0.55	10.5
72	ENELCO 2-mast	None	0.48	10.6
74	ENELCO 2-mast	None	0.25	4.1
75	ENELCO 2-mast	None	0.16	2.1
76	ENELCO 2-mast	None	0.31	3.9
77	ENELCO 2-mast	None	0.43	6.9
78	ENELCO 2-mast	None	0.72	15.1
79	ENELCO 2-mast	Pipe (3-mast)	0.28	6.4
80	ENELCO 2-mast	None	0.21	5.2
81	ENELCO 2-mast	None	0.14	3.4
82	ENELCO 2-mast	None	0.21	5.2
86	ENELCO 3-mast	None	0.02	0.5
87	ENELCO 3-mast	None	0.0024	0.1
88	ENELCO 3-mast	None	0	0
89	ENELCO 3-mast	None	0	0
97	ENELCO 3-mast (positive plate)	None	0.02	0.8
98	ENELCO 3-mast (positive plate)	None	0	0.1
99	Diamond plate (positive plate)	None	0	0
101	EERC (positive plate)	None	0.0009	0.2
102	EERC (positive plate)	None	0.01	0.4
103	ENELCO 2-mast (positive plate)	None	0.0043	0.2
104	ELEX (positive plate)	None	0.01	0.4
105	Vertical wire (positive plate)	None	0	0
106b	ENELCO 2-mast (positive plate)	None	0	0
107	ENELCO 2-mast (positive plate)	None	0	0
108	ENELCO 2-mast (positive plate)	None	0.0028	0.1

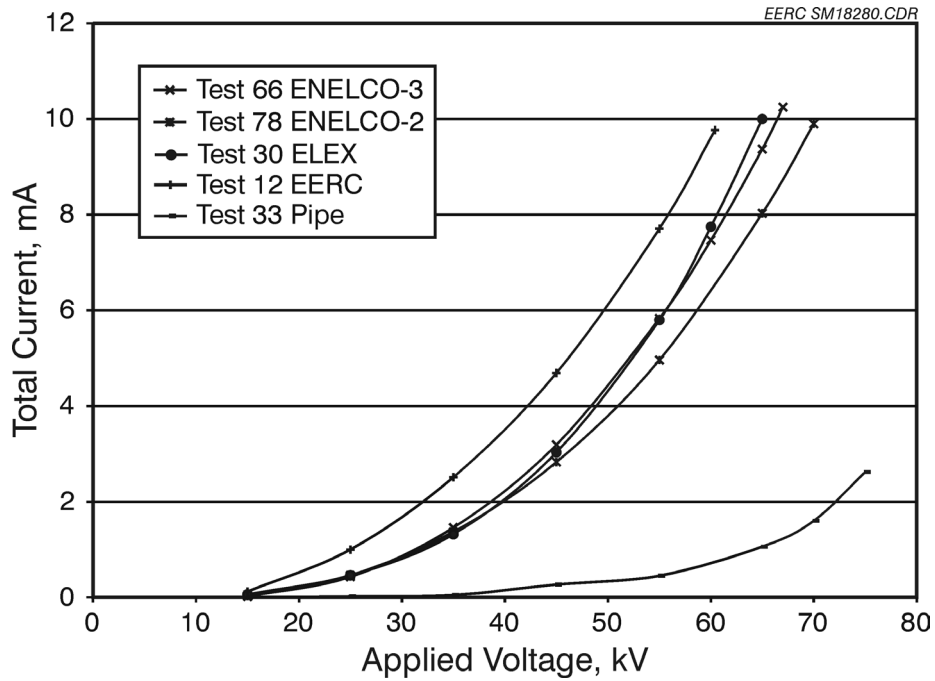


Figure 3.3-3. Effect of electrode on V-I characteristics (ratio - 1.25, plate spacing - 600 mm, bags - CBNM).

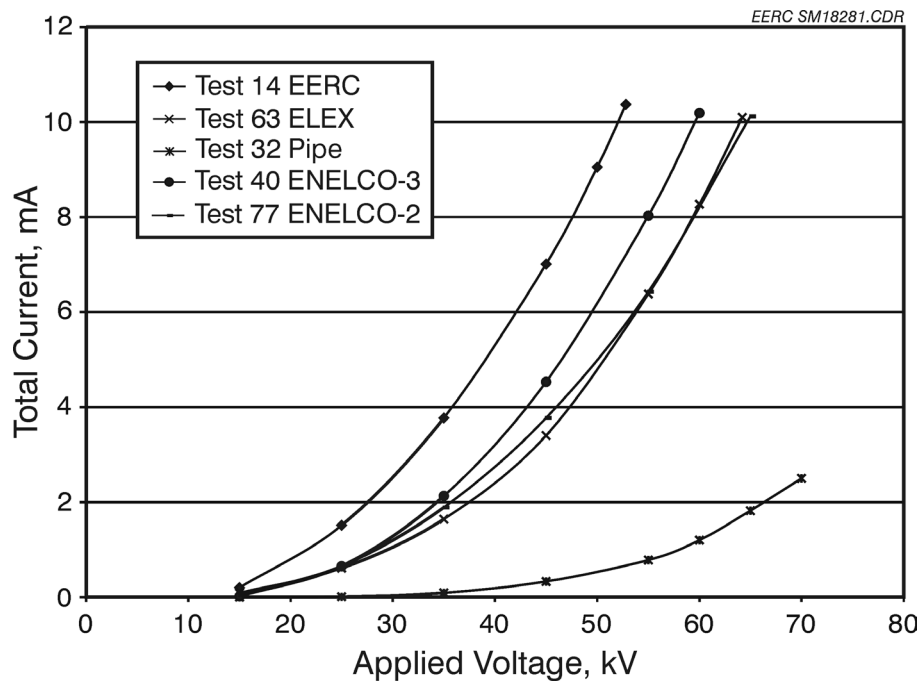


Figure 3.3-4. Effect of electrode on V-I characteristics (ratio - 1.65, plate spacing - 600 mm, bags - CBNM).

The current to bags was also measured at the same time for the two spacing ratios as shown in Figures 3.3-5 and 3.3-6. The ELEX electrode induced up to 3.38–4.5 mA current to the filter bags at the spacing ratios of 1.65 and 1.25 with an applied voltage of 65 kV, accounting for 48% of the total generated corona current. ENELCO-3-mast-type electrodes generated almost the same total current as that of ELEX under similar operating conditions (shown in Figures 3.3-3 and 3.3-4), but only around 22% of the total corona current reached the bags. The pipe electrodes had less than 0.5 mA current to bags at an applied voltage of 60 kV, but this was more than 50% of the total corona current generated. The EERC electrode demonstrated a low current to bags of 0.5 mA at an applied voltage of 60 kV, which was only 5.0% of the total corona current.

These experimental results indicated the EERC electrode was the best in terms of higher total corona current and lower current to bags, followed by the ENELCO-type electrodes which also had satisfactory results. The ELEX electrodes had a high total corona current yield, but a large portion of the current went to bags, which is more likely to create back corona on the filter bag surface. The pipe electrodes minimized current to the bags, but the total current was too low to use in the AHPC.

Experiments were then conducted to examine the effects of bag type, plate spacing, and spacing ratio on the current to the bags in the presence of different types of electrodes. The effectiveness of metal-grounded grids on suppression of the back corona on the filter bags was also investigated.

3.3.1.2 EERC Electrode Tests

The EERC electrode produced a high total corona current yield with a low level of current to bags. The EERC electrode was further examined in the following tests to determine the bag current under various conditions. The filter bags used were GORE-NO STAT[®] filter bags (GORE-TEX[®] membrane/GORE-TEX[®] felt).

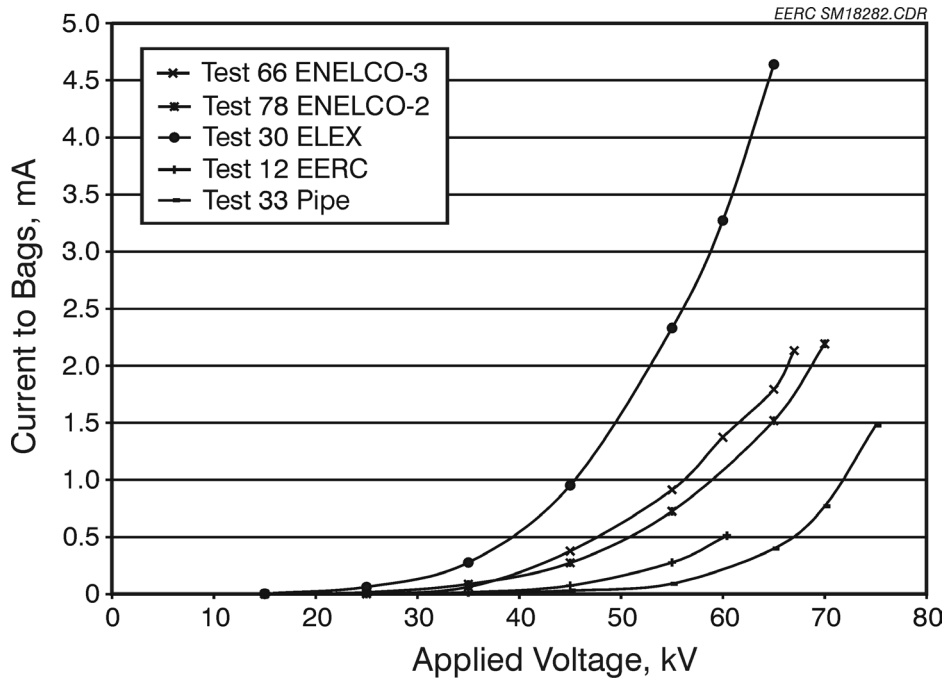


Figure 3.3-5. Effect of electrode on current to bags (ratio - 1.25, plate spacing - 600 mm, bags - CBNM).

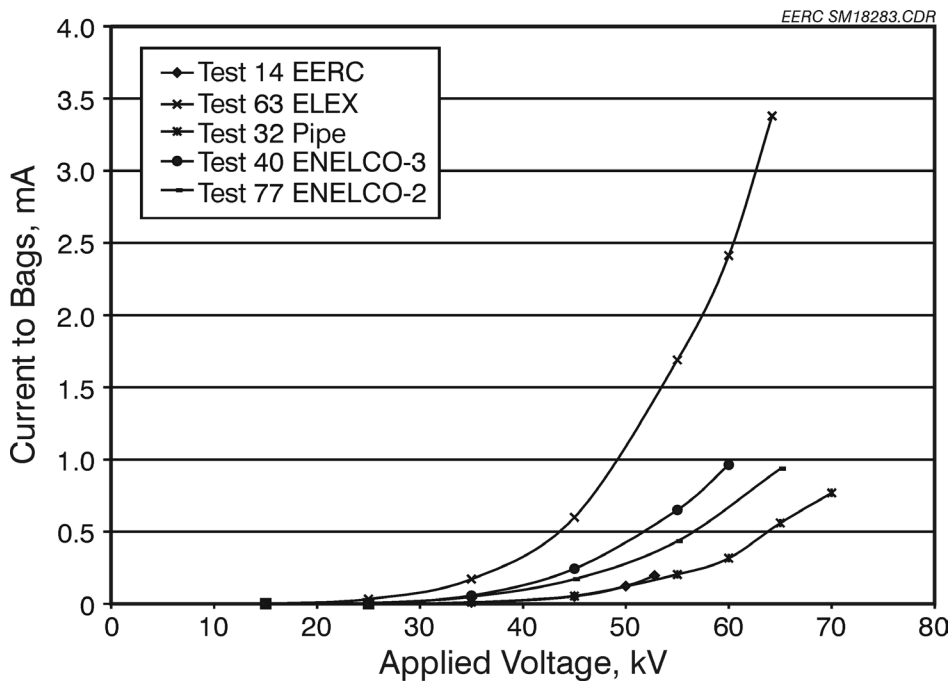


Figure 3.3-6. Effect of electrode on current to bags (ratio - 1.65, plate spacing - 600 mm, bags - CBNM).

3.3.1.2.1 Spacing Ratio Experiments

The relative position of the electrode between the filter bags and the collection plates is very critical for the corona current distribution within the AHPC chamber. The spacing ratio, (defined as the distance of the bag to the electrode divided by the distance of the electrode to the plate) was used to evaluate the effect of the position of the discharging electrode on the bag current. The higher the spacing ratio, the closer the electrodes were to the collection plates compared to the distance from the electrodes to the bags. The total current to the bags was measured as a function of the applied voltage under the various spacing ratios ranging from 1.00 to 2.00, and the results are plotted in Figure 3.3-7. The highest current to bags was observed for all the applied voltages at the spacing ratio of 1.00. The bag current decreased with increasing spacing ratios, as a result of the lower electric field existing in the space between the electrodes and the filter bags compared to that between the electrodes and the collection plate. The total current to the bags nearly dropped to zero when the spacing ratio was 2.00. However, with a spacing ratio of 2.00, part of the electric precipitation zone was sacrificed to achieve a lower current level to the bags, which would result in deteriorated AHPC performance.

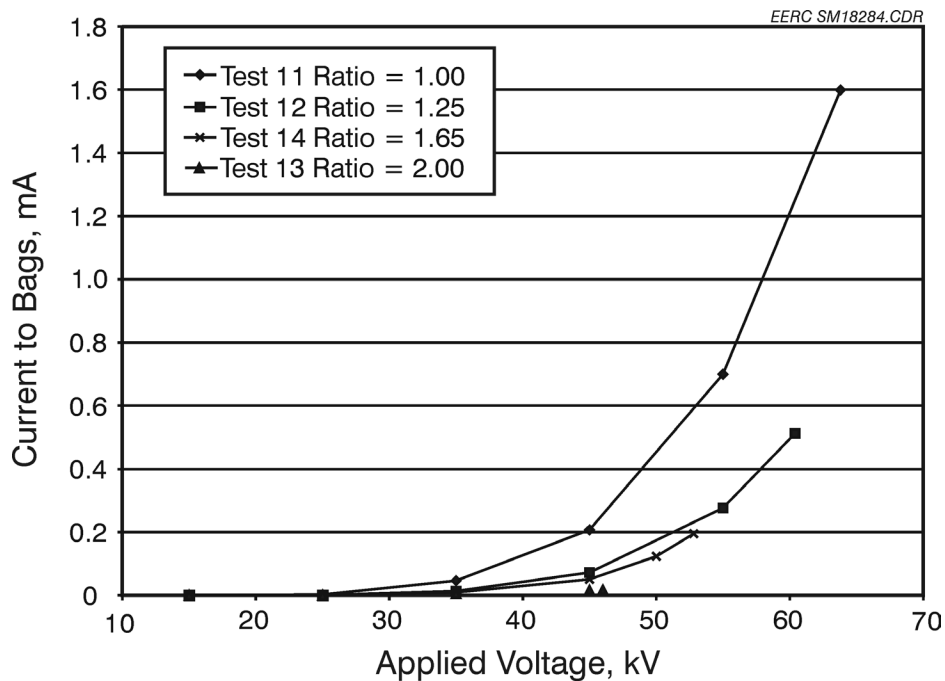


Figure 3.3-7. Effect of spacing ratio on bag current (EERC electrode, bags – CBNM, plate spacing – 600 mm).

3.3.1.2.2 Plate-Spacing Experiments

Another approach to reduce the current to the bags was increasing the plate spacing from 23.6 in. to 31.5 in. (600 mm to 800 mm). The current to bag (shown in Figure 3.3-8), recorded at the two plate spacings of 23.6 to 31.5 in. (600 to 800 mm) as a function of the applied voltage, showed a lower current to the filter bags at the wider plate spacing of 31.5 in. (800 mm). The bag current at the applied voltage of 60 kV was 1.6 mA at the plate spacing of 23.6 in. (600 mm) and significantly decreased to 0.4 mA at the plate spacing of 31.5 in. (800 mm). It is noted that even though the total corona current to the bags was significantly higher for the narrower plate spacing of 23.6 in. (600 mm), the percentage of current to bag was 14.9% for the plate spacing of 31.5 in. (800 mm) which was only slightly lower than the 17.4% for the plate spacing of 23.6 in. (600 mm).

3.3.1.2.3 2-Wire Grid Experiments

One solution to reduce the current to the bags is to install grounded wires between the discharging electrodes and the filter bags, which should intercept the ion current to the bags and

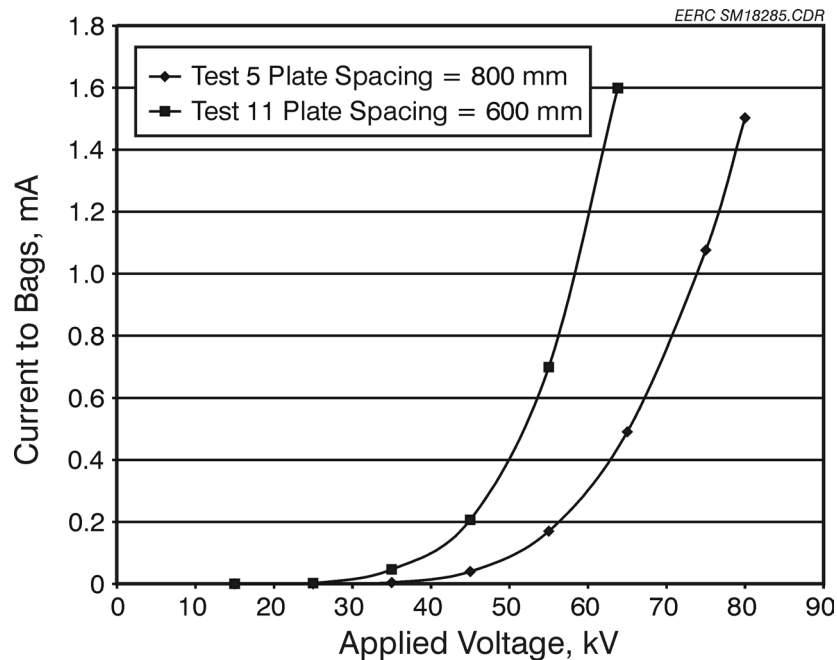


Figure 3.3-8. Effect of plate spacing on bag current (EERC electrode, ratio – 1.00).

also reduce the electric field around the bag surface. The 2-wire grounded grids (3 mm in diameter, spaced 60 mm apart) were installed to examine their effect on bag current reduction. The plate spacing was set at 23.6 in. (600 mm) with a spacing ratio of 1.00. The total current to bags, measured as a function of applied voltage, is shown in Figure 3.3-9. The current to bags was slightly decreased in the presence of the 2-wire grounded grid when the applied voltage was over 50 kV, indicating the 2-wire grounded grids did not provide significant bag protection.

3.3.1.3 ELEX Electrode Tests

The ELEX electrode is a commercially available product widely used in ESPs and will likely be used in larger-scale AHPCs. Experiments were, therefore, carried out to investigate its V-I characteristics under various conditions.

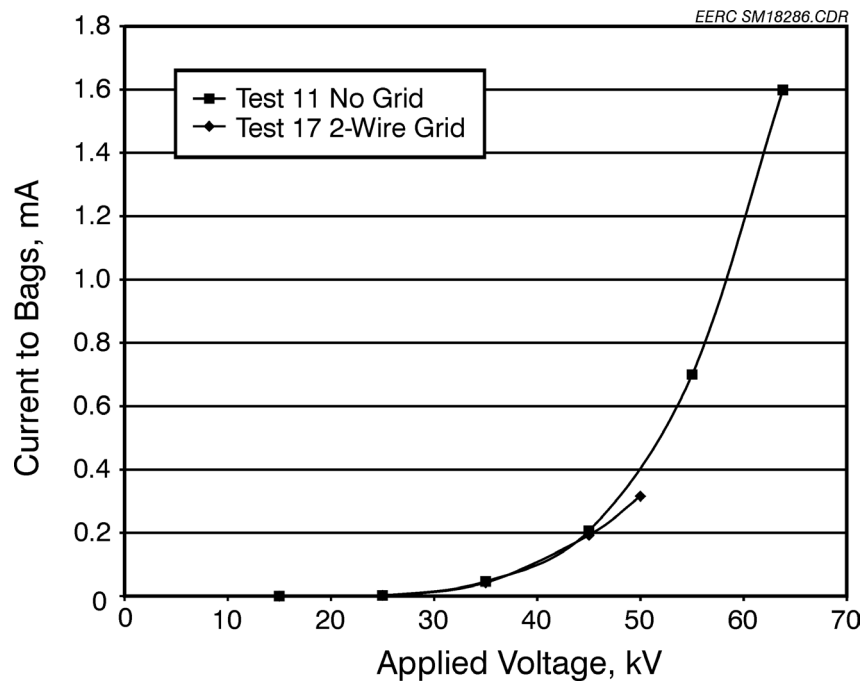


Figure 3.3-9. Effect of grid on bag current (EERC electrode, ratio – 1.00, plate spacing – 600 mm).

3.3.1.3.1 Spacing Ratio Experiments

The total current to the bags was measured as a function of the applied voltage under spacing ratios ranging from 1.25 to 2.00 at a fixed plate-to-plate spacing of 23.6 in. (600 mm), as shown in Figure 3.3-10. The current to the bags decreased with increasing spacing ratio, similar to the EERC electrode tests. At an applied voltage of 55 kV, the total current to the bag was reduced from 2.5 mA at the spacing ratio of 1.25 to 1.09 mA at the spacing ratio of 2.00. However, with the ELEX electrode, the current level to the filter bags, at the ratio of 2.00, was still high enough to be of concern.

Back corona on the bags, which was observed for all three spacing ratio tests, was very bright at the ratio of 1.25 and became faint at the ratio of 2.00. In addition to the corona emitting from the electrode tips pointed toward the plates, corona in some locations was also seen to point from the electrodes toward the filter bags. Back corona off the bags was observed to be much brighter in locations opposite these corona discharge points. This suggests that the ELEX electrode is not highly directional and explains why much higher bag currents were seen with this

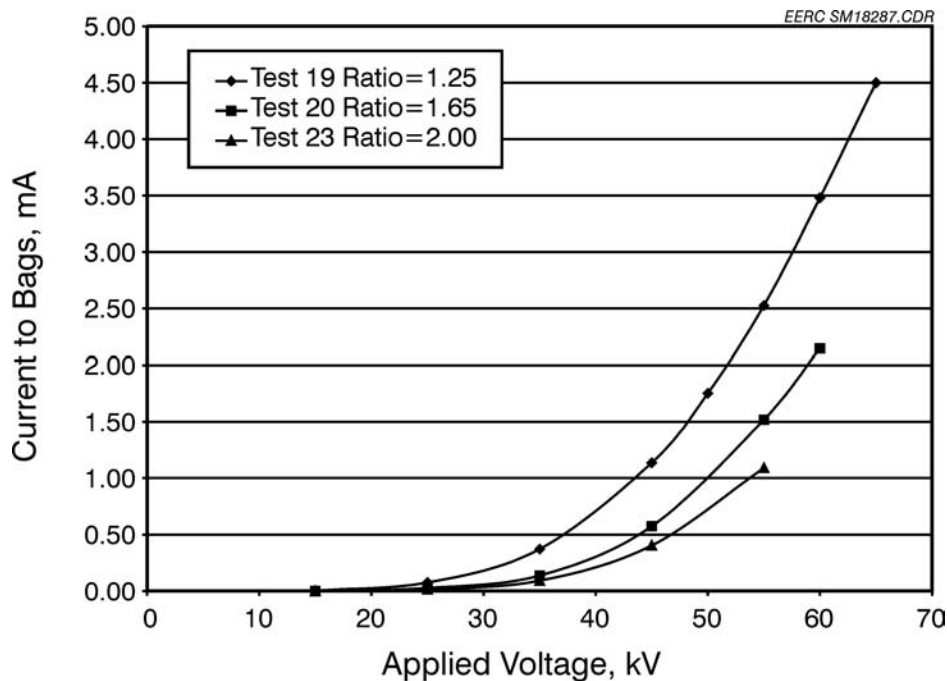


Figure 3.3-10. Effect of ratio on current to the bags (EX electrode, bags – CBNM, plate spacing – 600 mm).

design. It also suggests that the lack of directional specificity is a likely contributor to the bag damage seen in the field tests (the ELEX electrodes were installed in the 9000-acfm [255 m³/min] AHPC at the Big Stone Power Plant at the beginning of Phase III).

3.3.1.3.2 Bag-Type Experiments

Five different bag types were tested with the ELEX electrode to investigate the effect of bag type on the current to the bags with a plate-to-plate spacing of 23.6 in. (600 mm) and two different ratios of 1.25 and 2.00. The bag current results are plotted as a function of the applied voltage and shown in Figures 3.3-11 and 3.3-12. GORE-NO STAT[®] filter bag (GORE-TEX[®] antistatic membrane/GORE-TEX[®] felt) demonstrated the best performance in terms of the minimum current to the bags compared to the other type of bags. GORE-NO STAT[®] filter bags (GORE-TEX[®] membrane/GORE-TEX[®] felt) had the highest current to the bags under the two spacing ratios, reaching 4.5 mA at the applied voltage of 60 kV at a spacing ratio of 1.25. However, there was still significant current to the bags for all of the bag types for both ratios. Therefore, a change in bag type alone is not likely to sufficiently lower the bag current for the ELEX electrode.

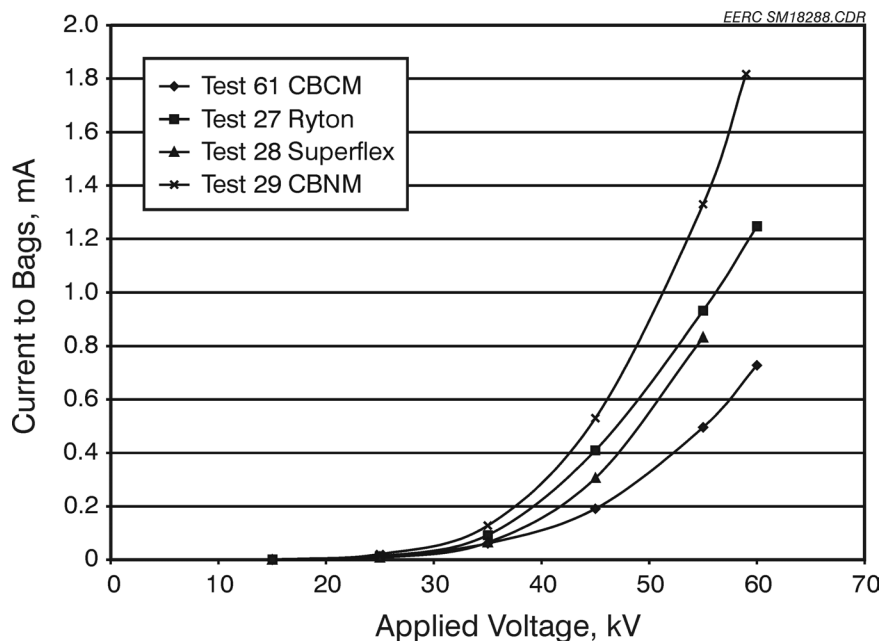


Figure 3.3-11. Effect of bag type on current to the bags (EX electrode, plate spacing – 600 mm, ratio – 2.00).

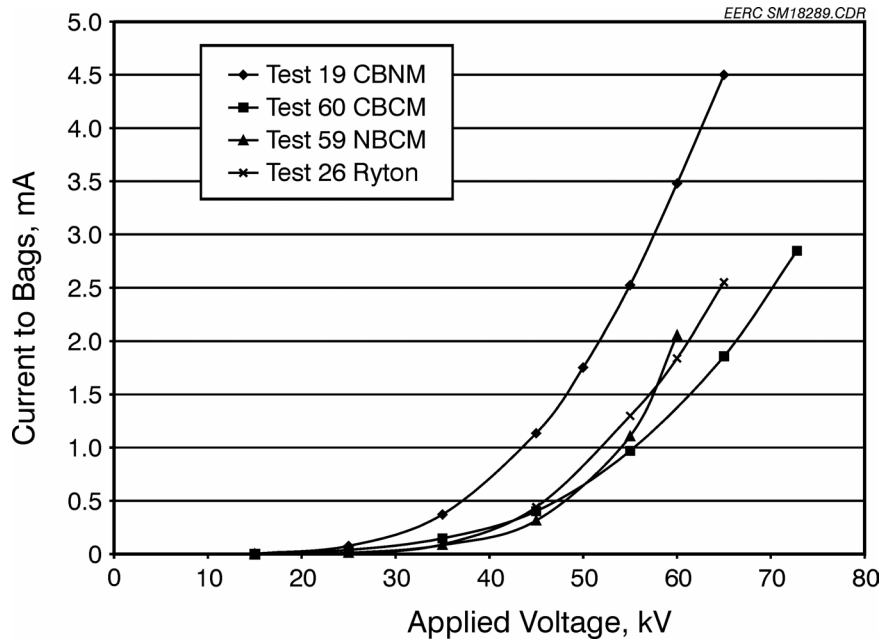


Figure 3.3-12. Effect of bag type on current to the bags (EX electrode, plate spacing – 600 mm, ratio – 1.25).

3.3.1.3.3 Grounded-Grid Experiments

The ELEX electrode resulted in a significant current to the bags even at a high spacing ratio and using GORE-TEX[®] antistatic membrane/GORE-TEX[®] felt filter bags. In order to further reduce the current to bags, two grounded grids, 2-wire and diamond mesh, were installed between the bags and the electrodes. The tests were conducted at a plate spacing of 23.6 in. (600 mm) with a spacing ratio of 2.00. The bag currents in the presence of the two grounded grids were recorded as a function of the applied voltage and plotted in Figure 3.3-13. The bag currents without grounded grids were also included in Figure 3.3-13 for comparison. The current to the bags was reduced from 1.1 mA at an applied voltage of 55 kV without grounded grid protection to 0.42 mA in the presence of the 2-wire grounded grid and nearly dropped to zero by using the diamond mesh grounded grid. These results demonstrated the diamond mesh could provide a much better protection of the filter bags than the 2-wire grounded grid in terms of reducing the current to the bags.

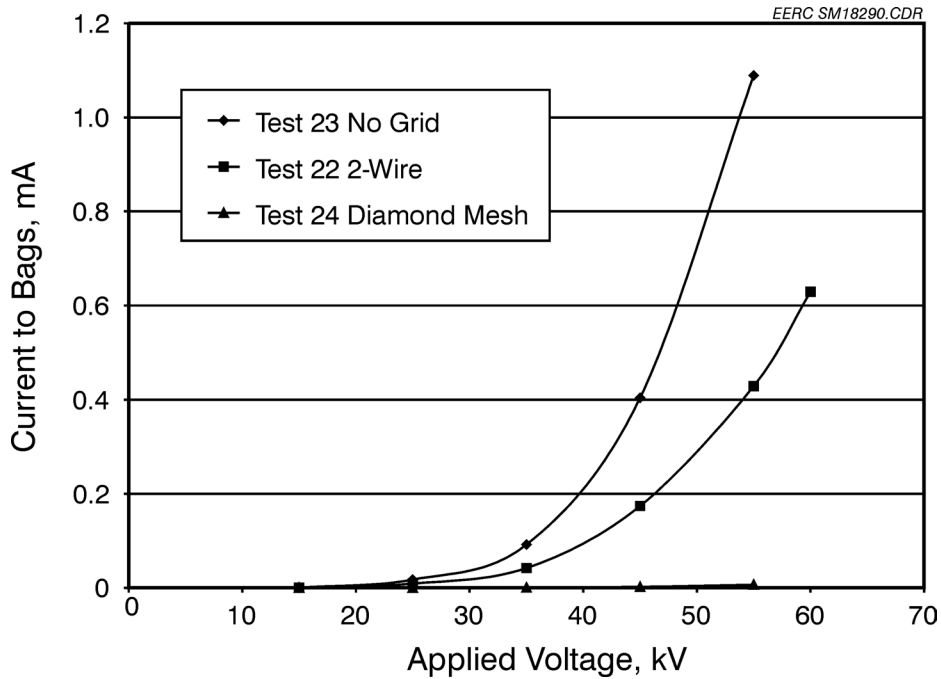


Figure 3.3-13. Effect of grounded grid on current to the bags (EX electrode, plate spacing – 600 mm, ratio – 2.00).

3.3.1.4 ENELCO Electrode Tests

3.3.1.4.1 Spacing Ratio Experiments

Experiments were carried out to investigate the interactions between the ENELCO-3-mast electrode and the filter bags under spacing ratios of 1.25, 1.65, and 2.00. Figure 3.3-14 shows the current to the bags at a plate spacing of 23.6 in. (600 mm). The bags used here were GORE-NO STAT[®] filter bags (GORE-TEX[®] antistatic membrane/GORE-TEX[®] felt). The higher spacing ratio resulted in a lower current to the bags, similar to that observed for the other electrode tests. The current to the bags was more than 2 mA at the ratio of 1.25 under the applied voltage of 60 kV and was significantly reduced to 0.5 mA when the spacing ratio was adjusted to 1.65.

The plate spacing was then increased to 27.6 in. (700 mm), and the filter bags were switched to GORE-NO STAT[®] filter bags (GORE-TEX[®] membrane/GORE-TEX[®] felt). The bag

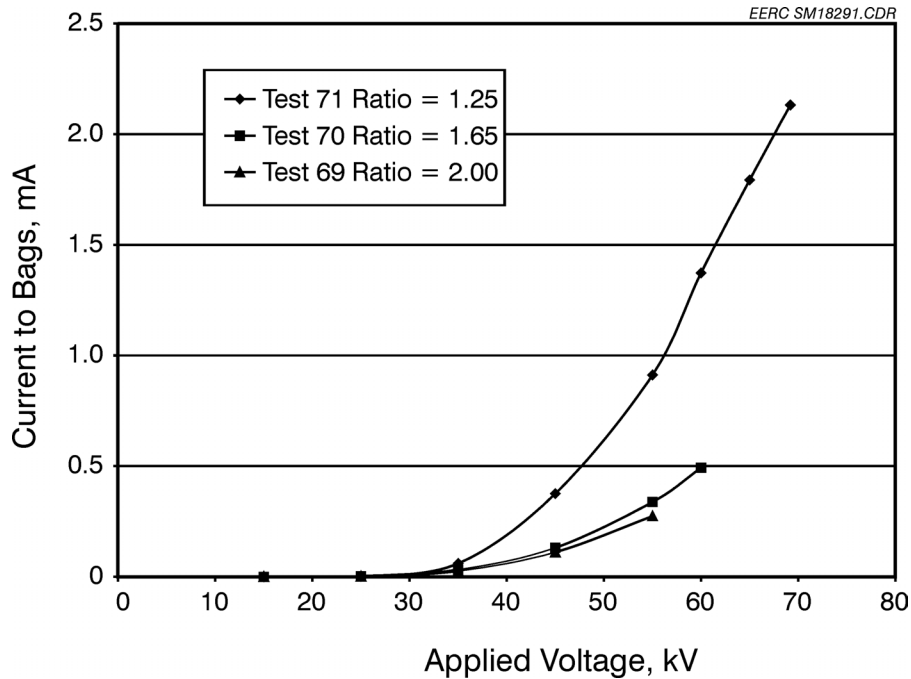


Figure 3.3-14. Effect of ratio on current to the bags (EN-3 electrode, plate spacing – 600 mm, bags – CBCM).

currents were measured and are shown in Figure 3.3-15. The same trend of decreasing current to the bags at a higher spacing ratio was also observed with GORE-NO STAT[®] filter bags (GORE-TEX[®] membrane/GORE-TEX[®] felt), as shown in Figure 3.3-15. Some back corona was also observed on these filter bags at all of the ratios tested.

3.3.1.4.2 Bag-Type Experiments

Experiments were then performed to investigate the current to the bags as a function of bag type at a plate-to-plate spacing of 23.6 in. (600 mm) and a spacing ratio of 1.25. Three different types of bags were examined. A filter cage (no bag) considered an ideal electrical conductor was also used to compare with results from the other bag tests. The experimental data (Figure 3.3-16) showed the cage wire had the lowest current at all of the applied voltages followed by GORE-NO STAT[®] filter bags (GORE-TEX[®] antistatic membrane/GORE-TEX[®] felt). Both the Ryton and GORE-NO STAT[®] filter bags (GORE-TEX[®] membrane/GORE-TEX[®] felt) induced higher currents, similar to the results observed in the ELEX electrode tests.

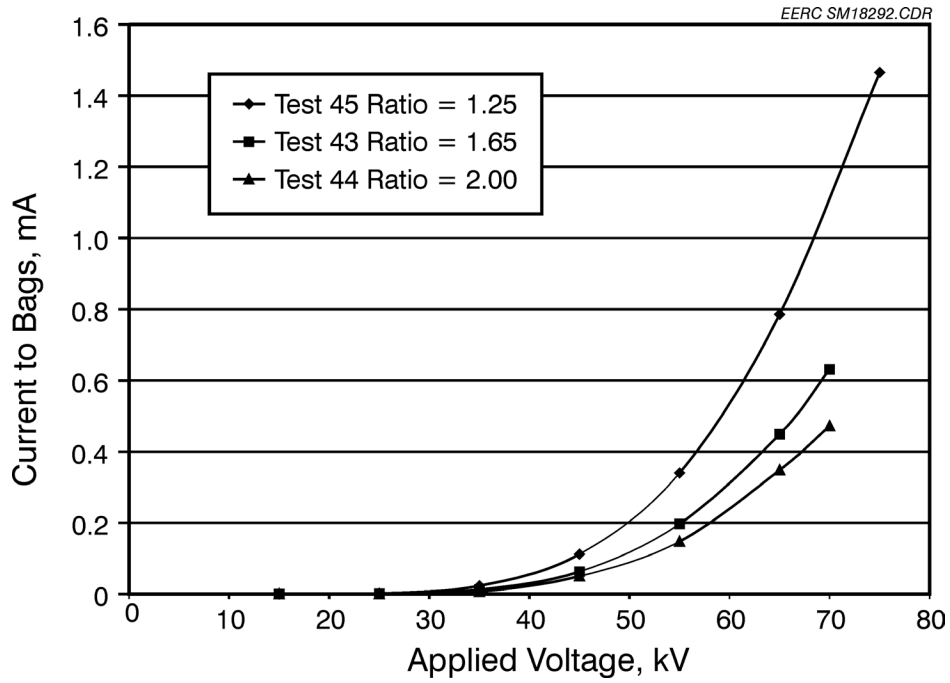


Figure 3.3-15. Effect of ratio on current to the bags (EN-3 electrode, plate spacing – 700 mm, bags – CBNM).

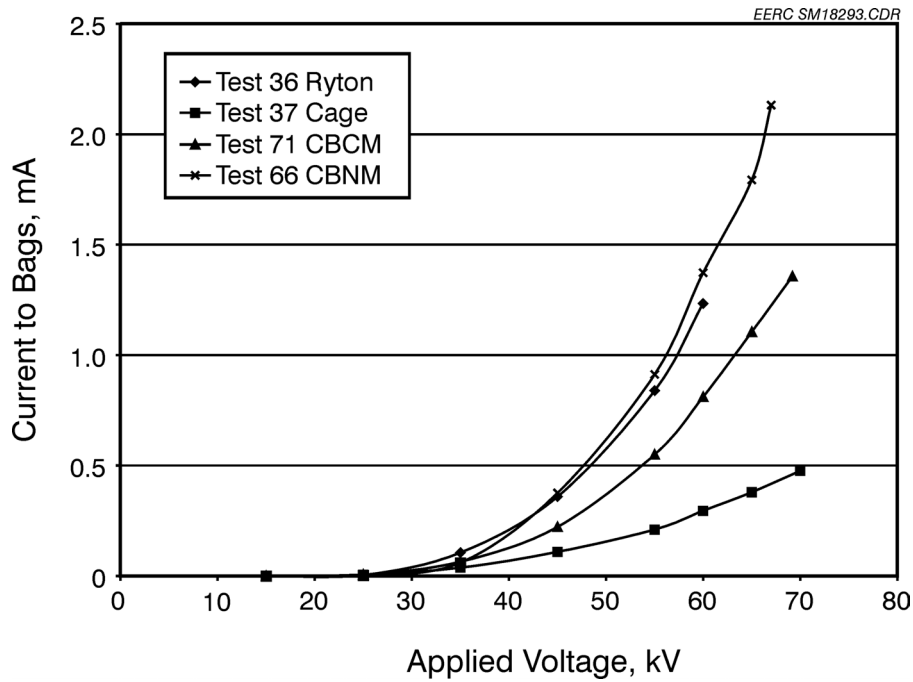


Figure 3.3-16. Effect of bag type on current to the bags (EN-3 electrode, plate spacing – 600 mm, ratio – 1.25).

The effectiveness of grounded grids on the reduction of current to bags was examined by using the 3-wire grounded grid in the presence of different bag types. The current to the bags, shown in Figure 3.3-17, was dramatically decreased because of the presence of the 3-wire grounded grids between the discharging electrodes and the filter bags compared to the bag current without a grounded grid shown in Figure 3.3-16. For example, the current to the GORE-NO STAT[®] filter bags (GORE-TEX[®] membrane/GORE-TEX[®] felt) (Figure 3.3-16) was reduced from 2.0 mA at 65 kV to less than 0.2 mA by the 3-wire grounded grid.

3.3.1.5 Summary of Pilot-Scale Cold-Flow Tests at the EERC

- Electrode type, bag type, spacing ratio, plate-to-plate spacing, and grounded grids were all evaluated for their effects on reducing the current to the bags in cold-flow tests without dust. The most significant factors were electrode type, spacing ratio, and the presence of a grounded grid.

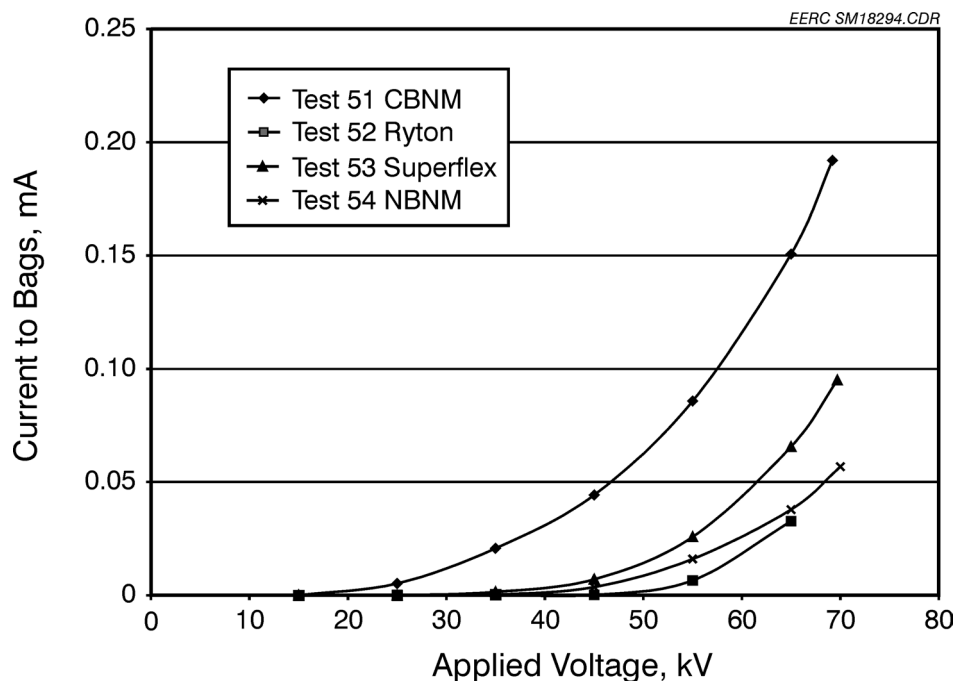


Figure 3.3-17. Effect of bag type on current to the bags in the presence of a grounded grid (EN-3 electrode, plate spacing – 600, ratio – 1.25, 3-wire grid).

- A significant finding was that the ELEX-type electrode, which is the type installed on the Big Stone AHPC, had the highest current to the bags and appeared to be less directional than either the EERC or ENELCO types.
- Spacing ratio was also a major factor affecting the amount of current to the bags. The spacing ratio tests indicate that the amount of current to the bags can be significantly reduced by increasing the ratio, but this approach would likely result in a deterioration of ESP performance.
- The grounded-grid tests show that a simple wire grid can greatly reduce the current to the bags, but that a more dense arrangement such as a diamond pattern, expanded metal grid can reduce the current to almost zero.
- The plate-to-plate spacing tests showed that, at the same spacing ratio, wider plate-to-plate spacing will also reduce the current to the bags.
- The GORE-NO STAT[®] filter bag (GORE-TEX[®] antistatic membrane/GORE-TEX[®] felt) had a lower bag current than the GORE-NO STAT[®] filter bag (GORE-TEX[®] membrane/GORE-TEX[®] felt). Since the GORE-NO STAT[®] filter bags (GORE-TEX[®] membrane/GORE-TEX[®] felt) were the type previously used at Big Stone, an approach to reduce the amount of current to the bags is to replace them with the GORE-NO STAT[®] filter bag (GORE-TEX[®] antistatic membrane/GORE-TEX[®] felt) type.

The highest bag current observed occurred for some of the ELEX-type electrode tests. In some cases, the bag current was over 2 mA, which represented over 40% of the total current. Low current could be achieved for all of the electrode types when a grounded grid was employed. This provided confidence that with the right geometric configuration, the current to the bags could be virtually eliminated. While the cold-flow tests without dust showed clear effects of these variables on the level of current to the bags, the results needed to be verified under real flue gas conditions.

3.3.2 Pilot-Scale Coal Combustion Hot-Flow Tests at the EERC

3.3.2.1 PTC-CR-621 Series Tests

Following the extensive cold-flow studies completed at the EERC, several strategies were proposed and tested in the pilot-scale coal combustion hot-flow experiments to examine their effectiveness on reducing current to the bags without deteriorating overall AHPC performance. Four of the conditions were tested for about 24 hr each, and the fifth condition was tested for 100 hr. A summary of the AHPC configurations is listed in Table 3.3-3.

TABLE 3.3-3

AHPC Configurations Tested in PTC-CR-621 Series					
	PTC-CR-621-1	PTC-CR-621-2	PTC-CR-621-3	PTC-CR-621-4	PTC-CR-621-5
Test Duration, hr	24	24	24	24	100
PTP, ¹ in. (mm)	23 (575)	23 (575)	23 (575)	23 (575)	31 (790)
Electrode	ENELCO-2-mast	ENELCO-2-mast	ENELCO-2-mast	Spike on diamond grid	ELEX
Power Supply	Positive on plate	Negative on electrode	Negative on electrode	Positive on plate	Negative on electrode
Grounded Grid	None	None	3/4" perforated plate (51% opening)	Diamond grid	3/4" perforated plate (51% opening)
ETP, ² n. (mm)	5.0 (127)	30 (76.2)	(30) 76.2	5.0 (127)	6.0 (152.4)
ETB, ³ in. (mm)	3.8 (96.8)	5.8 (147.6)	5.8 (147.6)	3.0 (76.2)	7.0 (177.8)
Spacing Ratio	0.76	1.94	1.94	0.6	1.17
Pulse Trigger Pressure, in. H ₂ O (kPa)	8.0 (2.0)	8.0 (2.0)	8.0 (2.0)	8.0 (2.0)	8.0 (2.0)
A/C ratio, ft/min (m/min)	12 (3.7)	12 (3.7)	12 (3.7)	12 (3.7)	12 (3.7)

¹ Plate-to-plate spacing.

² Electrode-to-plate spacing.

³ Electrode-to-bag spacing.

These tests were designated PTC-CR-621-1 through PTC-CR-621-5. The CR designation is for the Cordero Rojo complex coal used for the tests, which was the same type being burned at the Big Stone Power Plant.

3.3.2.1.1 PTC-CR-621-1

In Test PTC-CR-621-1, a positive-polarity HV power supply was used to apply positive voltage on the collection plates, while the discharge electrodes and the filter bags were grounded. The corona current from the discharge electrodes, under this configuration, was toward the collection plates rather than toward the filter bags because both the discharge electrodes and the filter bags were at the same zero electric potential. The AHPC unit was operated at 8.0 in. (0.2 mm) pulse trigger pressure with a constant A/C ratio of 12 ft/min (3.7 m/min). The current to the bags was maintained at less than 5 μ A during the 24-hr testing period. The total current generated under the positive collection plate configuration was very low (0.2–0.5 mA shown in Figure 3.3-18), which resulted in poor AHPC performance. The bag-cleaning interval (Figure 3.3-19) varied between 5 to 10 min because of inefficient ESP performance, which is verified by the high K_2C_i values ranging from 12 to 20 (Figure 3.3-20). The K_2C_i value was increased to over 60 when the AHPC unit was operated in baghouse mode without electric power, causing the bag-cleaning interval to drop below 5 min. The residual drag was around 0.5 in. W.C./ft/min at the end of the 24-hr test (Figure 3.3-21). These results show that the poor AHPC performance was the result of poor ESP performance rather than bag cleanability. Even though this configuration protected the bags, AHPC performance was significantly compromised.

3.3.2.1.2 PTC-CR-621-2

In Test PTC-CR-621-2, the power source was switched back to negative polarity HV power supply applied to the discharge electrodes. The spacing ratio was increased to 1.94 to minimize the current to the filter bags, as observed in the cold-flow tests. For direct comparison with the previous test, the total corona current was kept at a low level of 0.5 mA during most of the 24-hr testing period except for short-term tests at the end of the experiments when the current was set from 1.0 to 1.5 mA. The bag-cleaning interval shown in Figure 3.3-22 started at 40 min but gradually decreased to 5–10 min. The poor performance was caused by inadequate ESP

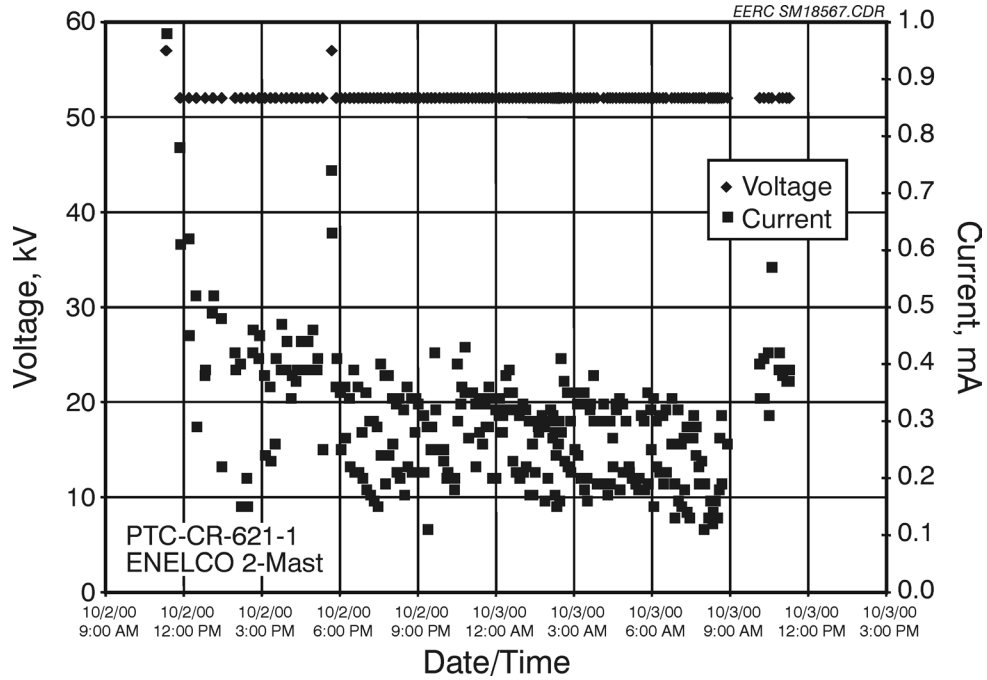


Figure 3.3-18. Current and voltage for PTC-CR-621-1.

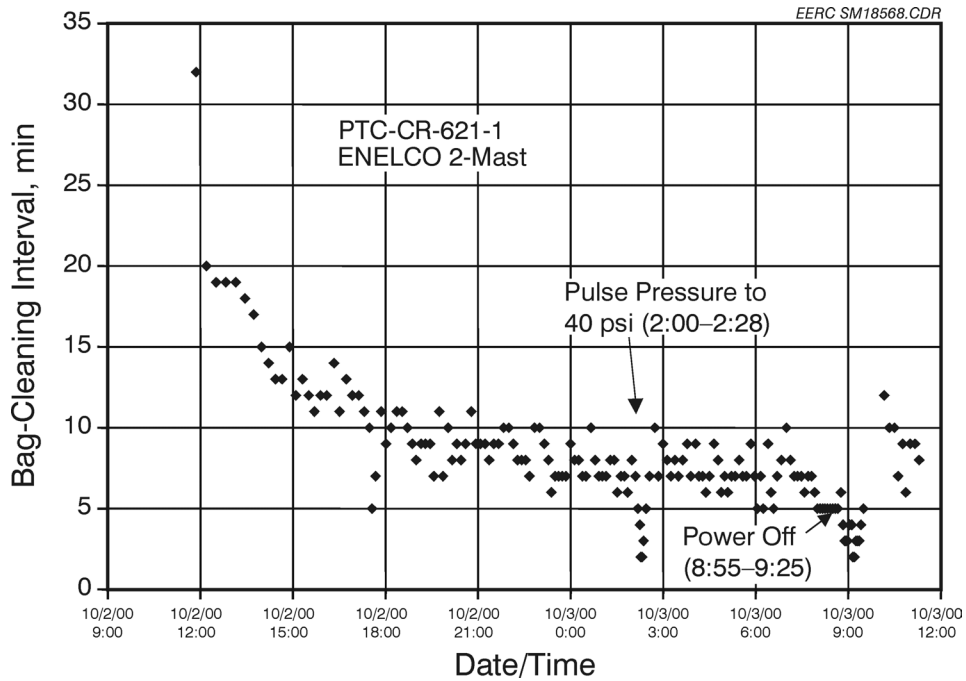


Figure 3.3-19. Bag-cleaning interval for PTC-CR-621-1.

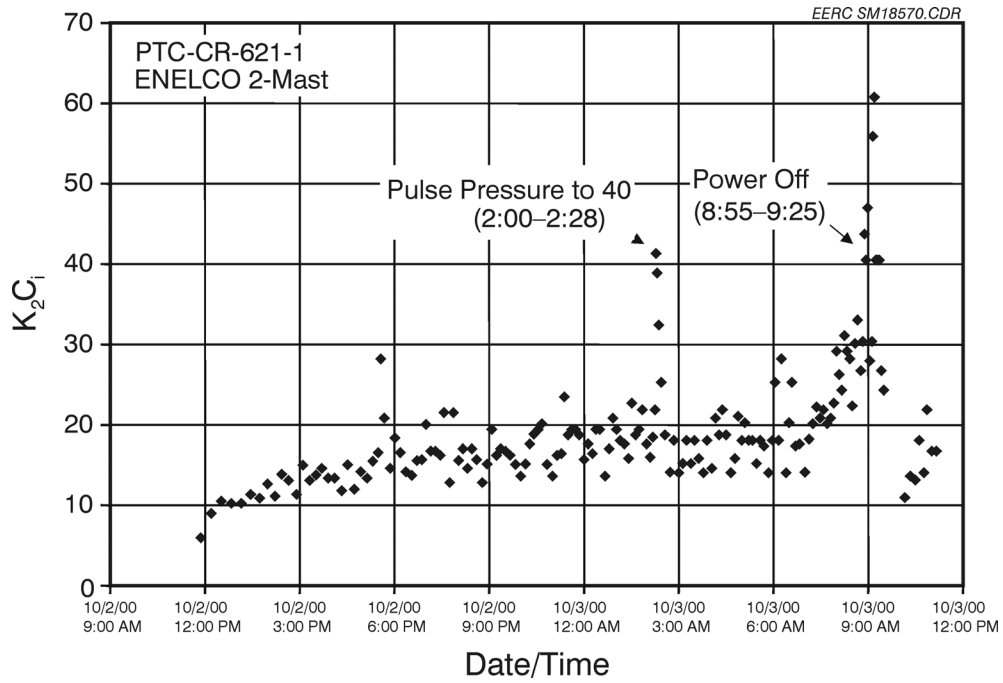


Figure 3.3-20. K_2C_i for PTC-CR-621-1.

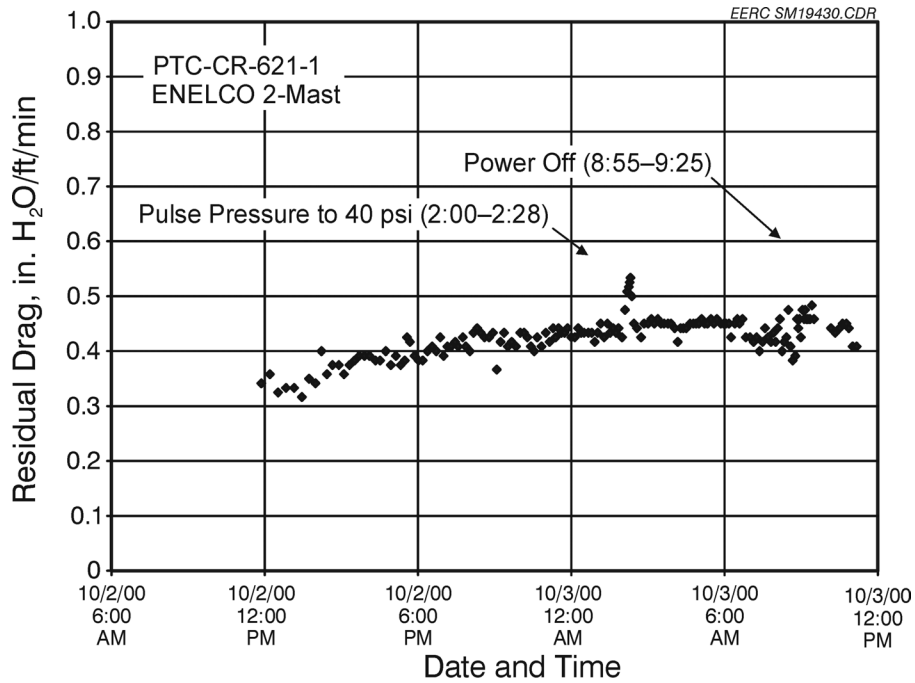


Figure 3.3-21. Residual drag for PTC-CR-621-1.

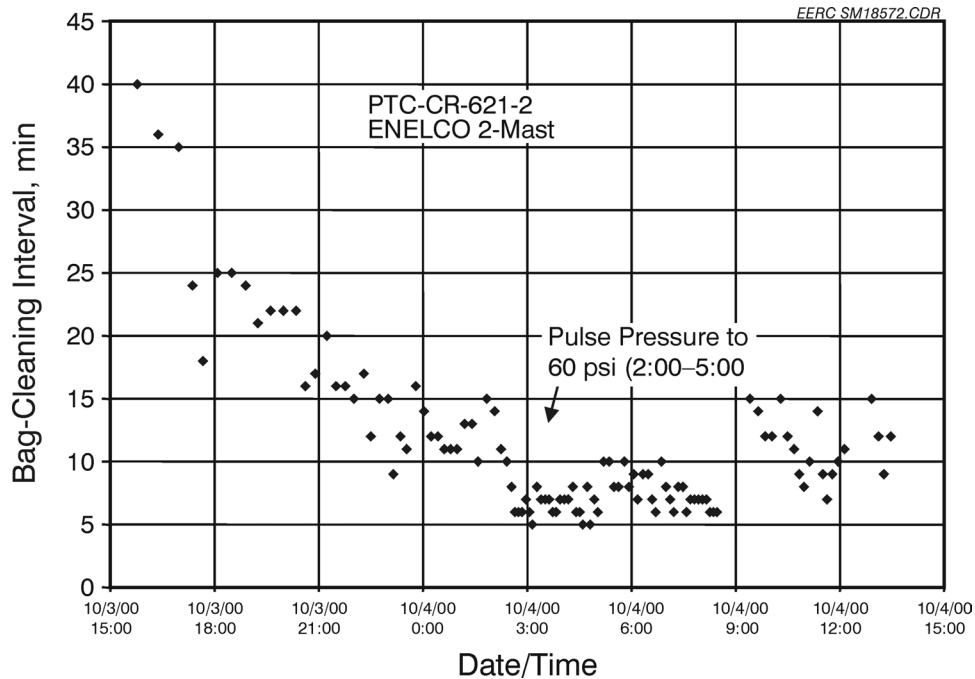


Figure 3.3-22. Bag-cleaning interval for PTC-CR-621-2.

performance, the result of the low current level. The bag-cleaning interval did increase somewhat to 10–15 min at the higher current of 1.5 mA. The K_2C_i , representing the ESP performance (shown in Figure 3.3-23), ranged from 10–20 at the current of 0.5 mA and decreased to around 10 when current was increased to 1.5 mA. The residual drag (Figure 3.3-24) was reasonable, ranging from 0.37 in. W.C./ft/min at the beginning to 0.47 in. W.C./ft/min at the end of the test. In the middle of the test, by reducing the pulse-cleaning pressure from 90 to 60 psi (621 to 414 kPa), the residual drag jumped to over 0.5 in. W.C./ft/min from the previous 0.417 in. W.C./ft/min, showing better bag cleaning under the higher pulse-cleaning pressure. The current to the bags was very low, an average of 17 μ A for each bag.

3.3.2.1.3 PTC-CR-621-3

In the PTC-CR-621-3 test, negative voltage was still applied on the discharge electrodes, while grounded perforated plates (0.75 in. hole in diameter with a 51% opening area) were installed between the filter bags and the electrodes to protect the bags. The spacing ratio was set

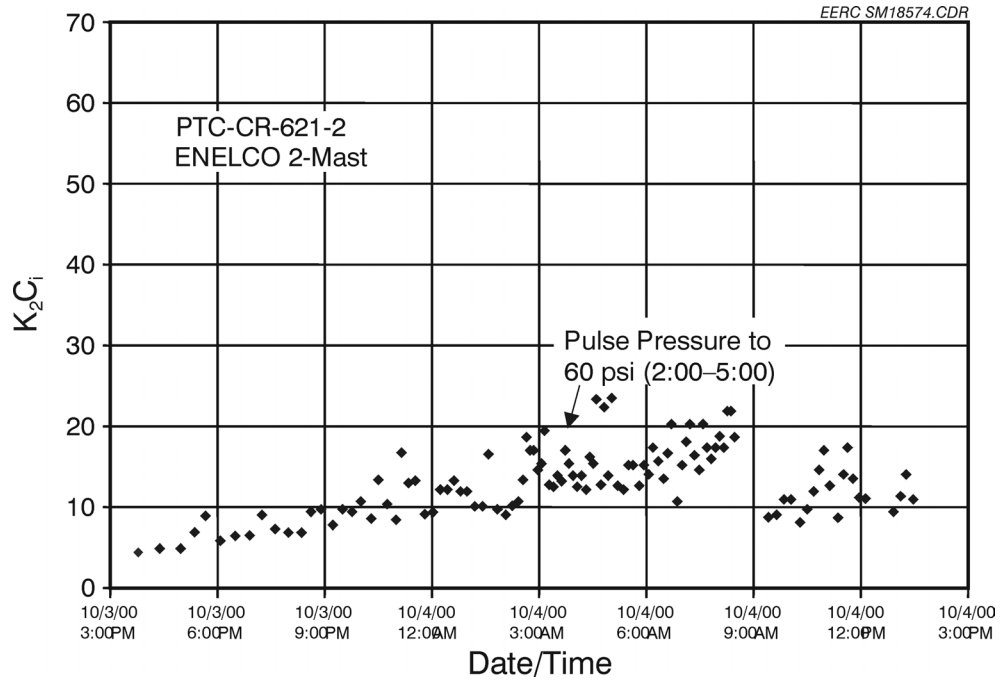


Figure 3.3-23. K_2C_i for PTC-CR-621-2.

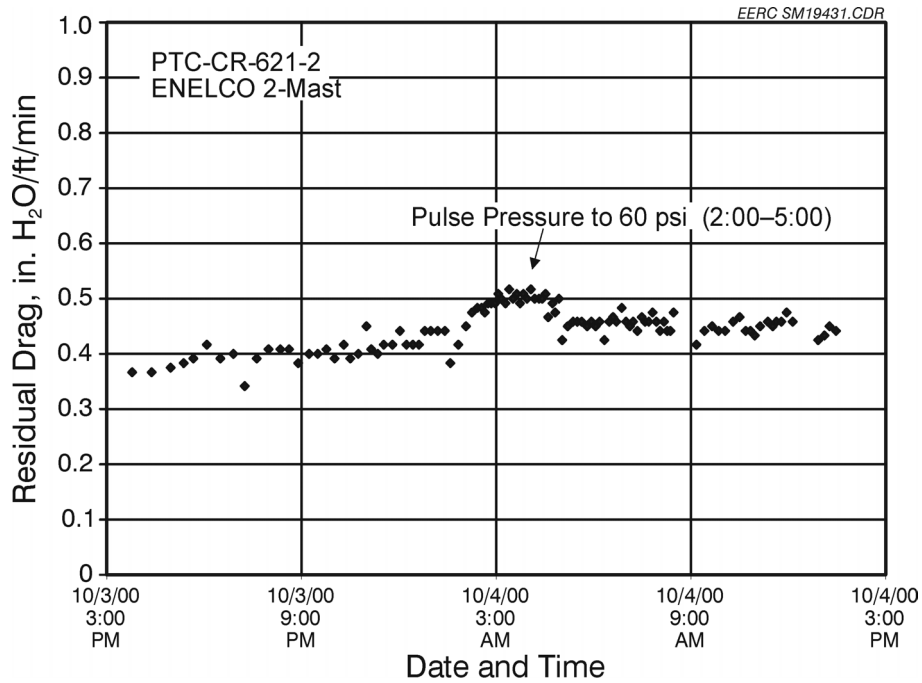


Figure 3.3-24. Residual drag for PTC-CR-621-2.

at 1.94, the same as in Test PTC-CR-621-2. The current to the bags was kept at an extremely low level, an average of 0.4 μA for each bag in the 24-hr test, demonstrating excellent bag protection with the perforated plates. The corona current was varied from 1.0 to 1.5 mA for most of the testing period except for a short-term test without electric power at the end of the experiments. A noticeably better AHPC performance with a bag-cleaning interval (shown in Figure 3.3-25) of 15 min was observed at the end of the test with the current level in the range of 1.0–1.5 mA. While this bag-cleaning interval was not as good as the 30–40 min observed in previous tests, it showed that acceptable performance could be achieved while adequately protecting the bags from electrical damage. Better AHPC performance was also proven by the reduced K_2C_i values, shown in Figure 3.3-26. The K_2C_i was around 10 at the current level 1.0–1.5 mA and increased up to 60 due to the shutdown of the electric power. The residual drag, shown in Figure 3.3-27, ranged from 0.33 to 0.42 in. W.C./ft/min. Again, the reduced pulse-cleaning pressure of 60 psi (414 kPa) resulted in increased residual drag, demonstrating poorer bag cleaning at the lower pulse-cleaning pressure. Without ESP power, the result was short bag-cleaning intervals less than 5 min, increased residual drag, and higher K_2C_i values.

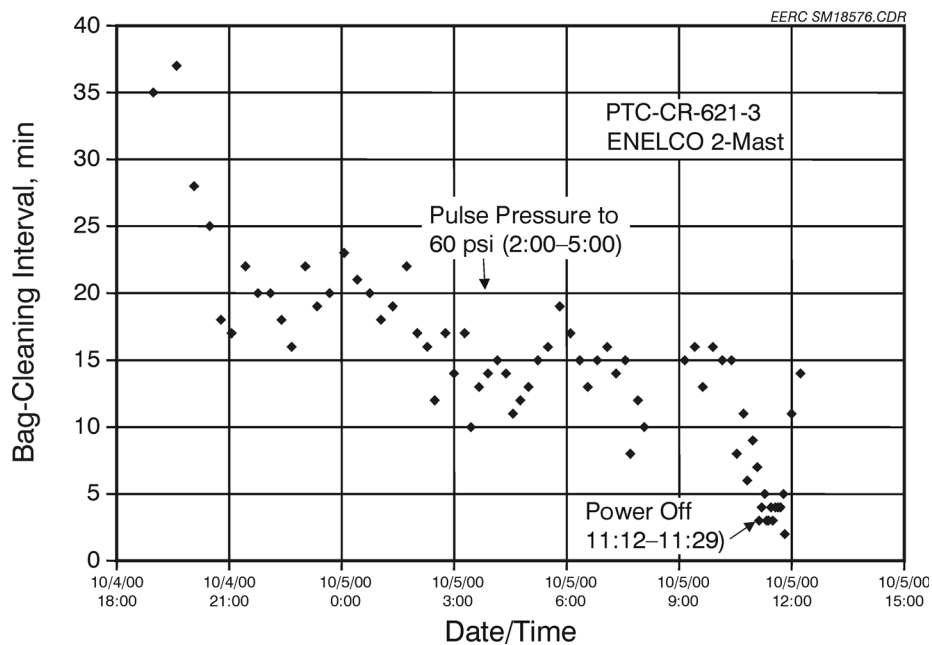


Figure 3.3-25. Bag-cleaning interval for PTC-CR-621-3.

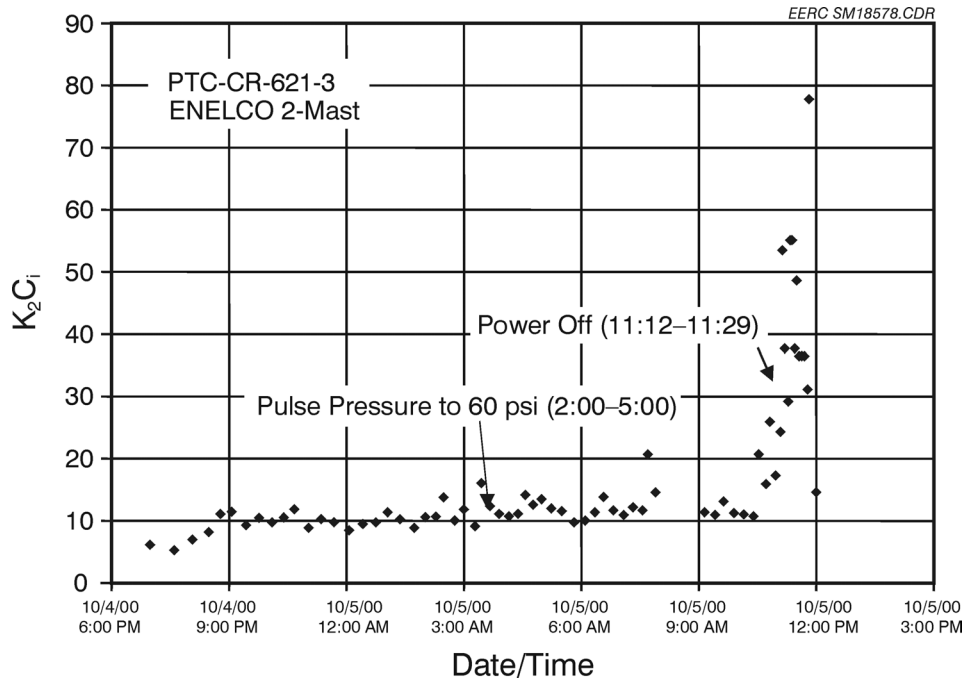


Figure 3.3-26. K_2C_i for PTC-CR-621-3.

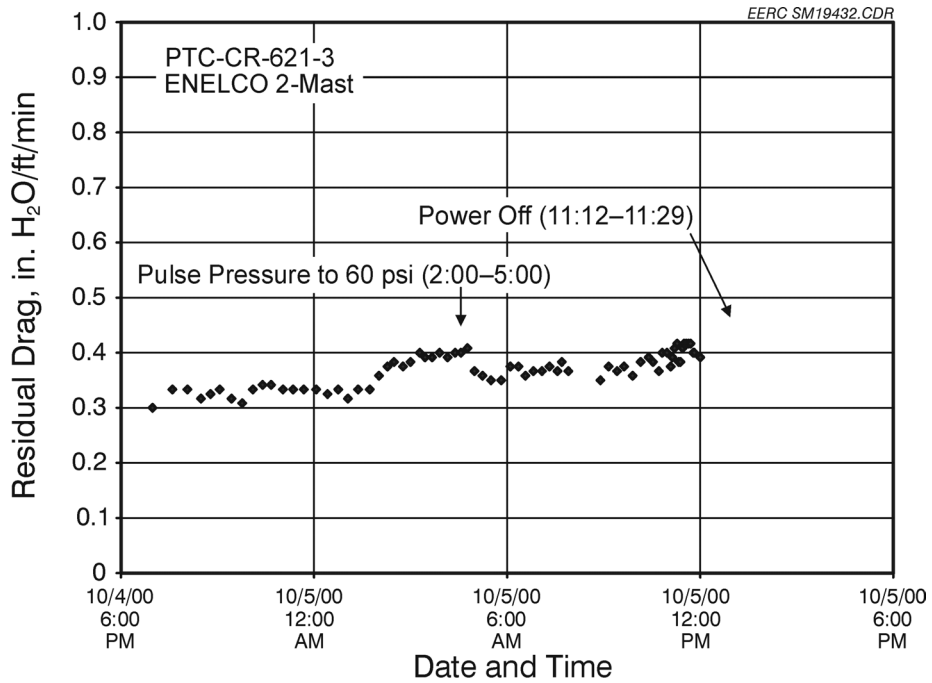


Figure 3.3-27. Residual drag for PTC-CR-621-3.

3.3.2.1.4 PTC-CR-621-4

In the PTC-CR-621-4 test, the ENELCO-2-mast electrodes (used in the last three tests) and the perforated plates were replaced with diamond mesh with 20 spikes (facing toward the collection plates), serving as both discharging electrodes and protection grids. The positive polarity power supply was used to apply the HV on the collection plates to generate a corona current from 0.2 to 0.7 mA in the 24-hr test. The bag-cleaning interval, shown in Figure 3.3-28, was below 10 min at the end of the test because of the low current level in the AHPC chamber under this configuration. The poor ESP performance resulted in high values of K_2C_1 (plotted in Figure 3.3-29) in the range of 10–25. This also resulted in a short bag-cleaning interval and impaired the bag-cleaning ability with high residual drag (shown in Figure 3.3-30). The current to the bags was near zero for all four bags in the presence of the diamond mesh in front of the filter bags, but AHPC performance was not acceptable.

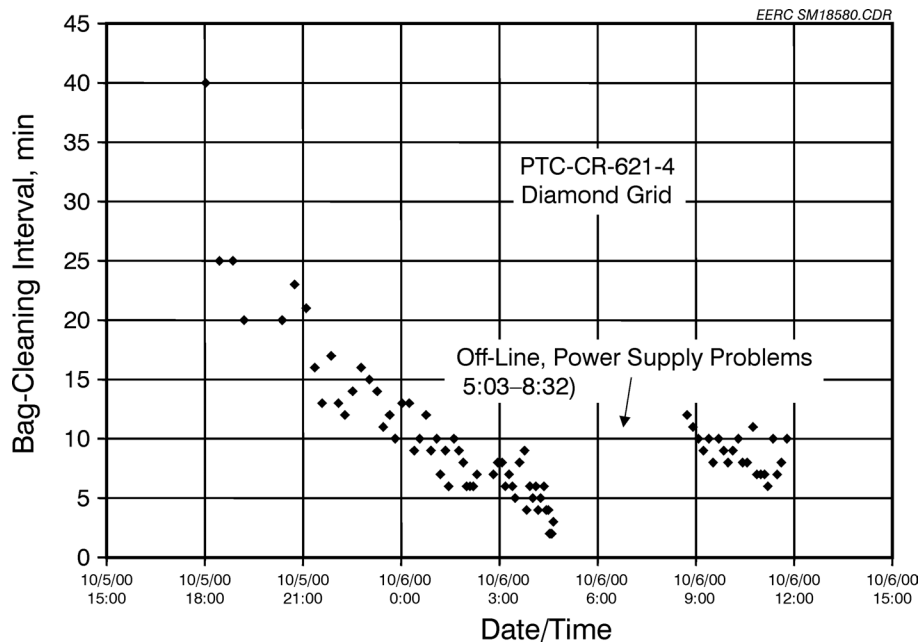


Figure 3.3-28. Bag-cleaning interval for PTC-CR-621-4.

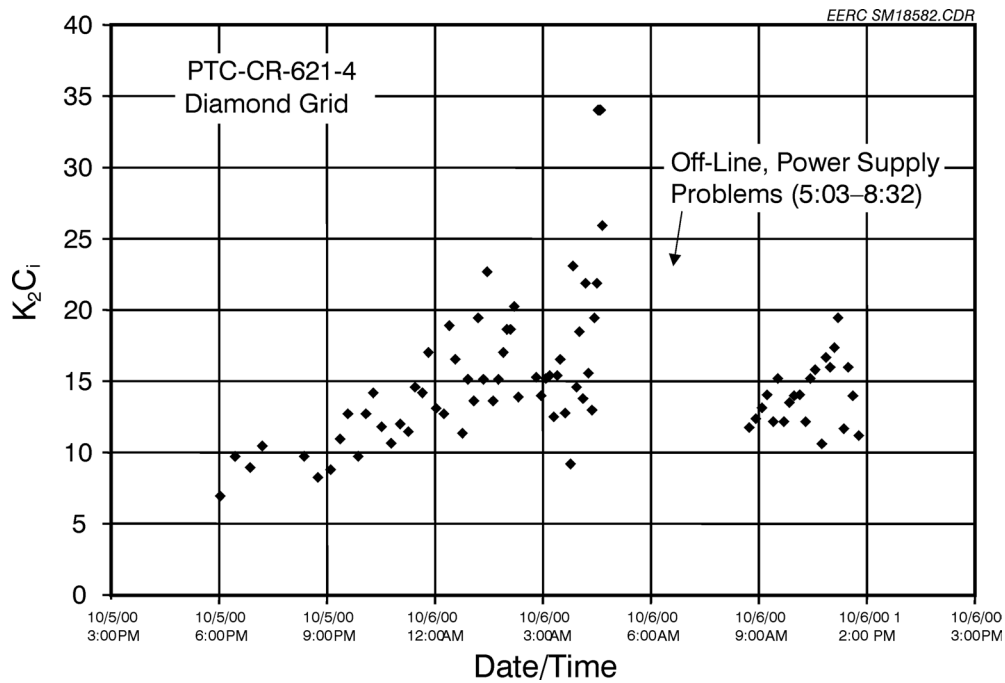


Figure 3.3-29. K_2C_i for PTC-CR-621-4.

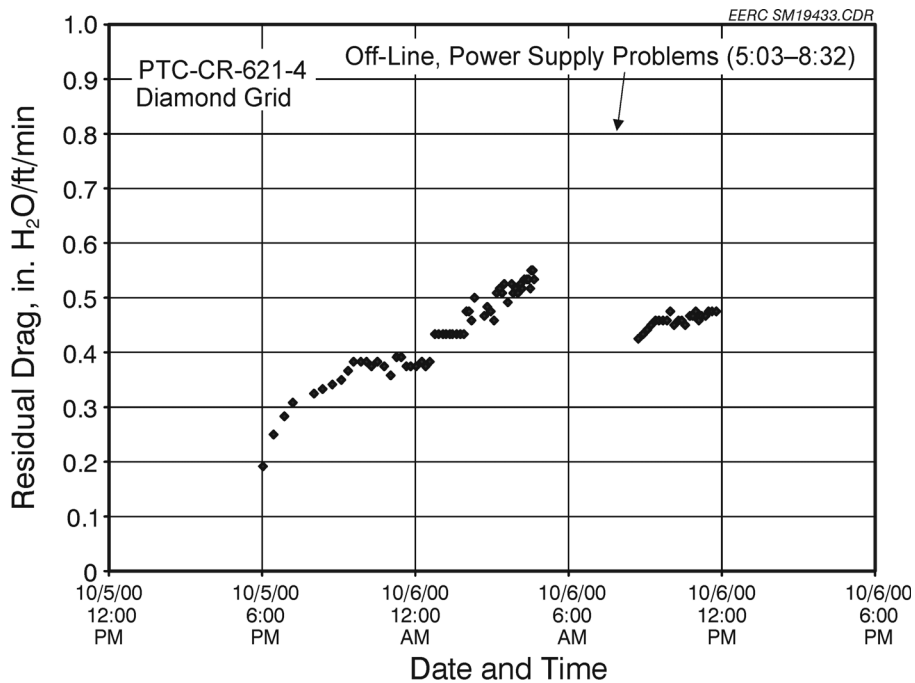


Figure 3.3-30. Residual drag for PTC-CR-621-4.

3.3.2.1.5 PTC-CR-621-5

For Test PTC-CR-621-5, a combination of several modifications was implemented to improve AHPC performance and reduce current to the bags. The plate-to-plate spacing was extended to 31.1 in. (790 mm), and 3/4-in. (19.1-mm)-hole-sized perforated plates (51% opening area) were installed between the collection plates and the filter bags and on the opposite side of the discharge electrodes. The perforated plates served both as protective grounded grids and the ESP collection surface. ELEX electrodes were used instead of the ENELCO-2-mast electrodes in this test, with negative voltage applied on the discharge electrodes. The test was started on October 9, 2000, and ended on October 13, 2000. Since poor ESP performance under low current was observed in the last four tests, the corona current was set at 4.0 mA during most of the 100-hr test except for a short time when the current was reduced to 1.5 mA. The test was conducted at an A/C ratio of 12 ft/min (3.7 m/min), and the bags were pulse-cleaned when the tube sheet pressure drop reached 8 in. W.C. (2.0 kPa). This configuration produced the best results achieved with the AHPC to date. The bag-cleaning interval with this configuration is shown in Figure 3.3-31, and the residual drag is shown in Figure 3.3-32. Note in Figure 3.3-31 that the bag-cleaning interval was initially at 6 hr and then decreased to about 3.25 hr after 24 hr of testing, where it remained steady for the remainder of the 100-hr test. Initially, the plan was to run this test for only 24 hr, but because of the excellent results, the decision was made to extend the test time to 100 hr to see if the bag-cleaning interval and the residual drag would stabilize. In retrospect, the decision to extend the testing was fortuitous, because if the testing had been stopped after 24 hr and the data extrapolated, it would have appeared that the bag-cleaning interval would continue to decrease and the residual pressure drop increase. In contrast, from Figures 3.3-31 and 3.3-32 with this configuration, both the bag-cleaning interval and residual drag appeared to be stable for the last 50 hr of the test. Shown in Figure 3.3-31 and 3.3-32, when the corona current was reduced by 64% (from 4.2 to 1.5 mA), the bag-cleaning interval dropped to about half the previous level, while the residual drag drop did not appear to change, maintaining the extremely low level of 0.29 in. W.C./ft/min. This result is highly encouraging because it shows that there is a wide margin to reduce power consumption under this configuration and still maintain a long bag-cleaning interval and excellent bag cleanability.

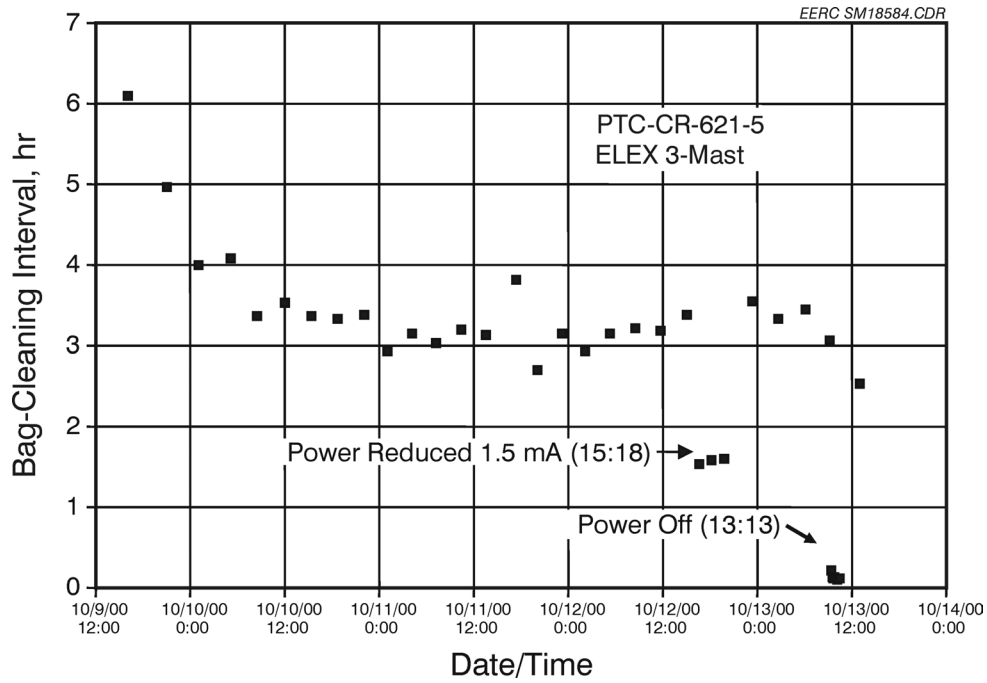


Figure 3.3-31. Bag-cleaning interval for PTC-CR-621-5.

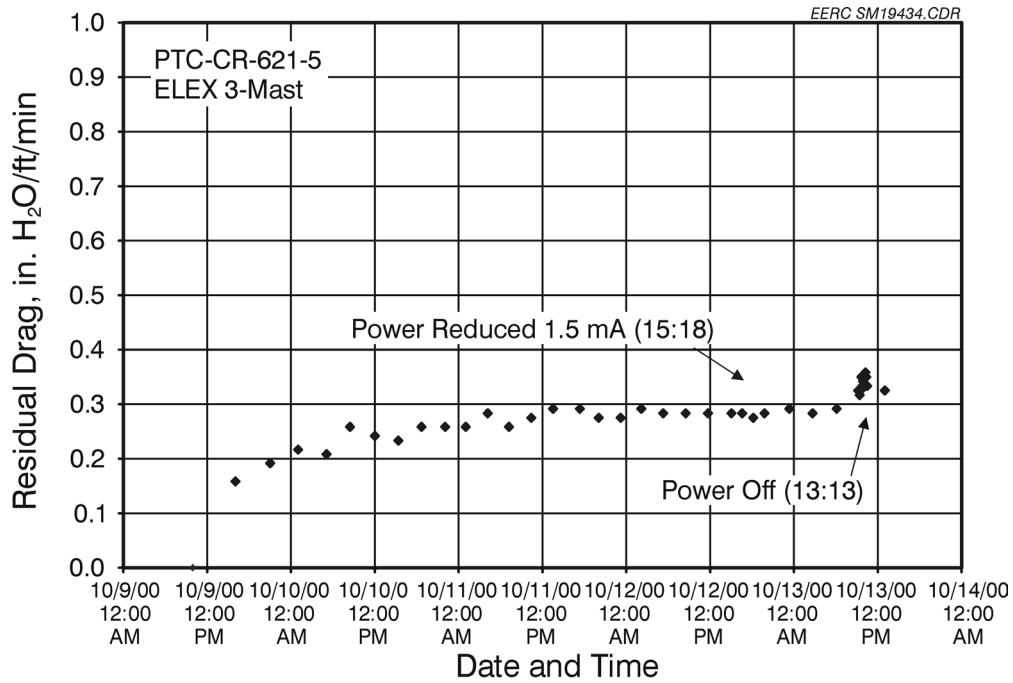


Figure 3.3-32. Residual drag for PTC-CR-621-5.

These results represented a significant improvement in overall AHPC performance with the modified configuration and were further evaluated in additional tests.

3.3.2.2 PTC-CR-622 and PTC-CR-623 Series Tests

3.3.2.2.1 Test Configuration Description

The results from PTC-CR-621-5 test showed the AHPC system with the perforated plates not only appeared to be the best solution to solving the bag damage problem by blocking the electrical field from the bag surface and intercepting current to the bags, but also offers many other advantages such as operation at higher A/C ratios, lower residual drag, longer bag-cleaning intervals, and an even more compact geometric arrangement. Additional pilot-scale coal combustion hot-flow tests were then carried out to further understand the effect of the perforated plate on bag protection and overall AHPC performance and to optimize the perforated-plate design. Tests PTC-CR-622 and 623 were sponsored separately by DOE and Gore under Jointly Sponsored Research Program Cooperative Agreement No. DE-FC26-98FT40321, but the experimental results are also included here to provide a more comprehensive understanding of perforated-plate AHPC performance.

For these tests, grounded perforated plates were placed between the filter bags and the discharge electrodes (Figure 3.3-34, which shows the 4-bag pilot AHPC system with the front removed). In this case, no perforated plates were installed on the outside of the discharge electrodes to more closely simulate a multirow AHPC chamber.

The pilot-scale experiments were performed to investigate the effect of perforated-plate design on overall AHPC performance. Different perforated plates, in terms of hole size and opening area percentage, were selected and evaluated in the coal combustion system. The spacing from the perforated plates to bags (PTB) was varied to examine the effect on bag protection and AHPC performance. Three different bags manufactured by Gore were evaluated. These bags were used with different electrodes, i.e., bidirectional ELEX-2-mast, directional ELEX-2-mast,



Figure 3.3-34. AHPC pilot-scale configuration at the EERC.

and directional ELEX-with mast-only second electrode, to evaluate their performance under different configurations. Operating parameters such as corona current, pulse trigger pressure, and dust loading were also varied. A summary of the variables tested in the pilot-scale experiments is listed below.

Bag Types

- GORE-TEX[®] membrane/GORE-TEX[®] felt filter bag
- GORE-NO STAT[®] filter bag (GORE-TEX[®] membrane/GORE-TEX[®] antistatic felt,)
- GORE-NO STAT[®] filter bag (GORE-TEX[®] antistatic membrane/GORE-TEX[®] antistatic felt)

Perforated Plates

- Hole size (ID = 1.5–2.0 in. [38–51 mm])
- Opening area (48%–52%)

- Geometric alignment (PTB = 2.0–3.0 in. [0.051–0.076 m])

Electrodes

- Bidirectional ELEX-2-mast
- Directional ELEX-2-mast
- Directional ELEX-mast-only second

Operating Conditions

- Current (0–3.0 mA)
- Pulse trigger pressure (6.5–8.0 in. W.C. [1.65–2.0 kPa])

To quantitatively evaluate the effect of the perforated plate on bag protection, the current to the bags was measured under the different perforated-plate configurations for the three different bags. Secondary current and voltage, bag-cleaning interval, and tube sheet pressure drop were monitored.

A total of five configurations were selected and evaluated in the hot-flow coal combustion tests, as listed in Table 3.3-4. The CR designation is for the Cordero Rojo complex coal used for the tests. Two GORE-NO STAT[®] filter bags (GORE-TEX[®] antistatic membrane/GORE-TEX[®] felt), one GORE-NO STAT[®] filter bag (GORE-TEX[®] membrane/GORE-TEX[®] felt), and one GORE-TEX[®] membrane/GORE-TEX[®] felt filter bag were installed in the AHPC pilot unit to examine bag protection and their performance in the modified configuration.

The bidirectional ELEX-2-mast electrodes used in PTC-CR-622-1 forced the fly ash particles to migrate both to the perforated plates and outside wall surface of the AHPC vessel. Directional ELEX-2-mast electrodes were then used in the following experiments to minimize collection of dust on the outside vessel walls. Directional ELEX-mast-only second electrodes (no electrode tips on the second mast) were used at the end of Test PTC-CR-623-3 to concentrate the corona current at the AHPC inlet.

TABLE 3.3-4

Experimental Parameters for the AHPC Pilot Test				
Test No.	Duration, hr	Electrode	PTB ¹	Plate Type
PTC-CR-622-1	24	Bidirectional ELEX-2-mast	2.0	1.5 in. (38 mm), 48% open
PTC-CR-622-2	35	Directional ELEX-2-mast	2.0	1.5 in. (38 mm), 48% open
PTC-CR-622-3	40	Directional ELEX-2-mast	2.0	2.0 in. (51 mm), 52% open
PTC-CR-623-1	54	Directional ELEX-2-mast	3.0	1.5 in. (38 mm), with solid section 42% open
PTC-CR-623-3	57	Directional ELEX-2-mast and Directional ELEX-mast-only second	3.0	1.5 in. (38 mm), 48% open

¹ Spacing from perforated plate to the bags.

By adjusting the perforated-plate position in the AHPC, the PTB spacing was varied from 2.0 to 3.0 in. (0.051 to 0.076 m) to examine the effects on bag protection and bag-cleaning ability. Secondary current and voltage, bag-cleaning interval, and tube sheet pressure drop were measured, and K_2C_i and residual drag were calculated for all of the tests.

3.3.2.2.2 Results for PTC-CR-622 Test

Test PTC-CR-622-1 was run (January 15–16, 2001) with an A/C ratio of 12 ft/min (3.7 m/min) and a pulse trigger pressure of 8.0 in. W.C. (2.0 kPa). Perforated plates (1.5 in. [38 mm], and 48% opening area) were installed. Figure 3.3-35 shows the 1.5-in. holes (38-mm) are uniformly distributed over the perforated plate in a staggered pattern. The PTB spacing was set at 2.0 in. (51 mm), which provided enough protection of the bags from electrical damage and also prevented any possible contact between the bag and the plate during the bag pulsing. The bidirectional ELEX-2-mast standard electrodes were used in the experiment. The secondary current was at 1.5 mA throughout the test period except for a gradual current reduction at the end of the test. The bag-cleaning interval (shown in Figure 3.3-36) was initially at 120 min and then dropped and remained steady around 100 min after 24 hr of testing. The residual drag plotted as a function of running time in Figure 3.3-37 was in the range of 0.25 to 0.35 in. W.C./ft/min during the test, indicating an excellent bag-cleaning ability even at a relatively low current level

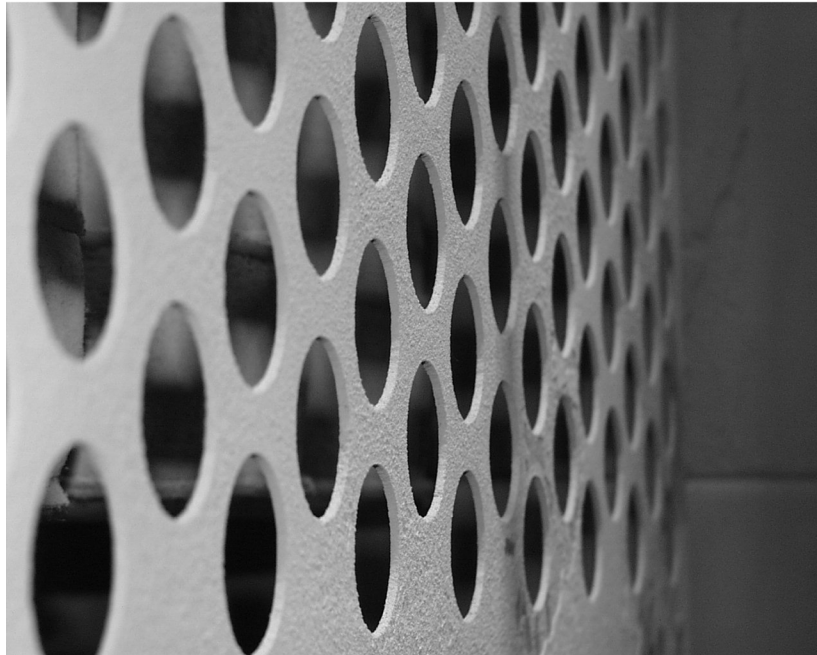


Figure 3.3-35. Photo showing the 1.5-in. (38-mm) holes uniformly distributed over the perforated plate in a staggered pattern.

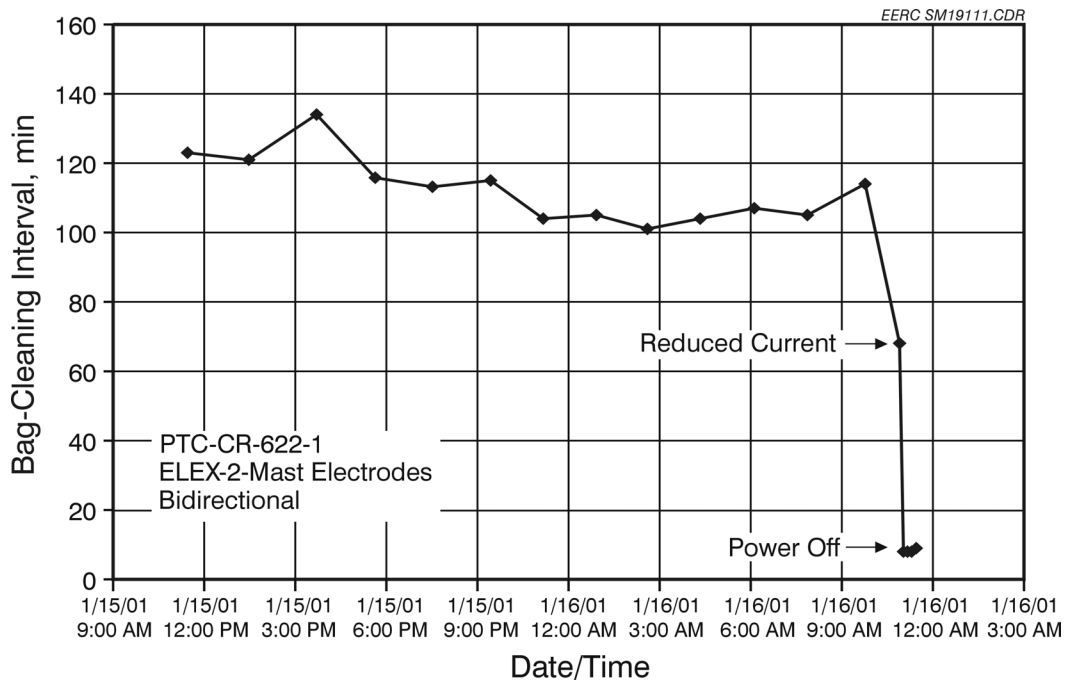


Figure 3.3-36. Bag-cleaning interval for PTC-CR-622-1.

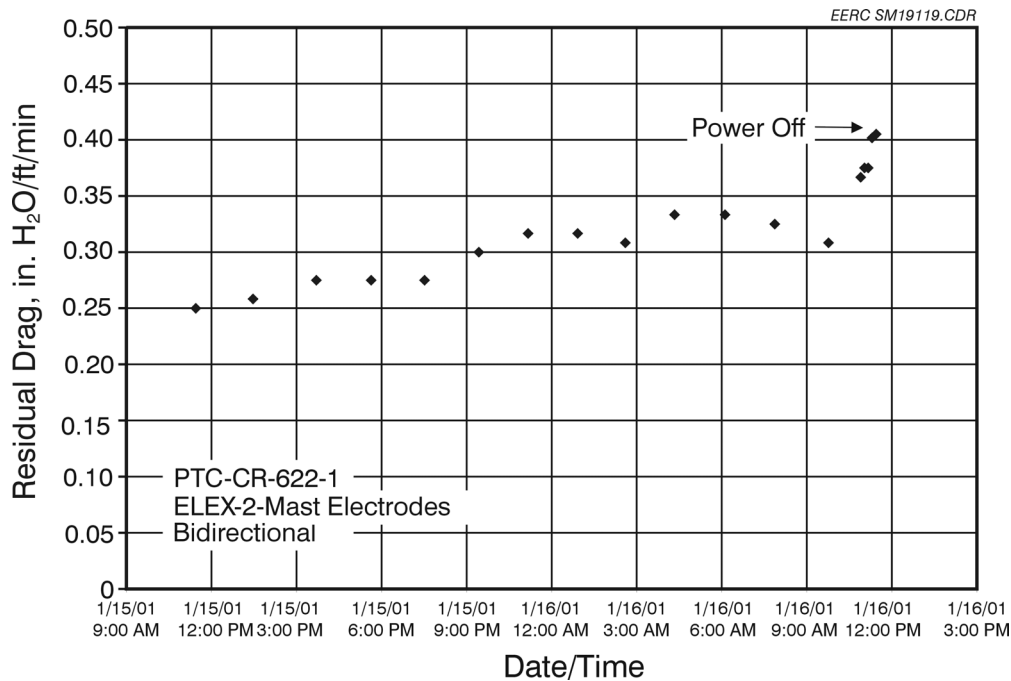


Figure 3.3-37. Residual drag for PTC-CR-622-1.

of 1.5 mA. However, it is noted that the residual drag might climb in longer-term operation. The calculated K_2C_i (in Figure 3.3-38) remained at a value of 2 during the test when the current was only 1.5 mA, showing that the ESP functioned extremely well at the low current in this perforated-plate configuration. The HV power was shut down at the end of Test PTC-CR-622-1 to examine perforated-plate AHPC performance under a conventional baghouse operation mode. Without the presence of corona current and electrical field, the fast accumulation of fly ash on the filter bags resulted in a dramatic increase of K_2C_i up to 22 (Figure 3.3-38), indicating no electrostatic precipitation occurred. Also, the bag-cleaning interval was reduced to 7 min with a relatively higher residual drag of 0.4 in. W.C./ft/min. The above results not only show the enormous benefits of the synergism between the ESP and filtration within the AHPC, but also show that the AHPC could operate for short periods without ESP power. This could be very important in full-scale AHPC operation, because the AHPC could treat all of the flue gas without an increase in emissions during periods of interruption to the ESP power. The photo (Figure 3.3-39) shows ash deposition on the perforated plates after plate rapping. The ash deposition pattern observed was the result of the specific electrode design. The ash deposited on

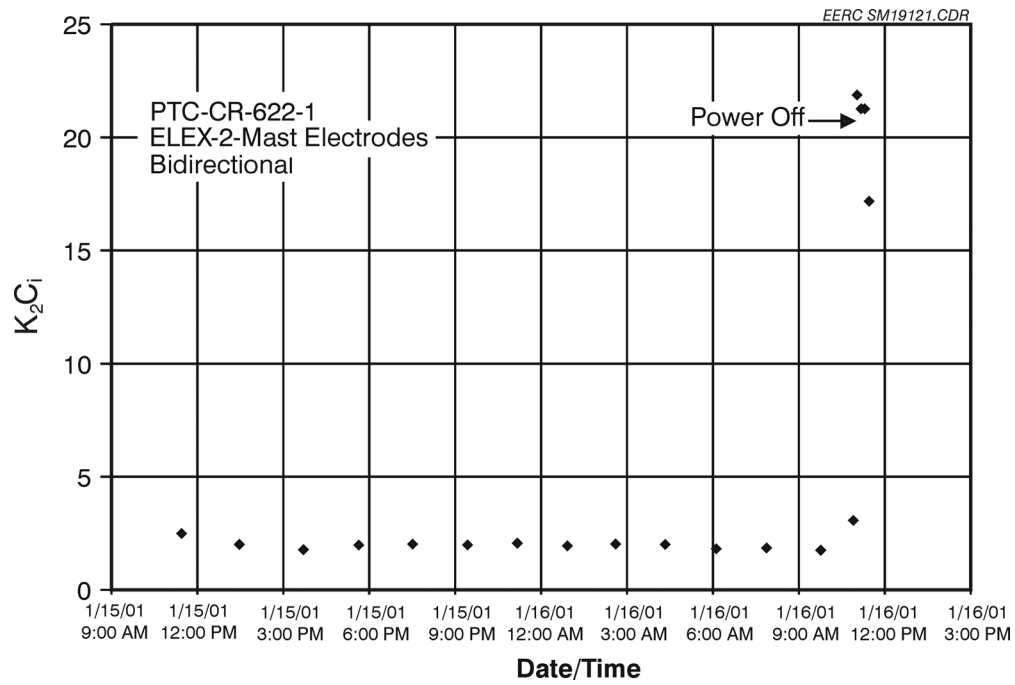


Figure 3.3-38. K_2C_i for PTC-CR-622-1.

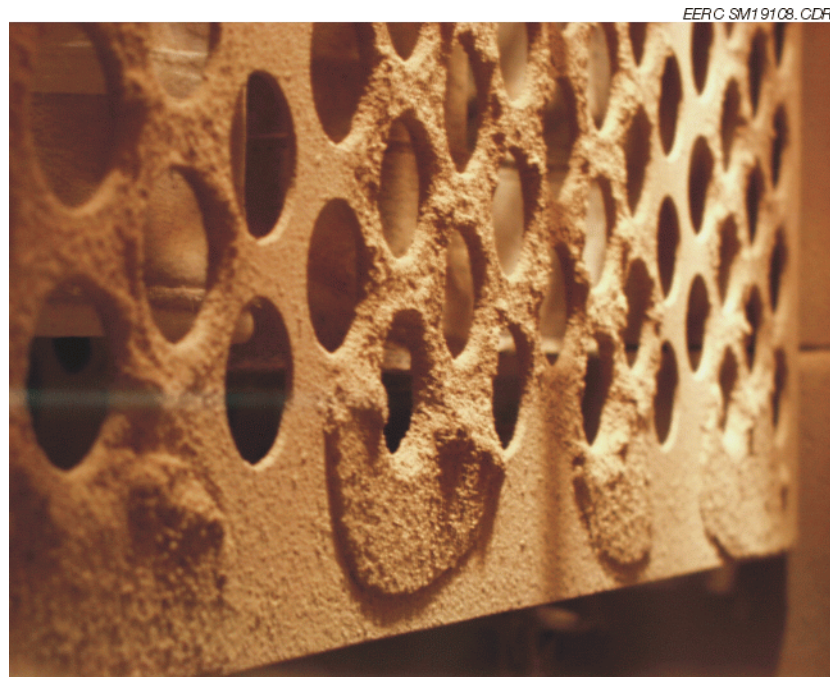


Figure 3.3-39. Fly ash-deposited pattern on the perforated plates at the pilot-scale AHPC.

the perforated-plate section facing toward the discharging electrode tips remained on the plates after rapping because of the existing higher electrical field, implying regular power-off rapping might be helpful to clean the perforated plate more efficiently.

Current to the filter bags was less than 2 μA during the testing period, which showed very good protection on the bags by the perforated plates with 1.5-in. hole size and 48% open area.

Tests PTC-CR-622-2 (35 hr) and PTC-CR-622-3 (40 hr) were carried out to examine AHPC performance under two different perforated plate designs: 1.5-in. (38-mm) hole size and 2.0-in. (51-mm) hole size. Directional ELEX-2-mast electrodes instead of the bidirectional ELEX-2-mast electrodes were used to force more fly ash to migrate toward the perforated plates rather than the outside walls of the vessel. The secondary current was increased to 3.0 mA during the two test periods except during Run Hours 18 to 23 when current level was reduced to 1.5–0.5 mA to investigate the corresponding AHPC performance. The bag-cleaning intervals shown in Figure 3.3-40, 375 min for PTC-CR-622-2 and 594 min for PTC-CR-622-3, were the longest bag-cleaning intervals achieved to date. The bag-cleaning interval dropped to 205 min (PTC-CR-622-2) and 280 min (PTC-CR-622-3) at the end of the tests because of bag seasoning. The observed bag-cleaning intervals of less than 100 min in the middle of the experiments were due to the lower current level at that time. The improved bag-cleaning intervals in the two tests compared to the data in PTC-CR-622-1 are attributed to the higher current level, resulting in better ESP performance, which is also reflected in the K_2C_i shown in Figure 3.3-41. The K_2C_i at the current level of 3 mA was as low as 1.0 at the end of the test, which is the best achieved to date. The residual drag (Figure 3.3-42) during the two tests was maintained less than 0.3 in. W.C./ft/min at the end of the experiments, demonstrating better cleaning ability in the two configurations than that in PTC-CR-622-1, partially due to the better ESP performance at the higher current level. PTC-CR-622-3 showed better performance than PTC-CR-622-2 in terms of the longer bag-cleaning interval and the lower residual drag. Except for a different hole size, operating conditions—pulse trigger pressure, current level, and A/C ratio—were the same. This suggests that the 2.0-in. (51-mm) hole perforated-plate design might be the better option in improving overall AHPC performance. However, there was concern that the 2.0-in. (51-mm)

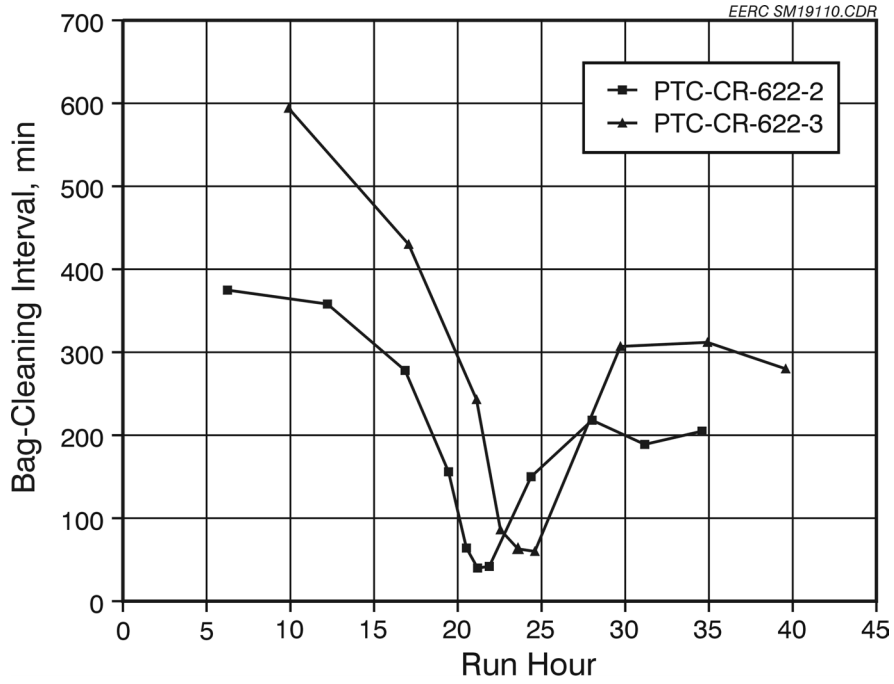


Figure 3.3-40. Bag-cleaning intervals for PTC-CR-622-2 and PTC-CR-622-3.

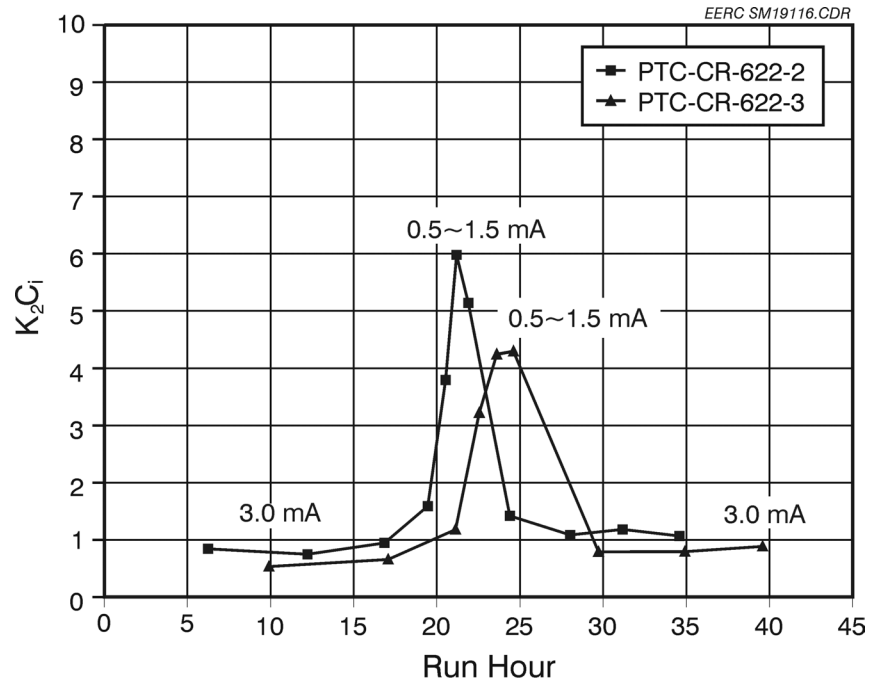


Figure 3.3-41. K_2C_i for PTC-CR-622-2 and PTC-CR-622-3.

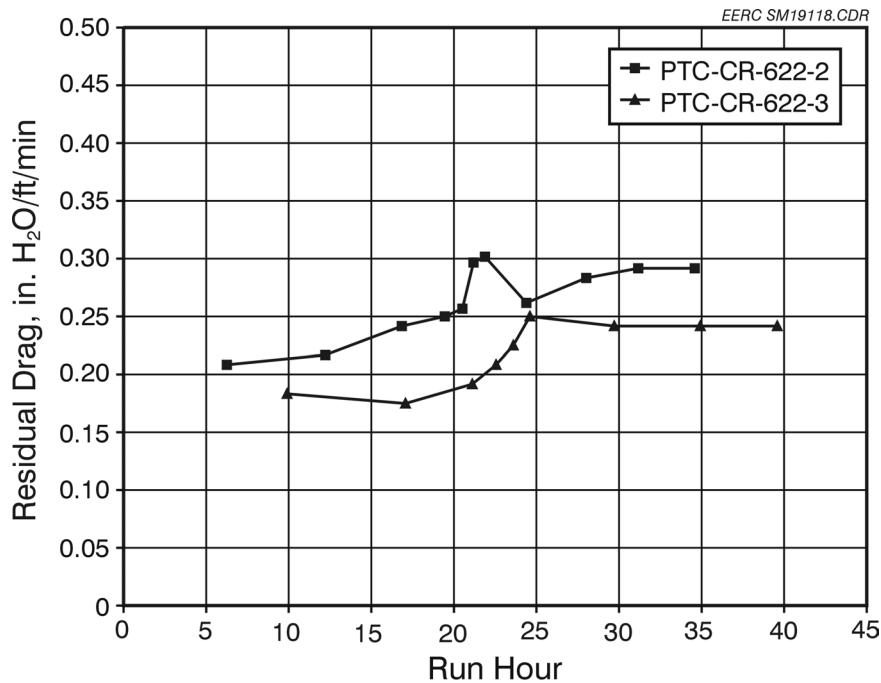


Figure 3.3-42. Residual drag for PTC-CR-622-2 and PTC-CR-622-3.

hole size may not provide as good bag protection as the 1.5-in (38-mm) hole size. Bag current for the 2.0-in. (51-mm) hole size was approximately 7.9 μ A at 63 kV compared to 5.8 μ A at 63 kV for the 1.5-in. (38-mm)-sized holes, but both of these provided excellent bag protection.

The PTC-CR-622 series experiments were exceptionally successful, achieving long bag-cleaning interval, low residual drag, and reasonable power consumption. These results show the perforated-plate design can not only protect the bag from electrically induced damage, but also substantially improve overall AHPC performance.

3.3.2.2.3 Results for Test PTC-CR-623

The perforated-plate design was then modified in an effort to provide better protection of the bags. A nonuniform hole distribution on perforated plates was designed and manufactured for the PTC-CR-623-1 test as shown in Figure 3.3-43. The hole pattern on the perforated plate was changed so that the plate section directly opposite of the bags was solid to reduce the electrical field around the bag surface and current to the bags. Tests PTC-CR-623-1 (1.5-in.

[38-mm] hole with solid section) and PTC-CR-623-3 (1.5-in. [38-mm] hole without solid section) were then carried out from February 5–10, 2001. The directional ELEX-mast-only second electrodes were used at the end of Test PTC-CR-623-3 to optimize the electrical field within the AHPC vessel by concentrating corona current at the AHPC inlet. The perforated plates were also moved closer to the electrodes so that the spacing from the perforated plate to the bag surface was increased to 3.0 in. (76 mm) to examine its effect on bag protection. Experiments were then performed to evaluate AHPC performance under the modified configurations. Other parameters such as current and pulse trigger pressure were also tested during the two experiments. Current was 1.5 mA except for short-term low-current-level (0.5–0.75-mA) tests. The tube sheet pressure drop is shown in Figures 3.3-44 and 3.3-45 for PTC-CR-623-1 and PTC-CR-623-3, respectively. The pulse trigger pressure was reduced to 6.5 in. W.C. (1.62 kPa) for part of the time. Additional fly ash was injected into the system during Test PTC-CR-623-3 on February 9, 2001, 14:23–18:13, to examine AHPC performance under a high dust-loading environment. The supplemental dust injection resulted in an extremely high dust loading of 22.8 grains/scf (52 g/m³) which was 14 times the baseline loading.

The bag-cleaning interval, residual drag, and K_2C_i results are plotted in Figures 3.3-46–3.3-51 for the two tests. Figures 3.3-46 and 3.3-47 show that the bag-cleaning interval dropped to about half the previous level when the current and trigger pressure were reduced. The observed shorter bag-cleaning interval of 18 min in PTC-CR-623-3, caused by the high dust loading, is still encouraging because anything over 10 min is considered acceptable under a high A/C ratio of 12 ft/min (3.7 m/min). The residual drag (Figures 3.3-48 and 3.3-49) only increased slightly at a low trigger pulse pressure and low current levels. This is also encouraging because it shows that there is a wide margin to reduce power consumption and still maintain a long bag-cleaning interval and excellent bag-cleaning ability. The calculated K_2C_i (Figures 3.3-50 and 3.3-51) shows its strong dependence on current level.

Decreasing the trigger pressure from 8 in. W.C. to 6.5 in. W.C. (2.0 kPa to 1.62 kPa), however, does not result in a significant increase of K_2C_i . It is noted that, by using ELEX-mast-

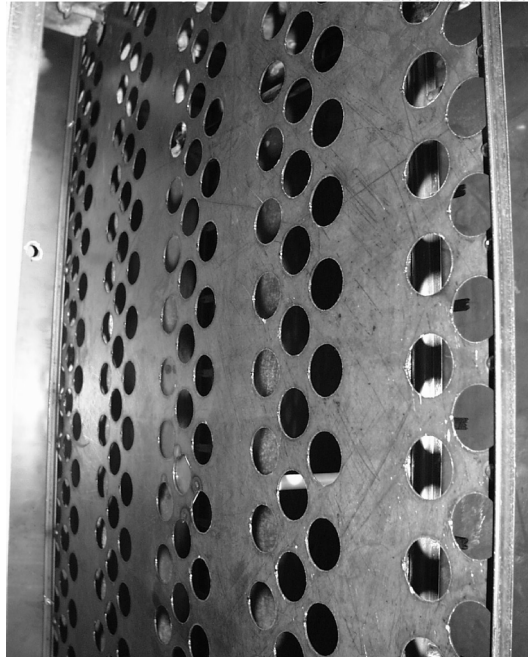


Figure 3.3-43. A nonuniform hole distribution on perforated plates.

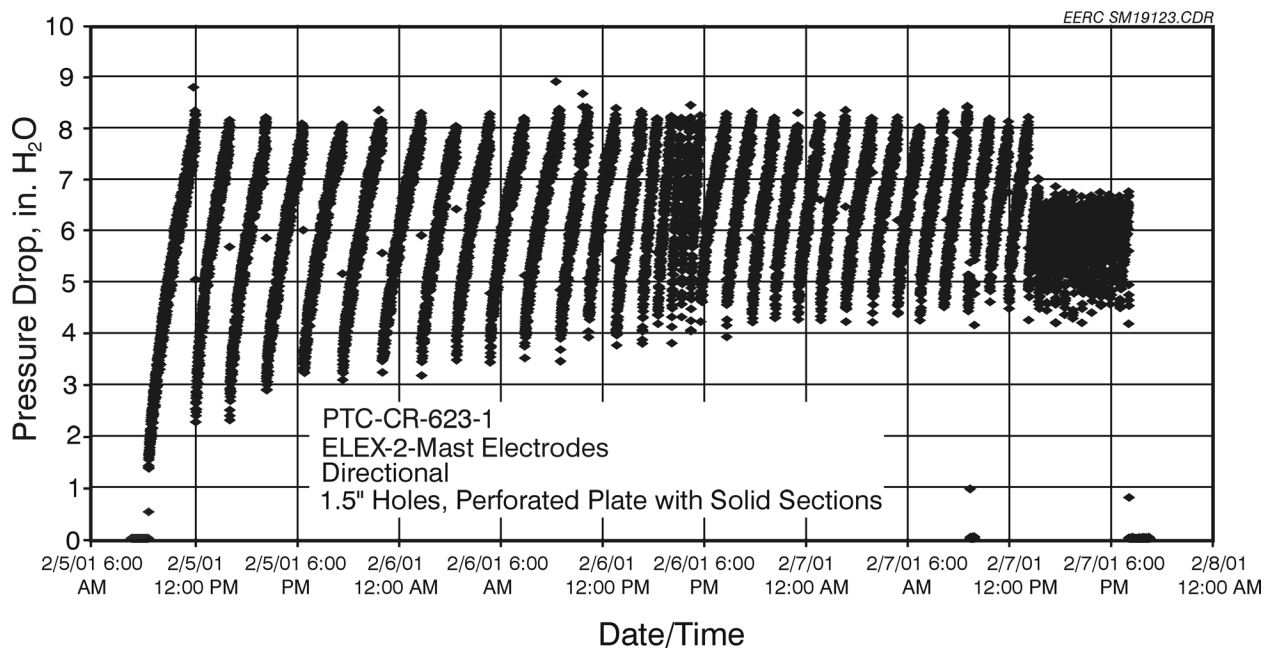


Figure 3.3-44. Pressure drop for PTC-CR-623-1.

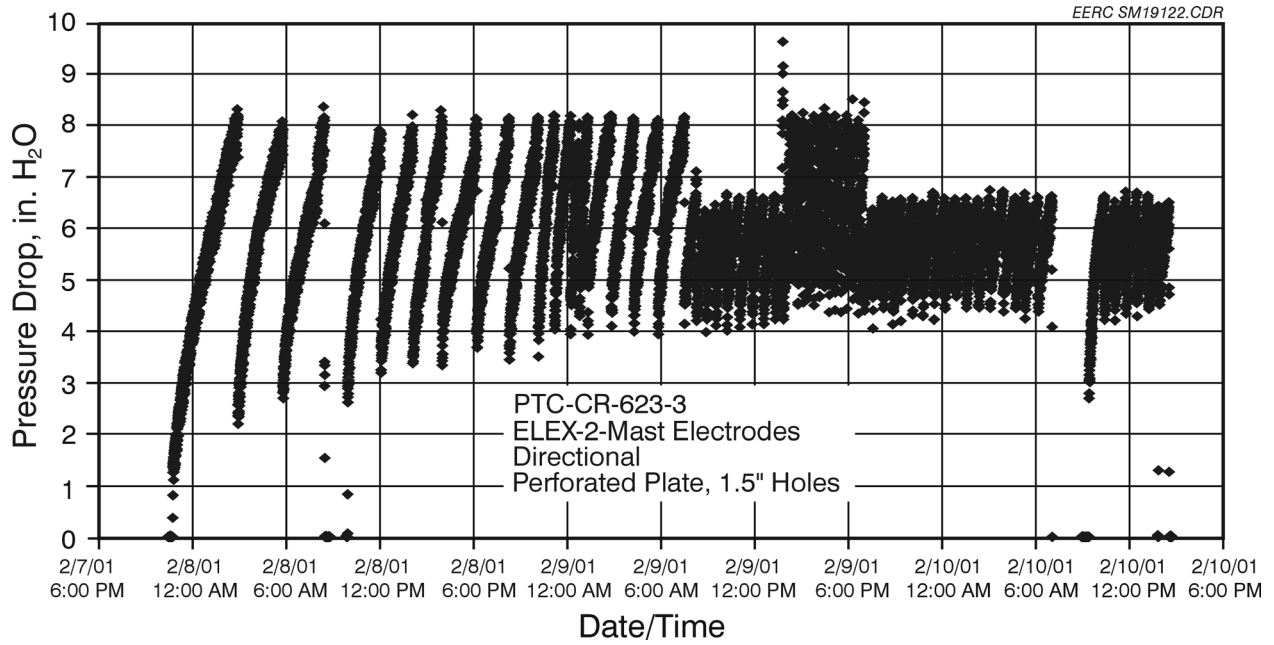


Figure 3.3-45. Pressure drop for PTC-CR-623-3.

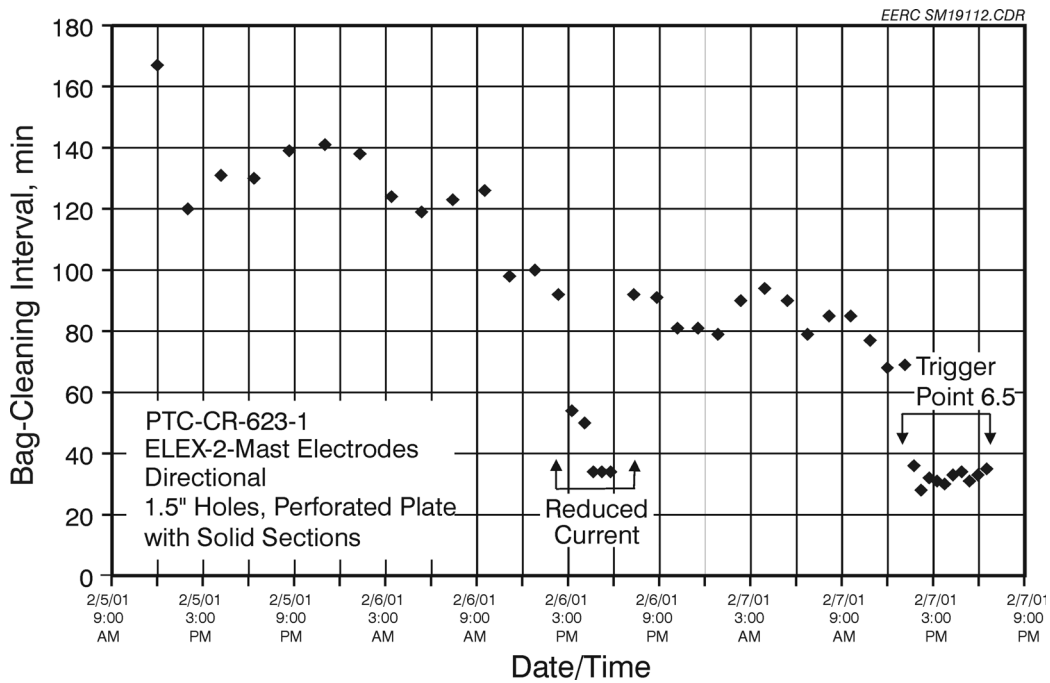


Figure 3.3-46. Bag-cleaning interval for PTC-CR-623-1.

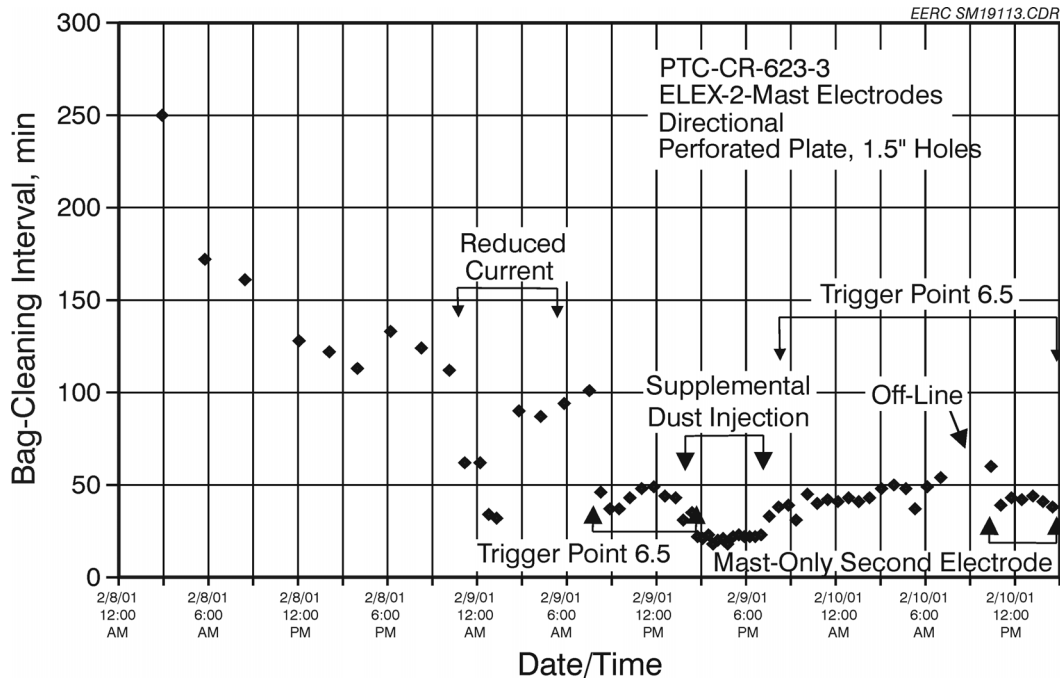


Figure 3.3-47. Bag-cleaning interval for PTC-CR-623-3.

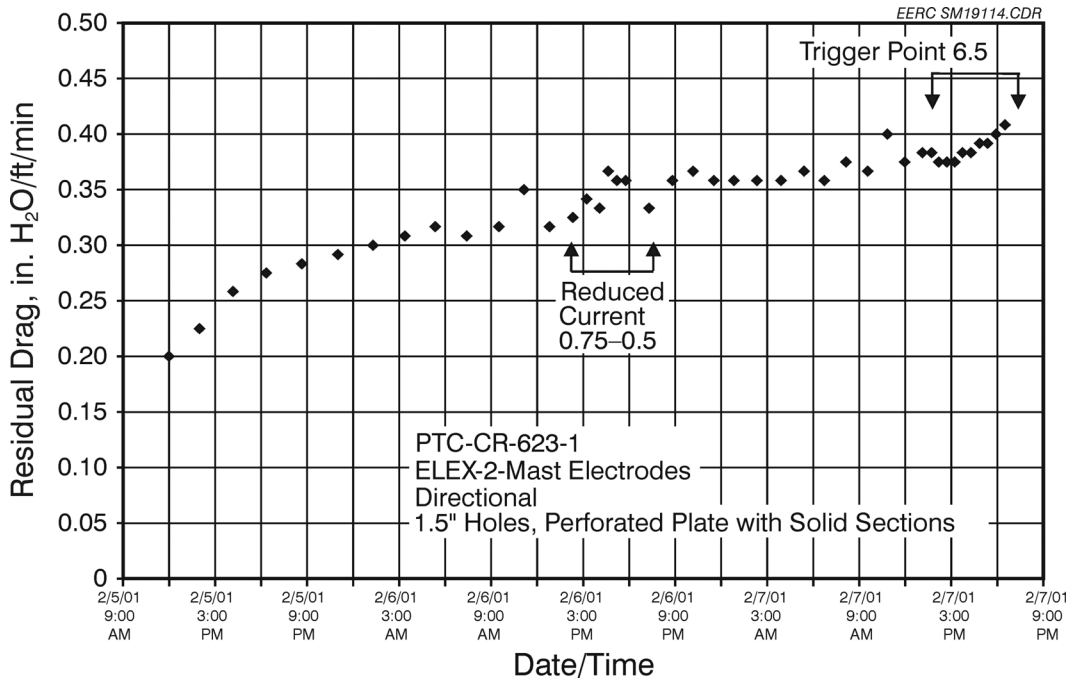


Figure 3.3-48. Residual drag for PTC-CR-623-1.

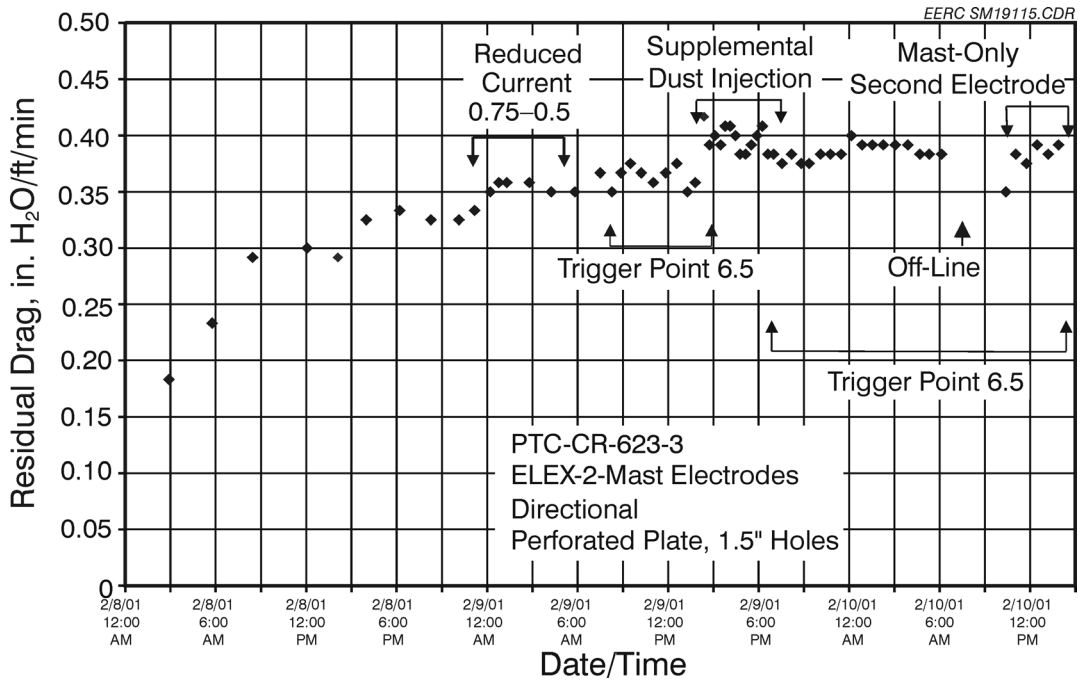


Figure 3.3-49. Residual drag for PTC-CR-623-3.

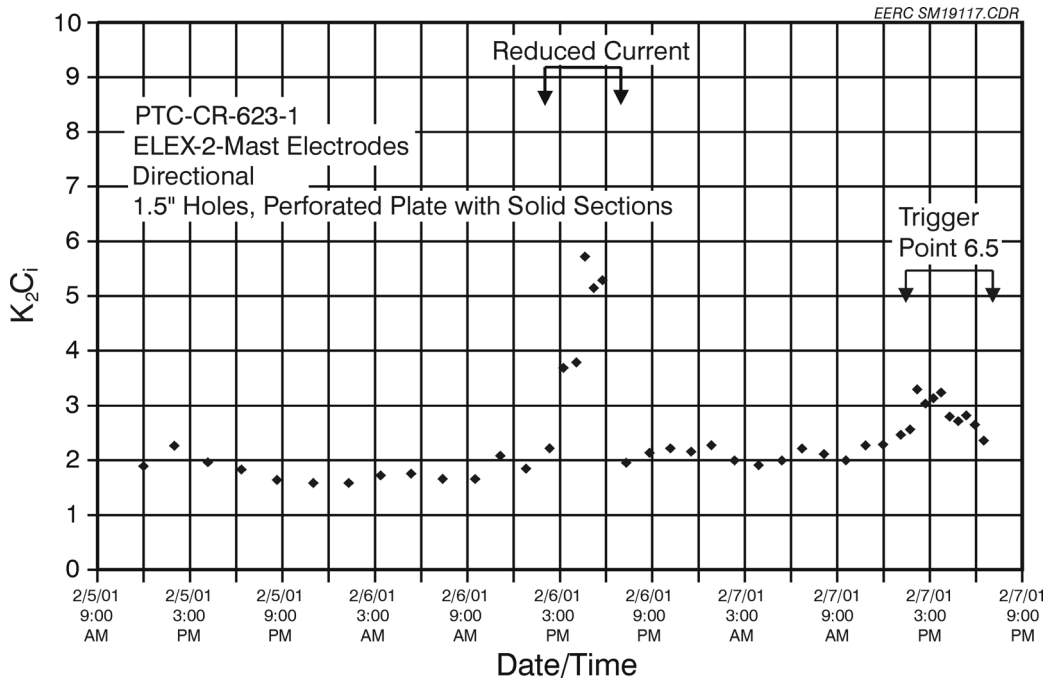


Figure 3.3-50. K_2C_i for PTC-CR-623-1.

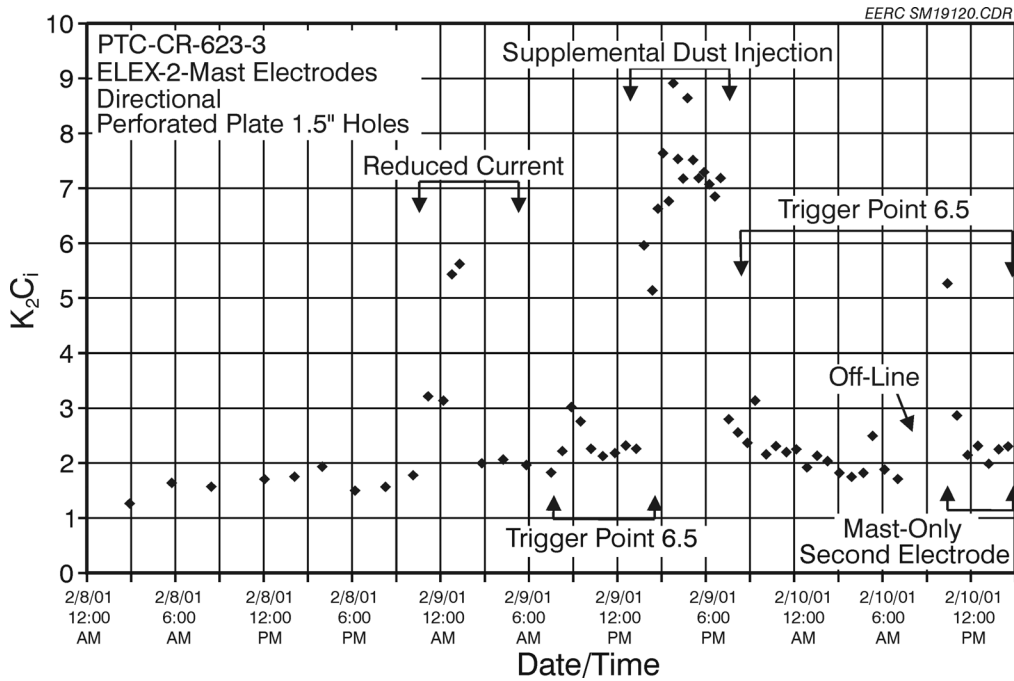


Figure 3.3-51. K_2C_i for PTC-CR-623-3.

only second electrodes instead of directional ELEX-2-mast electrodes, there was no significant difference observed with regard to bag-cleaning interval, residual drag, and K_2C_i . This shows the potential of using mast-only-type electrodes in the AHPC to reduce ESP power without deteriorating AHPC overall performance.

There were no significant differences with regard to overall AHPC performance for the two perforated-plate designs (with and without solid section). The adjustment of PTB to 3.0 in. (76 mm) also did not significantly affect AHPC performance.

The current to the bags was maintained at less than $3 \mu\text{A}$ in the presence of the perforated plates during the testing periods. All the bags were sent back to Gore for analysis, and no bag damage was observed for all three types of bags.

To further investigate bag cleanability, the residual dust cake weights on the bags were determined by comparing the new bag weight with the bag weight at the end of the tests (Table 3.3-5).

TABLE 3.3-5

Residual Dust Cake Weights						
Test No.	Bag 1, g	Bag 2, g	Bag 3, g	Bag 4, g	Average, g	Average, lb
PTC-CR-623-1	20.7	25.2	14.7	19.0	19.9	0.0439
PTC-CR-623-3	15.0	20.4	17.3	13.9	16.65	0.0367

The residual dust cake weight W_R can be calculated as: $W_R = W/(\pi \cdot d \cdot L + \pi d^2)$

$$\text{PTC-CR-623-1: } W_R = 9.359 \times 10^{-3} \text{ (lb/ft}^2\text{)}$$

$$\text{PTC-CR-623-3: } W_R = 7.824 \times 10^{-3} \text{ (lb/ft}^2\text{)}$$

For viscous flow, the pressure drop across fiber filters is further developed as:

$$dP = K_f V + K_2'' W_R V + K_2 C_i V^2 t / 7000 \quad [\text{Eq. 3.3-1}]$$

where:

- dP = differential pressure across baghouse tube sheet (in. W.C. [kPa])
- K_f = fabric resistance coefficient (in. W.C.-min/ft)
- V = face velocity or A/C ratio (ft/min [m/min])
- K_2'' = specific residual dust cake resistance coefficient (in. W.C.-ft-min/lb)
- K_2 = specific dust cake resistance coefficient (in. W.C.-ft-min/lb)
- W_R = residual dust cake weight (lb/ft²)
- C_i = inlet dust loading (grains/acf)
- t = filtration time between bag cleaning (min)

The first term in Equation 3.3-1 accounts for the pressure drop across the fabric. The new GORE-TEX® membrane filter media has a pressure drop across the fabric of approximately 1.5 in. W.C. (0.37 kPa) at an A/C ratio of 12 ft/min (3.7 m/min).

The second term in Equation 3.3-1 accounts for the pressure drop contribution from the permanent residual dust cake that exists on the surface of the fabric. For operation at high A/C ratios, the bag cleaning must be sufficient to maintain a very light residual dust cake and ensure that the pressure drop contribution from this term is reasonable. The contribution to pressure drop from this term is one of the most important indicators of longer-term bag cleanability.

The third term in Equation 3.3-1 accounts for the pressure drop contribution from the dust accumulated on the bags since the last bag cleaning. K_2 is determined primarily by the fly ash particle-size distribution and the porosity of the dust cake.

From the known pressure drop across the filter bag, residual dust cake weight, and calculated K_2C_i , K_2'' was calculated based on the experimental data (Table 3.3-6).

The K_2'' values for the two runs are not significantly different, but the slightly higher value of K_2'' in Test PTC-CR-623-3 could be the result of double pulses at the end of the experiment.

During the experiments, a sampling probe was installed at the location between the perforated plates and the filter bags. The dust loading toward the filter bags was measured by U.S. Environmental Protection Agency (EPA) Method 5 (Table 3.3-7).

The K_2 values shown in Table 3.3-7 are remarkably similar to the K_2'' values in Table 3.3-6. This is an encouraging result because it implies that the dust did not pack or penetrate into the fibers deeply, which could result in a significant increase in K_2'' over K_2 .

TABLE 3.3-6

Calculated Results of K_2 "				
Time	Running Time, hr	K_2C_i	K_2 "	Average, K_2 "
PTC-CR-623-1				
2/7/01 13:43	52.5	2.56	27.6	
2/7/01 14:11	52.9	3.29	27.6	
2/7/01 14:43	53.5	3.04	26.7	
2/7/01 15:14	54.1	3.14	26.7	
2/7/01 15:44	54.5	3.24	26.7	
2/7/01 16:17	55.1	2.80	27.6	
2/7/01 16:51	55.6	2.72	27.6	
2/7/01 17:22	56.2	2.82	28.5	
2/7/01 17:55	56.7	2.65	28.5	
2/7/01 18:30	57.3	2.36	29.4	
				27.7
PTC-CR-623-3				
2/10/01 3:04	52.3	1.82	34.1	
2/10/01 3:54	53.2	1.75	34.1	
2/10/01 4:42	53.9	1.82	34.1	
2/10/01 5:19	54.6	2.50	33.1	
2/10/01 6:08	55.4	1.88	33.1	
2/10/01 7:02	56.3	1.71	33.1	
				33.6

TABLE 3.3-7

Calculated Results of K_2				
Test No.	Sampling Date and Time	C_i , grains/scf	K_2C_i	K_2
PTC-623-1	02/06/01, 10:45	0.076	1.95	25.68
PTC-623-3	02/08/01, 15:10	0.064	1.69	26.55

3.3.2.2.4 Evaluation of ESP Performance in the AHPC Unit under the Perforated-Plate Configuration

In order to evaluate ESP performance with the perforated-plate configuration, a series of experiments was conducted to measure fly ash particle concentrations in the AHPC unit. Two sampling locations were selected: the inlet of the AHPC and the location between the perforated plates and bags. The dust loading, measured by EPA Method 5, was 1.674 grains/scf at the inlet of the AHPC and 0.064 grains/scf in front of the bag when the current was 1.5 mA. The resulting collection efficiency of the ESP alone was 96.2%, significantly higher than the ESP collection efficiency of 95% achieved in the previous Phase I and II AHPC studies, even though the current was only 1.5 mA. This indicates an improvement of electrostatic precipitation of the AHPC system with the perforated plates compared to the previous design. The results are also in agreement with the observed low K_2C_1 values. Fine-particle concentration was measured in front of the bag (between the perforated plate and bag) under different current levels with the APS system. The number median diameter of the fly ash particle flowing toward the bag was 1.4 μm , and the mass median diameter was 6.6 μm under several conditions. The respirable mass concentrations, plotted as a function of corona current, are shown in Figure 3.3-52. The respirable mass concentration was 205.8 mg/m^3 at a current of 0.37 mA and 93.8 mg/m^3 at a current of 1.5 mA, a 54.4% decrease. However, the respirable mass concentration was only reduced to 65.7 mg/m^3 when the current was further increased to 3 mA. This indicates that the ESP section in the AHPC can function very well even at a relatively low current level. The average respirable mass concentration in front of the bag (between the perforated plate and bag) when the power was off was approximately 660 mg/m^3 , which corresponds to 85.8% and 89.6% ESP collection efficiency of respirable mass at the currents of 1.5 and 3.0 mA, respectively. Both are higher than the 83% ESP collection efficiency of respirable mass in the previous design in the Phase I and II studies. Again, the results demonstrate better ESP performance of the perforated- plate AHPC system compared to the previous design.

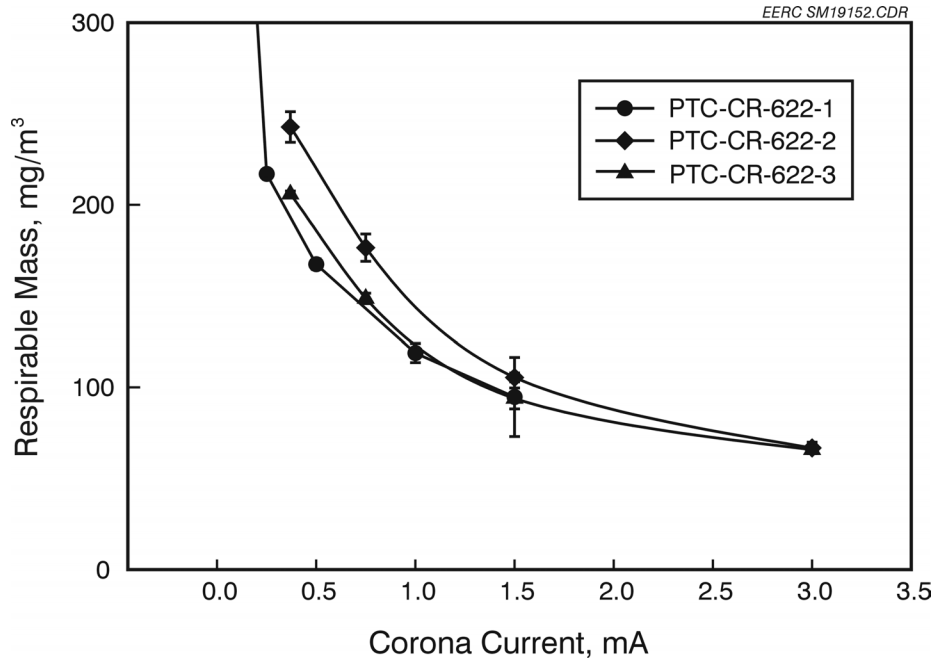


Figure 3.3-52. Effect of corona current on respirable mass in AHPC.

3.3.2.2.5 Summary of Perforated-Plate Testing

The AHPC performed extremely well even at a low current level (1.5–3.0 mA) and a low pulse trigger pressure of 6.5 in. W.C. (1.62 kPa). The longest bag-cleaning interval was 594 min, which is the best achieved to date. The residual drag was reduced to the range from 0.25 to 0.35 in. W.C./ft/min, showing excellent bag-cleaning ability under the perforated-plate configurations. The K_2C_i at the current level of 3 mA was as low as 1, indicating excellent ESP performance. The current to bags, measured for all the tests in the presence of the perforated plates, was below 1.5 μ A, which is extremely low compared to 100 μ A at the same corona current level without perforated plates, indicating excellent bag protection in terms of reducing bag current. No electrically induced damage was observed for all bags tested based on the visual inspection at the end of the experiments. The results show the perforated plates can provide extremely good protection of the different bags.

3.3.3 Bench-Scale Experiments and Theoretical Calculation for AHPC Perforated-Plate Configuration

In order to better understand the effect of the perforated plates on bag protection, a bench-scale experimental system was designed and built to measure the current to the bags under several perforated-plate configurations. Also, a theoretical model was developed to simulate the electrical field in the AHPC pilot unit in the presence of perforated plates to examine its effects on bag protection.

3.3.3.1 Effect of Perforated-Plate Hole Size on Bag Current

Experimental results in the pilot-scale studies clearly demonstrated that the perforated-plate configuration effectively reduced the current to the bags, which was believed to correlate with the observed bag damage. To better understand the interactions between the electrical field and bag fabric in the presence of a perforated plate, a bench-scale experimental system was designed and built to measure the current to the bags under several perforated-plate configurations. The schematic diagram of the system is shown in Figure 3.3-53. HV from the DC power unit is

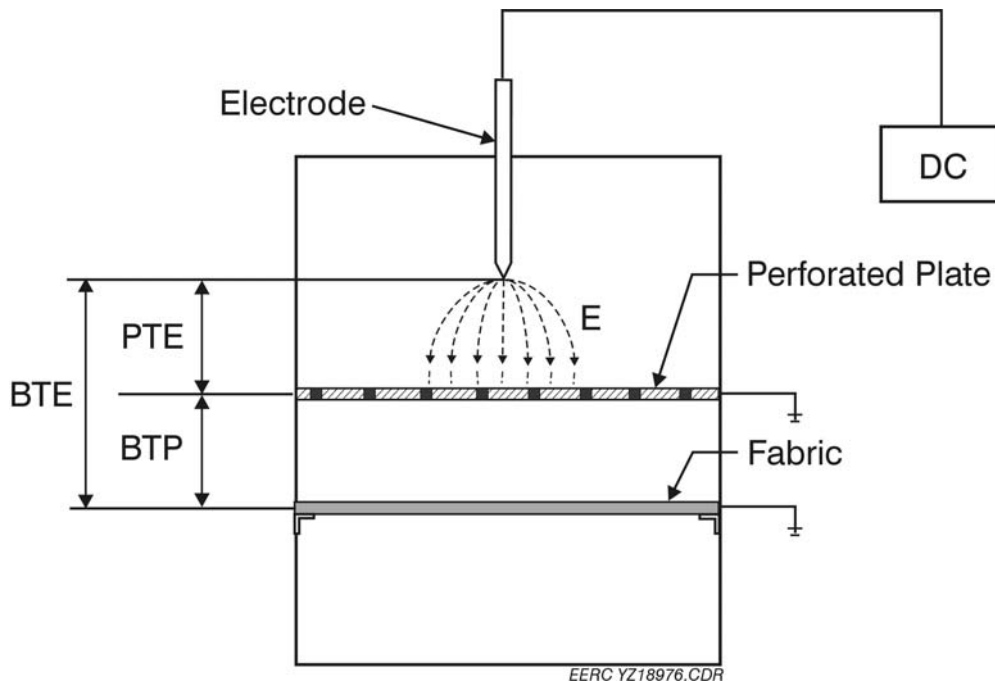


Figure 3.3-53. Schematic of the bench-scale AHPC.

applied to the electrode to generate corona. The ionic current, flowing downstream (as shown in Figure 3.3-53) toward the fabric surface, is intercepted by the installed perforated plate because of the diversion of the electrical field to the plate. The spacings between the electrode, the perforated plate, and the bag surface are adjustable. The bag fabric is isolated from the chamber to measure the current to the bag by using an ammeter. The evaluated parameters are listed in Table 3.3-8.

TABLE 3.3-8

Parameters Evaluated in the Bench-Scale Experiments	
PTB Spacing, in. (mm)	1.5–2.5 (38.1–63.5)
ETP Spacing, in. (mm)	2.5–4.5 (63.5–114.3)
ETB Spacing, in. (mm)	4–6 (101.6–152.4)
Perforated-Plate Hole Size, in. (mm)	0.75, 1.00, 1.50 (19.1, 25.4, 38.1)

The current to the fabric was first measured as a function of ETB without the perforated plate for two different bag fabrics: GORE-NO STAT[®] filter bag (GORE-TEX[®] antistatic membrane/GORE-TEX[®] felt) and GORE-NO STAT[®] filter bags (GORE-TEX[®] membrane/GORE-TEX[®] felt). The VI curves are shown in Figures 3.3-54 and 3.3-55 (as a function of ETB). At an applied voltage of 65 kV and a ETB spacing of 6 in. (152.4 mm), a normal operating condition for the AHPC system, the current to the bag was 65 μ A for (GORE-TEX[®] antistatic membrane/GORE-TEX[®] felt) and 131.4 μ A for GORE-NO-STAT[®] filter bags (GORE-TEX[®] membrane/GORE-TEX[®] felt), respectively, accounting for more than 50% of the total generated current. The experimental results showed the current to the bag increased with decreasing distance between the electrode and the bag for both fabrics.

The perforated-hole size is very important to AHPC performance. It will determine the extent of the reduced bag current as well as the dust loading toward the bags. The effect of the hole size on the perforated plate on bag current was investigated by measuring the current to bags at ETB = 4.0 in. (101.6 mm) and PTB = 1.0 in. (25.4 mm) for three different hole sizes: 0.75,

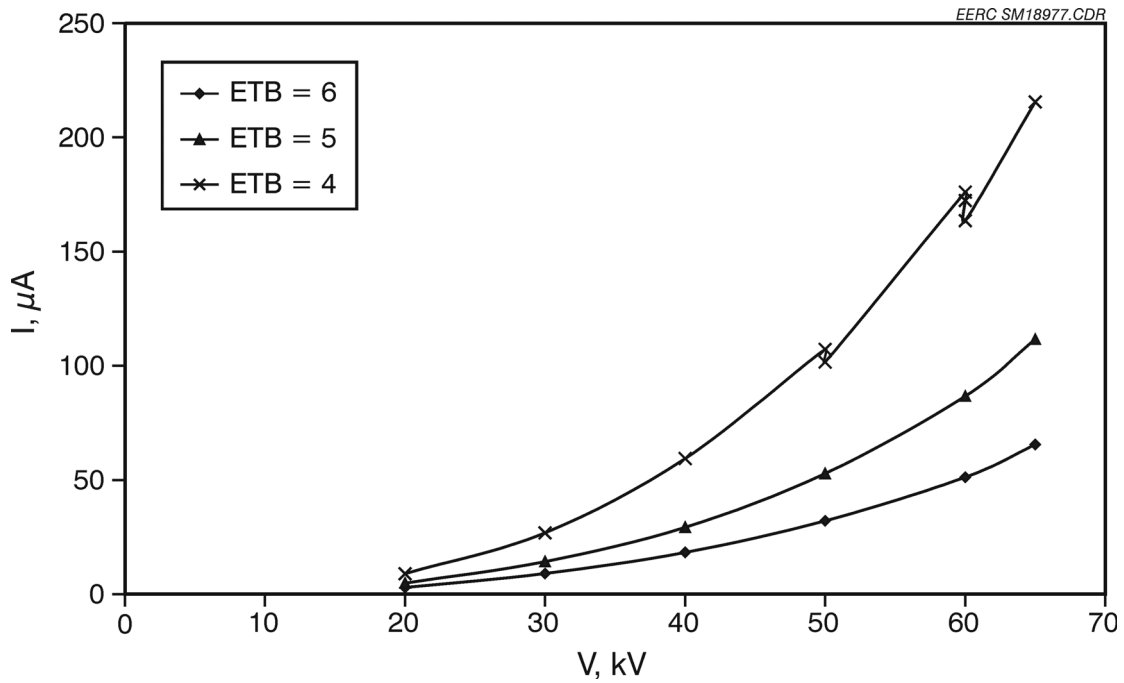


Figure 3.3-54. Current to the bags as a function of spacing between the electrode and the bag (no perforated plate, CBCM).

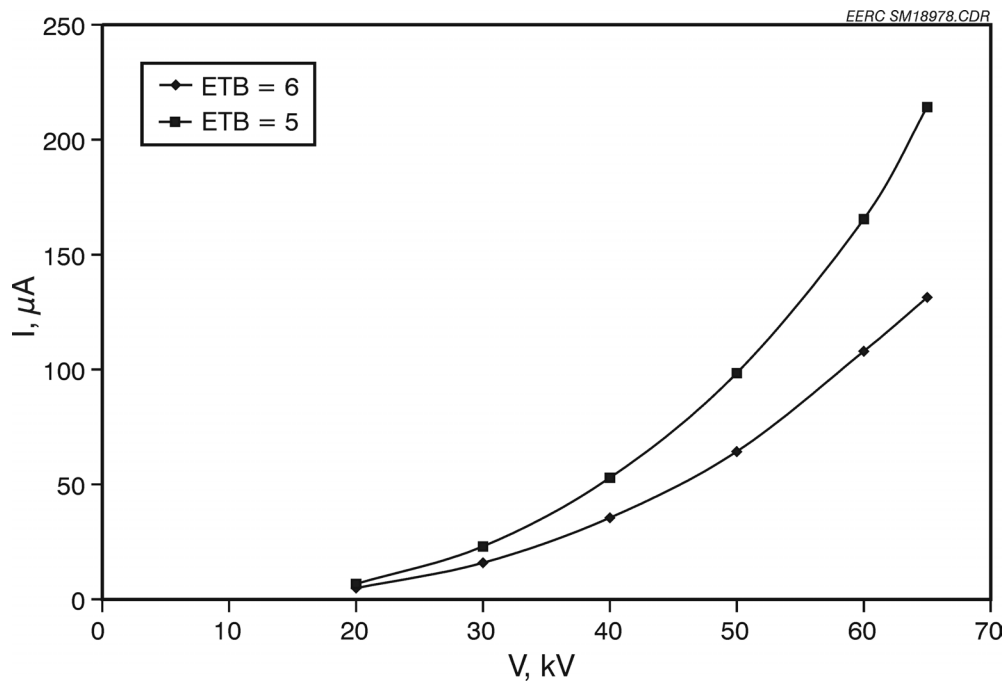


Figure 3.3-55. Current to the bags as a function of spacing between the electrode and the bag (no perforated plate, CBNM).

1.0, and 1.5 in. (19.1, 25.4, 38.1 mm). The bag current was 3.4 μA for the perforated plate with a hole size of 0.75 in. (19.1 mm) and increased to 11.9 μA for the 1.5-in. (38-mm)-hole-sized perforated plate when they were both at the same voltage of 65 kV (Figure 3.3-56). This indicates the perforated plate with smaller hole size protected the bag better than that of a larger hole size in terms of reducing bag current. It is noted that even the perforated plate with a hole size of 1.5 in. (38.1 mm) can remove more than 95% of the initial current flow to the bag.

A cold-flow test was then carried out in the AHPC pilot unit under the perforated-plate configuration to confirm the bench-scale results. Both the perforated plate hole size and the bag-to-perforated plate spacing were varied to examine their corresponding effects on the bag current. Figure 3.3-57 shows the bag current as a function of the applied voltage in the presence of perforated plates with different hole sizes: 0.75, 1.5, and 2.0 in. (19, 38, and 51 mm) at a PTB spacing of 2.0 in. (51 mm). The filter bags used were GORE-NO STAT[®] filter bags (GORE-TEX[®] antistatic membrane/GORE-TEX[®] felt). The bag current was less than 1 μA for the perforated plate with a 0.75-in. (19-mm) hole size for the entire applied voltage range. The bag current level increased with larger hole size, reaching 2.9 μA at the applied voltage of 60 kV for the 1.5-in. (38-mm)-hole-sized perforated plate and 5.3 μA at the applied voltage of 60 kV for the 2.0-in. (51-mm)-hole-sized perforated plate. The smaller-hole-sized perforated plate resulted in a lower current to the bags, similar to the results obtained in the bench-scale experiments. However, by using the perforated plate with the 2.0-in. (51-mm)-hole size, the current to the bags was still significantly reduced compared to the bag current without the perforated plate, indicating good bag protection.

Spacing between the perforated plate and the filter bags (PTB) was then set to 3.0 in. (76 mm), and the current to the filter bag was measured again as a function of the applied voltage and shown in Figure 3.3-58. The same correlation between the perforated plate hole size and bag current was observed at the PTB of 3.0 in. (76.2 mm) as that shown in Figure 3.3-57. The bag current was 2.4 μA at a PTB of 3 in. (76.2 mm) (Figure 3.3-58) under an applied voltage of 50 kV for the 2-in. (51-mm)-hole-sized perforated plate and increased to 3.3 μA when the PTB was adjusted to 2.0 in. (51 mm) (Figure 3.3-57), indicating some dependence of bag current on the distance from the bag to the perforated plate. The above experimental results demonstrated sufficient protection to the bags by using perforated plates, even at a large hole size.

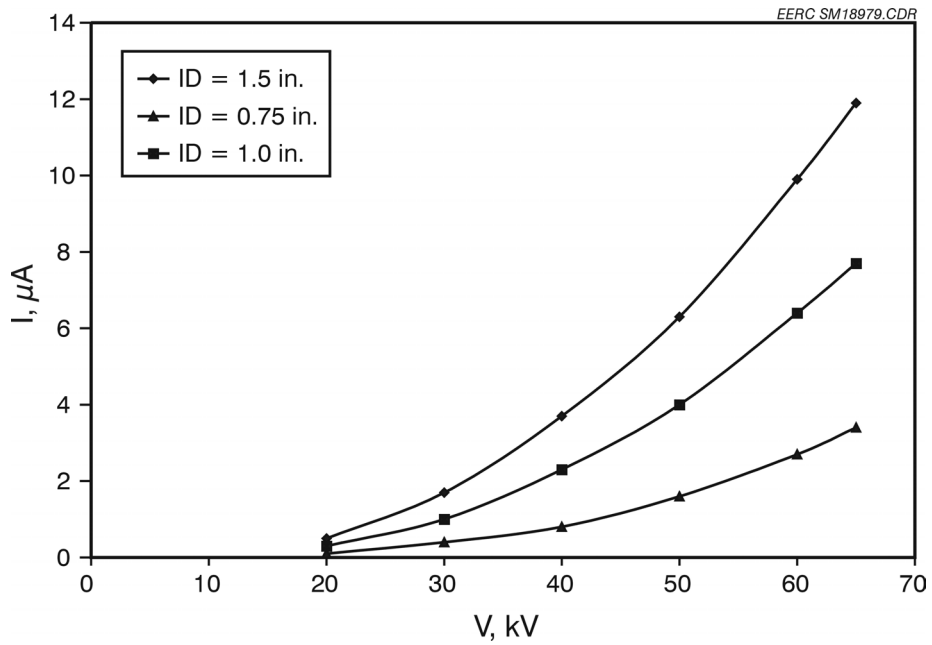


Figure 3.3-56. Current to the bag in the presence of different perforated plates (bench-scale, CBCM, $PTB:ETP = 1:3$).

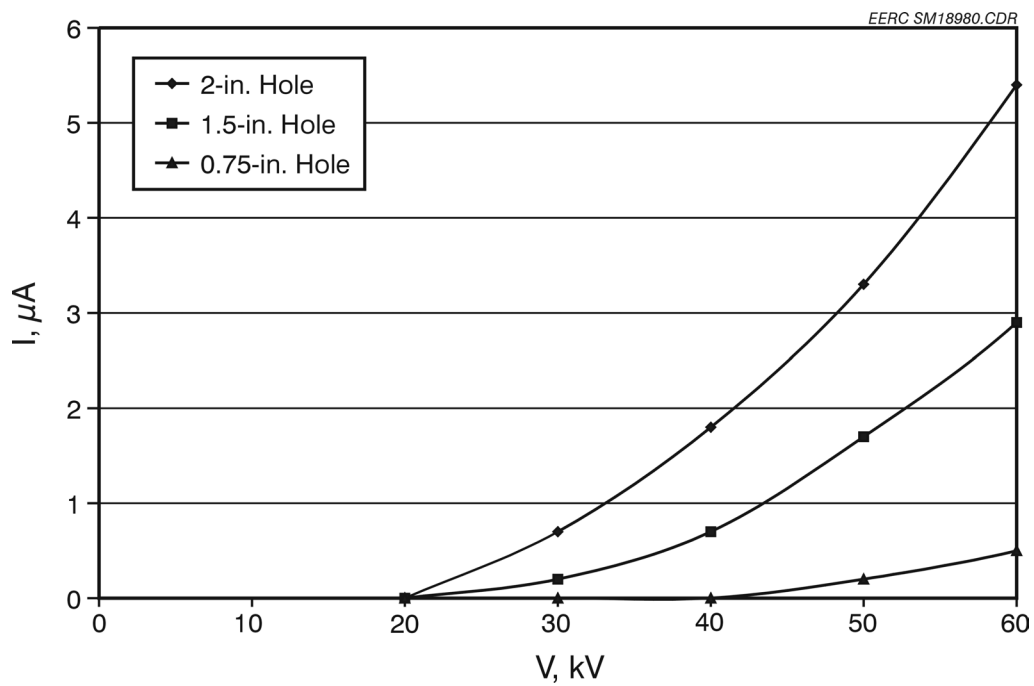


Figure 3.3-57. Current to the bag in the presence of different perforated plates (pilot unit, CBCM, $PTB = 2 \text{ in.}$).

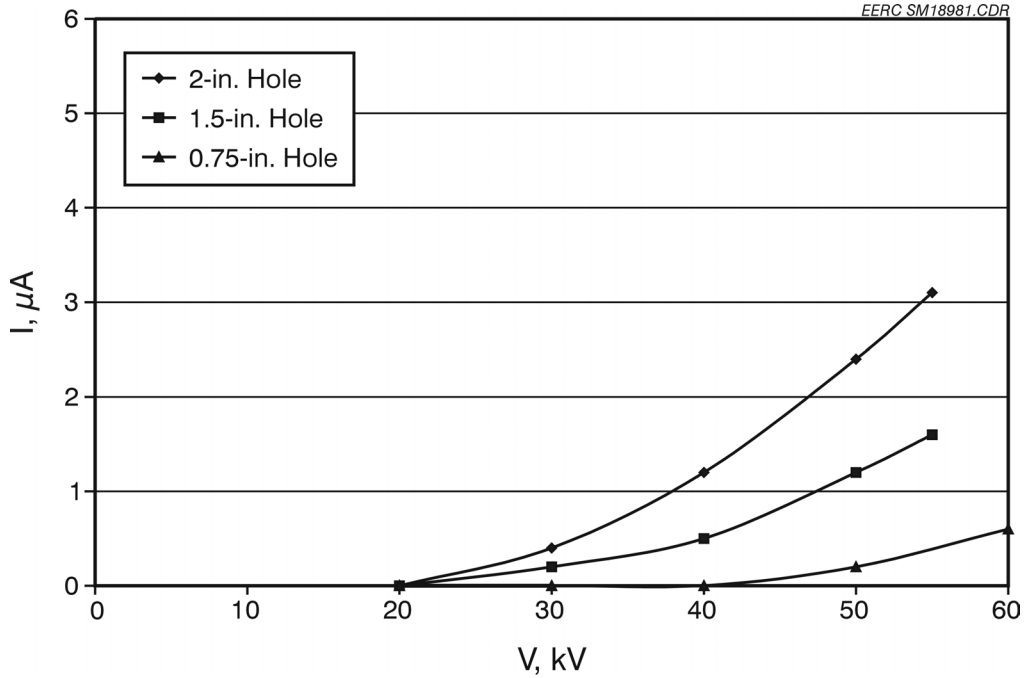


Figure 3.3-58. Current to the bag in the presence of different perforated plates (pilot unit, CBCM, PTB = 3 in.).

3.3.3.2 Electrical Field Distribution in the Perforated-Plate Configuration

To evaluate the effect of the perforated plate on the electric field strength, a theoretical 2-D dimensional model was developed to simulate the electrical field in the AHPC pilot-scale configuration in the presence of perforated plates of different hole sizes. The governing electrostatic equation for the region outside of the corona sheath is Poisson's equation:

$$\nabla^2 \phi = -\frac{\rho}{\epsilon} \quad [\text{Eq. 3.3-2}]$$

By assuming steady-state, the conservation of current equation is:

$$\nabla \cdot (\rho \beta E) = 0 \quad [\text{Eq. 3.3-3}]$$

where ϕ is electrical potential, ρ is ionic space charge density, g is a constant (gas permittivity), E is electrical field, and β is negative ion mobility. Current density is related to electric field by:

$$J = \beta \rho E \quad [\text{Eq. 3.3-4}]$$

$$E = -\nabla \phi \quad [\text{Eq. 3.3-5}]$$

An applied voltage of 60 kV, a normal operating condition for the AHPC system, was used as a boundary condition on the electrode surface. The electrical potentials on the AHPC wall surface, filter bag surface, and the perforated-plate surface were assumed to be zero because of the grounding. The ionic space charge density was calculated based on the corona current measured in the experiments. By assuming the corona is uniform and extends over the entire electrode surface, the above equations were solved by the finite element method to compute the electrical field distribution in the system. The electrical potential was set to 60 kV on the electrode, and the dimensions used in the simulation matched the pilot-scale AHPC unit. The calculated equipotential lines are shown in Figures 3.3-59–3.3-62. Without the presence of the perforated plates to protect the filter bags, the electric potential, starting at 60 kV on the discharging electrode, was in the range of 2000–4000 V around the bag surface, as shown in Figure 3.3-62. By installing the perforated plates in front of the filter bags, the electrical potential around the bag surface was dramatically decreased to 200 V (shown in Figure 3.3-59–3.3-61). The hole size evaluated in the simulation was from 1.0 to 2.5 in. (25.4 to 63.5 mm) in diameter and shows that the smaller the hole size on the plate, the lower the voltage around the filter bags, which is in agreement with the experimental results. The model predicted the bags were well protected even at a larger hole size of 2.5 in. (63.5 mm).

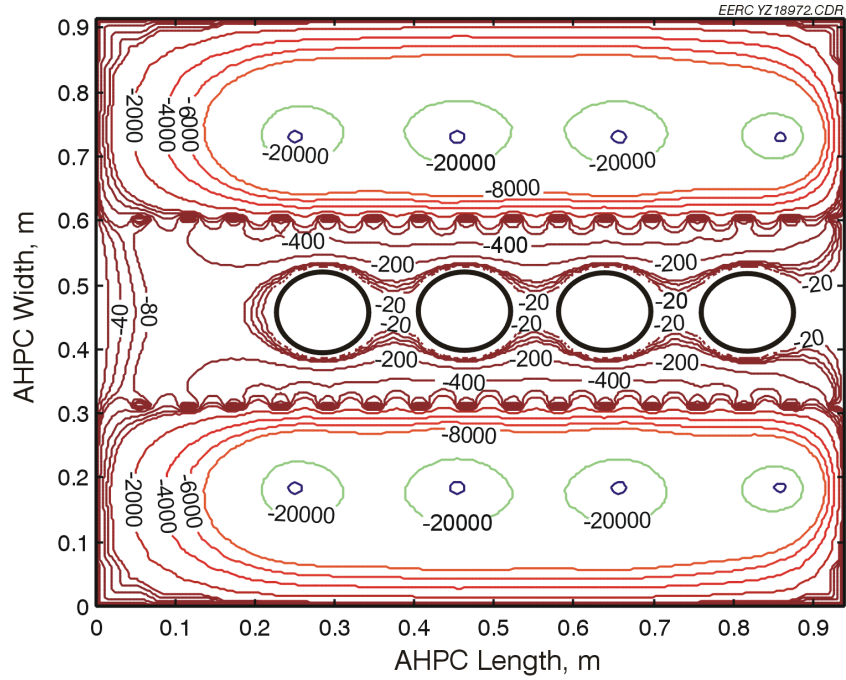


Figure 3.3-59. Electrical potential distributed in the pilot unit AHPC with the 1.0-in. (25-mm)-hole-size perforated plates.

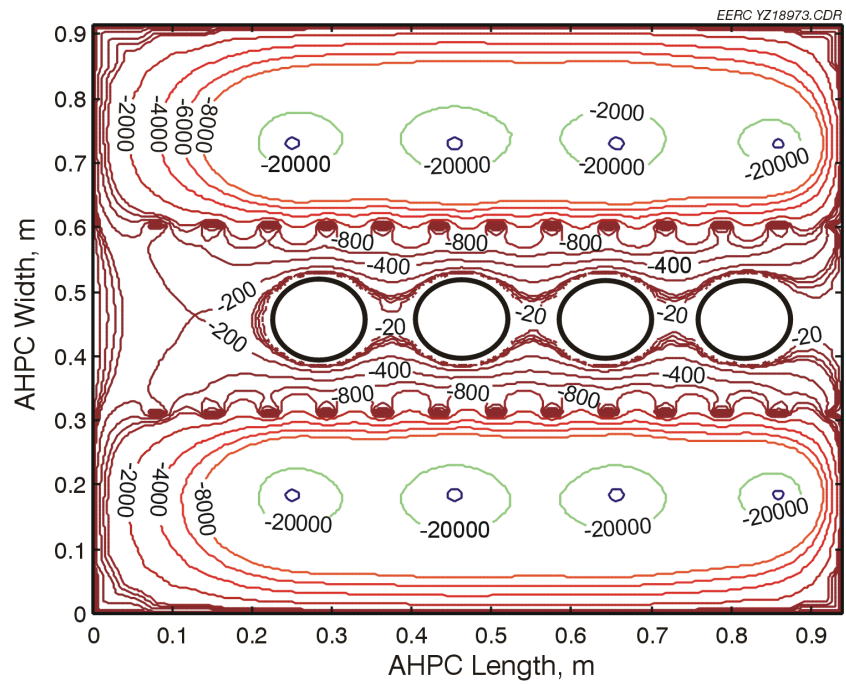


Figure 3.3-60. Electrical potential distributed in the pilot unit AHPC with the 2.0-in. (51-mm)-hole-size perforated plates.

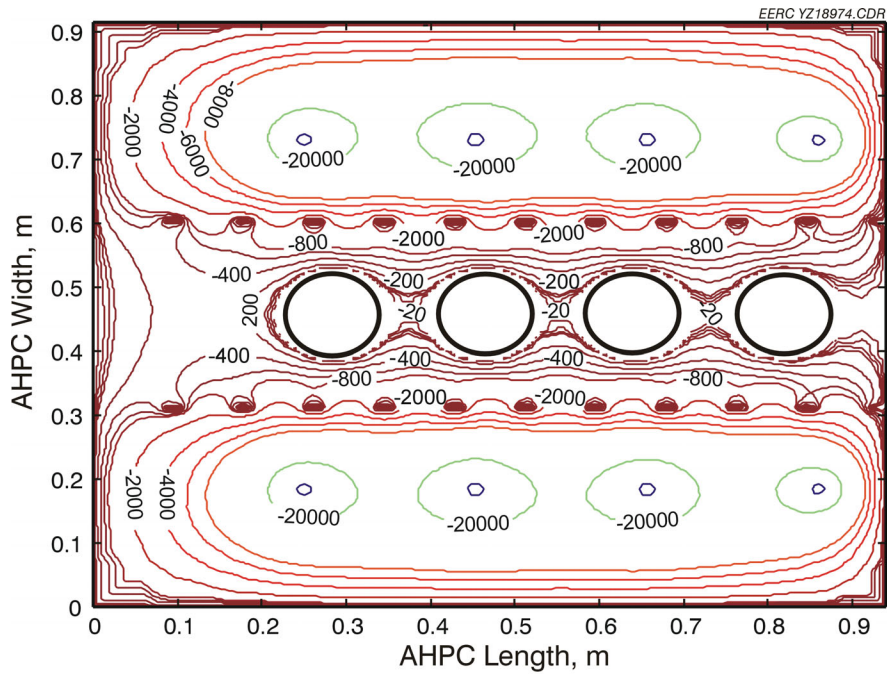


Figure 3.3-61. Electrical potential distributed in the pilot unit AHPC with the 2.5-in. (64-mm)-hole-size perforated plates.

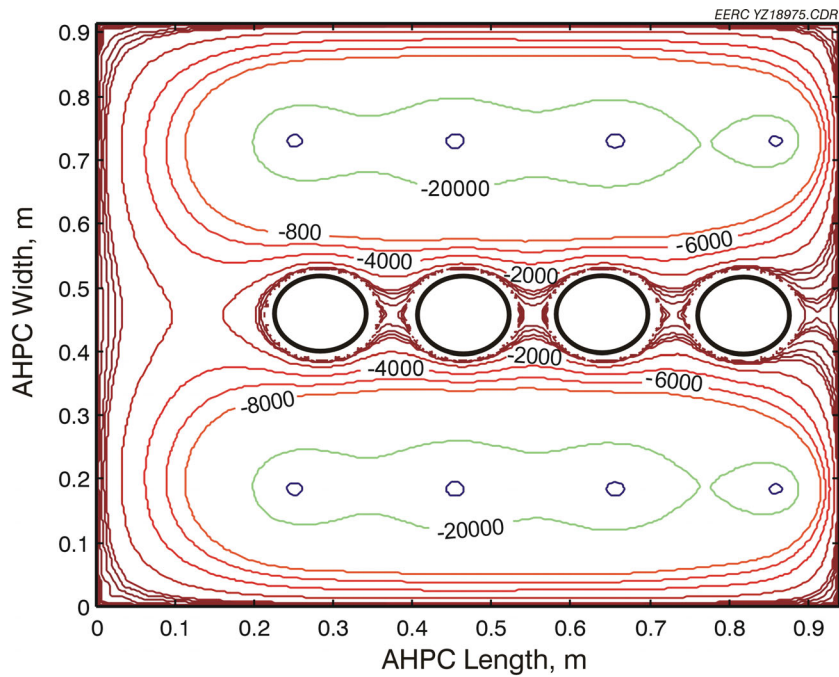


Figure 3.3-62. Electric potential distribution in the AHPC pilot unit without the perforated plates.

3.4 AHPC Field Study at Big Stone Power Plant (January – July 2001)

3.4.1 *Modifications of the Perforated-Plate AHPC at Big Stone Power Plant*

Based on the experimental results from the pilot-scale and bench-scale studies conducted at the EERC, a perforated-plate configuration was designed and installed on the 9000-acfm (255-m³/min) slipstream pilot unit at the Big Stone Power Plant. The differences between the new perforated-plate design and the previous AHPC can be seen by comparing Figures 3.4-1 and 3.4-2. Figure 3.4-1 is a simplified top view of the 9000-acfm (255-m³/min) AHPC configuration at the start of Phase III, which had a plate-to-plate spacing of 23.6 in. (599.4 mm). This arrangement was already more compact than the original Phase II AHPC configuration, which had a plate-to-plate spacing of 29 in. (736.6 mm). Since the overall size of the housing was not changed, this resulted in unused space, shown in Figure 3.4-1. In both cases, the bag row spacing is the same as the plate-to-plate spacing. Figure 3.4-3 (back side of the perforated plate) shows the uniform hole distribution pattern on the perforated plate. The beam at the bottom of the plate prevents any possible contact between the filter bags and the plates, which might cause abrasion damage on the filter bags. For the perforated-plate configuration (Figure 3.4-2), the bag spacing was not changed to allow using the same tube sheet as in the previous configuration (Figure 3.4-1). However, by installing the perforated plates in front of the filter bags, the distance from the discharge electrodes to the plates increased to 5.5 in. (139.7 mm), compared to 3.9 in. (99.1 mm) previously. With this configuration, the distance from the bags to the perforated plates was selected to be 3 in. (76.2 mm) in order to be on the conservative side. If this distance were reduced to 2 in. (50.8 mm) and the ETP distance were reduced to 4 in. (101.6 mm), the bag rows could potentially be moved 5 in. (127 mm) closer, which would correspond to a 21% reduction in footprint area, compared to the arrangement shown in Figure 3.4-2. Therefore, one of the obvious advantages of the new perforated-plate configuration is the potential to make the AHPC significantly more compact than the earlier design.

Another difference is that directional electrodes are not required with the perforated plate design. With the previous design, directional electrodes (toward the plate) were needed to

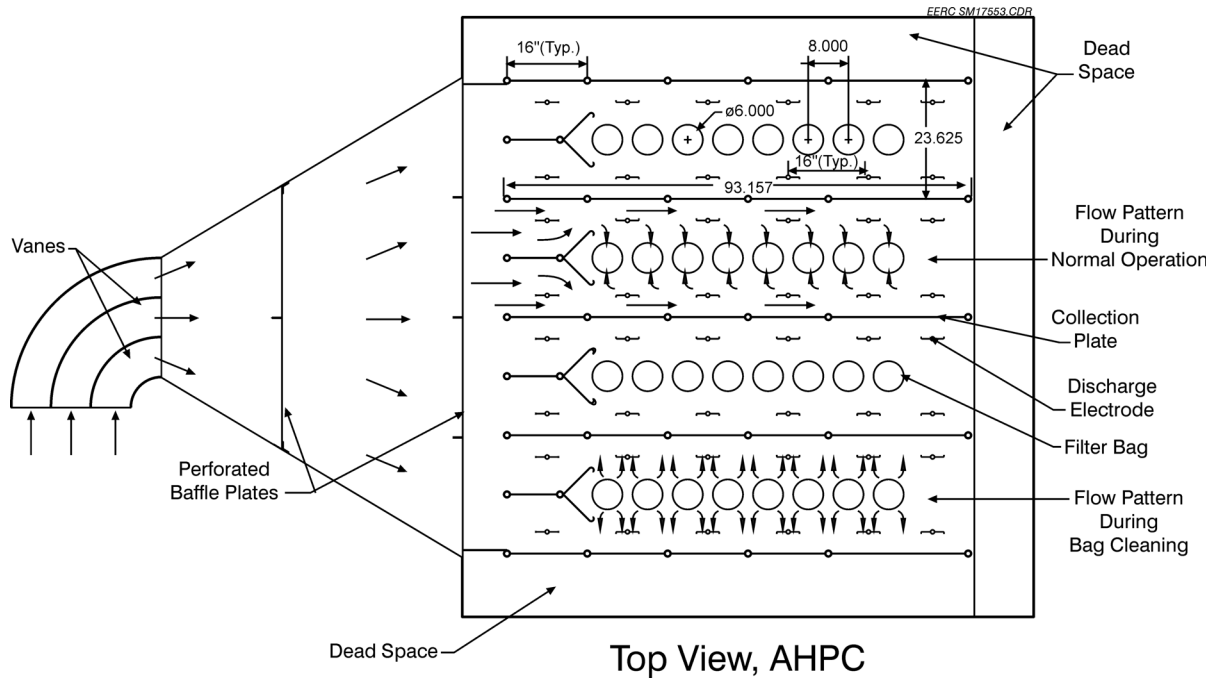


Figure 3.4-1. Top view of the 9000-acfm (255-m³/min) AHPC, as modified at the start of Phase III.

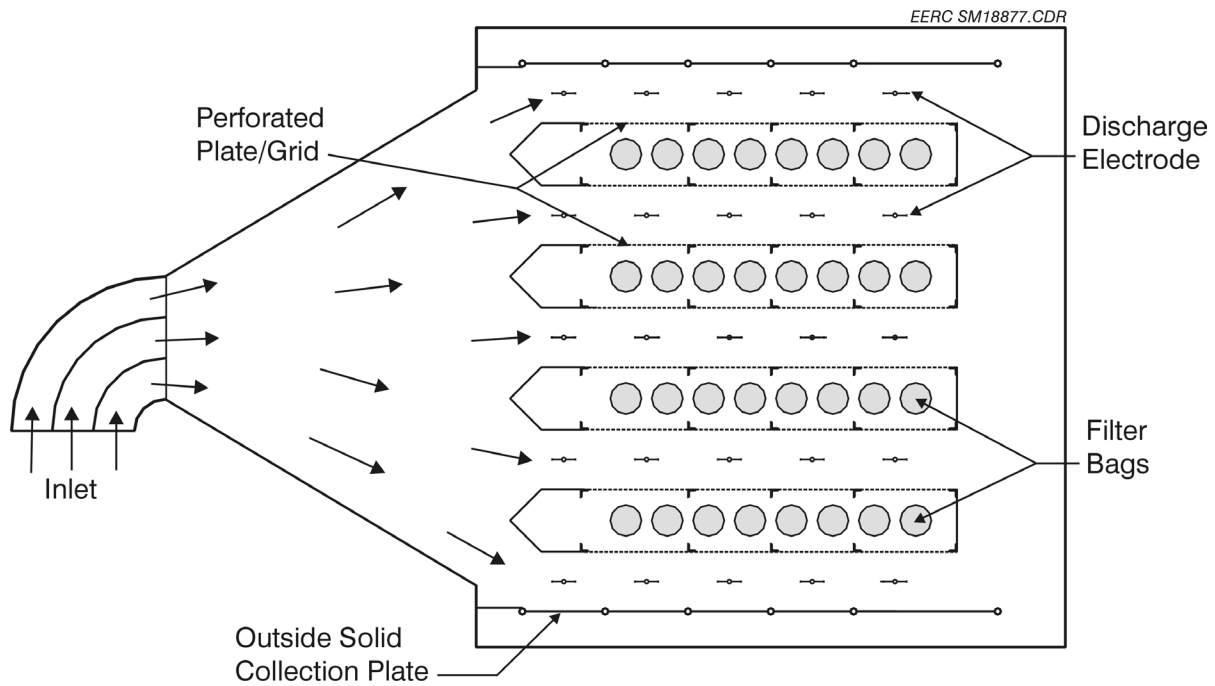


Figure 3.4-2. Top view of the perforated-plate configuration for the 9000-acfm (255-m³/min) AHPC.

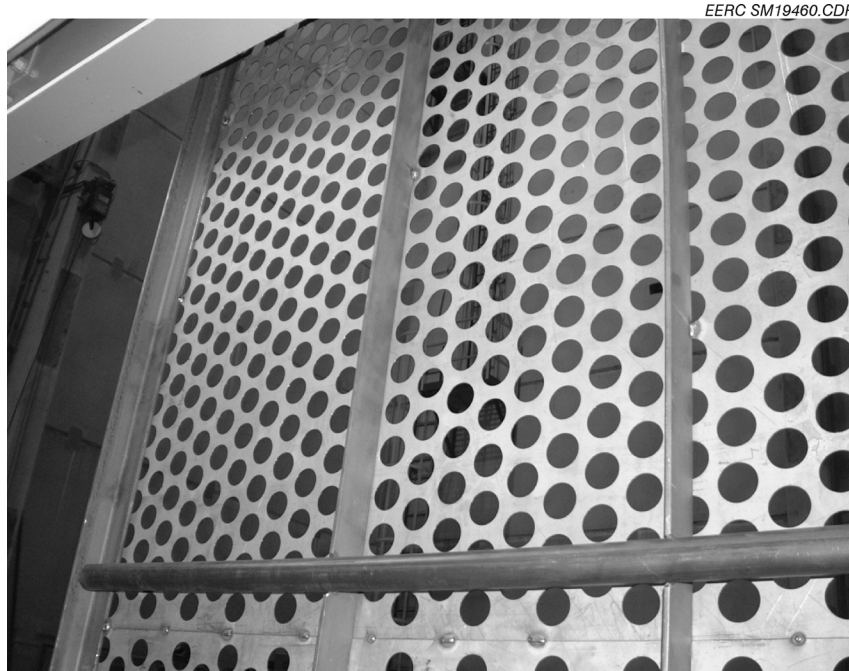


Figure 3.4-3. Photo of the back side of the perforated plate showing the uniform hole distribution pattern.

prevent possible sparking to the bags. This means that conventional electrodes can now be used with the AHPC. Electrode alignment is also now less critical because an out-of-alignment electrode would simply result in potential sparking to the nearest grounded perforated plate, whereas with the old design, an out-of-alignment electrode could result in sparking to a bag and possible bag damage.

While the overall AHPC concept is unchanged in that precollection of >90% of the dust and enhanced bag cleaning are key features, the purpose of the plates is somewhat different. The perforated plates serve two very important functions: as the primary collection surface and as a protective grid for the bags. With approximately 45% open area, the hope was that there would be adequate collection area on the plates to collect the precipitated dust while not restricting the flow of flue gas toward the bags during normal filtration. During pulse cleaning of the bags, the hope was that most of the reentrained dust from the bags would be forced back through the perforated plates into the ESP zone. From results to date, it appears that this configuration provides better ESP collection than the previous design and does not impair bag cleanability.

The better ESP collection efficiency is likely the result of forcing all of the flue gas through the perforated-plate holes before it reaches the bags. This ensures that all of the charged dust particles pass within a maximum of one-half of the hole diameter distance of a grounded surface. In the presence of the electrical field, the particles then have a greater chance of being collected. In the old AHPC design, once the gas reached the area between the electrodes and bags, it would be driven toward the bags rather than the plates, and a larger fraction of the dust was likely to bypass the ESP zone. Figure 3.4-4 shows the installation of the perforated plates in the AHPC Big Stone unit. Figure 3.4-5 shows a top view of the perforated plate AHPC Big Stone unit after modification. Figure 3.4-6 shows the bidirectional discharging electrodes centered between the two perforated plates.

Several other modifications were made during the 3.5-month field test. One was the design and installation of a new pulse system in a cross-row configuration. A schematic is shown in Figure 3.4-7. In the previous pulse system, four pulse tubes (solid line) cleaned the bags in the order from Row 1 to 4 with eight bags each time. In this new cross-row pulse system, a total of eight pulse tubes (dashed line) were installed. Each blow tube had four nozzles to pulse-clean four bags at the same time. Figure 3.4-8 shows the newly installed cross-row pulse system with Goyen pulse valves. A PLC system provided control over the pulsing trigger, pulse duration, and time interval between pulsing successive rows. The new pulse system with a modified control program also enabled control of the pulse sequence order. For example, Cross-Row Pulse 1–8 indicates the pulse cleaning started from Bag 1, followed by Bag 2, and ended with Bag 8, while Cross-Row 8–1 is in reverse order. Cross-Row Pulse 71538264 is an alternate pulsing mode to suppress the reentrainment of the fly ash (blown off during pulsing) toward adjacent bags. The primary purpose of the cross-row pulsing system is to allow flexibility in design of a full-scale AHPC. In some cases, especially retrofits, cross-row pulsing may be necessary to facilitate installation with minimal change to existing components. By comparing cross-row pulsing with conventional in-row pulsing, engineering data would be available to determine if cross-row pulsing is a viable design option for full-scale systems.



Figure 3.4-4. Installing the perforated plates in the 9000-acfm (255-m³/min) AHPC at the Big Stone Power Plant, March 2001.



Figure 3.4-5. Perforated plates as installed in the 9000-acfm (255-m³/min) AHPC before the tube sheet is replaced. Bags fit inside each pair of perforated plates.



EERC SM19449.CDR

Figure 3.4-6. Photo showing the bidirectional discharging electrodes.

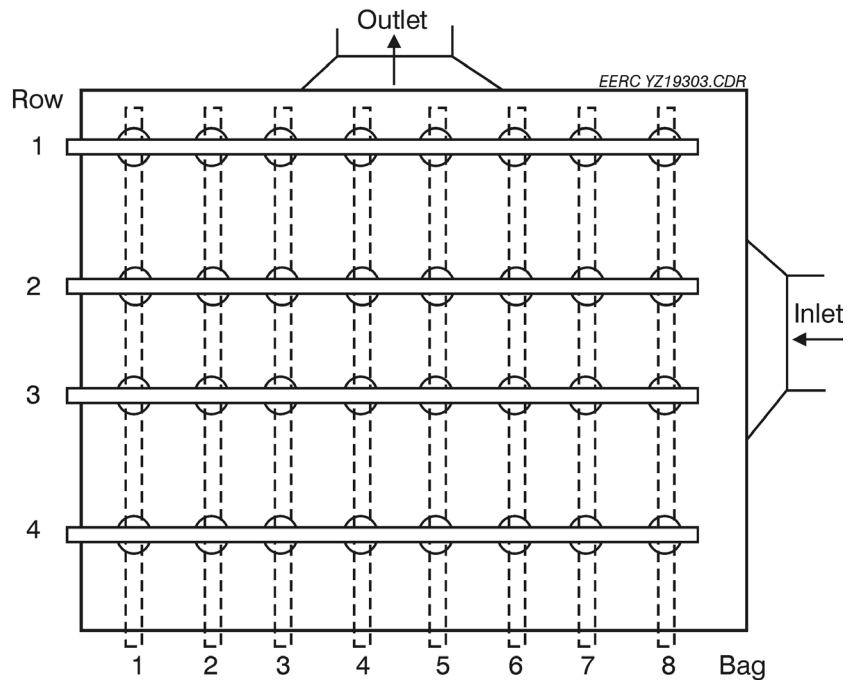


Figure 3.4-7. AHPC pulse system (top view).

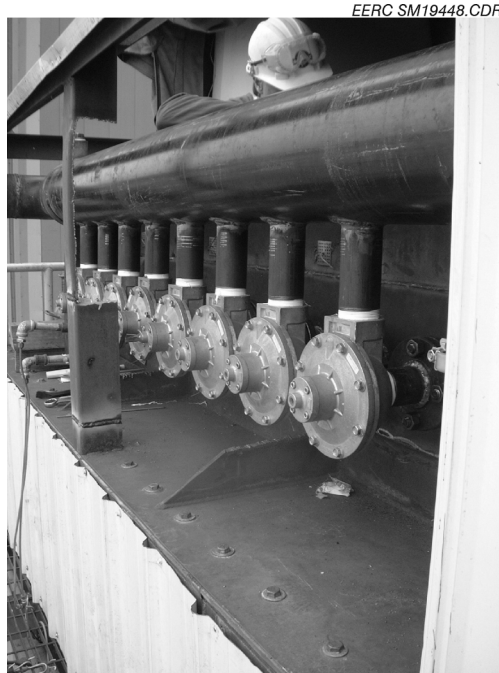


Figure 3.4-8. Photo showing the newly installed cross-row pulse system with Goyen pulse valves.

According to previous studies, temperature in the AHPC vessel played an important role in AHPC operation. Because of the very-high-resistivity fly ash, even at the lower operating temperatures, the AHPC performance was limited by ash resistivity. A humidification system, therefore, was also designed and installed in the AHPC unit at Big Stone to control the AHPC temperature by water injection. The water droplet size, produced with a single dual-fluid nozzle, was fine enough to allow injection into the 2-ft. (0.61-m)-diameter AHPC inlet pipe. The use of humidification allowed operation at a temperature where AHPC performance would not be limited by ash resistivity. Operation at this condition is more representative of expected AHPC performance for cases with lower-resistivity ash.

One further modification completed in June was the installation of bidirectional discharge electrodes in place of the mast-only electrodes, which were used in the last electrode position. The original purpose of the mast-only electrodes at the back of the AHPC was to force more current to the front of the AHPC where the dust loading is higher. However, there was concern that the mast-only electrodes did not provide enough corona current to enhance bag cleaning.

3.4.2 Overview for March 15, 2001 – June 28, 2001

After modifications were completed to the perforated-plate AHPC at the Big Stone Power Plant, the field AHPC was started on March 15, 2001, and operated continuously for 3.5 months except for an unplanned plant outage on March 25–26, 2001, and an annual power plant outage from May 8–16, 2001. The field testing was divided into three test periods. Test Period 1 was from March 15, 2001, to May 8, 2001. After the annual power plant outage, the AHPC was started again on May 16, 2001, and operated continuously until June 15, 2001, when the AHPC unit was shut down for electrode replacements. Test Period 3 was from June 17–28, 2001. June 28, 2001 marked the end of the AHPC Phase III field testing at Big Stone.

During the 3.5-month testing, the AHPC unit experienced very challenging operating conditions such as usage of various coals with high resistivity, fly ash high flue gas temperature, and fluctuating power plant loads. The operational parameters for the AHPC unit were also changed to examine their corresponding effects on the perforated-plate AHPC operation. A summary of operating parameters is listed below:

- Bag type: GORE-NO STAT[®] filter bag (GORE-TEX[®] antistatic membrane/GORE-TEX[®] felt), GORE-NO STAT[®] filter bags (GORE-TEX[®] membrane/GORE-TEX[®] felt)
- Secondary current, mA: 55–85 mA
- A/C ratio, ft/min (m/min): 8–14 (2.4–4.3)
- Trigger pressure, in. W.C. (kPa): 7.3–8.0 (1.8–2.0)
- Pulse pressure, psi (kPa): 50–80 (345–552)
- Pulse duration, ms: 200–400

A daily average of A/C ratio across the filter bags for the entire testing period is plotted as a function of operating time in Figure 3.4-9. During most of the testing, the A/C ratio was controlled in the range of 11–12 ft/min (3.4–3.7 m/min), meeting the goal of operating the AHPC

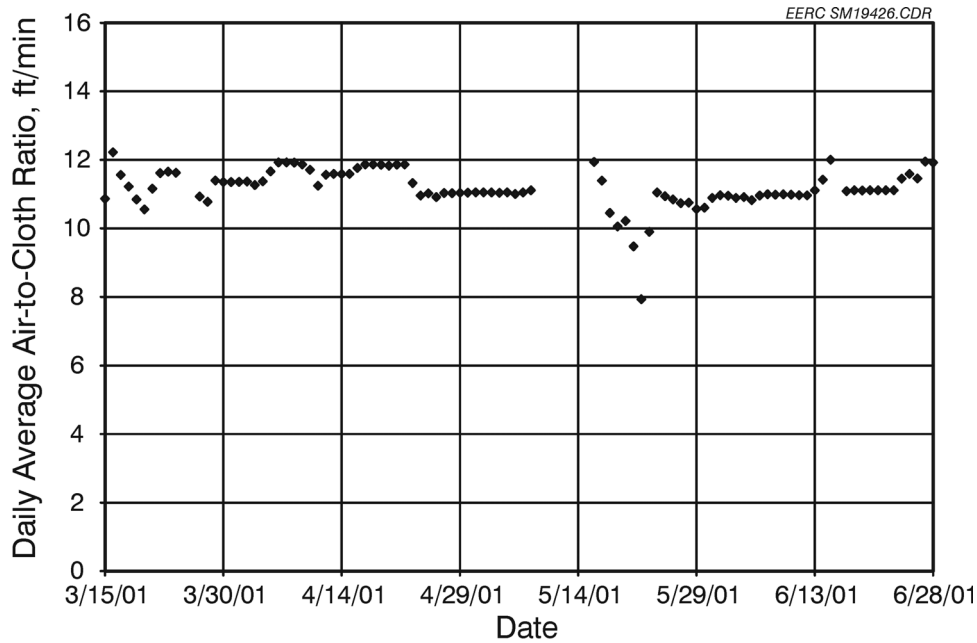


Figure 3.4-9. Daily average A/C ratio.

unit at a high A/C ratio. For some shorter-term tests, the A/C ratio was reduced to allow operation at lower pressure drop. By setting the pulse trigger pressure, the daily average pressure drop across the AHPC unit was controlled within the range from 6.0 to 8.0 in. W.C. (1.5 to 2.0 kPa) shown in Figure 3.4-10, which is acceptable in full-scale systems. The daily average pressure drop started at 5.5 in. W.C. (1.4 kPa) and was steady at 7.0 in. W.C. (1.7 kPa) with an A/C ratio of 11 ft/min (3.4 m/min) at the end of Testing Period 1. In order to achieve good AHPC performance under difficult operating conditions such as switching of coal, high flue gas temperature, etc., in Tests 2 and 3, the pulse trigger pressure was increased. This resulted in an increase in the average pressure drop across the system to the range of 7.5–8.0 in. W.C. (1.9–2.0 kPa), which is still acceptable for the AHPC operation. The perforated-plate AHPC functioned well in terms of long bag-cleaning interval, low residual drag, and K_2C_i , as shown in Figures 3.4-11–3.4-13. Figure 3.4-11 shows an integrated daily bag-cleaning interval as a function of operating time for the testing period. For a total of 85 days, the daily integrated bag-cleaning interval was over 20 min, accounting for 89% of the total testing period. The shortest interval was 15 min, and the longest bag-cleaning interval was as high as 70 min, well above the benchmark goal of over 10 min. The daily average K_2C_i (plotted in Figure 3.4-12) was maintained at a very low level of 2.0–3.0 during Test Period 1, which were the lowest levels

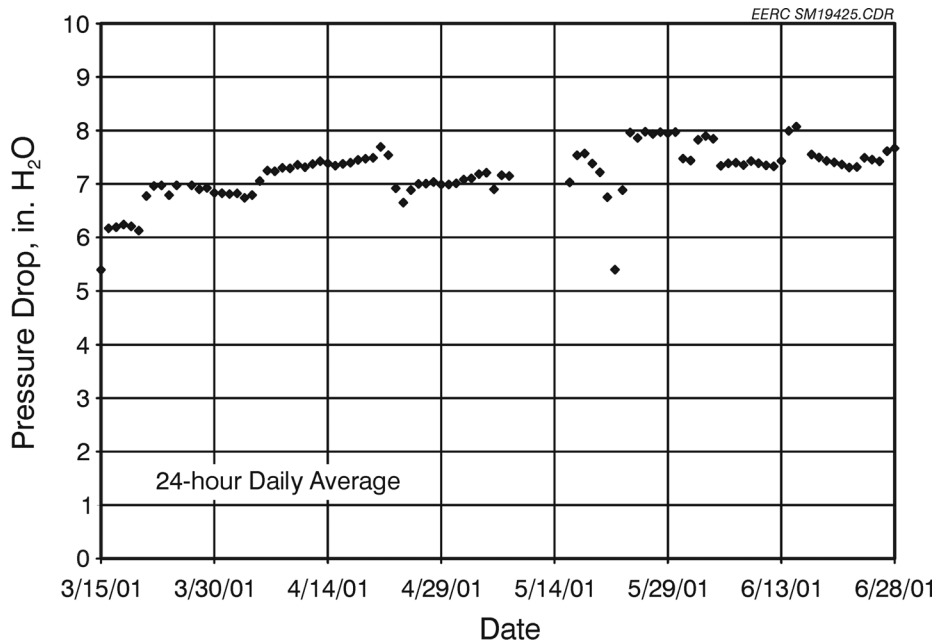


Figure 3.4-10. Daily average pressure drop.

obtained in the field study, indicating the ESP functioned extremely well under the perforated-plate configuration. The K_2C_i was increased to 2.4–5.5 during Test Periods 2 and 3 (caused by high resistivity of fly ash), which was still excellent compared to K_2C_i values of 6.6–17.1 in previous field testing. The daily average residual drag, plotted in Figure 3.4-13, started at 0.33 in. W.C./ft/min and gradually increased and stabilized around 0.6 in. W.C./ft/min at the end of the test. The highest residual drag of 0.7 in. W.C./ft/min observed in Test 2 was caused by high-resistivity fly ash and variable power plant operating conditions.

3.4.3 Results for Test Period 1 (March 15 – May 8, 2001)

3.4.3.1 Plant Conditions – Fuel, Load, and Temperature

When the AHPC unit was started on March 15, 2001, the Big Stone Power Plant burned an Eagle Butte coal and switched to Buckskin coal on April 2, 2001. At the end of this test period, just prior to plant shutdown, the plant started to use Cordero coal. The detailed analyses are discussed in Section 3.4.7.

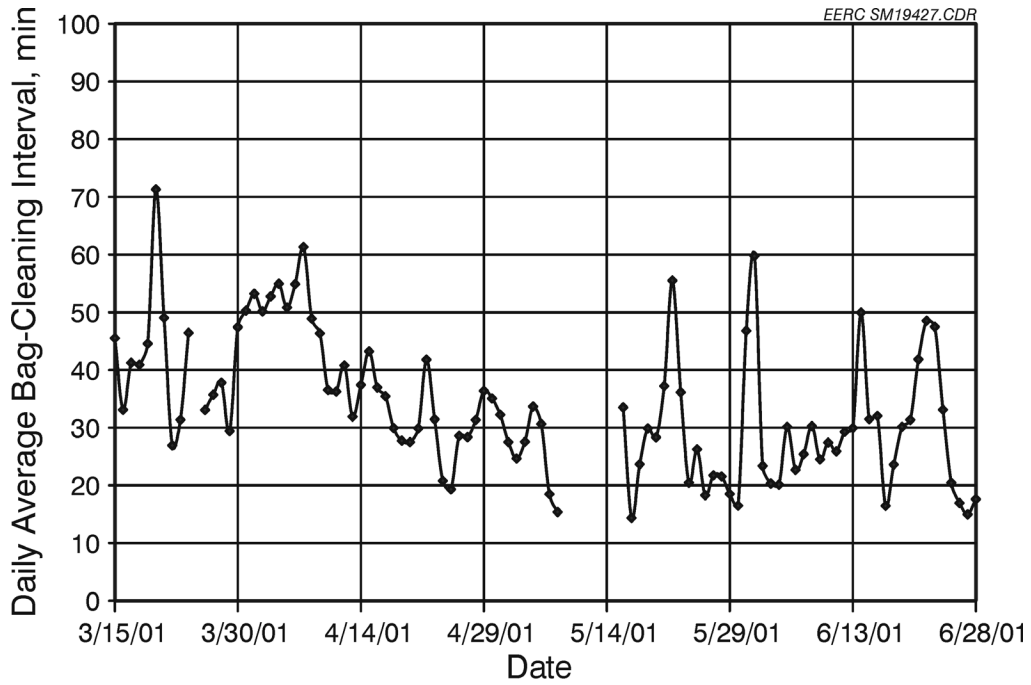


Figure 3.4-11. Daily average bag-cleaning interval.

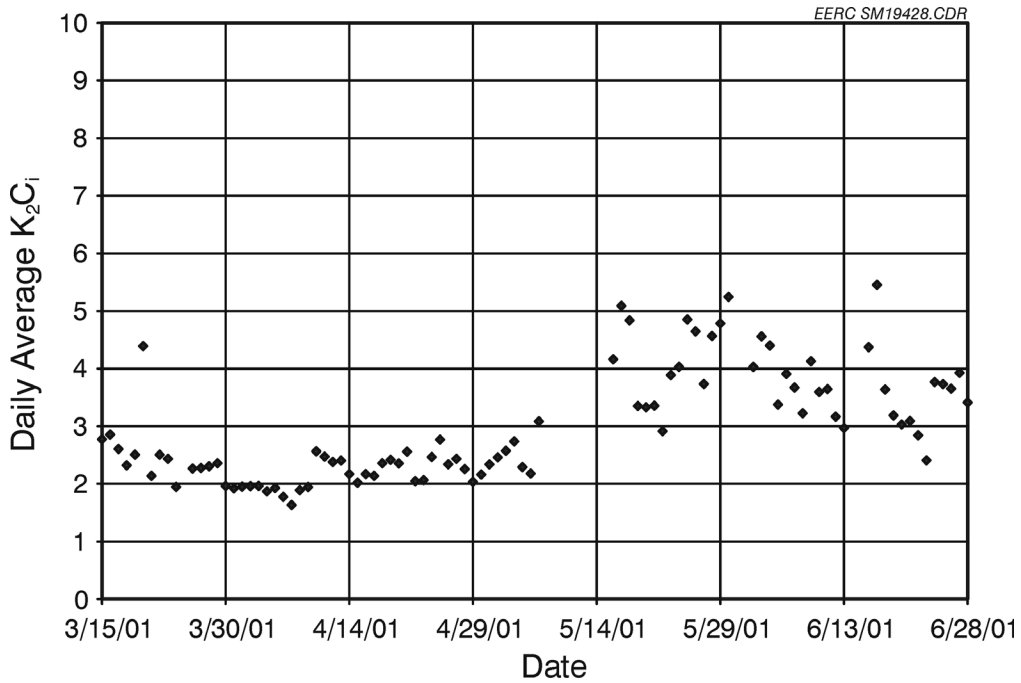


Figure 3.4-12. Daily average K_2C_i .

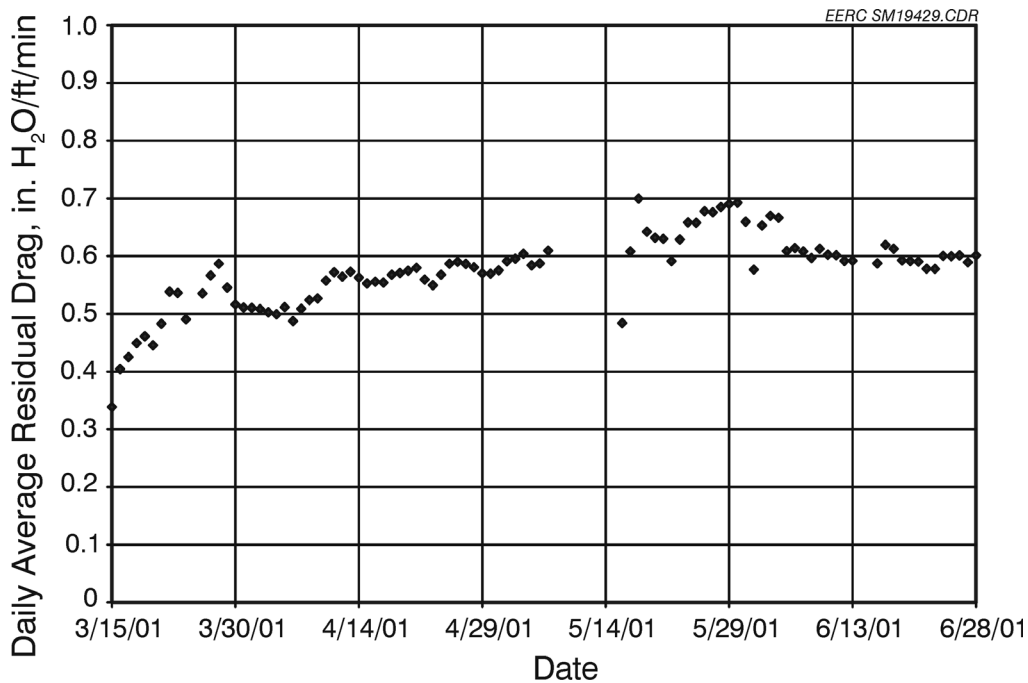


Figure 3.4-13. Daily average residual drag.

The gross load of the power plant and the plant ESP inlet temperature during this period are shown in Figure 3.4-14. It is seen that, except for an unplanned 1-day plant outage on March 25, 2001, the power plant operated at a very stable gross load of 450 MW, with an ESP inlet temperature in the range of 260E–330EF (127E–166EC). The stable operating conditions of the power plant provided a stable dust loading to the AHPC unit with a stable flue gas temperature.

3.4.3.2 Electrical Conditions

One of the major functions for the installed perforated plates between the bags and the electrodes is to prevent the filter bags from electrically induced damage. The secondary current was set at 60 and 70 mA during the majority of this test period, except for short-term tests when the current was 50 and 80 mA to examine the current effect on AHPC operation. The daily sparking number is shown in Figure 3.4-15. When the secondary current was maintained at 60 mA or less, there was almost no sparking. Even when the secondary current was increased to 70 mA, the daily sparking number was still kept at a low level of 400 sparks per day or less for

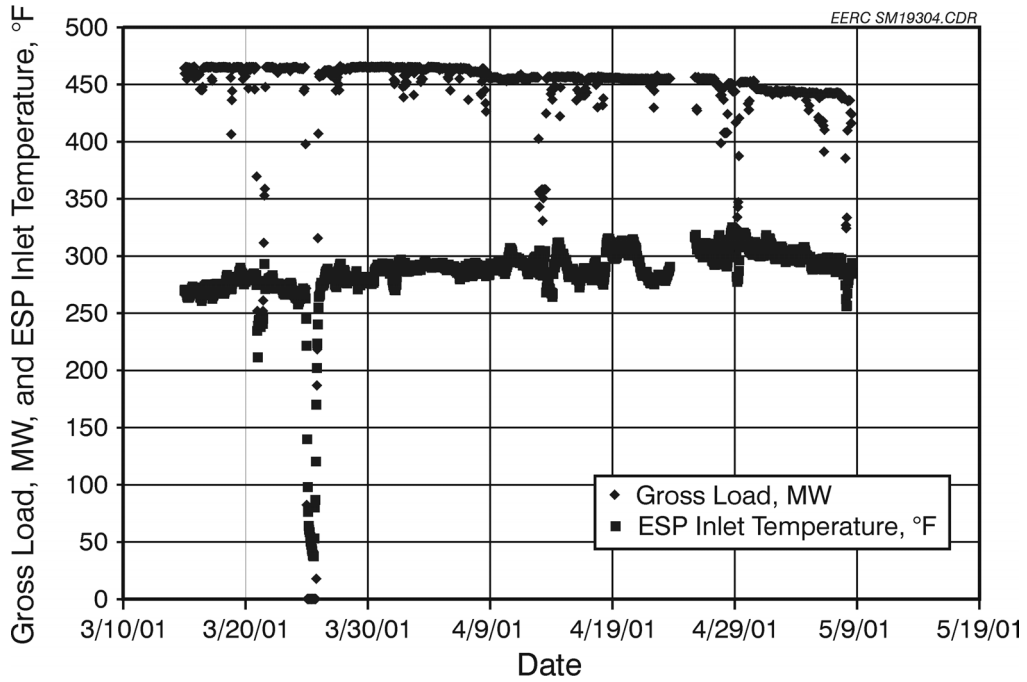


Figure 3.4-14. Big Stone Power Plant gross load and ESP inlet temperature (test period March 15 - May 8, 2001).

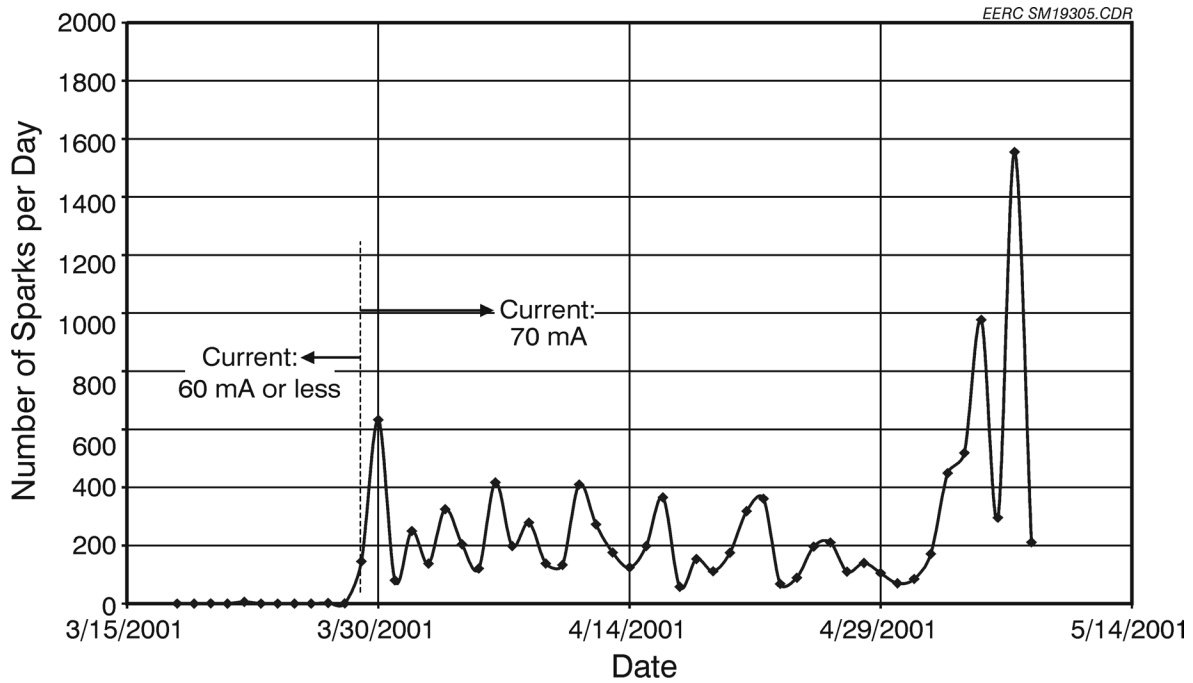


Figure 3.4-15. Number of sparks per day (Test Period 1).

most of the testing periods. The highest daily sparking number was 1555 on May 7, 2001. A total of 11,045 sparks occurred during the 53-day test, with a daily average of 212 sparks. Compared to the daily sparking over 10,000 (at the same current level) observed in the summer 2000, the present perforated-plate configuration dramatically reduced the daily sparking number. Visual inspection through the sight ports showed the sparking was always between the discharge electrodes and the perforated plates. Since no sparking was observed between the perforated plates and the filter bags, the plates appeared to be an effective shield, providing good protection for the bags.

3.4.3.3 Perforated-Plate AHPC Performance

Experiments carried out in this test period (March 15 – May 8, 2001) were aimed at examining perforated-plate AHPC performance under different operating conditions. The operational parameters tested are listed below:

Pulse trigger pressure:	7.3, 7.5, and 8.0 in. W.C. (1.8, 1.9, and 2.0 kPa)
A/C ratio:	11.1, 11.4, 11.7, and 12 ft/min (3.4, 3.5, 3.6, and 3.7 m/min)
Secondary current:	55, 70, and 85 mA
Pulse-cleaning pressure:	50, 65, 75, and 80 psi (345, 448, 517, and 552 kPa)
Pulse duration:	200 and 400 ms

The bag-cleaning interval results ranged from 10–70 min at a pressure drop less than 7.5 in. W.C. (1.9 kPa). The K_2C_i ranged from 1.54 to 4.26, and the residual drag was from 0.50 to 0.62 in. W.C./ft/min (0.41 to 0.51 kPa/m/min). The observed gradual increases of K_2C_i and residual drag were partially due to bag seasoning, but can also be ascribed to the changes in operating conditions as a result of the varying power plant gross load and temperature. The experimental data including bag-cleaning interval, residual drag, and K_2C_i at the same operating conditions were grouped together and are shown in Figures 3.4-16–3.4-24.

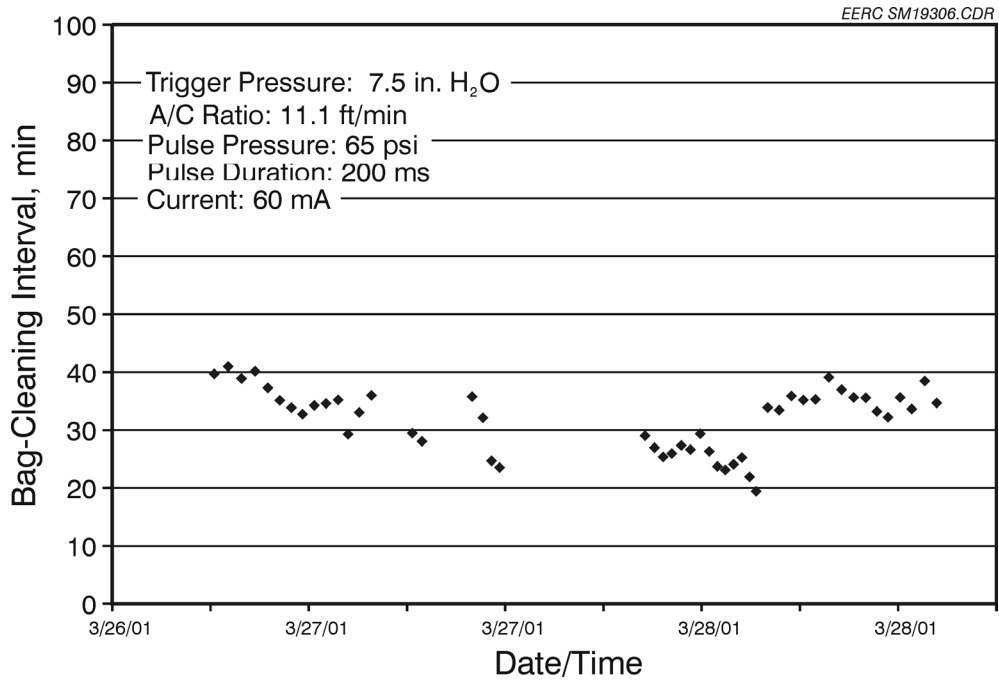


Figure 3.4-16. AHPC bag-cleaning interval (March 27–28, 2001).

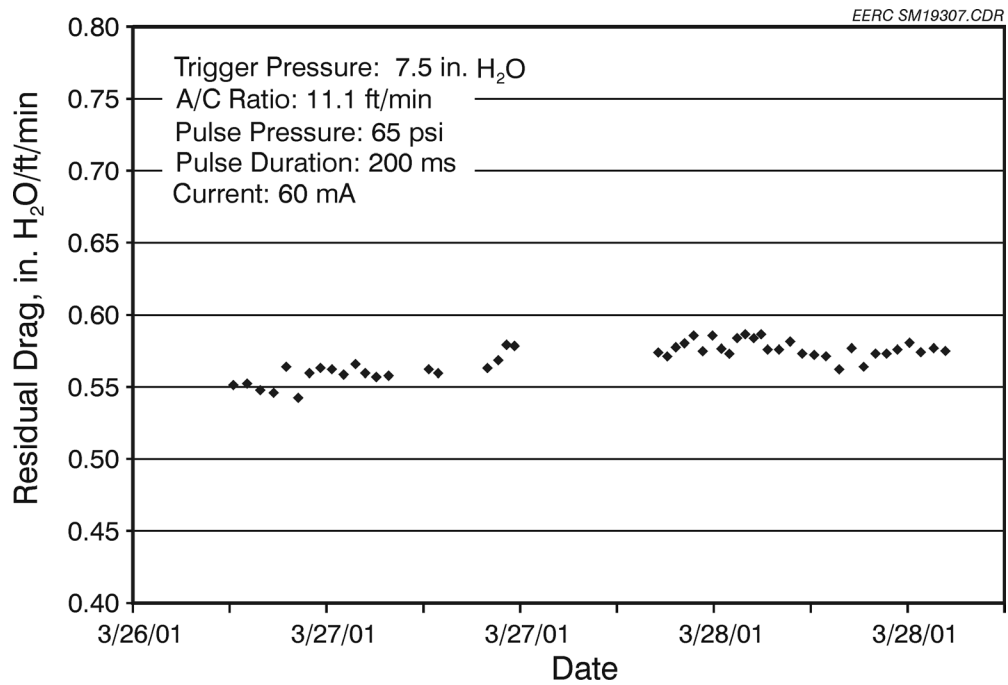


Figure 3.4-17. AHPC residual drag (March 27–28, 2001).

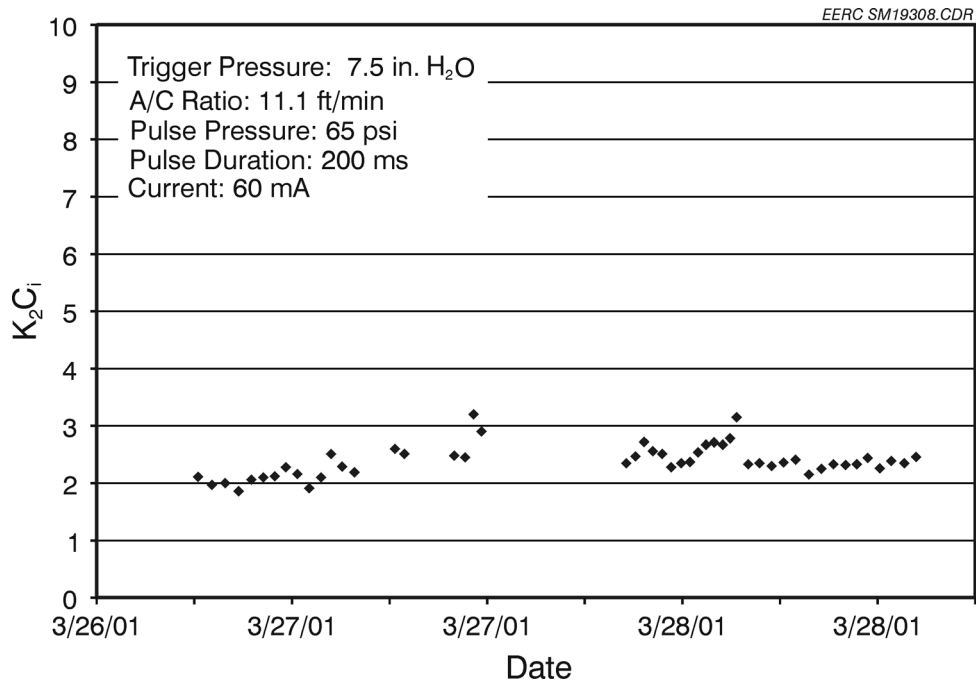


Figure 3.4-18. AHPC K_2C_i (March 27–28, 2001).

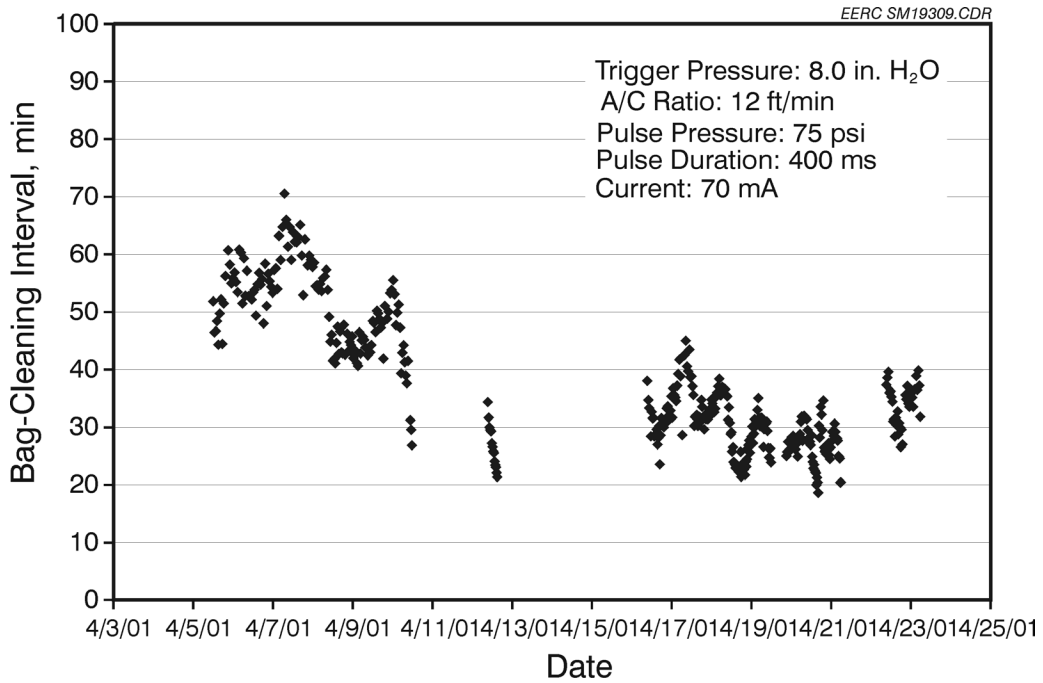


Figure 3.4-19. AHPC bag-cleaning interval (April 5–23, 2001).

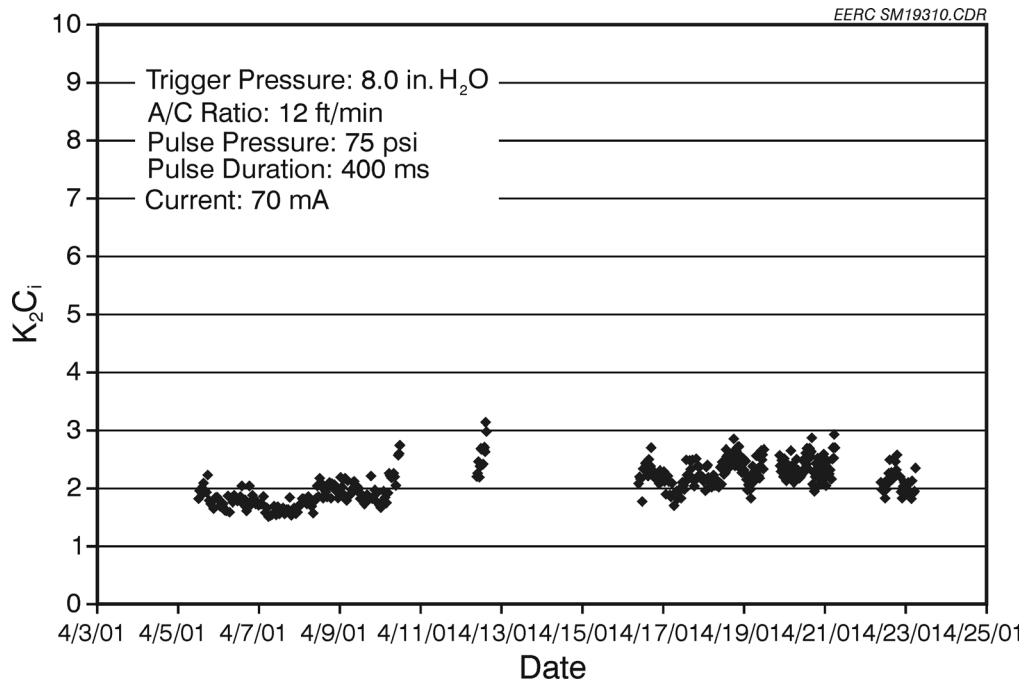


Figure 3.4-20. AHPC K_2C_i (April 5–23, 2001).

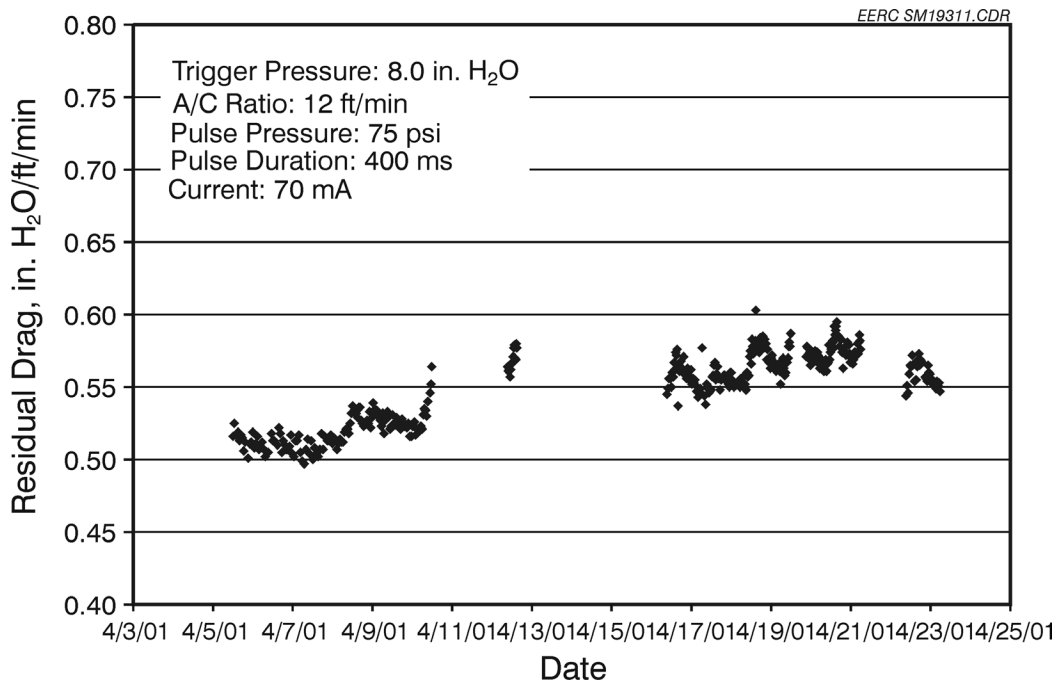


Figure 3.4-21. AHPC residual drag (April 5–23, 2001).

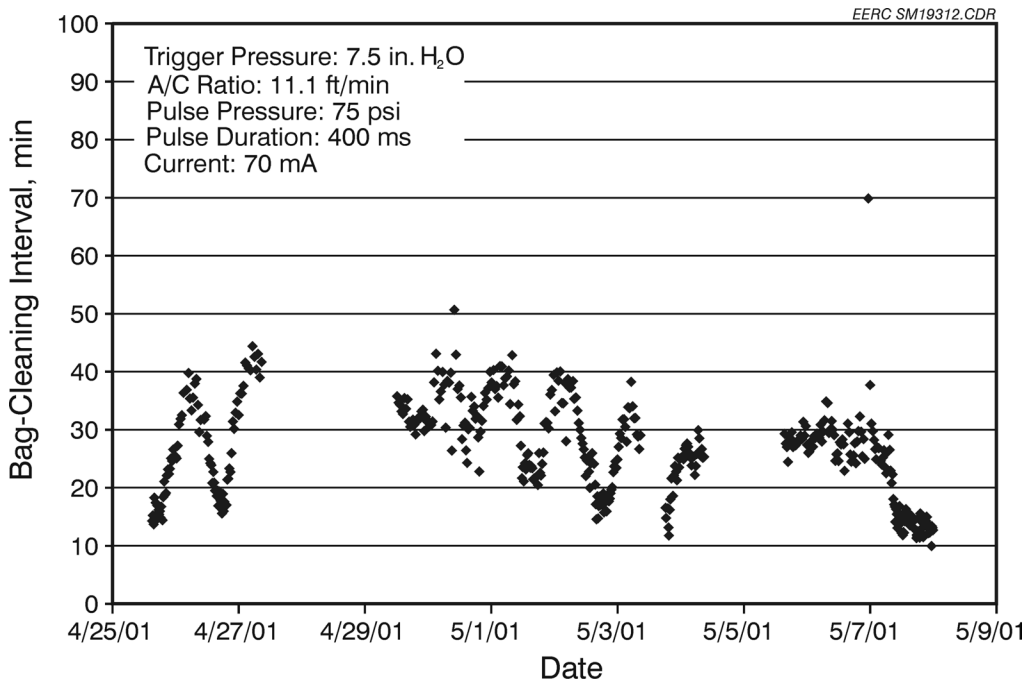


Figure 3.4-22. AHPC bag-cleaning interval (April 25 – May 8, 2001).

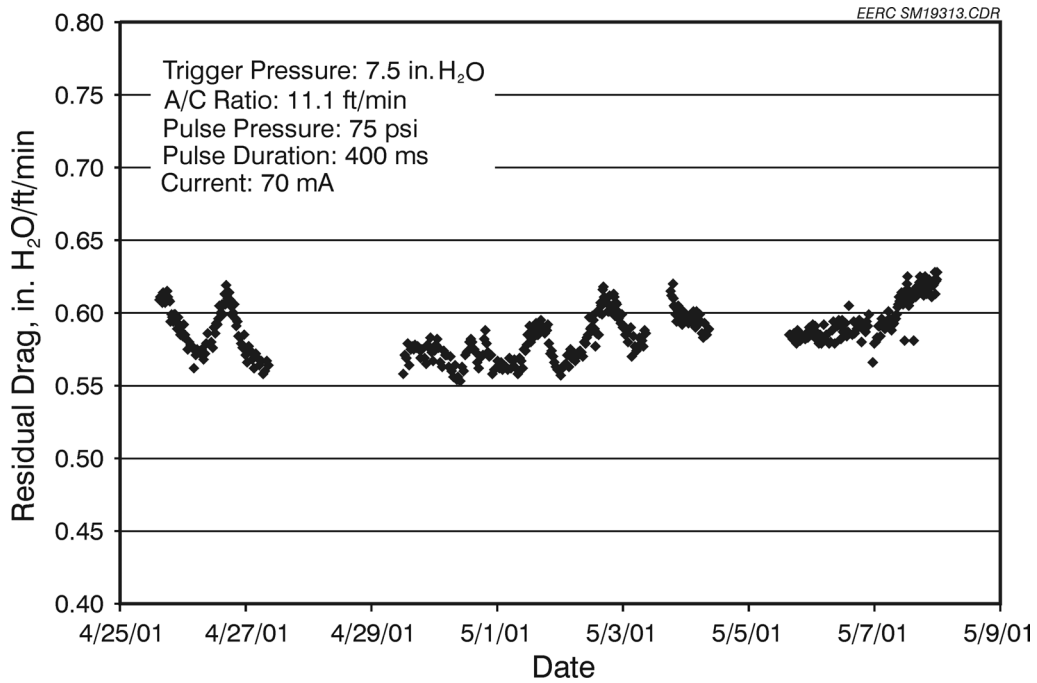


Figure 3.4-23. AHPC residual drag (April 25 – May 8, 2001).

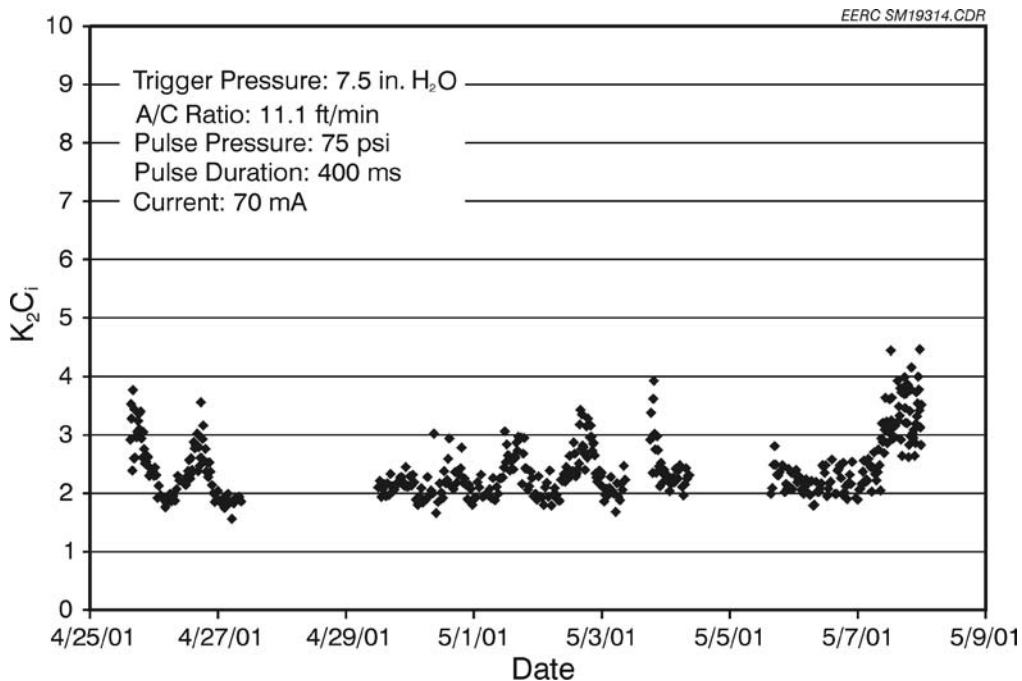


Figure 3.4-24. AHPC K_2C_i (April 25 – May 8, 2001).

Figures 3.4-16–3.4-18 show the bag-cleaning interval, residual drag, and K_2C_i when the pulse cleaning was triggered at 7.5 in. W.C. (1.9 kPa) pressure drop across the system with an A/C ratio of 11.1 ft/min (3.4 m/min) during March 27–28, 2001. The pulse-cleaning pressure was 65 psi (448 kPa) with a pulse duration of 200 ms. The current level was at a constant 60 mA. The bag-cleaning interval was in the range of 20–40 min with a pressure drop across the system of less than 7.0 in. W.C. (1.7 kPa) during the 36-hr test period. The integrated average bag-cleaning interval of this test period was calculated at 32.6 min, much longer than the goal of 10 min. The residual drag, an indicator of bag-cleaning ability, leveled off in the range of 0.54–0.59 with an integral average value of 0.57, demonstrating very good bag cleaning under the low pulse cleaning pressure of 65 psi (448 kPa). The low K_2C_i varied from 2 to 3, indicating the ESP functioned very well under the perforated-plate configuration.

In order to achieve the combined goal for the AHPC of a bag-cleaning interval of at least 10 min at an A/C ratio of 12 ft/min (3.7 ft/min) and an 8.0-in.-W.C. (2.0-kPa) pressure drop, the A/C ratio was increased to 12 ft/min (3.7 ft/min) with a higher pulse-trigger pressure setting at

8.0 in. W.C. (2.0 kPa). The secondary current, pulse-cleaning pressure, and pulse duration were also increased to 70 mA, 75 psi (517 kPa), and 400 ms, respectively, to ensure good ESP performance and bag-cleaning ability. The resulting experimental data are shown in Figures 3.4-19–3.4-21. The bag-cleaning interval (Figure 3.4-19) initially was over 60 min and gradually leveled off in the range of 20–40 min. The calculated integral average bag-cleaning interval during the 425-hr test was 39 min. Compared to the experimental data shown in Figure 3.4-16 (integrated bag-cleaning interval of 32.6 min), the elevated secondary current level and pulse trigger pressure extended the bag-cleaning interval and allowed the AHPC to operate at the higher A/C ratio of 12 ft/min. Average pressure drop for the period was 7.5 in. W.C. (1.9 kPa). The K_2C_i values (Figure 3.4-20) varied from 1.54 to 3, showing the higher current of 70 mA improved ESP operation at the high A/C ratio of 12 ft/min (3.7 m/min). The residual drag (Figure 3.4-21) was 0.497–0.595 with an integral value of 0.544. These results are extremely encouraging and demonstrate better AHPC performance under the new perforated-plate configuration compared to previous results obtained in Phase II and III.

From the previous results, there is a trade-off between pressure drop and A/C ratio. To further test this effect, the pulse trigger pressure and the A/C ratio were reduced to 7.5 in. W.C. (1.9 kPa) and 11.1 ft/min (3.4 m/min) to examine their effect on AHPC performance. The bag-cleaning interval, residual drag, and K_2C_i results are presented in Figures 3.4-22–3.4-24. The bag-cleaning intervals were in the range of 10–50 min with an average pressure drop across the system of 7.0 in. W.C. (1.7 kPa). The K_2C_i values were in the range of 1.6–4.4 with a residual drag of 0.55–0.63. Therefore, by reducing the A/C ratio to 11.1 ft/min (3.4 m/min) and setting the pulse trigger pressure at 7.5 in. W.C. (1.9 kPa), the AHPC was operated at a lower pressure drop as planned. During this test, the bag-cleaning interval results were maintained in the same range as at the higher A/C ratio of 12 ft/min (3.7 m/min) with a higher pulse trigger pressure of 8.0 in. W.C. (2.0 kPa). Both the K_2C_i and residual drag shown in Figures 3.4-23 and 3.4-24 were slightly higher than the experimental data shown in Figures 3.4-20 and 3.4-21, possibly because of continued bag seasoning and higher ash resistivity. The overall AHPC performance is still regarded as excellent, confirming the trade-off between pressure drop and A/C ratio.

More specific studies were then carried out to optimize operating parameters such as pulse trigger pressure, secondary current, pulse-cleaning pressure, pulse duration, and A/C ratio.

3.4.3.4 Pulse Trigger Pressure Experiments

During the test period from April 23–27, 2001, the pulse trigger pressure was set at 7.0 and 7.5 in. W.C. (1.7 and 1.9 kPa) to examine its effect on AHPC performance. The other operating parameters were 11.1 ft/min (3.4 m/min) A/C ratio, 70 mA secondary current, 75 psi (517 kPa) pulse-cleaning pressure, and 400 ms pulse duration. The bag-cleaning interval, residual drag, and K_2C_i results are plotted in Figures 3.4-25–3.4-27. Figure 3.4-25 shows that when the pulse trigger pressure was increased from 7.0 (1.7 kPa) to 7.5 in. W.C. (1.9 kPa), the K_2C_i did not change significantly. The integrated average K_2C_i was in the range of 2.35–2.28 for the two different pulse trigger pressures. The residual drag (Figure 3.4-26) was slightly increased with the increasing trigger pressure (integrated averages of 0.562 at 7.0 in. W.C. [1.7 kPa] and 0.585 at 7.5 in. W.C. [1.9 kPa]), showing that the perforated-plate AHPC configuration could maintain good bag-cleaning ability under a lower pulse trigger pressure. The trigger pressure of 7.5 in.

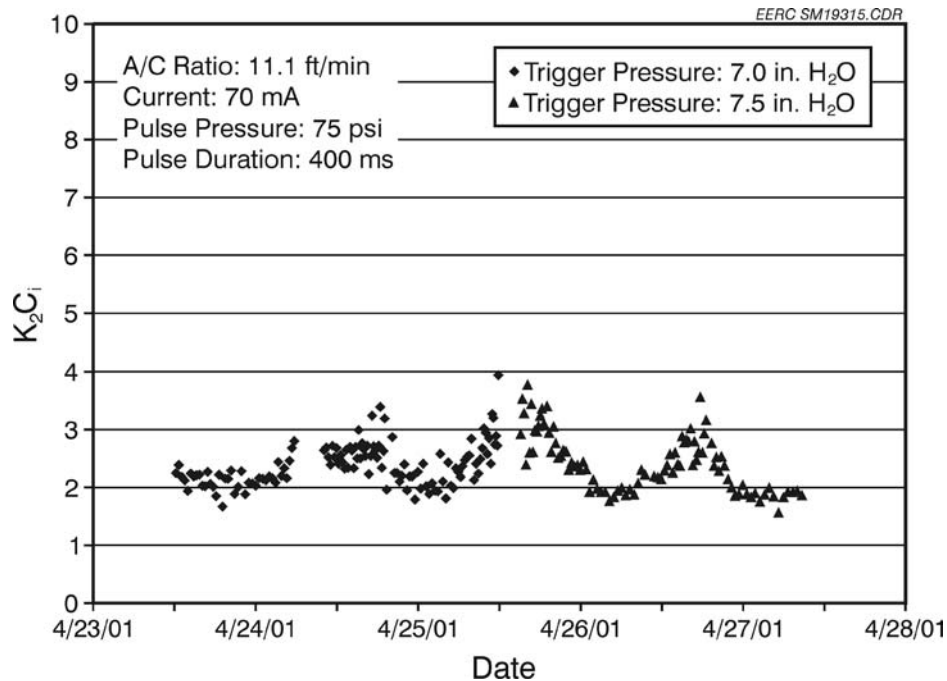


Figure 3.4-25. Trigger pressure effect on AHPC K_2C_i (April 23–27, 2001).

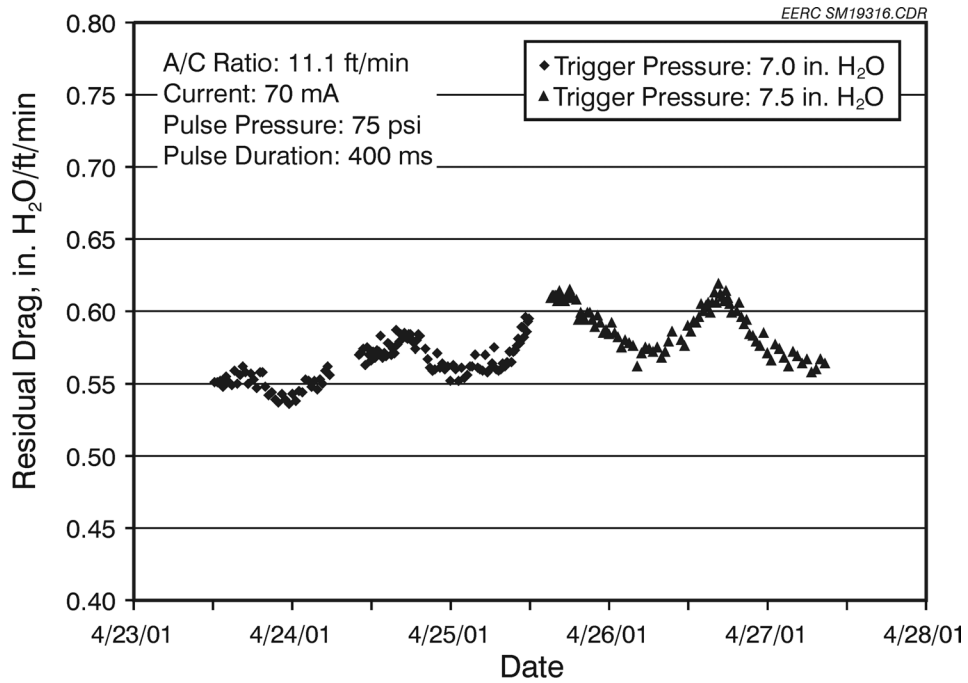


Figure 3.4-26. Trigger pressure effect on AHPC residual drag (April 23–27, 2001).

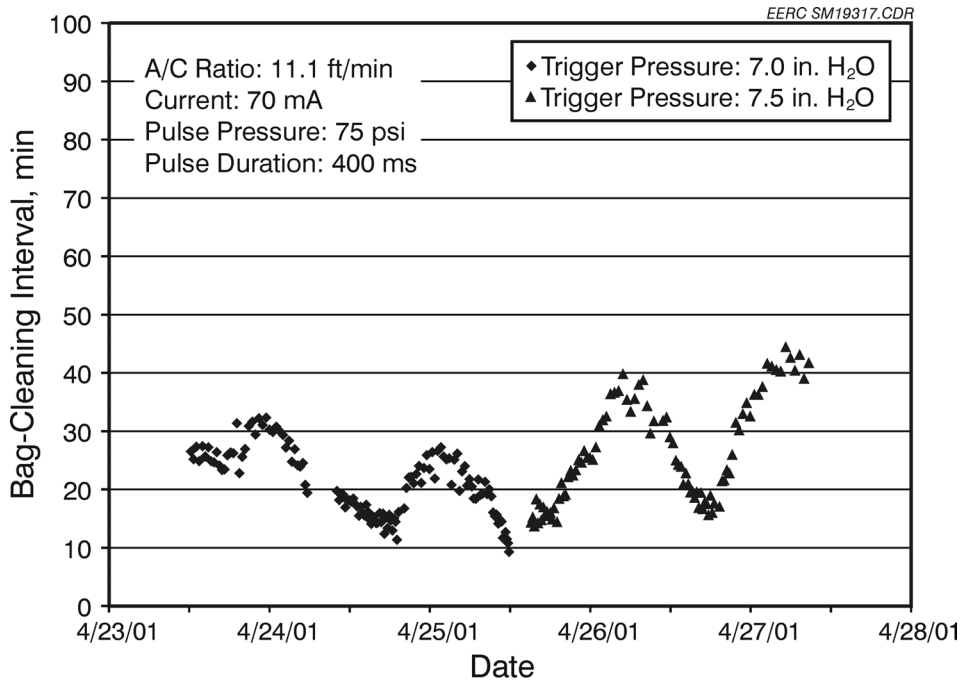


Figure 3.4-27. Trigger pressure effect on AHPC bag-cleaning interval (April 23–27, 2001).

W.C. (1.9 kPa) resulted in a longer bag-cleaning interval of 29.2 min (integral average value) compared to 22.2 min at the pulse trigger pressure of 7.0 in. W.C. (1.7 kPa) (shown in Figure 3.4-27). A longer bag-cleaning interval is the expected benefit of a higher pulse trigger pressure.

3.4.3.5 A/C Ratio Experiments

Experiments were carried out where the A/C ratio was varied in the range of 11.4–12.0 ft/min (3.5–3.7 m/min). The K_2C_i , residual drag, and bag-cleaning interval results are plotted in Figures 3.4-28–3.4-30. With the increase of A/C from 11.4 to 12.0 ft/min (3.5 to 3.7 m/min), the K_2C_i and residual drag were not changed dramatically. The integrated average values for both K_2C_i and residual drag (Table 3.4-1) were almost the same, 2.0–2.27 for K_2C_i and 0.55–0.56 for residual drag, respectively. The bag-cleaning interval, however, was initially maintained at approximately 40 min at the lower A/C ratios of 11.4 and 11.7 ft/min (3.5 and 3.6 m/min) and dropped to 31.7 min when the A/C ratio increased to 12 ft/min (3.7 m/min). The experimental results show that when the pulse trigger pressure was 8.0 in. W.C. (2.0 kPa),

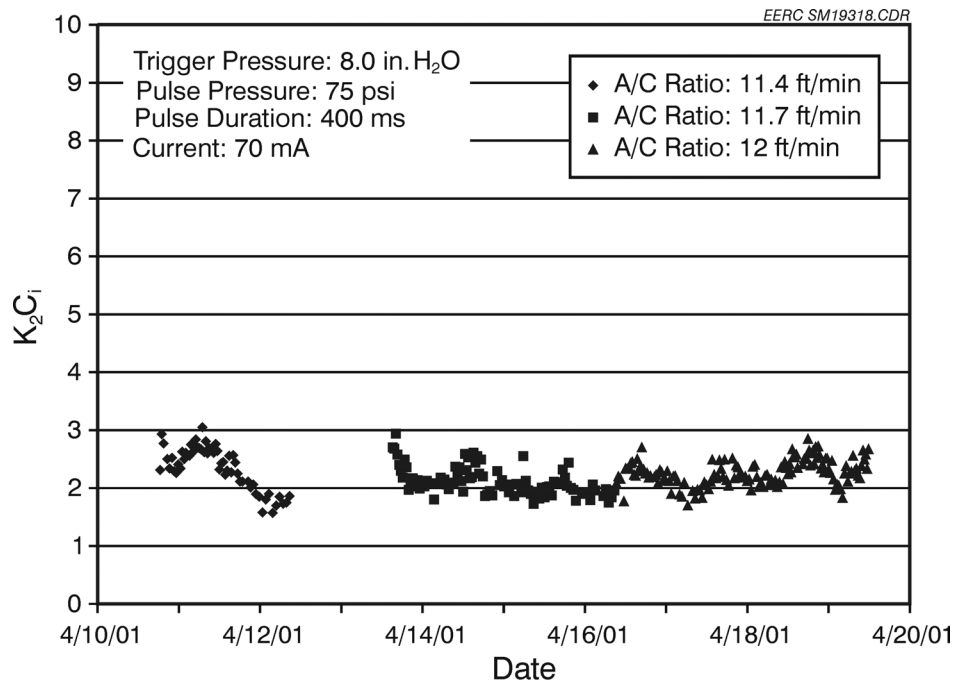


Figure 3.4-28. A/C ratio effect on AHPC K_2C_i (April 11–19, 2001).

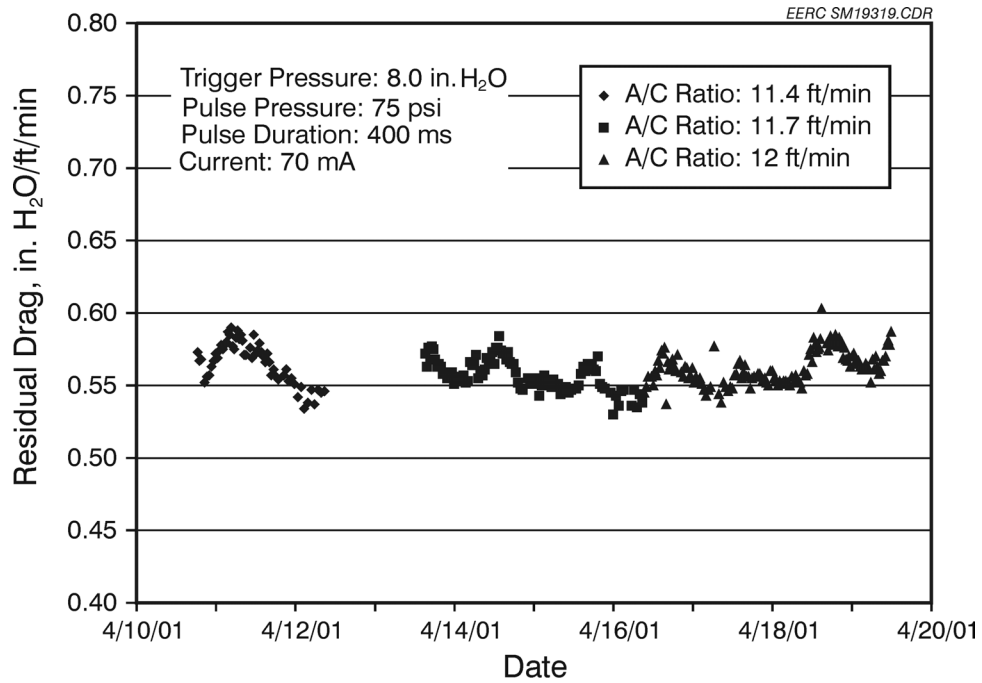


Figure 3.4-29. A/C ratio effect on AHPC residual drag (April 11–19, 2001).

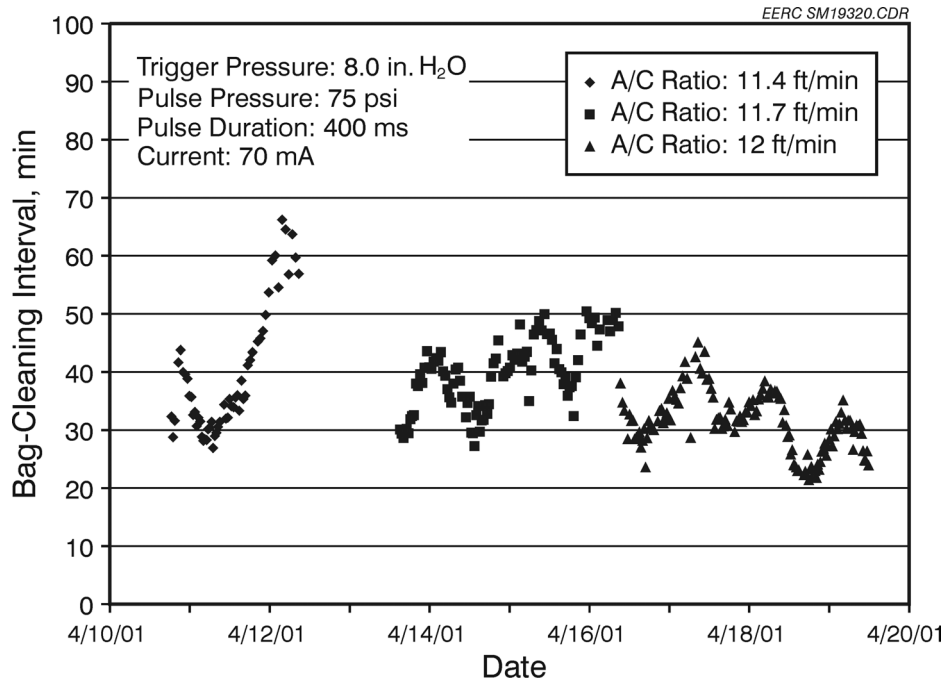


Figure 3.4-30. A/C ratio effect on AHPC bag-cleaning interval (April 11–19, 2001).

TABLE 3.4-1

AHPC Settings and Results at Different A/C Ratios

Operational Setting			
Pulse Trigger Pressure: 8.0 in. W.C. (2.0 kPa)			
Pulse-Cleaning Pressure: 75 psi (517 kPa)			
Pulse Duration: 400 ms			
Secondary Current: 70 mA			
A/C Ratio: 11.4, 11.7, and 12.0 ft/min (3.5, 3.6, and 3.7 m/min)			
Operational Results (integral average values)			
A/C	K_2C_i	Residual Drag	Bag-Cleaning Interval
11.4 (3.5)	2.27	0.562	42.4
11.7 (3.6)	2.07	0.555	40.9
12.0 (3.7)	2.23	0.561	31.7

secondary current was 70 mA, and the pulse cleaning pressure was 75 psi (517 kPa) with a 400-ms pulse duration, within the range of A/C ratio of 11.4 to 12 ft/min (3.5 to 3.7 m/min), the perforated-plate AHPC performed better overall at an A/C ratio of 11.7 ft/min (3.6 m/min) compared to 12 ft/min (3.7 m/min). However, performance during this test period at 12 ft/min (3.7 m/min) was excellent and significantly better than the performance goals.

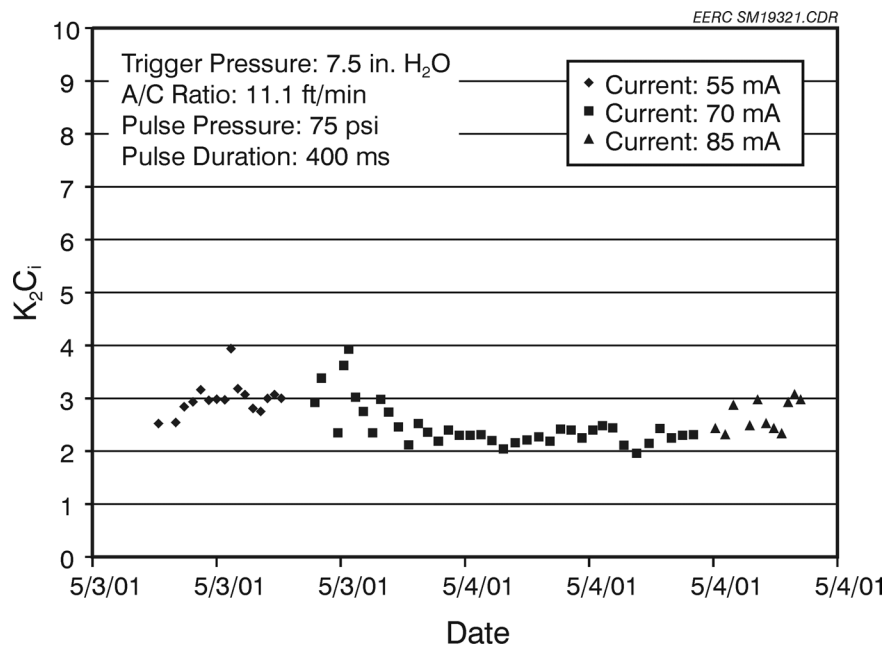
3.4.3.6 Secondary Current Experiments

The secondary current is a critical operating parameter affecting AHPC performance, but higher current requires more electrical power and may cause back corona and sparking. During the test period from May 3–4, 2001, short-term tests were carried out to investigate the effect of secondary current on AHPC performance under the following operating conditions: 7.5 in. W.C. (1.9 kPa) pulse trigger pressure, 11.1 ft/min (3.4 m/min) A/C ratio, 75 psi (517 kPa) pulse-cleaning pressure, and 400 ms pulse duration. The secondary current was initially 55 mA and gradually increased to 70 and 85 mA. K_2C_i , the indicator for ESP performance plotted in Figure 3.4-31, was around 3.0 at a current of 55 mA and decreased to 2.38 when the current reached 70 mA, indicating improvement in ESP performance. However, on further increasing current to 85 mA, the K_2C_i was around 2.65, implying that the ESP performance did not improve with increasing current. This suggests that the ESP had reached its limiting performance;

however, the 85 mA current was during a time of increasing temperature, so the negative effect of increasing ash resistivity may have overpowered any benefit of increased current. The effect of the secondary current on residual drag was not significant. The residual drag was kept around 0.60 during the test period when the current was increased from 55 to 85 mA (Figure 3.4-32). The bag-cleaning interval (Figure 3.4-33) was 18.2 min at 55 mA, increased to 23.7 min at a higher current of 70 mA, and then decreased to 19.5 min when the current was further increased to 85 mA. Again, the effect of changing temperature during this test period may have overshadowed the current effect.

3.4.3.7 Pulse-Cleaning Experiments

Short-term tests (March 21–24, 2001, and April 19–21, 2001) were carried out to investigate the pulse-cleaning pressure effect on bag-cleaning ability. The operational parameters are listed in Table 3.4-2.



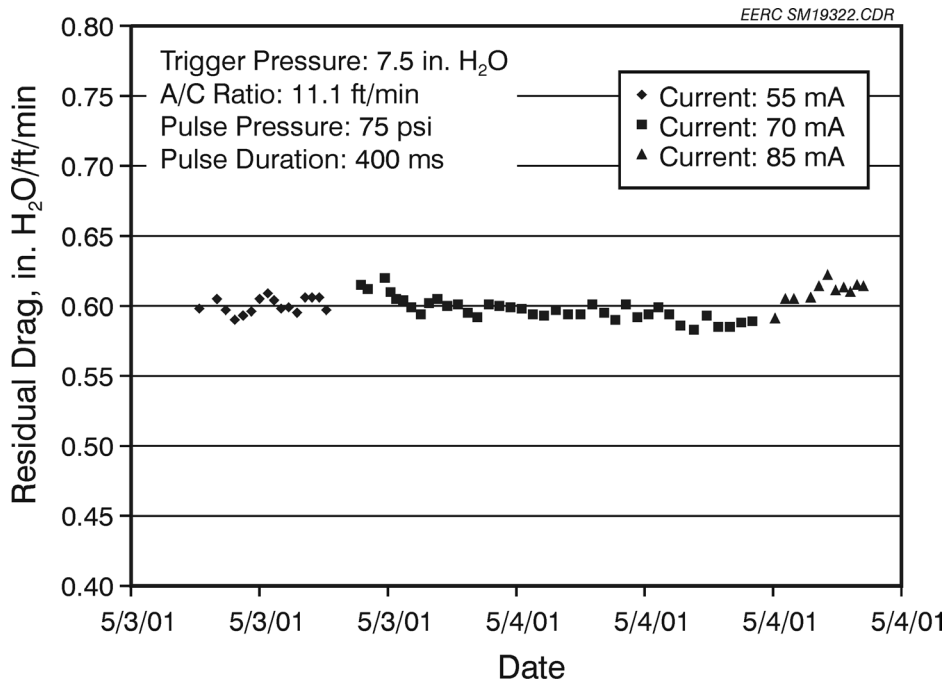


Figure 3.4-32. Current effect on AHPC residual drag (May 3–4, 2001).

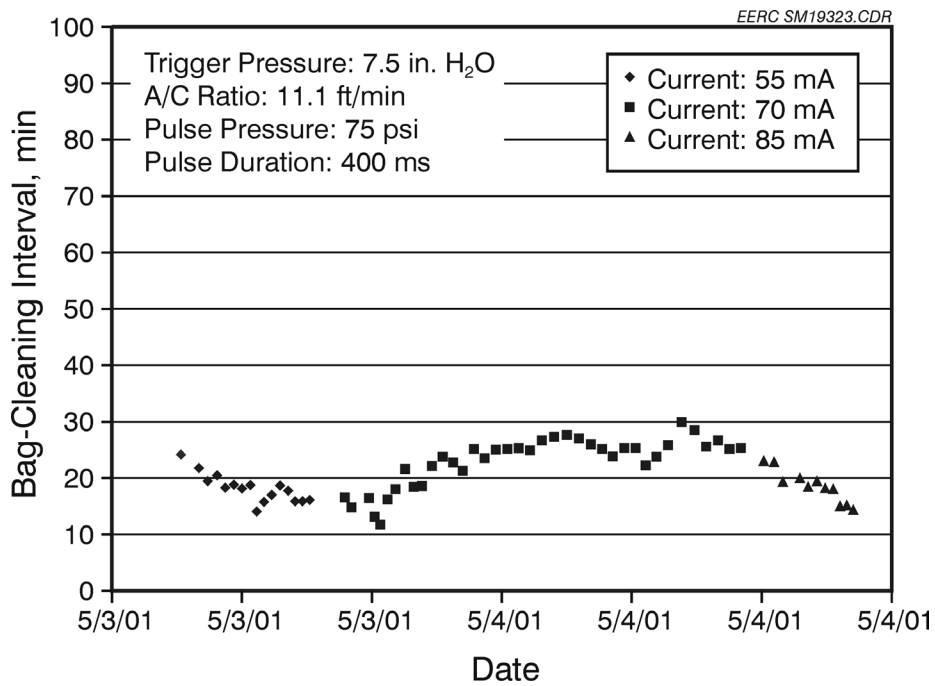


Figure 3.4-33. Current effect on AHPC bag-cleaning interval (May 3–4, 2001).

TABLE 3.4-2

AHPC Settings at Different Pulse-Cleaning Pressures		
Test Date:	3/21/01–3/24/01	4/19/01–4/21/01
Operational Setting		
Trigger Pressure	7.5 in. W.C. (1.9 kPa)	8.0 in. W.C. (2.0 kPa)
A/C Ratio	11.7 ft/min (3.6 m/min)	11.2 ft/min (3.4 m/min)
Current	60 mA	70 mA
Pulse-Cleaning Pressure	50, 65 psi (345, 448 kPa)	75, 85 psi (517, 586 kPa)
Pulse Duration	200 ms	400 ms

The residual drag for the two tests is plotted and shown in Figures 3.4-34 and 3.4-35, respectively. When the pulse-cleaning pressure was increased from 50 to 65 psi (345 to 448 kPa) (Figure 3.4-34), the residual drag was reduced dramatically from 0.566 to 0.497, demonstrating an impressive improvement in bag-cleaning ability. The further increase of pulse-cleaning pressure from 75 to 85 psi (517 to 586 kPa) (Figure 3.4-35) did not result in a significant reduction in residual drag. However, the 85-psi (586-kPa) test was completed with a smaller-volume tank. This demonstrates that similar bag-cleaning effectiveness can be achieved with

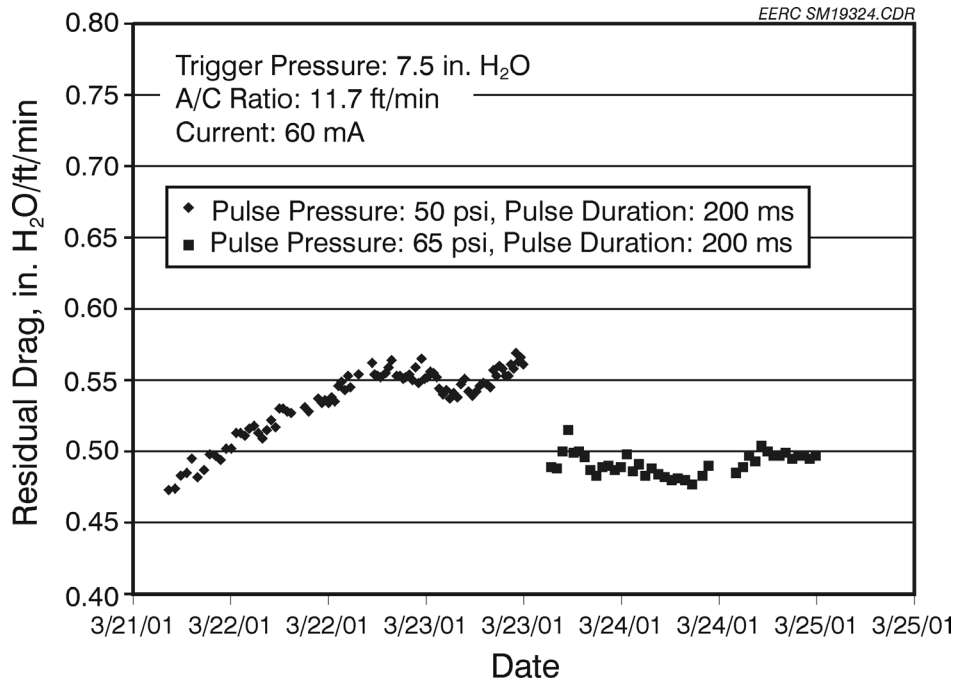


Figure 3.4-34. Pulse pressure effect on AHPC residual drag (March 21–25, 2001).

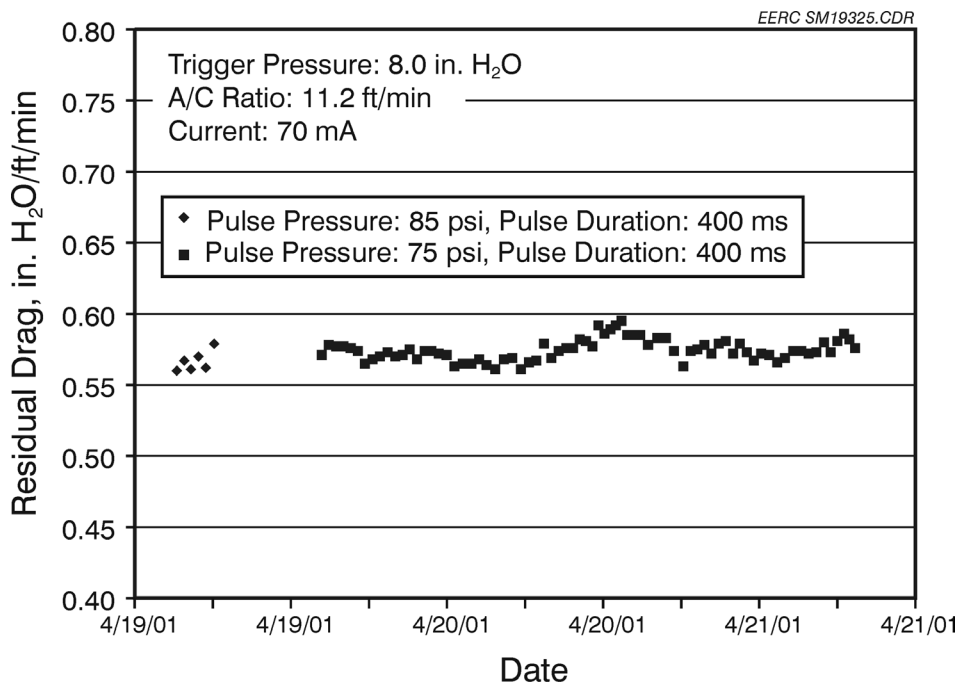


Figure 3.4-35. Pulse pressure effect on AHPC residual drag (April 19–21, 2001).

increased pressure but reduced volume. The difference in residual drag observed in the two tests is due to bag seasoning. The corresponding bag-cleaning intervals are shown in Figures 3.4-36 and 3.4-37. The integral average of bag-cleaning interval (Figure 3.4-36) was 28.2 min at the pulse-cleaning pressure of 50 psi (345 kPa) and increased to 45.7 min at the higher pulse-cleaning pressure of 65 psi (448 kPa). The bag-cleaning interval was kept around 27 min (Figure 3.4-37) when the pulse-cleaning pressure changed from 75 to 85 psi (517 to 586 kPa).

The AHPC system was shut down on May 8, 2001, to correspond with a planned plant maintenance outage. Photos were taken inside the AHPC chamber to examine the fly ash deposition on the plates. Figure 3.4-38 shows the nonuniform ash pattern on the perforated plates caused by the electrical field in the AHPC vessel. The perforated plates were reasonably clean after 1300 hr of operation, showing the plate-rapping system was effective. A power-off rapping was carried out, and a photo was taken (Figure 3.4-39) to evaluate the rapping's effectiveness on plate cleaning. As seen in Figure 3.4-39, the perforated plate was very clean with only a thin uniform ash deposit, implying that regular power-off rapping may benefit AHPC operation.

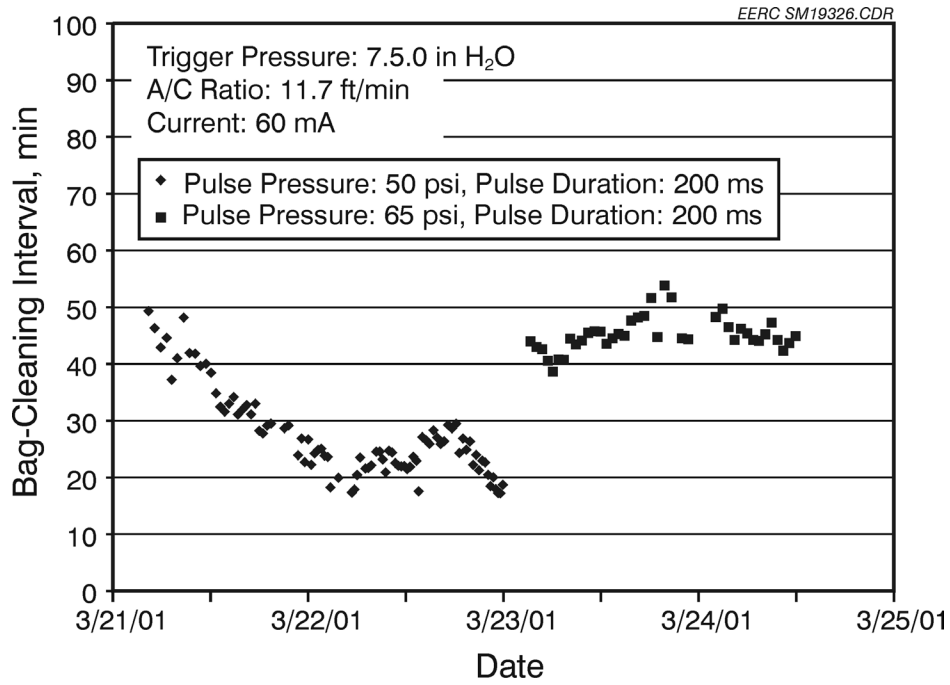


Figure 3.4-36. Pulse pressure effect on AHPC bag-cleaning interval (March 21–25, 2001).

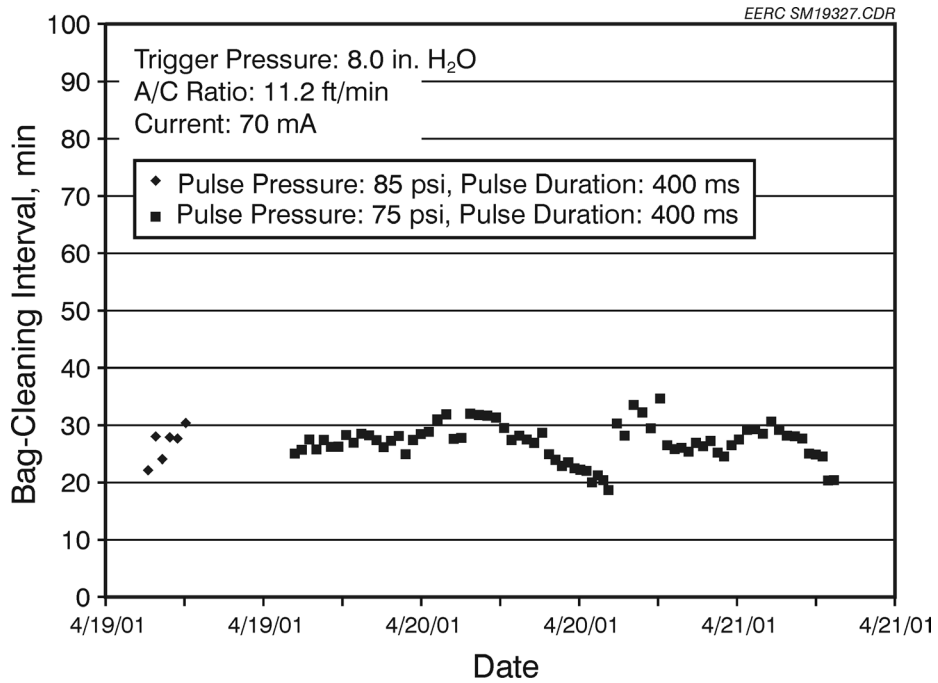


Figure 3.4-37. Pulse pressure effect on AHPC bag-cleaning interval (April 19–21, 2001).

EERC SM19461.CDR

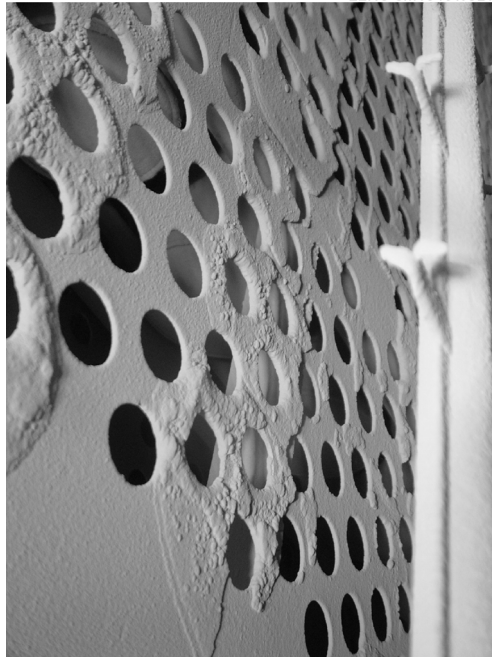


Figure 3.4-38. Photo showing the nonuniform ash pattern on the perforated plates caused by the electrical field in the AHPC vessel.

EERC SM19462.CDR

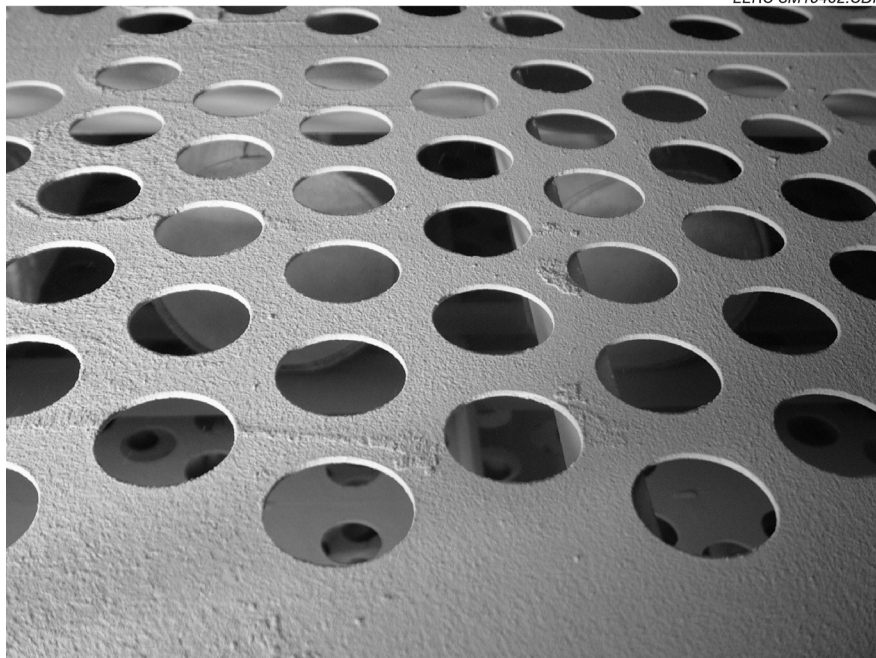


Figure 3.4-39. Photo showing a very clean perforated plate with only a thin uniform ash deposit after a power-off rap.

Several bags were pulled out for visual inspection. No electrically induced damage was observed, indicating excellent bag protection by the perforated plates. The ash attached to the bags was very easy to brush off. Figure 3.4-40 shows the extremely clean bag surface after brush-off. Several new bags were installed in the AHPC system to replace the ones sent back to Gore for microscopic analysis. More detailed bag analysis results are discussed in Section 3.4.6.

3.4.4 Results for Test Period 2 (May 16 – June 15, 2001)

3.4.4.1 Plant Conditions – Fuel, Load, and Temperature

The AHPC was started again on May 16, 2001, following the plant outage. During this test period, the power plant burned several different coals, including Cordero, Black Thunder, Cordero Rojo, and Eagle Butte. The fly ash resistivity of these coals varies widely. The highest resistivity was over 10^{12} ohm-cm, which can cause a significant deterioration in ESP performance. More detailed analyses on fly ash resistivity are provided later. Also, the power



Figure 3.4-40. Photo showing the extremely clean bag surface after brush-off.

plant gross load and ESP temperature fluctuated, as shown in Figure 3.4-41. The gross load reached a full load value of 450 MW during the daytime and dropped to around 350 MW at night. The AHPC temperature, therefore, also varied widely from 250E–320EF (121E–160EC), which significantly affected AHPC performance. Except for a 9-hr shutdown on May 31, 2001, to switch to a cross-row pulsing system, the AHPC was in a continuous operating mode until June 15, 2001, when the system was shut down briefly to change electrodes.

3.4.4.2 Electrical Conditions

The secondary current was set at 70 mA during the entire testing period. The daily sparking number was recorded and is shown in Figure 3.4-42. Except for 4709 sparks and 1233 sparks observed on May 25, 2001, and June 11, 2001, respectively, the daily sparking number was far less than 1000 during the rest of the testing period. A total of 10,760 sparks occurred during the 30-day test, with a daily average of 359 sparks, which was still much better than the previous results in summer 2000.

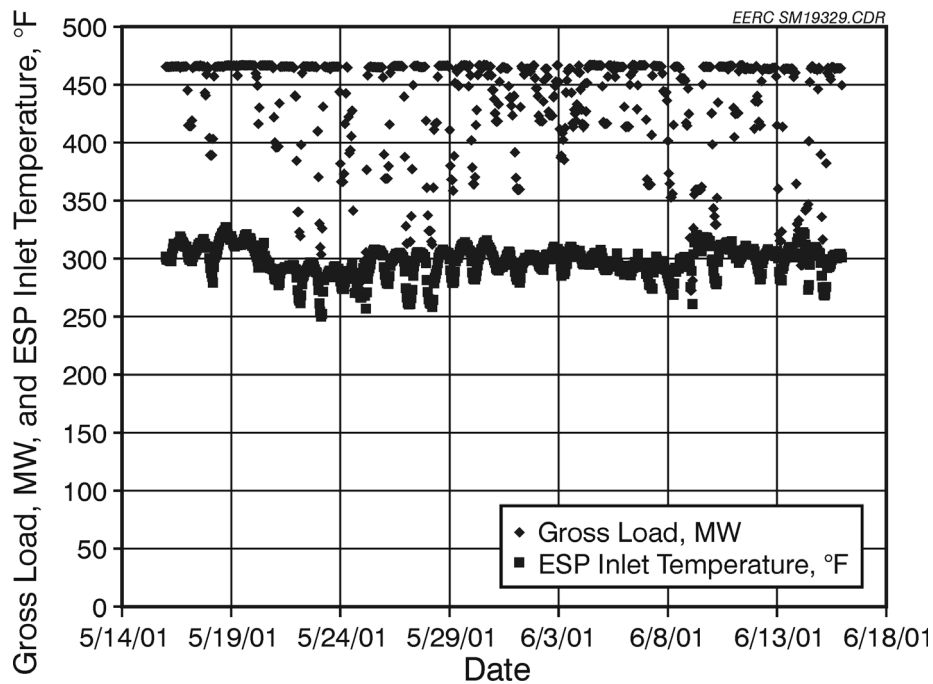


Figure 3.4-41. Big Stone Power Plant gross load and ESP inlet temperature (Test Period May 16 – June 15, 2001).

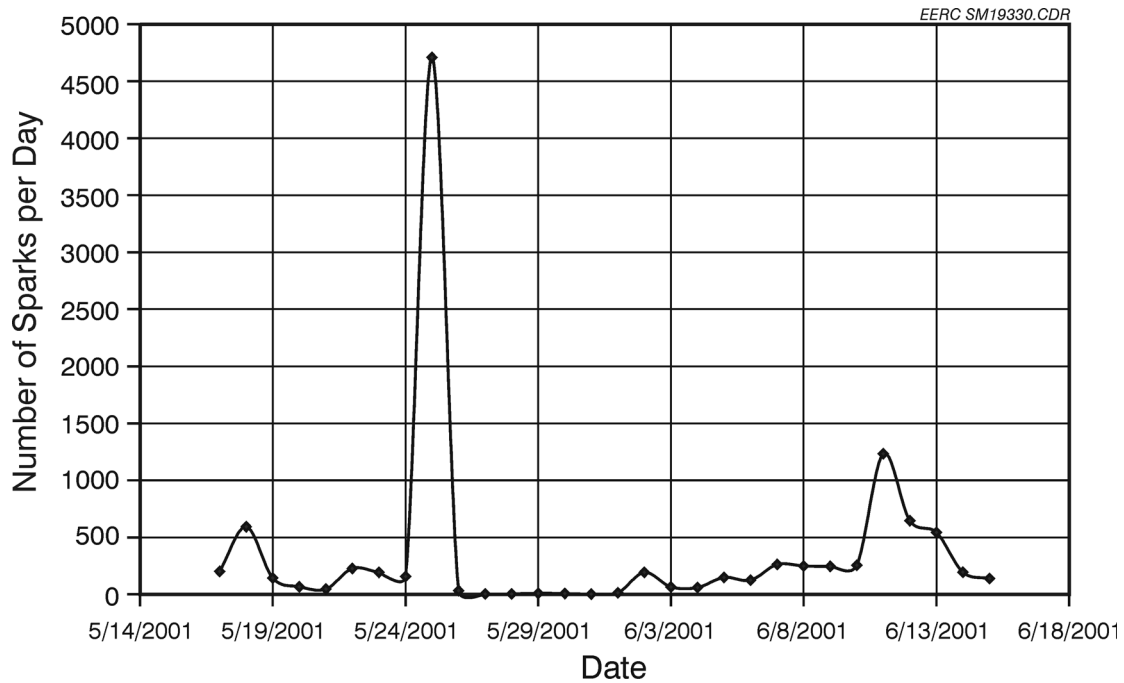


Figure 3.4-42. Number of sparks per day (May 16 – June 16, 2001).

3.4.4.3 Perforated-Plate AHPC Performance

The AHPC was started at an A/C ratio of 12 ft/min (3.7 m/min), with a pulse trigger pressure of 8.0 in. W.C. (2.0 kPa). The secondary current was 70 mA, and the pulse-cleaning pressure was 75 psi (517 kPa), with a duration time of 400 ms. The bag-cleaning interval, initially at 60 min, dropped below 10 min on May 17, 2001, as shown in Figure 3.4-43. In order to operate the AHPC system with a reasonable bag-cleaning interval over 10 min, the A/C ratio was gradually cut down to 11.1, 10.8, and 10.5 ft/min (3.4, 3.3, and 3.2 m/min). The observed decreasing bag-cleaning interval (shown in Figure 3.4-43) correlated with poor ESP (high K_2C_i) and poor bag-cleaning ability (high residual drag), as shown in Figures 3.4-44 and 3.4-45. The residual drag started at a low value of 0.42 but climbed up to 0.67 in. W.C./ft/min even though the A/C ratio was reduced. The residual drag reached 0.63–0.67 in. W.C./ft/min at an A/C ratio of 10.5 ft/min (3.2 m/min), which is higher than that observed in Test Period 1 at the same operating conditions. The calculated K_2C_i ranged from 4–7 during this test period, which is also not as good as observed in Test Period 1. The bag-cleaning interval was around 16 min with a

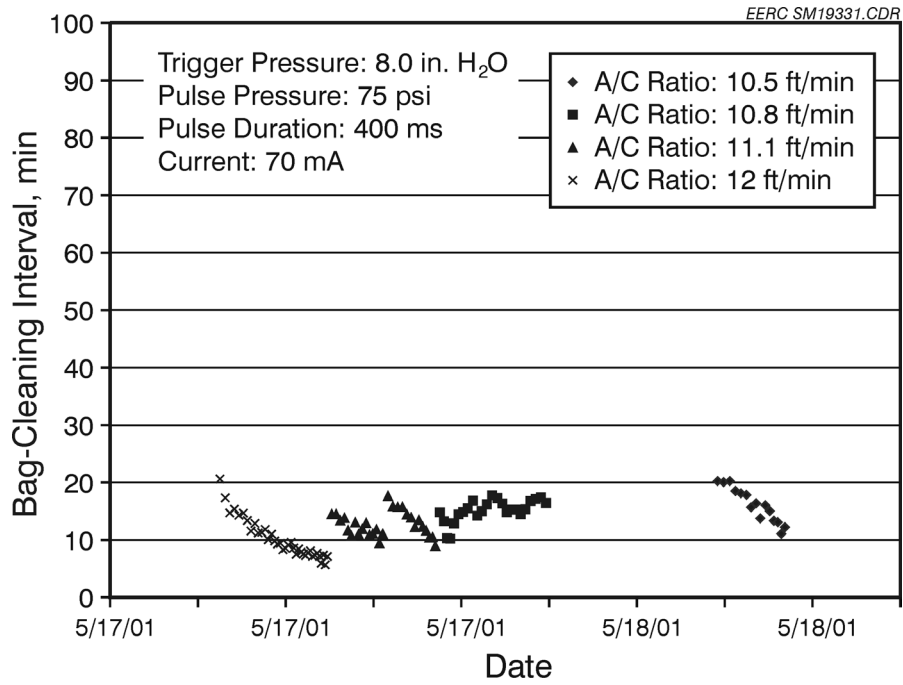


Figure 3.4-43. A/C ratio effect on AHPC bag-cleaning interval (May 17–18, 2001).

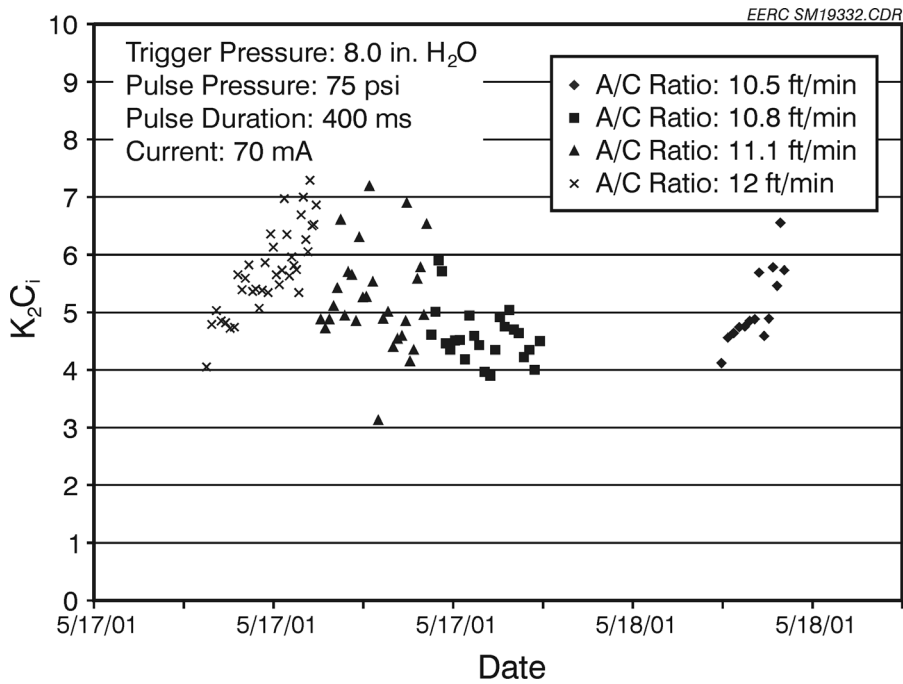


Figure 3.4-44. A/C ratio effect on AHPC K_2C_i (May 17–18, 2001).

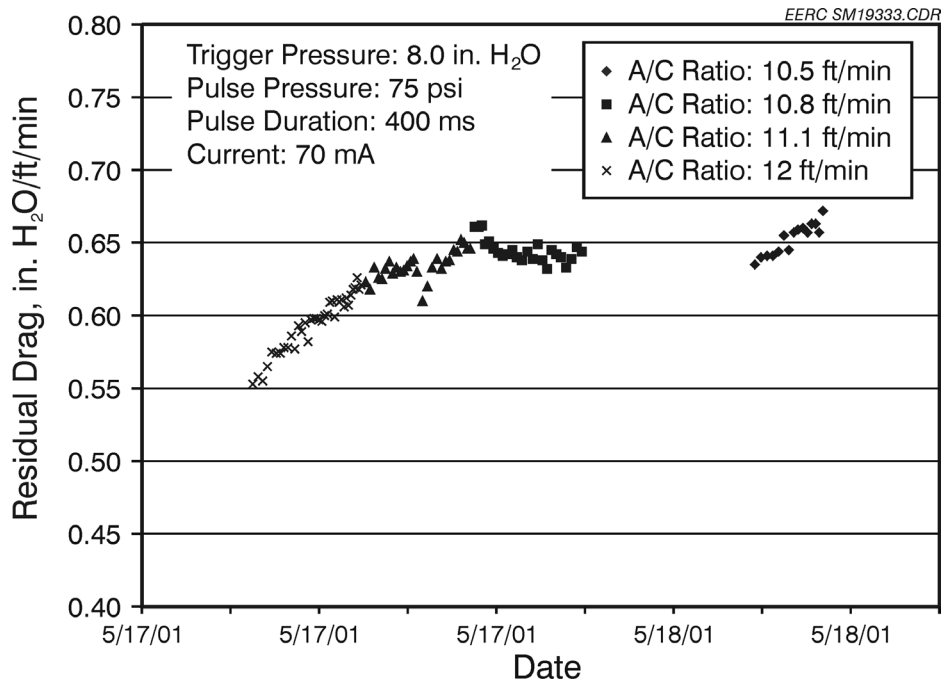


Figure 3.4-45. A/C ratio effect on AHPC residual drag (May 17-18, 2001).

K_2C_1 of 4.98 and an A/C ratio of 10.5 ft/min (3.2 m/min). Since all of the operating parameters were kept at a range similar to Test Period 1, the observed poorer AHPC overall performance was likely the result of changes in power plant conditions such as the higher temperature and higher resistivity of the fly ash because of coal switching.

3.4.4.4 Fixed Bag-Cleaning Interval Experiments

One reason for the short bag-cleaning interval was the high residual drag (over 0.65), which indicated the fly ash attached to the bag surface was not efficiently removed after pulsing. In order to improve the bag-cleaning ability, the AHPC was operated in a controlled bag-cleaning-interval mode, which meant the bag-cleaning pulse was triggered by a filtration time such as a 30-min interval rather than by the pressure drop across the system. It is expected that the fine fly ash particles on the bag surface will agglomerate better under an extended bag filtration time, which, in turn, facilitates bag cleaning. Therefore, the AHPC was operated at a fixed bag-cleaning interval of 10 and 30 min (May 18-21, 2001), to evaluate the effect on residual drag. The A/C ratio was set at 10.3 ft/min (3.1 m/min), with a secondary current of

70 mA, a pulse-cleaning pressure of 75 psi (517 kPa), and a pulse duration time of 400 ms. The residual drag and K_2C_i results are shown in Figures 3.4-46 and 3.4-47. The residual drag was reduced to some extent but not significantly under the 30-min bag-cleaning interval operation compared to the data in the 10-min operation mode. It is concluded that there was no significant difference in terms of residual drag between the 10- and 30-min operating modes. Most of the K_2C_i values at the bag-cleaning interval of 30 min were in the range of 3.0–4.0, with an integral average of 3.29, indicating somewhat better ESP performance compared to that of the 10-min bag-cleaning interval mode (Figure 3.4-47). The average pressure drop across the system was around 7.4 in. W.C. (1.8 kPa) for the 30-min operating mode and 7.1 in. W.C. (1.8 kPa) at the 10-min operating mode, which shows there is some benefit to reduced pressure drop with a shorter bag-cleaning interval.

3.4.4.5 Pulse Sequence Experiments with Cross-Row Pulsing

The cross-row pulse system (as described in an earlier section) was installed on May 31, 2001, and the pulse controller program was modified to allow full control of the pulse sequence.

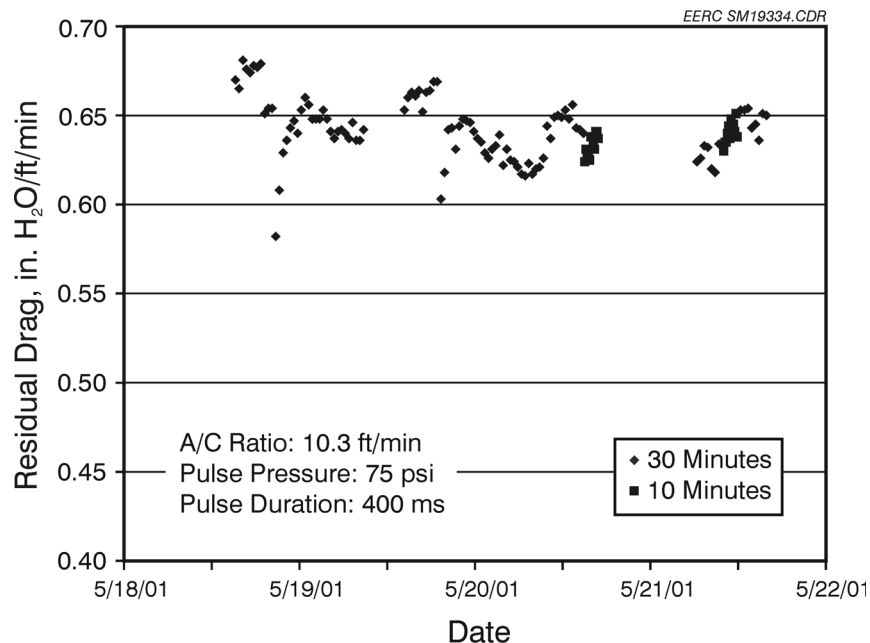


Figure 3.4-46. AHPC residual drag performance at 10- and 30-min bag-cleaning intervals (May 18–21, 2001).

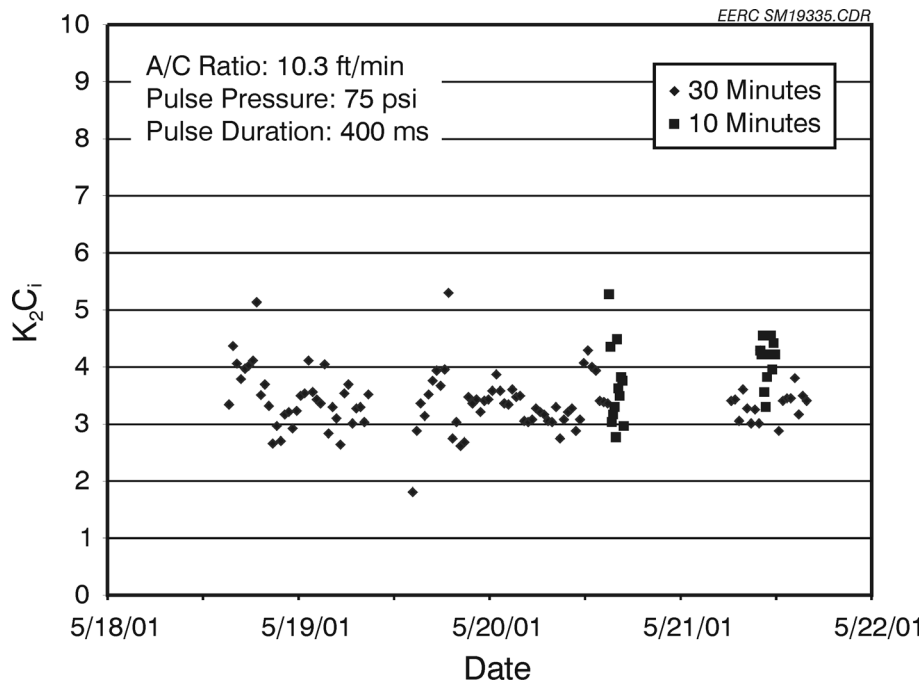


Figure 3.4-47. AHPC K_2C_i performance at 10- and 30-min bag-cleaning intervals (May 18–21, 2001).

Cross-Row Pulse 1–8 indicates that the pulse cleaning started at Bag 1, followed by Bag 2, and ended with Bag 8, while Cross-Row Pulse 8–1 was in the reverse order (shown in Figure 3.4-7). Cross- Row Pulse 71538264 was an alternate pulsing mode to suppress the reentrainment of the fly ash (blown off during pulsing) toward the adjacent bags. The A/C ratio was 11.1 ft/min (3.4 m/min), and the pulse trigger pressure was set at 8.0 in. H_2O (2.0 kPa), with a pulse-cleaning pressure of 75 psi (517 kPa) and a pulse duration time of 400 ms. The bag-cleaning interval, residual drag, and K_2C_i results from June 7–13, 2001, are shown in Figures 3.4-48–3.4-50. The power plant was operated under changing load conditions during this test period, having a full gross load of 460 MW during the day and a low gross load of 375 MW at night. The varying gross load resulted in the variation of temperature in the AHPC unit, which significantly affected AHPC performance in terms of bag-cleaning interval, residual drag, and K_2C_i . The integral average values were calculated for the bag-cleaning interval, residual drag, and K_2C_i under the three different pulse sequence modes and are listed in Table 3.4-3. The bag-cleaning interval was maintained around 27–29 min, with a constant residual drag of 0.59. The results show no significant differences among the three pulse sequence modes, indicating the AHPC system

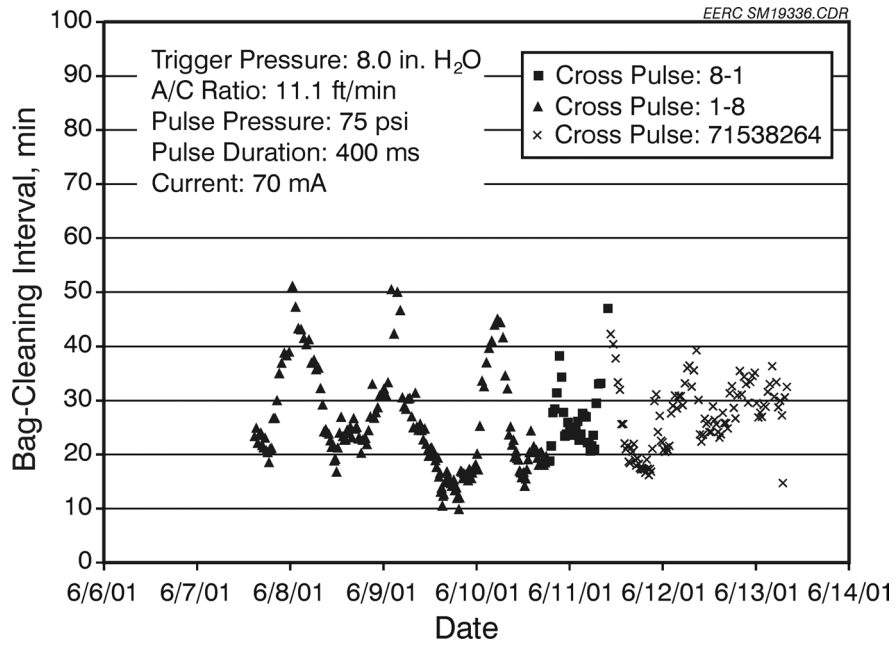


Figure 3.4-48. Pulse sequence effect on AHPC bag-cleaning interval (June 7–13, 2001).

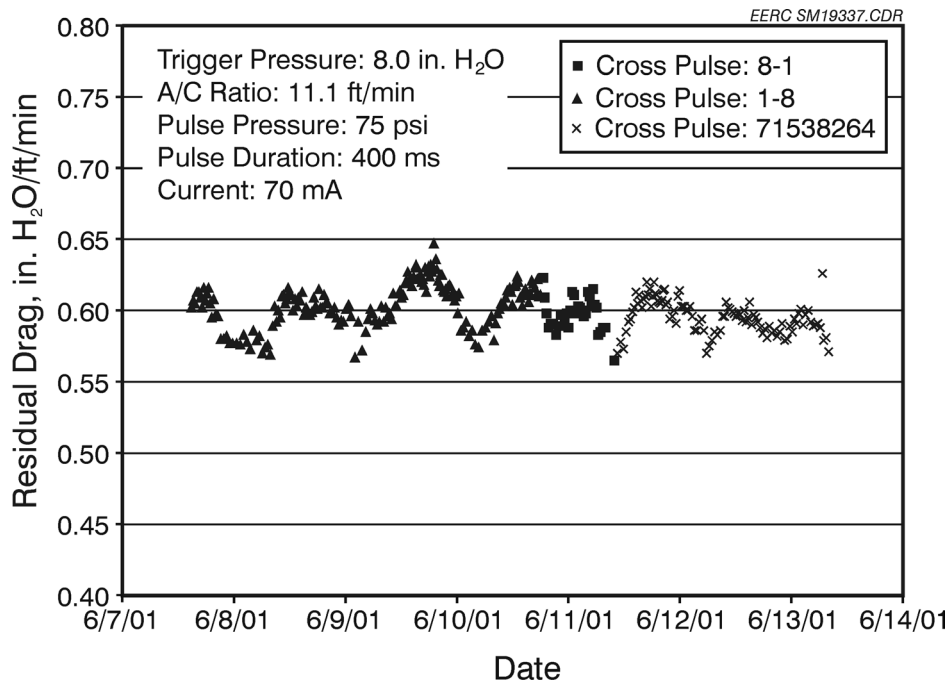


Figure 3.4-49. Pulse sequence effect on AHPC residual drag (June 7–13, 2001).

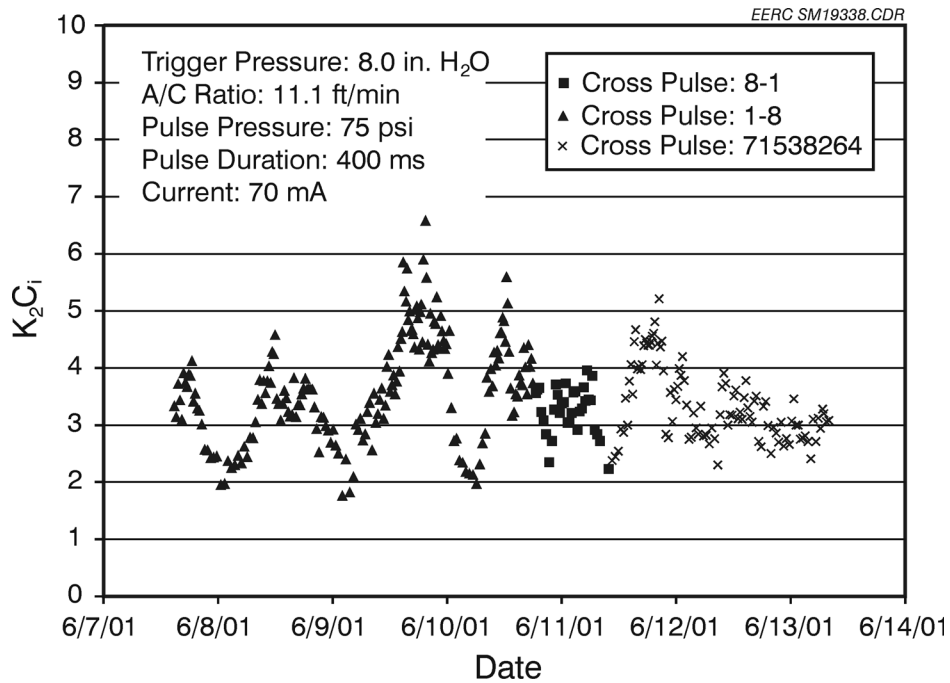


Figure 3.4-50. Pulse sequence effect on AHPC K_2C_i (June 7-13, 2001).

TABLE 3.4-3

AHPC Settings and Results at Different Pulse Sequence Modes

Operational Settings

Pulse Trigger Pressure: 8.0 in. W.C. (2.0 kPa)
 Pulse-Cleaning Pressure: 75 psi (517 kPa)
 Pulse Duration: 400 ms
 Secondary Current: 70 mA
 A/C Ratio: 11.1 ft/min (3.4 m/min)

Operational Results (integral average values)

Cross-Row Pulse Order	K_2C_i	Residual Drag	Bag-Cleaning Interval, min
1-8	3.37	0.599	27.5
8-1	3.11	0.593	29.2
71538264	3.25	0.594	27.8

can be operated under different pulsing sequence modes without compromising overall performance. Since the AHPC functioned very well under difficult operating conditions, the conclusion is that the cross-row pulsing system was as effective as the down-row pulsing. Therefore, cross-row pulsing appears to be a viable design alternative for full-scale systems.

3.4.5 Results for Test Period 3 (June 17–28, 2001)

3.4.5.1 Electrical Conditions

A total of four ELEX bidirectional electrodes was installed at the end electrode position (opposite the inlet) to replace the mast-only electrodes that were originally installed in March 2001. The secondary current was set at 70 and 80 mA during this test period. The daily sparking number was recorded and plotted in Figure 3.4-51. A total of only 1237 sparks occurred during the 12-day test, with a daily average of 112 sparks, which was again much better than the previous results in summer 2000. The bidirectional electrodes allowed an increase in total corona current without sparking.

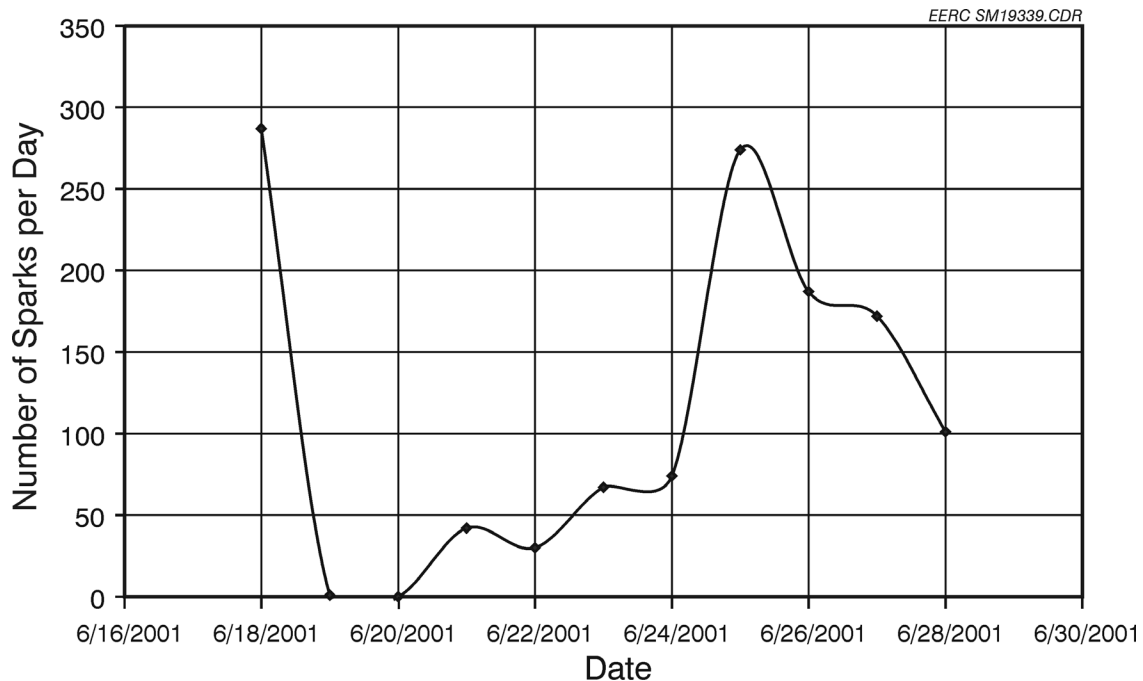


Figure 3.4-51. Number of sparks per day (June 18–28, 2001).

3.4.5.2 Pulse Sequence Experiments

A total of four different pulse sequences was tested during June 17–20, 2001, to examine their effect on AHPC performance. The A/C ratio was 11.1 ft/min (3.4 m/min), and the pulse trigger pressure was set at 8.0 in. W.C. (2.0 kPa), with a pulse-cleaning pressure of 75 psi (517 kPa) and a pulse duration time of 400 ms. The bag-cleaning interval, residual drag, and K_2C_i results are shown in Figures 3.4-52–3.4-54. The bag-cleaning interval varied widely from over 40 min to as low as 15 min. The bag-cleaning interval showed a periodical variation pattern during this test period, which was caused by the varying power plant gross load and the corresponding fluctuating temperatures of flue gas temperature to the AHPC system. The residual drag and K_2C_i may have slightly decreased when the pulse system operated in a cross-row pulsing order of 32187654, but because of the varying power plant operating conditions, it is very difficult to evaluate a small effect of pulse sequence on AHPC performance. Since the AHPC operated very well for all four pulse sequence modes, the exact pulse sequence does not appear to be an important factor affecting AHPC performance.

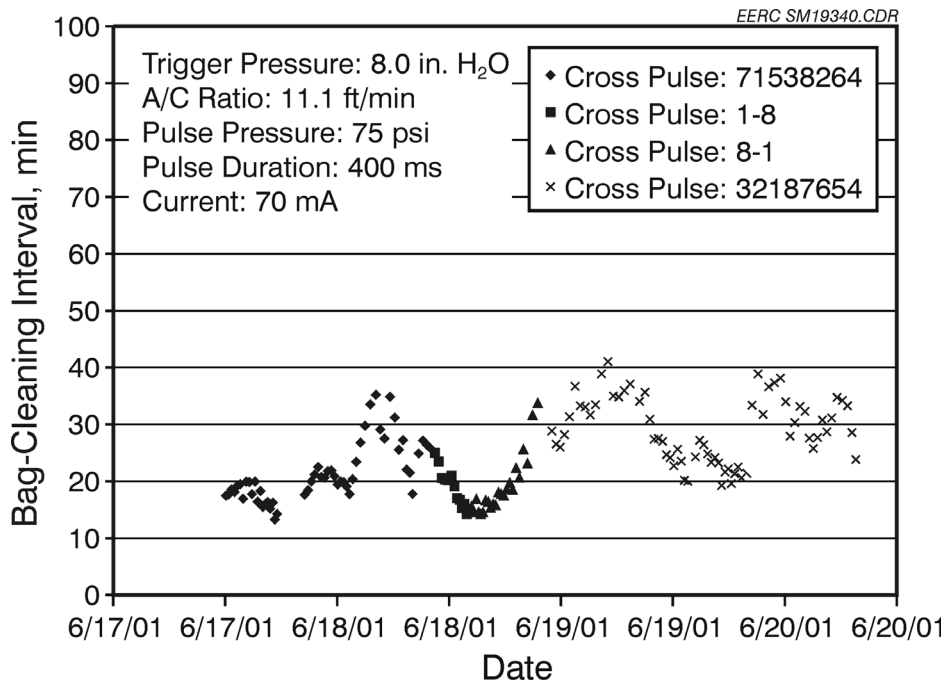


Figure 3.4-52. Pulse sequence effect on AHPC bag-cleaning interval (June 17–20, 2001).

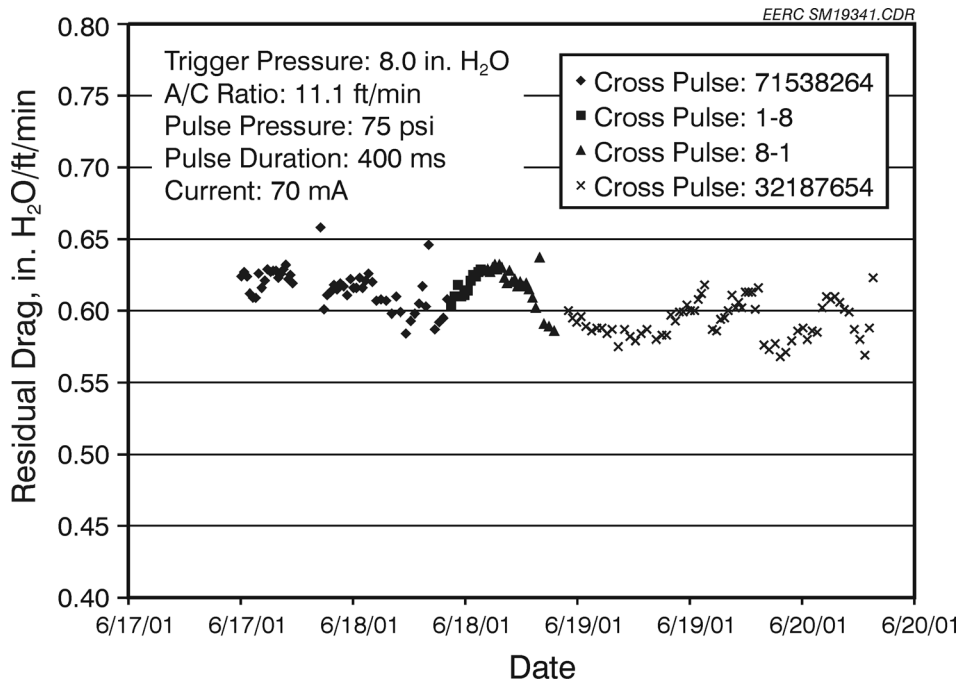


Figure 3.4-53. Pulse sequence effect on AHPC residual drag (June 17–20, 2001).

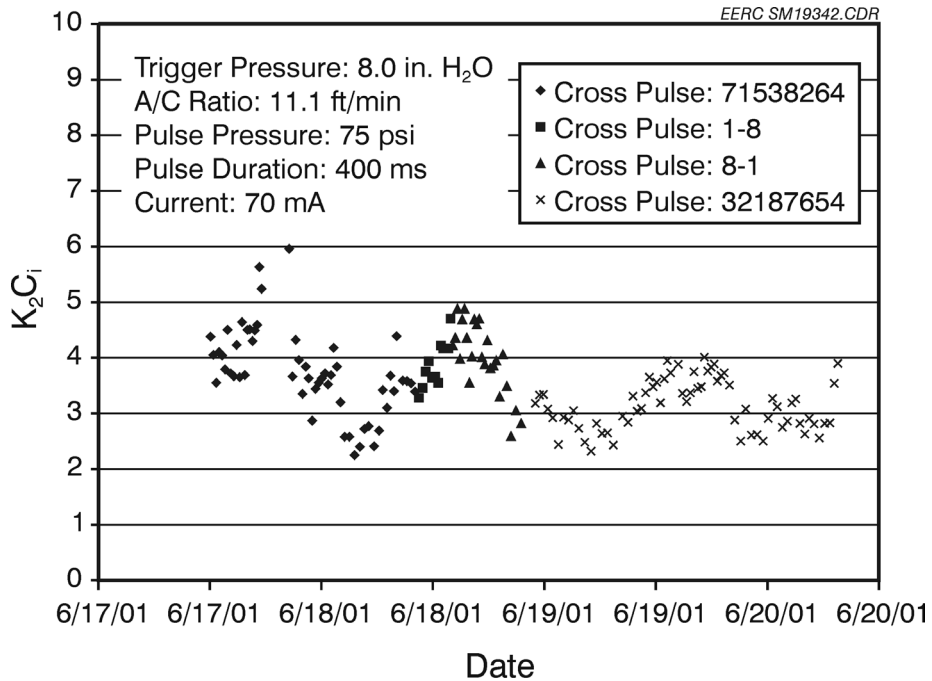


Figure 3.4-54. Pulse sequence effect on AHPC K_2C_i (June 17–20, 2001).

3.4.5.3 Humidification Experiments

From previous results, it is known that temperature has a significant effect on AHPC performance. When the temperature in the AHPC chamber was higher than 300EF (149EC), the fly ash resistivity was sometimes higher than 10^{12} ohm-cm, resulting in back corona, which severely limited ESP performance. A humidification system was, therefore, installed to inject water into the flue gas to reduce the temperature of the AHPC vessel to the range where the ESP was able to function well. The water injection rate was adjusted in the range from 0.5 to 1.0 gal/min (1.9 to 3.8 L/min) to control AHPC temperature within 220E–250EF (104E–121EC). Short-term tests were then conducted on June 25–27, 2001, to evaluate the humidification effect on AHPC performance. The pulse-trigger pressure was set at 8.0 in. W.C. (2.0 kPa), the current was 80 mA, and the A/C ratio was 11.9 ft/min (3.6 m/min), with a pulse-cleaning pressure of 75 psi (517 kPa) and 400 ms pulse duration time. The experimental data are plotted in Figures 3.4-55–3.4-57, showing the variations in bag-cleaning interval, residual drag, and K_2C_i with and without water injection. On June 25, 2001, 12:00 a.m.–8.00 a.m., the AHPC was operated without humidification, and the AHPC temperature during this time was around 310EF (154EC). The bag-cleaning interval results ranged from 10 to 20 min, with a constant residual

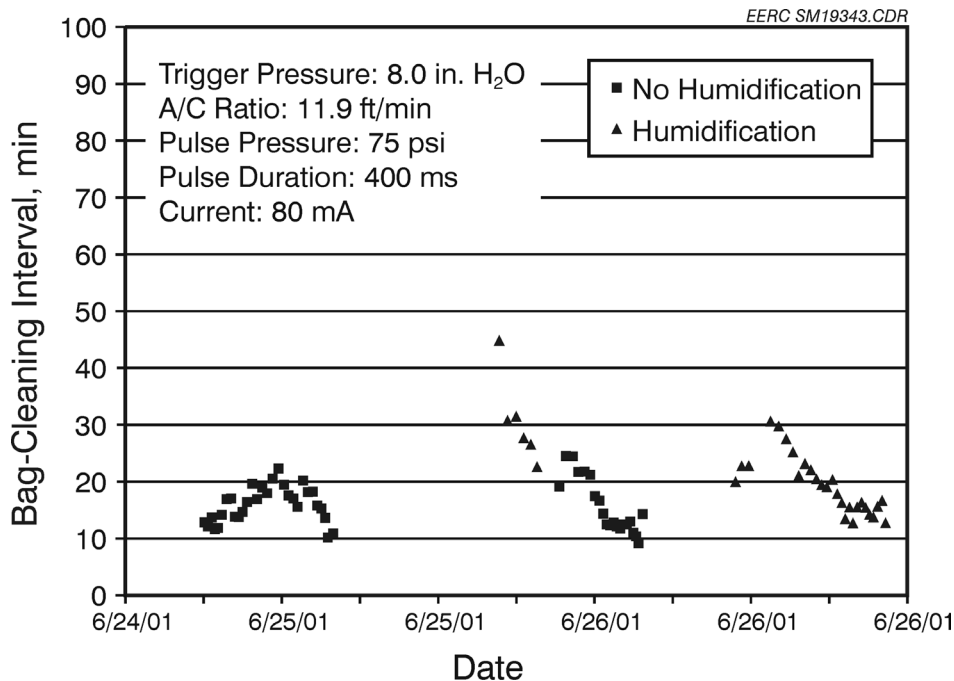


Figure 3.4-55. Humidification effect on AHPC bag-cleaning interval (June 25–26, 2001).

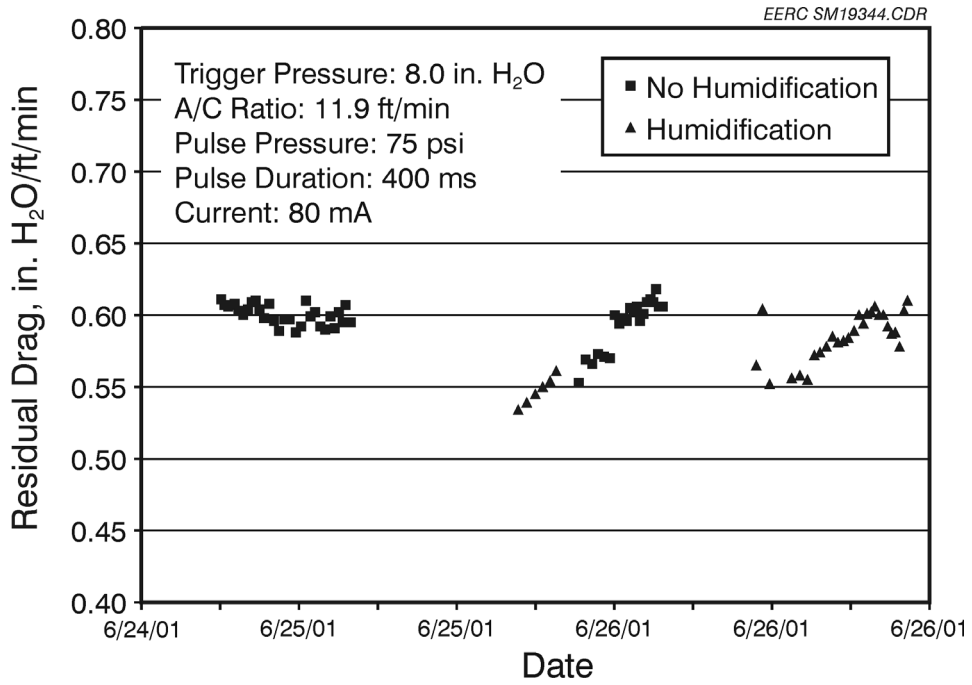


Figure 3.4-56. Humidification effect on AHPC residual drag (June 25–26, 2001).

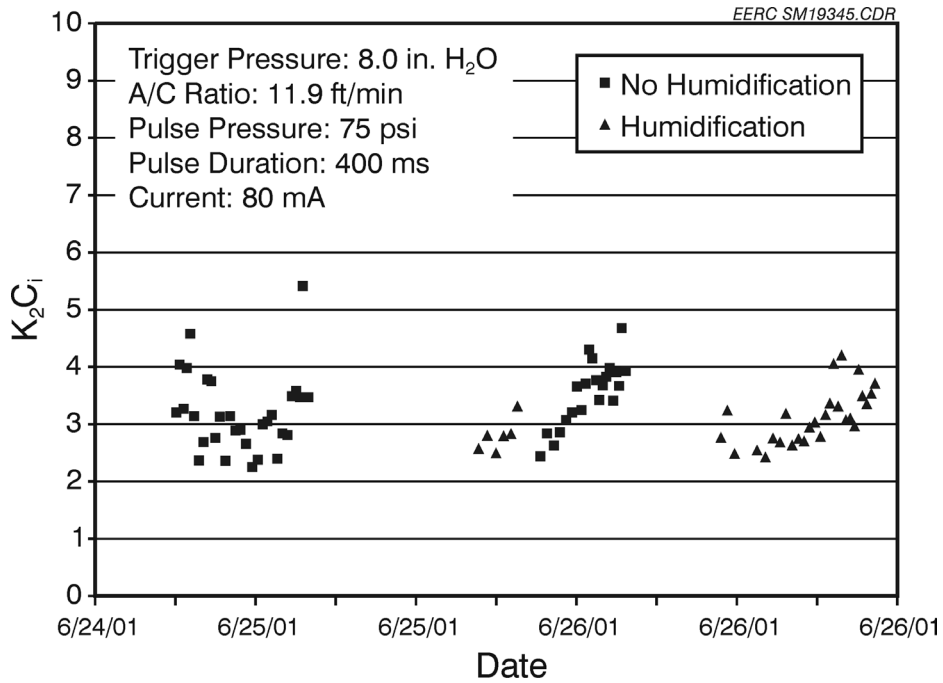


Figure 3.4-57. Humidification effect on K₂C_i (June 25–26, 2001).

drag of 0.6. The corresponding K_2C_i was in the range of 2.3–5.4. By injecting water at a rate of 0.5 gal/min (1.9 L/min), the AHPC temperature was reduced to 250EF (121EC). The bag-cleaning interval initially increased significantly up to 45 min and then fluctuated in the range of 22–30 min, better than that without humidification. The observed bag-cleaning interval increase was caused by reductions of both K_2C_i (2.5–3.3) and residual drag (0.53–0.56), shown in Figures 3.4-56 and 3.4-57, demonstrating the improvement in ESP performance and bag-cleaning ability with humidification. After the water injection was turned off on June 25, 2001, 9:00 p.m., the K_2C_i and residual drag increased to their previous levels, resulting in a bag-cleaning interval as low as 10 min. Short-term humidification was carried out again on June 26, 2001, at a higher water injection rate of 0.67–1.0 gal/min (2.5–3.8 L/min), further reducing AHPC temperature to 240EF (116EC) (Figure 3.4-57). AHPC performance was improved in terms of longer bag-cleaning interval (13–31 min), lower K_2C_i (2.42–4.20), and residual drag (0.55–0.60) compared to the results without humidification. In order to further clarify the effect of humidification on AHPC performance, integral average values of the above experimental results were calculated and are listed in Table 3.4-4. The calculated results

TABLE 3.4-4

AHPC Settings and Results with and Without Humidification			
Operational Settings			
Pulse Trigger Pressure: 8.0 in. W.C. (2.0 kPa)			
Pulse-Cleaning Pressure: 75 psi (517 kPa)			
Pulse Duration 400 ms			
Secondary Current: 80 mA			
A/C Ratio: 11.9 ft/min (3.6 m/min)			
Operational Results (integral average values)			
Temperature, EF (EC)	K_2C_i	Residual Drag	Bag-Cleaning Interval, min
310 (154), No Humidification	3.09	0.599	16.5
250 (121), Humidification	2.82	0.549	28.1
300 (149), No Humidification	3.46	0.591	16.8
240 (116), Humidification	2.98	0.580	21.2

clearly demonstrate the longer bag-cleaning interval and lower K_2C_i at the lower temperatures with humidification. The AHPC performance met the project goal of over 10 min at the A/C ratio of 12 ft/min (3.7 m/min) without humidification, but significantly improved to over 20 min in the presence of water injection with a reduced K_2C_i of 2.82–2.98 and residual drag of 0.549–0.580 in. W.C./ft/min.

On June 27, further humidification tests were completed to determine if the AHPC could operate at higher A/C ratios when performance was not limited by ash resistivity. Prior to starting humidification, the AHPC was operating at 11.1 ft/min (3.4 m/min) with a residual drag of 0.6. Immediately upon starting humidification so that the inlet temperature was reduced to 250EF (121EC), the residual drag dropped to 0.58, which allowed the A/C to be increased to 11.9 ft/min (3.6 m/min) without increasing the pressure drop. At that point, the water injection rate was increased to lower the inlet temperature to 220EF (104EC), which resulted in a further reduction in residual drag to 0.57 and allowed increasing the A/C ratio to 13.1 ft/min (4.0 m/min). Since operation under these conditions was stable, the A/C ratio was then increased to 13.9 ft/min (4.2 m/min) and the pulse trigger increased to 8.7 in. The bag-cleaning interval results were in the range of 8–10 min, but appeared to be very steady. The K_2C_i (Figure 3.4-58) was in the range of 3.1–5.9, indicating the ESP functioned well under the highest A/C ratio 13.9 ft/min (4.2 m/min) achieved so far. The residual drag was stable at around 0.58 under the high A/C ratio of 13.9 ft/min (4.2 m/min) with water injection, which is even better than the previous results obtained at lower A/C ratios without humidification. The humidification significantly improved performance so that the flow rate through the AHPC could be increased by 25% (A/C increase from 11.1 to 13.9 ft/min [3.4 to 4.2 m/min]). While these were very short-term tests (10-hr total), they clearly demonstrate the potential of the AHPC to operate at much higher face velocities than 12 ft/min (3.7 m/min) when performance is not limited by very-high-resistivity ash.

The above encouraging results suggest that the AHPC can be operated successfully at a higher A/C ratio with a reasonably long bag-cleaning interval at a lower temperature under humidification conditions, implying the possibility of a more compact AHPC design.

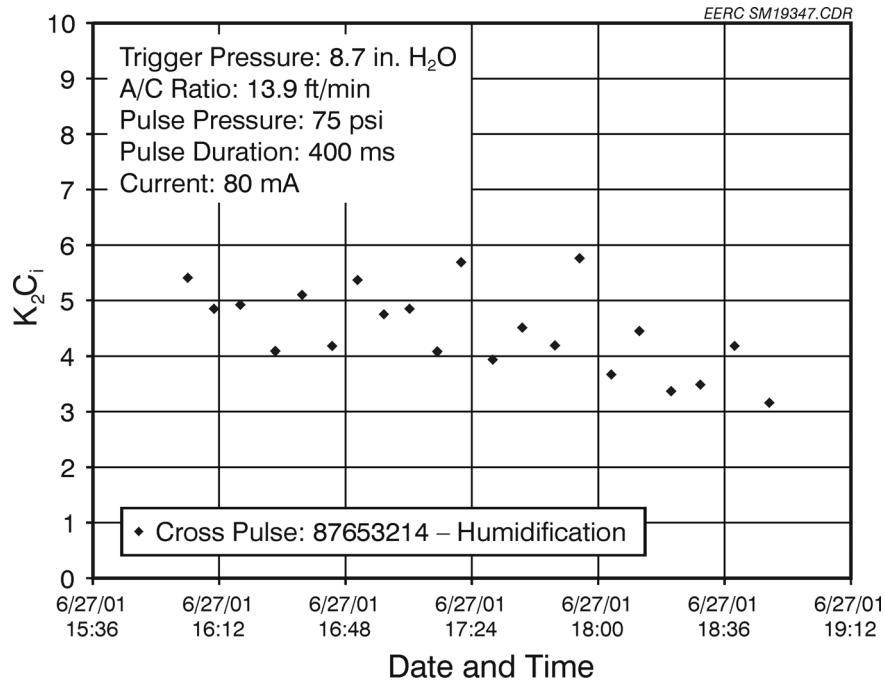


Figure 3.4-58. Humidification effect on K_2C_i (June 27, 2001).

3.4.6 AHPC Filter Bag Analysis

The AHPC pilot unit utilized GORE-NO STAT[®] filter bags, which were installed and pre-coated prior to start-up of the AHPC Phase III 2001 testing on March 15, 2001. Filter bags were removed from the unit for inspection and evaluation in May and June. The bags originally installed in March and removed in June experienced a total service time in the AHPC of 2300 hr (14 weeks).

Applications and specifications are as follows:

- Plant Location: Big Stone, South Dakota, Otter Tail Power Company
- Coal Type: Western subbituminous coal
- Dust Type: Fly ash from cyclone coal-fired boiler
- Filter Bag Type: GORE-NO STAT[®] filter bags (GORE-TEX[®] anti-static membrane/
GORE-TEX[®] anti-static felt)
- Bag Diameter: 5.75 in. (146 mm)

Length: 15 ft (4.6 m)
A/C ratio: 11–12 ft/min (3.4–3.7 m/min)

The AHPC operational parameters prior to shutdown were as follows:

Pulse pressure: 75 psi (517 kPa)
ESP current: 70 mA
A/C ratio: 11 ft/min (3.4 m/min)
Pulse pressure trigger: 7.6 in. W.C. (1.9 kPa)
Pulse duration: 200–400 ms

The shutdown sequence was to allow the pressure drop to build to 7.5 in. W.C. (1.9 kPa), commence pulsing the bags in multibank mode, and immediately shut down the fan, ESP power supply, and inlet/outlet dampers. After the shutdown procedure, the clean air plenum was opened up, and filter drag measurement was completed on each filter bag.

3.4.6.1 Filter Bag Drag Analysis

After shutdown, the clean-air plenum was opened up, and testing was conducted to determine the filter drag across individual bags while the bags remained installed in the collector. The measurement determines the permeability condition of a pulse-jet filter bag after operation has been stopped. The flow measurement and pressure drop test device consists of a 2-in. (51-mm)-diameter aluminum pipe 4 ft (1.2 m) in length that has a pitot tube mounted in the pipe to measure velocity pressure. The 4 ft length of pipe has, at one end, a cone-shaped transition piece that is placed over the top of the bag while the bag is in place in the collector tube sheet. The cone seals over the bag and cage to the tube sheet, thereby isolating the clean side of the bag. The other end of the pipe is connected to a flexible hose and a fan to pull air through the bag. The pressure drop across the bag and the airflow through the bag are recorded to determine filter drag for that individual bag. The filter drag is the pressure drop across the bag divided by the A/C ratio as measured at the time of the testing. All the filter bags were tested for individual filter drag.

The filter drag measurements were conducted after an on-line multibank cleaning at a pressure drop of 7.6 in. W.C. (1.9 kPa) in May, July, and August 2001 (after continued testing beyond Phase III). The May tests were completed with down row pulsing and the July–August tests were completed after cross-row cleaning. The detailed information is listed in Table 3.4-5. The experimental data from the tests contain 32 data points from the four down rows of eight bags. In this way, the performance of the AHPC zones or down row sets of bags can be compared for flow and loading distribution between the ESP and filter bag zones.

Table 3.4-5

Filter Drag Test Dates and AHPC Operating Parameters							
Test Date	Pulse Bags	Row Sequence	Pulse Pressure, psi (kPa)	Pulse On Time, msec	Nozzle Diameter, in. (mm)	A/C Ratio, ft/min (m/min)	Pressure Drop, in. W.C. (kPa)
5/8/2001	On-line	Down row	75 (517)	400	1.0 (25)	11.6 (3.5)	7.6 (1.9)
7/24/2001	On-line	Cross row	75 (517)	200	1.0 (25)	11.0 (3.4)	7.6 (1.9)
8/31/2001	On-line	Cross row	75 (517)	200	0.75 (19)	11.0 (3.4)	7.6 (1.9)

Figure 3.4-59 compares the average of the down row sets of bags. The levels in drag after on-line cleaning are similar for all four down rows within each test period and across all three test dates. The error bars represent one standard deviation between the eight bags tested per row. The data show the averages fall within one standard deviation of each row. The after-cleaning on-line filter drag is similar over the time period and across the four rows, indicating excellent operation of the AHPC system between the ESP zone and the filter bag zone.

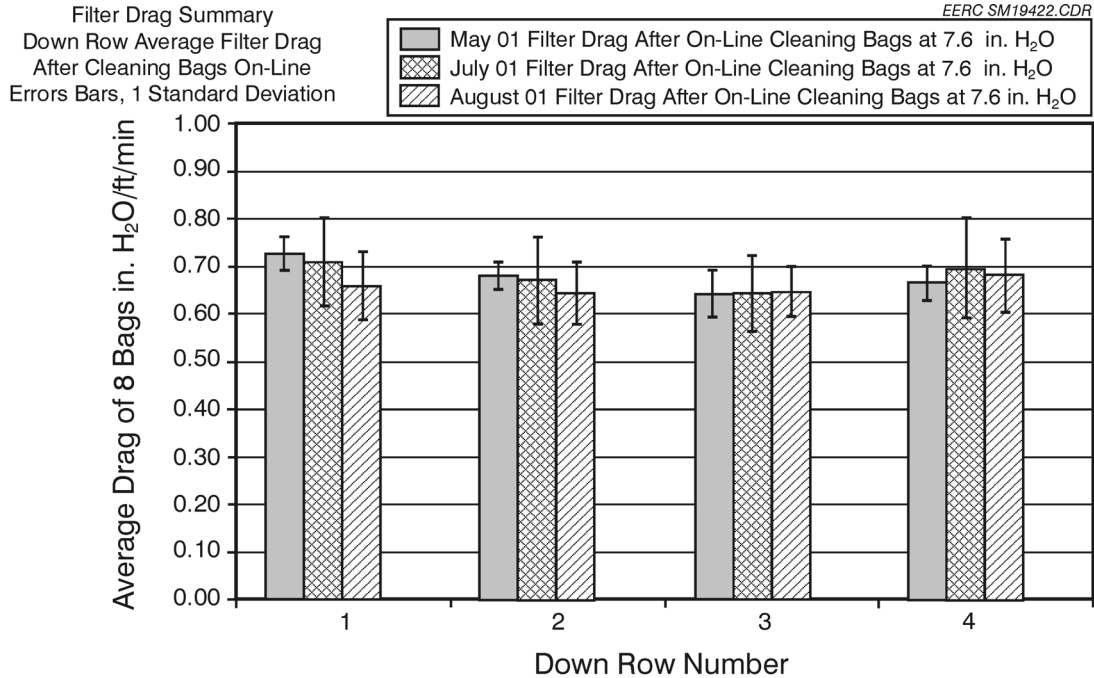


Figure 3.4-59. Average filter drag per row.

3.4.6.2 Filter Bag Field Analysis

In May 2001, four bags were removed from the unit and returned to Gore for lab analysis. They were lightly brushed, and the attached ash fell off very easily. The locations of the removed bags analyzed in the lab are presented in Figure 3.4-60. The one white membrane bag, R2B5, showed no small holes and no membrane damage along the cage wire from electrostatic discharge (ESD) or electric field effect (EFE). A few areas of abrasion from handling and installation were noticed, but the small amount is of no concern. The inside of the bag appeared clean and free of dust and pulse system/flue gas condensate contamination (see Figure 3.4-61). The three black anti-static membrane bags (R4B4, R4B8, and R2B1), shown in Figure 3.4-40, revealed a very clean bag surface after brush-off, and there were no holes and no damage to the membrane along the cage wires from ESD or EFE. The entire bag area was in excellent condition. Two of these bags received extensive lab analysis. In June 2001, eight additional bags were removed and analyzed in the lab.

Pulse Valve Header Side

	Row 4	Row 3	Row 2	Row 1
Bag 1	○	○	○	○
2	○	○	○	○
3	○	○	○	○
4	○	○	○	○
5	○	○	○	○
6	○	○	○	○
7	○	○	○	○
8	○	○	○	○

Transition Gas Inlet Dust Side

GORE-NO STAT* Filter Bag Removed for Laboratory Analysis

Figure 3.4-60. Location of removed bags for analysis.



Figure 3.4-61. Photo showing the top cuff, R3B4, and top of the bag.

3.4.6.3 Visual Observation

After arrival at the lab, the bags were carefully removed from the packaging and placed in a lab hood for analysis. The bag is laid out to its full length for analysis. The top cuff is examined for seal integrity and any signs of dust bypass between the bag snap ring and the tube sheet. All the bags maintained excellent seals, and no evidence of any leakage was observed. The surface of the bag and the dust cake is examined down the length of the bags for any signs of heavy cake buildup that would appear as clumps or nodules. None of these signs was observed on the bags. The bottom of the bag is analyzed for excessive wear or abrasion due to the bag restraining channel. These bags are manufactured with a double bottom cuff for added protection. The cuff on all of the bags showed no signs of excessive wear.

The surface of the filter bags contained a thin layer of fly ash dust on the membrane surface, typical of the bags examined in the past from the AHPC tests and from most coal-fired boiler applications with GORE-TEX[®] membrane filter bags. The primary dust cake was easily brushed off from the membrane bag to reveal a fully intact membrane. No dust was observed to have penetrated into the membrane surface nor through the membrane to the felt. Additional scanning electron microscopy images of the membrane cross section confirmed no dust penetration into the membrane surface. The inside of the bags appeared clean and free of dust.

The visual examination of the filter bags confirmed no ESD damage, excellent membrane integrity, and no unusual signs of wear of the filter bags.

3.4.6.4 Filter Bag Microscope Analysis

Visual analysis of a filter sample is often aided by the use of a light microscope. Determining the particulate interaction with the membrane filter surface and the condition of the microporous membrane surface is often critical in solving filter performance issues. Evidence of abrasion, ESD, and chemical and thermal effects is often enhanced by this analysis.

The filter bags were examined for membrane damage from ESD using a light microscope. Microscopic analysis along the membrane surface where the cage wire is closest to the collecting plates revealed no damage from ESD or EFEs as seen in summer 2000. The surface of the filter bags was lightly brushed before examination, allowing a clear view of the membrane surface. The microscope range was a magnification of 10–50×, allowing sufficient magnification of the membrane surface features. Locations at the top, middle, and bottom of each bag were evaluated. The membrane under the microscope is shown in Figure 3.4-62. The examinations revealed no damage to the membrane surface by ESD effects. Additional analytical analysis confirmed the visual findings.

The perforated-plate design with the addition of the antistatic membrane bags has eliminated the previously experienced effects of ESD on the filter bags. There was no evidence of bag abrasion and chemical or temperature attack on the filter bag felt media.



Figure 3.4-62. R3B5 membrane surface at 10–50× magnification.

3.4.6.5 Air Permeability Analysis

The air permeability analysis of the AHPC filter bag media was performed in the lab and measured by a device that produces a Frazier number. The Frazier number is defined as the volumetric flow rate, measured in cubic feet per minute (cfm), through a square foot of filter media at a pressure differential of 0.5 in. W.C. (0.1 kPa). The unit of measure is written as $\text{ft}^3/\text{min}/\text{ft}^2$ at 0.5 in. W.C. (0.1 kPa) or ft/min at 0.5 in. W.C. (0.1 kPa).

Samples of each filter bag were cut from the top, middle, and bottom bag locations. The sample size was 5 in. (127 mm) in the vertical bag length direction along the entire circumference of the bag. This enables three Frazier measurements to be taken per bag length location. The test produces a total of nine data points for each filter bag. A sample is tested for permeability in the condition it was received from the field and labeled (as-received). The as-received condition is the state of the bag as removed from the collector and immediately placed in plastic bags and carefully shipped to the lab. After the as-received permeability is measured, the membrane surface is lightly brushed to remove the residual dust cake and retested for permeability at the identical locations on the sample as previously tested. Each of the sets of nine readings is then averaged to create a bag permeability number for as-received and after-brushing. The after-brushing measurement is then compared to the bag condition when new. A significant reduction below the initial new permeability indicates further analysis is required.

The filter media permeability analysis results are shown in Table 3.4-6. As a baseline, the new Frazier number of the media used in Phase III 2001 tests is in the range of 3.0 to 5.0 ft/min (0.9 to 1.5 m/min) at 0.5 in. W.C. (0.1 kPa). The averaged as-received Frazier number for all of the bags was 1.7 ft/min (0.5 m/min) at 0.5 in. W.C. (0.1 kPa). After brushing, the averaged Frazier number for all of the bags was 3.0 ft/min (0.9 m/min) at 0.5 in W.C. (0.1 kPa). The after-brushing Frazier number for the filter bags is within the range of the new media permeability. This indicates the membrane is capturing the particles on the surface of the media while retaining a majority of its original permeability. These permeability data combined with the filter drag

TABLE 3.4-6

Filter Media Permeability as Measured in Lab					
AHPC Phase III May 2001		Service Life	R = Row B = Position	Permeability of Media	Permeability of Media
Date Installed	Date Removed	Hours	Bag Location	As-Received Frazier No.	After-Brushing Frazier No.
3/15/2001	5/8/2001	1300	R2B7	1.8	3.8
3/15/2001	5/8/2001	1300	R3B5	1.33	3.4
3/15/2001	6/28/2001	2300	R4B2	1.8	3.3
3/15/2001	6/28/2001	2300	R1B2	1.6	2.7
3/15/2001	6/28/2001	2300	R4B4	1.7	3.7
3/15/2001	6/28/2001	2300	R4B3	1.6	3.2
3/15/2001	6/28/2001	2300	R3B3	1.9	3.3
3/15/2001	6/28/2001	2300	R2B5	NA	2.2
3/15/2001	6/28/2001	2300	R3B7	NA	2.9
Average Values				1.7	3.0

testing results demonstrate the filter bags' ability to operate in the AHPC pilot unit and exhibit steady-state bag operation while maintaining excellent media permeability.

3.4.6.6 Dimensional and Mechanical Strength Analysis

The pressures and movements experienced by the bags during service include a negative static pressure or pressure drop across the bag, a positive pressure created inside the bag during pulse-jet cleaning, and the rapid flexing of the media between these two times. These forces combined with temperature and chemical exposure can lead to a loss of dimensional stability of a filter bag.

The flat width of the filter bags is the measured distance of the bag when it is placed flat against a straight surface and is used to determine any changes to the dimensional stability of the bag. The flat width is equal to one half the circumference. All the bags were cut and manufactured to the identical flat width specifications. The average flat width of the filter bags was 22.8 cm as measured in the lab after 1200 hr of operation. The bag width of new bags had

been measured as 22.9 cm. The bag inspection after 2300 hr of service produced measurements with average flat widths of 23.1 cm. The bags have maintained their dimensional stability during the 2300 hr (14 weeks) of operation.

The Mullen burst strength is a measure of the two-dimensional or planar strength of the media, measured in pounds per square inch. The sample is securely clamped over a rubber diaphragm which is pressurized with fluid until the fabric yields and the diaphragm breaks through the media. The pressure at breakthrough is recorded as the burst strength of the material. The effects on the filter from mechanical, chemical, or thermal stress are determined.

A Mullen burst test was performed on six filter bags and showed no loss in mechanical strength of the felt. The filter bags show no decrease in mechanical stress after 2300 hr (14 weeks) of operation.

3.4.7 Coal and Fly Ash Resistivity Analyses

During the 3.5 months from March 15 – June 28, 2001, five different coals were burned at the Big Stone Power Plant. The coal usage schedule is listed in Table 3.4-7. The varying coal usage resulted in challenging operating conditions for the AHPC system, such as variation of fly ash resistivity and particle size. Among these parameters, sodium content in coal is critical to AHPC performance, since a higher sodium content in the coal correlates with lower fly ash resistivity. The power plant was using higher-sodium coals (Eagle Butte [1.76%–1.8%] and Buckskin [1.57%–1.65%]) in March and April and then switched to lower-sodium coals (Cordero [1.1%–1.22%] and Cordero Rojo [1.1%–1.2%]) during May and most of June. The power plant burned Black Thunder coal from June 14–16, 2001, which had a low sodium content. The gradual conversion from the higher-sodium coals to the coals with lower sodium content caused an increase in fly ash resistivity. Fly ash from the AHPC hopper was collected and tested for resistivity under a constant humidity of 11%, which is normal for coal-fired power

TABLE 3.4-7

Coal Usage Schedule and Analysis Results					
	Eagle Butte	Buckskin	Cordero	Cordero Rojo	Black Thunder
Time	3/15–4/01, 6/17–6/20	4/02–5/04	5/06, 6/21–6/30	5/07–5/31, 6/04–6/13	6/14–6/16
Moisture, %, as received	30.67	30.14	29.4	29.7	26.95
Ash, %, as received	4.7	5.6	5.82	5.07	5.71
Btu/lb, %, as received	8384	8323	8400	8430	8786
Sulfur, %, as received	0.37	0.3	0.32	0.34	0.28
NaO, %, as received	1.76–1.8	1.57–1.65	1.1–1.22	1.1–1.2	0–1.6

plants. The analysis results presented in Figure 3.4-63 show that the electrical resistivity of the fly ash increased with the elevated temperature, reaching a maximum resistivity at a temperature of approximately 300EF (149EC), which was the normal operating temperature for the AHPC system. The results show the varying electrical resistivity of the fly ash for different coals because of the varied sodium contents in the coals, as discussed above. The resistivity of the fly ash for the Eagle Butte and Buckskin, in the range of 10^{11} – 10^{12} ohm-cm in the temperature range of 200E–378EF (93E–192EC), were lower than the resistivity for the Cordero Rojo, which was over 10^{12} ohm-cm. The increasing resistivity due to the switch to the low-sodium coals resulted in the deteriorated ESP performance observed in Test Periods 2 and 3. This explains why AHPC performance was better in Test Period 1 than in Test Periods 2 and 3. However, 10^{11} -ohm-cm resistivity is still high enough to limit ESP performance. With a lower ash resistivity, the AHPC would perform even better than the best observed performance for Test Period 1.

3.4.8 Particulate Emissions of the Perforated-Plate AHPC System

The dust loadings at the inlet and the outlet of the AHPC unit were measured by EPA Method 5 at the end of the 3.5-month test to evaluate the overall collection efficiency of the perforated-plate AHPC system. The sampling time was 45 min at the inlet and extended to 15 hr at the outlet to guarantee weighing accuracy. Flue gas moisture was 12%, with leak checks of the

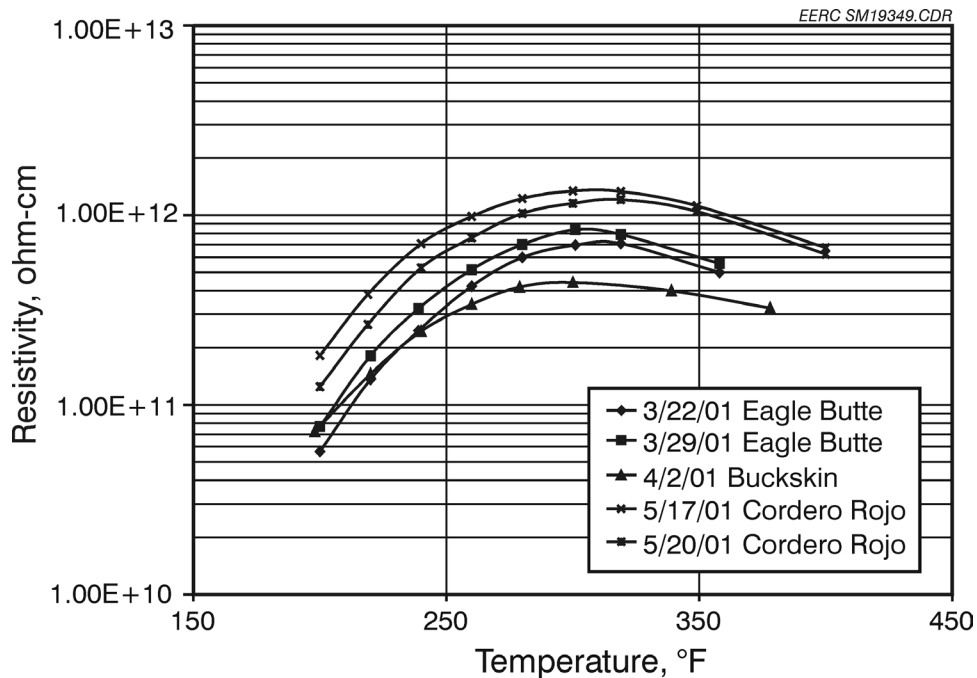


Figure 3.4-63. Fly ash resistivity at Big Stone Power Plant.

sampling trains before and after sampling, providing quality control checks, which indicated that flue gas volume was the actual volume sampled. The measured dust loadings and collection efficiency are shown in Table 3.4-8. The dust loading at the AHPC inlet was 5.362 g/m³ and dramatically reduced to an extremely low level of 0.00021 g/m³, providing an extraordinary high collection efficiency of 99.996%.

TABLE 3.4-8

AHPC Dust-Loading Measurements			
Dust Loading, g/m ³ (gr/scf)	H ₂ O, %	Sample Time	Removal Efficiency, %
Inlet			
5.362 (2.341)	12	20 min	
Outlet			
0.00021 (0.000092)	12	15 hr	99.996

The ultrahigh collection efficiency was confirmed by the perfectly clean outlet sampling filter. Another indication of ultrahigh collection is that inspection of the clean plenum area of the AHPC after 3.5 months of operation revealed a completely clean tube sheet.

To confirm the ultrahigh collection efficiency observed, fine particulate emissions were measured at the outlet of the AHPC by an APS, measuring particles in the range from 0.5 to 5 μm . According to the measured results, the mass median diameter of the emitted particles was 1.633 μm , with a standard deviation of 0.457. The measured respirable particulate mass at the outlet of the AHPC is shown in Figure 3.4-64 as a function of sampling time. The respirable mass was in the range of 0.002–0.006 mg/m^3 , with an integrated average value of 0.045 mg/m^3 , demonstrating an extremely low and stable emission level. By assuming a respirable mass particle concentration of 1.0 g/m^3 at the inlet of the AHPC, a typical value for a coal-fired plant, the fine-particle collection efficiency by the perforated-plate AHPC achieved the extremely high rate of 99.9995%. The respirable mass concentration of the ambient air was also measured at the same time and is plotted in Figure 3.4-64. Compared to the measured respirable mass of 0.013 mg/m^3 for ambient air, the perforated-plate AHPC removed the particulate so efficiently that the particle concentration in the emitting flue gas was even lower than that in the ambient air.

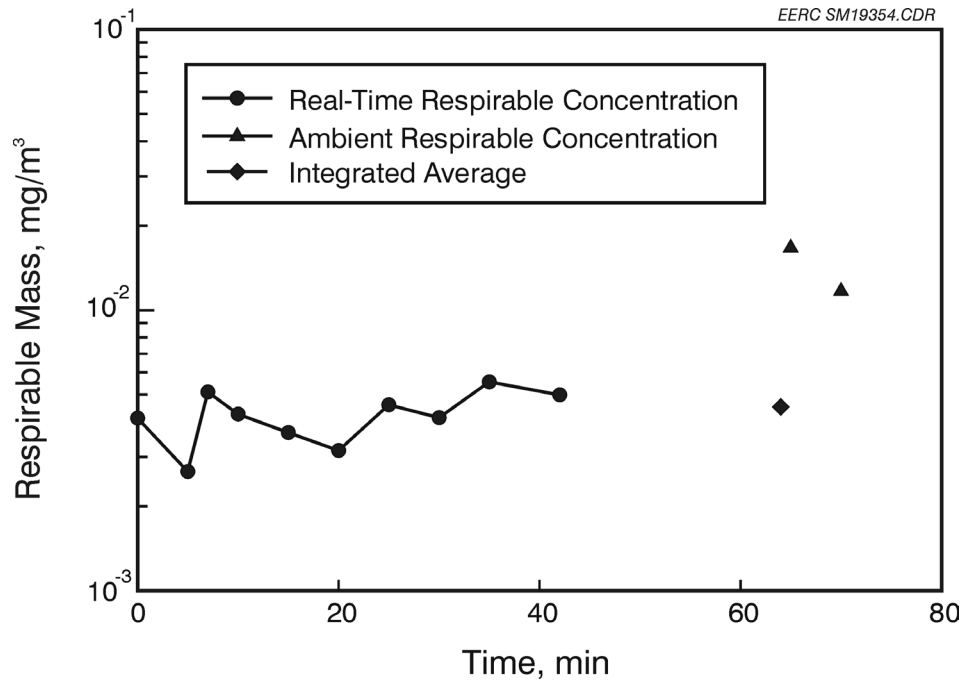


Figure 3.4-64. Respirable mass concentration at the outlet of the AHPC unit at the Big Stone Power Plant.

4.0 CONCLUSIONS AND DISCUSSIONS

- At the start of Phase III, the 9000-acfm (255-m³/min) AHPC was modified to include a side transition inlet, different discharge electrodes and plates, closer bag and plate spacing, and a preionization zone. The AHPC field unit was then successfully operated for a period of about 3 months from April to July 2000. The modified AHPC with significantly closer bag row spacing and bag-to-electrode spacing functioned very well according to theoretical expectations and within the previously established goals of a 10-min bag-cleaning interval at an A/C ratio of 12 ft/min (3.7 m/min) and 8.0 in. W.C. (2.0 kPa) pressure drop. Acceptable performance was achieved in spite of dealing with a fine-particle size, high-resistivity ash.
- The AHPC performance in summer 2000 demonstrated the bag-cleaning interval was quite sensitive to the A/C ratio and could be significantly increased by a small reduction in A/C ratio under a constant pulse-trigger pressure. Alternatively, the average pressure drop across the system could be significantly reduced by a small reduction in A/C ratio at a constant bag-cleaning interval. These results suggest there is a trade-off between pressure drop and A/C ratio.
- The use of high-resistivity fly ash (higher than 4×10^{11} ohm-cm) limits AHPC performance by affecting ESP operation.
- The filter bags were analyzed after more than 3 months' operation at the Big Stone unit in summer 2000. The results showed the filter bags retained permeability and strength. However, some damage was observed on the membrane, which appeared to be caused by electrical effects such as back corona, rather than from abrasion, temperature, or chemical attack.
- Bench- and pilot-scale tests were conducted to evaluate the effects of electrode type, bag type, spacing ratio, plate-to-plate spacing, and grounded grids on the current to the bags. It was found that the ELEX electrode induced the highest bag current and was less directional than either the EERC electrode or ENELCO-type electrodes. The bag current can be

significantly reduced by increasing spacing ratio, meaning that the greater the distance from the electrode to the filter bags, the lower the current to the filter bags. The GORE-NO STAT[®] filter bag (GORE-TEX[®] antistatic membrane/ GORE-TEX[®] felt) induced less current than the GORE-NO STAT[®] filter bags (GORE-TEX[®] membrane/GORE-TEX[®] felt).

- Among the several configurations tested in the pilot AHPC unit at the EERC, perforated plates installed between the discharge electrodes and the filter bags provided excellent protection of the filter bags from electrical damage and also improved AHPC performance in terms of longer bag-cleaning intervals and lower K_2C_i , and residual drag.
- Perforated plates with two different hole sizes of 1.5 and 2.0 in. (38 and 51 mm) were evaluated in hot-combustion tests at the EERC, with the spacing between the perforated plate and the filter bags varied from 2.0 to 3.0 in. (51 to 76 mm). Very low bag current was maintained for all the different filter bags tested under the perforated-plate configurations. The 2.0-in. (51-mm) diameter hole perforated plate demonstrated somewhat better AHPC performance than the 1.5-in. (38-mm) hole perforated plate in terms of longer bag-cleaning interval, lower K_2C_i , and lower residual drag. However, the 1.5-in. (38-mm) perforated plates may provide better bag protection.
- A perforated-plate configuration for the 9000-acfm (255-m³/min) AHPC at the Big Stone Power Plant was installed in January–March 2001, and 3 months of successful testing were conducted from March to June 2001 with the larger-scale AHPC.
- AHPC performance with the perforated-plate configuration was excellent for several different subbituminous fuels with ash resistivity over 10¹² ohm-cm. This demonstrates flexibility and ruggedness under varying and challenging conditions. With high-resistivity dust, some reduction in performance is expected compared to operation with moderate-resistivity ash. However, by a small reduction in A/C ratio or an increase in pressure drop, the AHPC can adequately handle dusts with very high ash resistivity. Overall, AHPC performance with the perforated plates was better than with the previous design.

- The cross-row pulsing configuration appeared to be as effective as the more conventional in-row pulsing approach. This means that additional flexibility is available to facilitate design of both new and retrofit applications for the AHPC. Adequate pulse cleaning was achieved for several different pulse sequences with the cross-row pulsing. Pulse order sequence appeared to be of minor significance.
- Pulse-cleaning pressure appears to be critical to adequately control residual drag. Significantly lower residual drag was achieved by increasing the pulse pressure from 50 to 65 psi (345 to 448 kPa). Stable, longer-term operation has been demonstrated with a pulse pressure of 75 psi (517 kPa).
- Particulate collection efficiency was again demonstrated to be well above the performance goal of 99.99%, and outlet emissions were measured to be cleaner than the surrounding ambient air.
- Short-term tests with humidification showed that the AHPC performance significantly improved when it was not limited by high ash resistivity. Operation at an A/C ratio of 13.9 ft/min (4.2 m/min) was achieved with humidification, demonstrating the potential of the AHPC to operate at much higher A/C ratios when conditions are more ideal.
- After 2300 hr of operation, the filter bags still maintained excellent permeability, retained their dimensional stability, and showed no decrease in mechanical strength. No sign of membrane damage, either from electrical effects or other factors such as abrasion, temperature, and chemical attack, was found by microscope analysis, proving excellent bag protection with the perforated-plate design.

5.0 REFERENCES

1. Miller, S.J.; Olderbak, M.R.; Zhuang, Y. *Advanced Hybrid Particulate Collector*; Final Technical Report, Phase I and II, for U.S. Department of Energy Contract No. DE-AC22-95PC95258; Energy & Environmental Research Center: Grand Forks, ND, Dec 2000.
2. Miller, S.J.; Jones, M.L.; Walker, K.; Gebert, R.; Darrow, J.; Krigmont, H.; Feeley, T.; Swanson, W. Field Testing of the Advanced Hybrid Particulate Collector, A New Concept for Fine-Particle Control. Presented at the 2000 American Chemical Society Symposium, San Francisco, CA, March 26–31, 2000.
3. Miller, S.J. Advanced Hybrid Particulate Collector. Presented at the 1998 International Mechanical Engineering Congress & Exposition, Anaheim, CA, Nov 15–20, 1998.
4. Miller, S.J.; Schelkoph, G.L.; Walker, K.; Gore, W.L.; Feeley, T.J.; Krigmont, H. Ultrahigh Collection of PM_{2.5} with the Advanced Hybrid Particulate Collector. Presented at the International Joint Power Generation Conference and Exposition and the International Conference on Power Engineering, San Francisco, CA, July 25–28, 1998.
5. Miller, S.J.; Schelkoph, G.L.; Walker, K.; Krigmont, H. Advanced Hybrid Particulate Collector, A New Concept for Fine-Particle Control. In *Preprint of the PARTEC 98 International Congress for Particle Technology, 4th European Symposium Separation of Particles from Gases*; Nürnberg, Germany, March 10–12, 1998; pp 256–265.
6. Miller, S.J.; Schelkoph, G.L.; Dunham, G.E.; Walker, K.; Krigmont H. Advanced Hybrid Particulate Collector, A New Concept for Air Toxics and Fine-Particulate Control. Presented at the EPRI–DOE–EPA Combined Utility Air Pollutant Control Mega Symposium, Washington, DC, Aug 25–29, 1997.
7. Miller, S.J.; Schelkoph, G.L.; Dunham, G.E.; Walker, K.; Krigmont, H. Advanced Hybrid Particulate Collector, A New Concept for Air Toxics and Fine-Particle Control. Presented at

- the Advanced Coal-Based Power and Environmental Systems '97 Conference, Pittsburgh, PA, July 22–24, 1997.
8. Miller, S.J. Advanced Hybrid Particulate Collector. Presented at the 1st Joint Power and Fuel Systems Contractors' Conference, Pittsburgh, PA, July 9–11, 1996.
 9. Dennis, R. et al. *Filtration Model for Coal Fly Ash with Glass Fabrics*, EPA-600/7-77-084, Aug 1977.
 - 10.. Leith, D.; Rudnick, S.N.; First, M.W. *High-Velocity, High-Efficiency Aerosol Filtration*, EPA-600/2-76-020, Jan 1976.
 11. Oglesby, S.; Nichols, G.B. *Electrostatic Precipitation*; Marcel Dekker: New York, NY, 1978.
 12. Miller, S.J.; Collings, M.E; Zhuang, Y., Gebert, R.; Davis, D.; Rinschler, C.; Swanson, W. The Advanced Hybrid Particulate Collector Field-Testing Results. Presented at the EPA-DOE-EPRI Combined Power Plant Pollutant Control Symposium, Chicago, IL, August 20–24, 2001.
 13. Gebert, R.; Davis, D.; Rinschler, C.; Miller, S.J.; Jones, M.L.; Collings, M E.; Swanson, W.; Krigmont, H. Advanced Hybrid Particulate Collector: Concept, Field Results, and Commercialization Potential. Presented at the Air Quality II: Mercury Trace Elements, and Particulate Matter, McLean, VA, Sept 19–21, 2000.
 14. Gebert, R.; Darrow, J.; Miller, S.J.; Feeley, T.; Swanson, W. Advanced Hybrid Particulate Collector: A New Method for Control of Fine Particles. Presented at the 93rd Air & Waste Management Association Annual Meeting, Salt Lake City, UT, June 18–22, 2000.